Use of Resistivity to Measure Deterioration of Engineered Soils

Chuxia Huang

Thesis submitted towards the degree of

Doctor of Philosophy

Sustainable Infrastructure Group

Department of Engineering

Durham University, Durham

United Kingdom

June 2022

Abstract

Climate change induced seasonal water content variations are likely to influence the soil parameters that determine the stability of engineered slopes. These slopes constitute a large amount of UK transport infrastructure, Repeated fluctuations of water content affect the soil water retention behaviour and hence the suction-dependent shear strength behaviour of engineered soils, resulting in deterioration in both the soil suction and shear strength, which impact the long-term slope stability. Resistivity methods can provide spatial information on the electrical properties of underground soils and therefore has a great potential to be used to monitor subsurface geotechnical property changes by applying geotechnical-geophysical transformation approaches. In order that the resistivity method can be used more effectively in slope monitoring, the interrelationships between soil geotechnical and geophysical properties need to be more fully understood. Therefore, this research focused on establishing an improved understanding of soil deterioration by investigating the effects of repeated drying and wetting cycles on soil property interrelationships and investigating the potential use of resistivity methods to qualitatively and quantitatively describe the property variation of engineered soils subjected to drying and wetting cycles.

In this thesis, three phases of laboratory-based experiment programmes were conducted to investigate the interrelationships between soil electrical and geotechnical properties on samples with different sizes by using different measurement techniques. In the first phase, several point measurement sensors were employed for estimating the soil water content, electrical resistivity, and suction on a cubic glacial till sample during cyclic drying and wetting. In the second phase, soil electrical resistivity, suction and shear strength were determined by a four-electrode resistivity probe, WP4C potential meter and performing Unconsolidated Undrained triaxial test on triaxial specimens with 38mm diameter made of three different types of soils. In the third phase, the 3D time-lapse ERT method was employed to map the in-time resistivity changes in a 1.2m diameter cylindrical lysimeter; point sensors were also used to provide water content and suction measurements on different depths within the lysimeter.

Soil water retention and shear strength behaviour under multiple drying-wetting cycles has been investigated in this research. Result showed that the both the SWRCs and the

undrained shear strength-water content relationships changes over time with drying-wetting cycling, indicating a hysteresis between drying and wetting paths and a deterioration over cycling. The hysteresis of SWRC and shear strength-water content relationship was found to be more pronounced in the first drying-wetting cycle and decreased over cycling. Deterioration in soil suction (i.e. negative pore water pressure) were found to be most significant between the first and the second cycle. Similar evolutionary trends were found in the cyclic swelling and shrinkage behaviour of the soils which may be a key factor to the hysteresis and deterioration. Furthermore, the spatial geotechnical information (i.e., the water content distributions) within the large lysimeter sample can be extrapolated from the ERT-derived resistivity data by applying the proxy relationships (i.e., the Waxman-Smits model).

Keywords: Unsaturated soils; Soil suction; Property relationships; Electrical resistivity method; Soil deterioration

Declaration

The work in this thesis is based on research carried out in the Sustainable Infrastructure Group, Department of Engineering, Durham University. No part of this report has been submitted elsewhere for any other degree or qualification and it is all my own work unless referenced to the contrary in the text.

Signed:_____

Date:_____

Acknowledgements

Firstly, I would like to acknowledge my supervisors Dr. Paul Hughes and Prof. David Toll for their untiring support, friendship and sharing of knowledge. Without their help and expertise, the big picture of the thesis cannot be constructed; the difficulties in the experimentations cannot be tackled.

I would also like to thank the members of the British Geological Survey (BGS) for their expertise and time. Notably, Prof. Jonathan Chambers for his help in developing the electrical resistivity tomography (ERT) system and providing the ERT instruments; Dr. Paul Wilkinson for his support and sharing of knowledge in developing the ERT arrays and the inverse modelling; Dr. David Gunn for kindly providing the testing soils and sharing knowledge from the geotechnical engineering perspectives.

The laboratory work would not have been possible without the assistance of Mr. Stephen Richardson and Mr. Kevan Longley. Many helpful ideas came from conversations with them who have lots of experiences in the laboratory works. Also, I would like to thank Dr. Jonathan Asquith for his friendship and help in setting up and calibrating the TDR system, Miss Anna Brooks for her assistants in the experiment.

In addition, I am grateful to my lovely friends who have contributed to this thesis in many ways during these years: Lei, Jianye, Dan, Arash, Joao, Difu and Sofia. Thanks for your company and encouragements.

Finally, and especially, I want to say thank you to Zhe Zhang and my parents, for their love and support over these years. Without your selfless love, I would not have enough motivation throughout this adventure.

Contents

List of Figures

List of Tables

Acronyms

AC	Alternative Current
ADR	Amplitude Domain Reflectometry
AEV	Air-Entry Value
ALERT	Automated Time-Lapse Electrical Resistivity Tomography
BEC	Bulk Electrical Conductivity
BGS	British Geological Survey
DC	Direct Current
DPT	Direct Penetration Test
ER	Electrical Resistivity
ERT	Electrical Resistivity Tomography
FDR	Frequency Domain Reflectometry
FEM	Finite Element Mesh
GWC	Gravimetric Water Content
HAEV	High Air-Entry Value
LVDT	Linear Variable Differential Transformers
NMR	Nuclear Magnetic Resonance
PSD	Particle Size Distribution
PVC	Polyvinyl Chloride
PWP	Pore-Water Pressure
RH	Relative Humidity
SEM	Scanning Electron Microscope
SWRC	Soil Water Retention Curve
TDR	Time Domain Reflectometry
UU	Unconsolidated Undrained
VWC	Volumetric Water Content

Nomenclature

σ'	Effective normal stress
σ	Total normal stress
u_w	Pore water pressure
χ	Bishop factor ranging between 0 and 1
u_a	Pore air pressure
ψ	Total suction
R	Universal gas constant
T	Absolute temperature
v_{w0}	Specific volume of water
ω_v	Molecular mass of water vapour
u_v	Partial pressure of water vapour
u_{v0}	Saturation pressure of water vapour
π	Osmotic suction
Θ	Normalized water content
θ	Volumetric water content
θ_s	Volumetric water content of soil at saturation
θ_r	Residual volumetric water content
ψ_b	Air entry value of the soil
$C_{(\psi)}$	Correction factor for SWRC
ψ_r	Residual suction
τ	Shear strength of soil
c'	Effective cohesion
ϕ'	Effective internal friction angle
w	Gravimetric water content
ε_a	Dielectric constant/permittivity
c	Velocity of light in free space
t	Time
L_a	Apparent length of TDR
L	Length of TDR wave guide

K_p	Probe constant
ρ	Electrical resistivity
σ_b	Bulk conductivity
R	Electrical resistance
I	Current
ΔV	Voltage difference
i	Current density
K	Geometric factor
C1/C2	Current electrodes
P1/P2	Potential electrodes
a	Electrode spacing
F_{3D}	Sensitivity function for 3D ERT
srv.	Format of the survey file in E4D
stg.	Format of the output data file for Surpersting system
S_r	Degree of saturation
F	Tortuosity factor
ρ_w	Pore water resistivity
ϕ	Porosity
B	Average ionic mobility of cations in the double diffuse layer
Q_v	Cation concentration per unit volume
C	Cation exchange capacity
G_s	Specific gravity
e_r	Reciprocal error
R_n	Resistance of normal measurements for ERT
R_r	Resistance of reciprocal measurements for ERT

1 Introduction

1.1 Background

A significant portion of the UK transport network is built on engineered slopes. Slope instability can cause serious financial and social problems. In recent years, climate change has been identified as a key factor affecting the stability of engineering infrastructure, including embankments, cuttings and other engineered slopes built with fine-grained soils (Dijkstra and Dixon, 2010). Future climate scenarios predict hotter and drier summers and wetter winters with more intense rainfall in the UK (Kilsby et al., 2009). The changing climate drives seasonal water fluctuations within the soil, which in turn causes changes in pore water pressure (Uchaipichat, 2010). As a consequence, the weather-driven moisture cycling in engineered slopes has been shown to cause a change in the soil water retention behaviour (Hen-Jones et al., 2014; Stirling et al., 2014; Toll et al., 2016) and a deterioration of soil fabric, resulting in a progressive loss in soil suction and shear strength (Stirling et al., 2020). Such soil deterioration accelerates the aging of engineered slopes and many other engineering infrastructures constructed from compacted clays, resulting in more slope failures. However, traditional geotechnical monitoring of slope stability is time-consuming and expensive. It is favourable to characterise geotechnical properties using more convenient and non-invasive geophysical methods (Cosenza et al., 2006) such as the electrical resistivity method, which is closely related to soil's geo-structural properties and water content and therefore considered one of the most suitable methods for monitoring slope stability and landslide risk (Di Maio and Piegari, 2012). The resistivity method can provide soil property information in 3D from the ground surface and is widely used to monitor subsurface moisture and geotechnical property changes (Gunn et al., 2015). For the resistivity method to be used effectively in slope monitoring, the relationships between soil geotechnical and geophysical properties need to be more fully understood.

This study concentrates on investigating the interrelationships between resistivity, water content, pore water pressure and shear strength of engineered soils under drying and wetting cycles. The outcomes of this study are improved understanding of the role of soil deterioration in soil property behaviour under cyclic drying and wetting processes and of

the potential uses of electrical resistivity methods in the monitoring and assessment of slope stability.

1.2 Aims and objectives

The aims of this thesis are to investigate how soil deterioration influences property relationships of engineered soils during successive moisture cycling through laboratory experimentation, and to investigate the potential use of resistivity methods for quantifying the changes in geotechnical properties of engineered soils in association with proxy relationships under drying and wetting cycles at laboratory scale.

In order to achieve the aim, the study has the following objectives:

1) To assess the performance of point sensors in measuring soil water content, suction and resistivity under successive drying and wetting cycles through laboratory experiments and compare with data obtained using other relevant techniques in this study.

2) To investigate soil water retention (SWR) behaviour of engineered soils under cyclic drying and wetting through laboratory experiments using different measurement techniques.

3) To investigate the mechanical behaviour of engineered soils under cyclic drying and wetting using unconsolidated undrained triaxial tests.

4) To investigate the electrical behaviour of engineered soils under cyclic drying and wetting through laboratory experiments using soil samples in different sizes.

5) To compare the interrelationships between soil water content, resistivity, shear strength and suction obtained using different measurement techniques.

6) To establish the soil geotechnical and geophysical property interrelationships in soil samples of different sizes (from a 38-mm triaxial sample to a large lysimeter sample) and to investigate the effect of sample size on soil property behaviour and interrelationships obtained from laboratory experiments.

7) To obtain an improved understanding of soil deterioration driven by the successive

drying and wetting cycles.

8) To observe the development of cracks and determine the resistivity distributions in large diameter lysimeter sample using the electrical resistivity tomography (ERT) method.

9) To evaluate the geotechnical property behaviour of soils under drying and wetting cycles using data derived from ERT methods.

1.3 Scope of the study

As defined in the aims and objectives, the work of this thesis concentrates on investigations of soil interrelationships under multiple drying and wetting cycles and the use of the electrical resistivity methods for soil testing in a laboratory scale. In this study, the interrelationships between soil properties (i.e., water content, suction, undrained shear strength and resistivity) are established for three types of clay soils (i.e., glacial till, London Clay and Hollin Hill clay) through a small-scale laboratory testing programme using 38mm-diameter triaxial specimens. The soil property interrelationships are also investigated with medium-scale (box lysimeter test) and large-scale (large cylindrical lysimeter test) laboratory testing programmes, and ultimately the ERT method is employed to conduct a quantitative assessment of the geotechnical properties of the glacial till in the large lysimeter test. Throughout the comprehensive testing programme, certain limitations to this project can be observed:

- All the testing programmes performed in this study are laboratory-based; field tests have not been considered in this study.

- Given the time limits and design of the testing programme, limited numbers of soil properties were investigated; some other properties that may also be relevant to soil deterioration were overlooked in this study, such as tensile strength, permeability, and stiffness.

- All the soil samples used in this study were clay materials and were remoulded to remove large particles and control the as-compacted conditions. These remoulded samples are more homogeneous than the original undisturbed soil sample from the field and therefore their property behaviour may not be completely

representative of field conditions.

- The unconsolidated undrained (UU) triaxial test used for unsaturated samples in this study is normally conducted on saturated samples to assess short-term stability related to a sudden failure in soils (Wood, 1990). This test was chosen because it provides rapid measurements of clay's undrained shear strength. However, the shear strength measured using UU triaxial test on unsaturated soil samples is not a "true" undrained shear strength, but the results are still representative of the shot-term maximum shear resistance of soil under an undrained condition.

1.4 Thesis structure

This PhD thesis is divided into five chapters. An introduction of the overall project is presented in Chapter 1.

Chapter 2 starts with a brief review on unsaturated soil mechanics, which is relevant to soil water retention behaviour, followed by a review of recent laboratory techniques for the determination of soil properties relevant to this thesis. At the end of Chapter 2, relevant research on the applications of resistivity methods is reviewed.

Chapter 3 presents a brief introduction to the three laboratory testing programmes and describes all the methodologies used in this study.

Chapter 4 presents the results of the three laboratory testing programmes in this study along with brief discussions for each through individual subchapters.

Chapter 5 provides a comprehensive discussion of and conclusions for the study together with recommendations for future work.

2 Literature review

2.1 Introduction

The literature review of this thesis forms the background information about the PhD project. The review introduces the definition of unsaturated soil, the different phases and properties of unsaturated soils from the saturated soils. Since soil water content plays an important role in the behaviour of unsaturated soil, the significance of monitoring soil water content and the potential effects from climate change are reviewed. In recent decades, a wide range of techniques has been developed to provide water content measurement. The principles, advantages and disadvantages for these popular water content measurement methods are reviewed. The soil water retention behaviour which is a main factor of unsaturated soil and is essential for understanding the mechanical behaviour of unsaturated soil is reviewed. In addition, the fundamental knowledge and applications of electrical resistivity methods for estimating the soil water content is presented. From the reviews, the fundamental and basic knowledge for the subsequent works in this thesis is established.

2.2 Unsaturated soils

Classical soil mechanics has led to an emphasis on specific type of soils, i.e. the saturated soils. However, any natural soils near the ground surface can be partially saturated with water, which results in materials having more than two phases, differing from the saturated soils which only have two phases (Fredlund and Rahardjo, 1993). An unsaturated soil is commonly defined as the soil consisting of three phases, i.e. the solid, the water and the air. However, Fredlund and Morgenstern (1977) suggested that there is a fourth phase for unsaturated soils, namely, the air-water interface due to its unique character.

In engineering practice, unsaturated soils are widely spread in most of the shallow earth structures, e.g. the engineered slopes, road embankments, dams, railways. More and more attention has been given to unsaturated soils due to their different nature and engineering behaviour that compared with the saturated soils. The most important factor of an

unsaturated soil that differs from the saturated soil is that their pore-water pressure is relatively negative to the pore-air pressure (Fredlund and Rahardjo, 1993).

2.2.1 Stress state variables for unsaturated soils

The mechanical behaviour of a soil can be described associated with the stress state variables. The stress state variable for a saturated soil has been defined as the effective stress by Terzaghi (1943). However, the stress state variables for unsaturated soils are more complex due to the three-phase system.

Since the 1950's, more and more researchers have attempted to extend the effective stress concept to unsaturated soils. Croney et al. (1958) proposed a form of effective stress equation for unsaturated soil in terms of the total normal stress, σ and the pore-water pressure, u_w:

$$\sigma' = \sigma - \beta' u_w \tag{2.1}$$

Where σ′ = effective normal stress, σ = total normal stress, β′ = a factor of holding or bonding and u_w = pore-water pressure.

Aitchison (1961) and Jennings (1961) proposed their effective stress equation for unsaturated soil in the expression of the same form:

$$\sigma' = \sigma + \psi p'' \tag{2.2}$$

Where, ψ is a parameter, and p″ is pore-water pressure deficiency defined by Aitchison, and the absolute value of pore-water pressure defined by Jennings.

Bishop (1959) was the first to propose the effective stress equation in terms of both pore-water pressure and pore-air pressure, expressed as:

$$\sigma' = (\sigma - u_a) + \chi(u_a - u_w) \tag{2.3}$$

Where, u_a is the pore air pressure, and χ is a factor varies between 0 and 1, related to the degree of saturation of the soil.

Jennings and Burland (1962) pointed out that the proposed effective stress equations did not fully describe the relationship between volume change and effective stress for most unsaturated soils below a critical degree of saturation, pointing out the difficulties of using any single stress state variable to explain unsaturated soil behaviour. The importance of

considering the stress state variables separately while dealing with the change from volume and shearing of partially saturated soil was emphasized.

Fredlund and Morgenstern (1977) suggested to use the combination of any two of three possible normal stress variables as the independent stress state variables to describe unsaturated soil behaviour. These are: 1) net normal stress, $(\sigma - u_a)$, 2) matric suction, $(u_a - u_w)$, and 3) effective normal stress, $(\sigma - u_w)$. The use of independent stress state variables solved the philosophical difficulty in finding a single-valued effective stress equation that is matching both the shear strength behaviour and the volume change behaviour of unsaturated soils. The independent stress state variables can then be applied to establish the constitutive equations to describe the shear strength and volume change behaviour of unsaturated soils. This approach has provided a more meaningful description of unsaturated soil behaviour and has been experimentally examined by Fredlund (1973).

2.2.2 Soil suction

2.2.2.1 Total suction

Soil suction is commonly defined in terms of the free energy state or relative vapour pressure of soil moisture, which can be determined from its partial vapour pressure (Edlefsen and Anderson, 1943). Sposito (1981) suggested that total suction could be described by Kelvin's equation from a thermodynamic standpoint, which expressed as:

$$\psi = -\frac{RT}{v_{w0}\omega_v}\ln\left(\frac{u_v}{u_{v0}}\right) \tag{2.4}$$

Where:

ψ = total suction (kPa);

R = universal gas constant ($m^3.Pa.K^{-1}.mol^{-1}$);

T = absolute temperature (K);

v_{w0} = specific volume of water ($m^3.kg^{-1}$);

ω_v = molecular mass of water vapour ($kg.mol^{-1}$);

u_v/u_{v0} = relative humidity (RH)

u_v = partial pressure of water vapour (kPa);

u_{v0} = saturation pressure of water vapour over a flat surface of pure water at same temperature (kPa).

The total soil suction, ψ consists of two components, metric suction $(u_a - u_w)$ and osmotic suction (π), i.e.

$$\psi = (u_a - u_w) + \pi \tag{2.5}$$

2.2.2.2 Matric suction

Matric suction is caused by capillary phenomenon due to the presence of surface tension at the curved air-water interfaces (meniscus) within the soil pores. Therefore, the matric suction is the difference between the pore air pressure (u_a) and pore water pressure (u_w) across the air-water interface. The matric suction decreases while the radius of curvature of the meniscus increases (Fredlund and Rahardjo, 1993). Thus, the matric suction is affected by the soil particle size distribution as the pore sizes of soil changes with the change in soil particle size which then affecting on the curvature radius of the meniscus and consequently the matric suction. The matric suction of soil is also controlled by soil water content where the matric suction of soil increases with an decrease in soil water content (Fredlund, 2006).

2.2.2.3 Osmotic suction

Osmotic suction is the osmotic potential produced by salts dissolved in the pore fluid, which also contributing to the total suction. Generally, the contribution of osmotic suction to a total suction is much less than it from matric suction in most engineering problems. Therefore, the osmotic suction is less important than matric suction (Fredlund and Rahardjo, 1993).

2.2.3 Soil water retention curves (SWRCs)

The soil water retention curve of an unsaturated soil is defined as the relationship between the amount of water and the suction present in a soil (Williams, 1982), and can be used

to estimate the soil parameters required for describing unsaturated soil behaviour. The amount of water in the soil can be expressed in various forms as: (1) the gravimetric water content, w, which is the ratio of water mass to the solid mass in a soil; (2) the volumetric water content, θ, which is the ratio of water volume to the total volume of soil; and (3) the degree of saturation, S_r, which is the proportion of voids in a soil that are filled with water. The volumetric water content is the most commonly used indicator for water content in the soil science (Fredlund and Xing, 1994).

2.2.3.1 Typical plot of SWRCs

The typical soil water retention curves along the desorption paths for a sandy soil, a silty soil and a clayey soil are shown in Figure 2.1, indicating that the shape of a soil water retention curve is nonlinear and dependent on the soil type. The differences between the SWRCs for the three types of soil illustrate that the saturated water content and the air-entry value are affected by the soil plasticity (Fredlund and Xing, 1994). Croney et al. (1958) pointed out that the SWRC is "primarily dependent upon the particle size distribution of the soil and the structure". Additionally, the key properties of SWRC are also related to the pore connectivity, shape and angularity of soil that are governed by the soil type, density and structure (Or and Tuller, 1999).

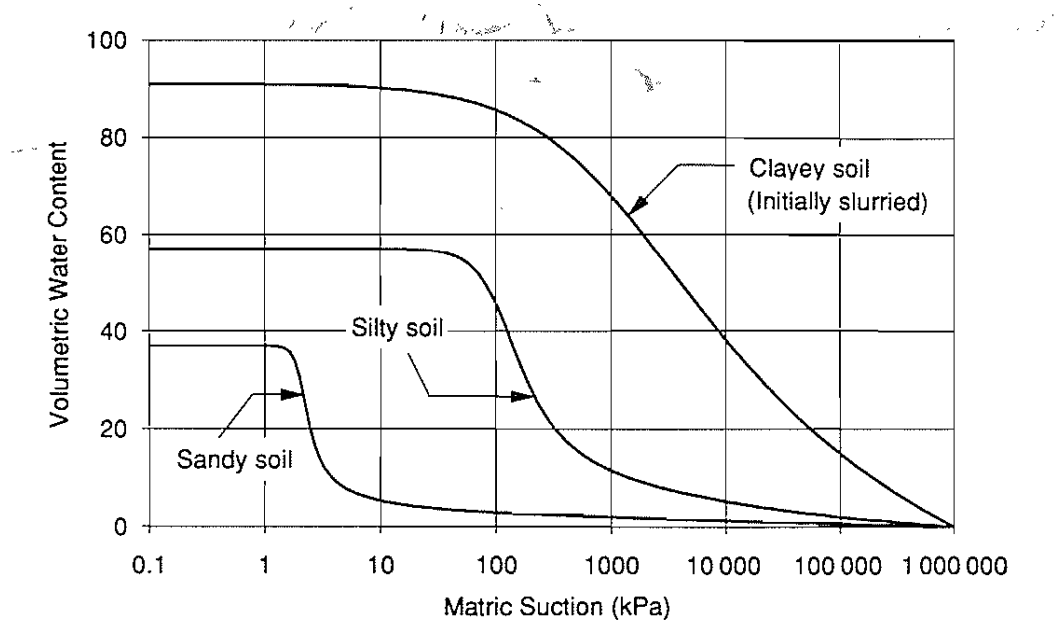

Figure 2.1 Typical soil water retention curves for different soils (Fredlund and Xing, 1994).

Figure 2.2 shows a typical SWRC plotted with the volumetric water content of soil along both the desorption (drying) and adsorption (wetting) curves. A number of soil parameters can be obtained from the SWRCs: the saturated volumetric water content,θ_s which is the volumetric water content of a soil at fully saturation; the air-entry value (AEV) of the soil, which is the matric suction at where the soil starts desaturation (i.e. air starts to enter the largest pores of soil); and the residual water content θ_r, which indicates the water content after where the significant increase in suction is required to remove the remaining amount of water within the soil. Klute (1986) pointed out that there might be a gap between the end point of the wetting path and initial point of the drying path due to the entrapped air in the soil.

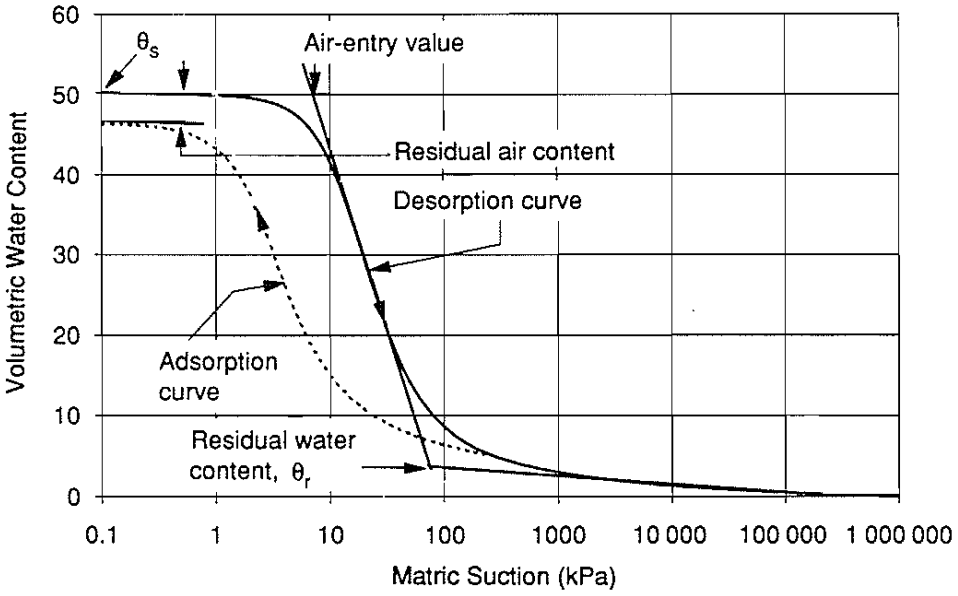

Figure 2.2 Characters of drying and wetting soil water retention curves (Fredlund and Xing, 1994).

2.2.3.2 Hysteresis of the SWRCs

Typically, the soil has different water retention behaviour on the drying and the wetting paths due to hysteresis (Haines, 1927; Croney, 1952; Mualem, 1984). Generally, the suction value of a soil on the drying path is higher than that on the wetting path, at a given water content (Figure 2.3a). The hysteretic behaviour of SWRC has been explained as a result of several mechanisms: (1) the 'ink bottle' effect that results from the heterogeneities in the pore size and shape of the connective pores in the soil, while the drying process is governed by the radius of the 'bottlenecks', *r* and the re-wetting is governed by the radius of widest part of pores, *R* (Figure 2.3c); (2) different contact angles between water and soil particle for advancing and reducing water menisci during

adsorption and desorption (Figure 2.3b); (3) the effect of entrapped air due to incomplete saturation during the wetting process; (4) volumetric changes of unsaturated soils due to swelling and shrinking behaviour of soil that is subjected to drying and wetting (Tuller and Or, 2004).

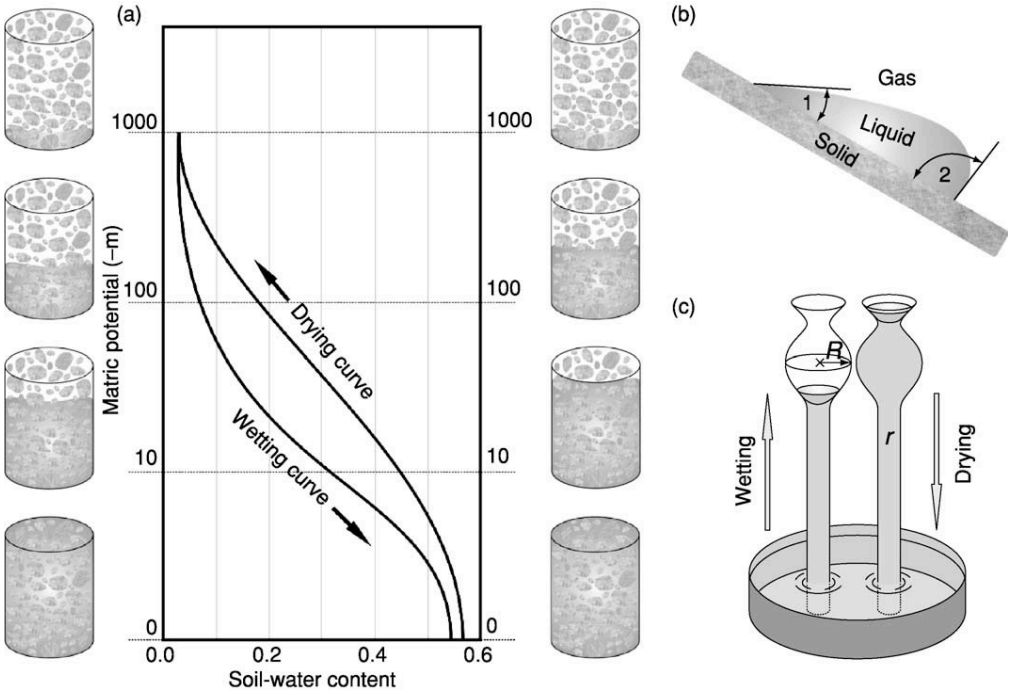

Figure 2.3 (a) Hysteretic behaviour in the SWRC. (b) The effect of contact angle and (c) The ink-bottle effect (Tuller and Or, 2004)

2.2.3.3 Equations for the soil water retention curve

In resent few decades, considerable efforts have been made to formulate the mathematical equations to describe the soil water retention behaviour of unsaturated soils. In a soil water retention curve equation, the normalized water content, Θ is a dimensionless value used to indicate the quantity of water contained in the soil, which is defined as:

$$\Theta = \frac{\theta - \theta_r}{\theta_s - \theta_r} \tag{2.6}$$

Where:

θ = volumetric water content of soil at any suction.

θ_s = volumetric water content of soil at saturation.

θ_r = residual volumetric water content of soil.

Brooks and Corey (1964) proposed the earliest SWRC equation in a form of the power relationship. The equation was proposed for describing the desaturation of the agricultural soils when the soil suction was greater than the air entry value:

$$\Theta = (\frac{\psi_b}{\psi})^{\lambda} \tag{2.7}$$

where:

ψ_b = the air entry value of the soil.

ψ = suction of soil at any water content.

λ = the pore size distribution index.

The materials tested in this study consisted of the sands, the glass beads, the fragmented mixture (clay and sand) and the silt loam, which had relatively stable structure. The equation has been proved valid for the suctions between the air entry value and residual conditions (Campbell, 1974; Clapp and Hornberger, 1978; Williams et al., 1983).

Williams et al. (1983) suggested a linear relationship between the logarithms of suction and the logarithms of water content to characterise the soil water retention behaviour of eight groups of soils (primarily sandy and clayey soils) from the Australian Great Soil Groups:

$$\ln \Theta = a_1 + b_1 \ln \psi \tag{2.8}$$

Where a_1 and b_1 are two fitting parameters for the curvature of the SWRC.

McKee and Bumb (1984) proposed an exponential relationship for the normalized water content and the soil suction referring to the Boltzmann distribution in order to describe the soil water retention curve for coal media:

$$\Theta = e^{-(\psi - a_2)/b_2} \tag{2.9}$$

Where a_2 and b_2 are curve-fitting parameters for the SWRC.

Equations (2.7) and (2.9) have been verified to be fitted to the SWR data when the soil suction values are greater than the air entry value, whereas they are not valid for the data

under the air entry value or after a residual condition. In order to maintain the validity of function in the whole suction range, McKee and Bumb (1987) modified their equation based on the Fermi distribution, which is given by:

$$\Theta = \frac{1}{1 + e^{(\psi - a_2)/b_2}} \tag{2.10}$$

The validity of the modified equation has been improved in the low suction range, while the equation is still not valid for the suction in the residual range.

A commonly used SWRC model was given by van Genuchten (1980), which is expressed as:

$$\Theta = \left[\frac{1}{1 + (\alpha\psi)^n}\right]^m \tag{2.11}$$

where:

α = fitting parameter primarily related to inverse of air-entry value.

n = fitting parameter related to the rate of water extraction from soil once the air entry value has been reached.

m = fitting parameter related to the residual water content.

Fredlund and Xing (1994) pointed out that the expression of the Van Genuchten model gives more flexibility to the water retention curve than the previous equations. However, the fixed relationship between parameter m and n (i.e., $m = 1 - 1/n$) reduces the flexibility. They modified the pore-size distribution function proposed by van Genuchten (1980) and introduced a correction factor $C_{(\psi)}$ into their equation, which is written as:

$$\Theta = C_{(\psi)} \left\{\frac{1}{\ln[e + (\psi/a)^n]}\right\}^m \tag{2.12}$$

Where a is a fitting parameter for the SWRC and the correction factor $C_{(\psi)}$ is defined as:

$$C_{(\psi)} = 1 - \frac{\ln(1 + \psi/\psi_r)}{\ln(1 + 1000000/\psi_r)} \tag{2.13}$$

Where ψ_r = the residual suction of soil at the residual water content. The value of 1000000 kPa is the maximum suction value of a soil at a water content approaching to zero from the experimental data (Croney and Coleman, 1961; Koorevaar et al., 1983). The Fredlund and Xing (1994) equation produces more flexible fitting curve to the experimental data than the van Genuchten (1980) equation as it unlinks the fixed relationship between *m* and *n* parameters. Numerous equations have been proposed over the years for describing the soil water retention curve. Most of the equations perform well for the particular soil types or in the limited suction ranges. Leong and Rahardjo (1997) evaluated the popular used SWRC equations and concluded that the equation proposed by Fredlund and Xing (1994) provided the best fit for various types of soil over the entire suction range from zero to 10^6 kPa.

Experimental studies have shown that the SWRC is a crucial tool for determining the particular geotechnical properties of unsaturated soils (Fredlund and Rahardjo, 1993). In geotechnical engineering practice, the permeability of an unsaturated soil can be estimated by using the SWRC and the saturated permeability coefficient of the soil (van Genuchten, 1980; Mualem, 1986; Fredlund and Xing, 1994). The SWRC has also been used for predicting the shear strength function of unsaturated soils (Fredlund et al., 1996; Vanapalli et al., 1996; Khalili and Khabbaz, 1998).

2.3 Suction measurement techniques

Numerous techniques have been developed to estimate the suction of soils, including pressure plate, filter paper, high-suction probe, transistor psychrometer, chilled mirror technique and so on. The detailed reference for the various suction measurement methods can be found in a list of literatures: (Fredlund and Rahardjo, 1993), Lee and Wray (1995), Rahardjo and Leong (2006) and Delage et al. (2008) among others. Only the techniques that are most commonly used and those which are related to this thesis are presented in this sub-chapter.

2.3.1 Pressure plate

The axis translation technique is the most commonly used technique for controlling and measuring soil matric suction. The pressure plate method uses the axis translation

technique to impose matric suction to the soil sample by controlling both the pore-air and pore-water pressure (Richards, 1941; Gardner, 1956).

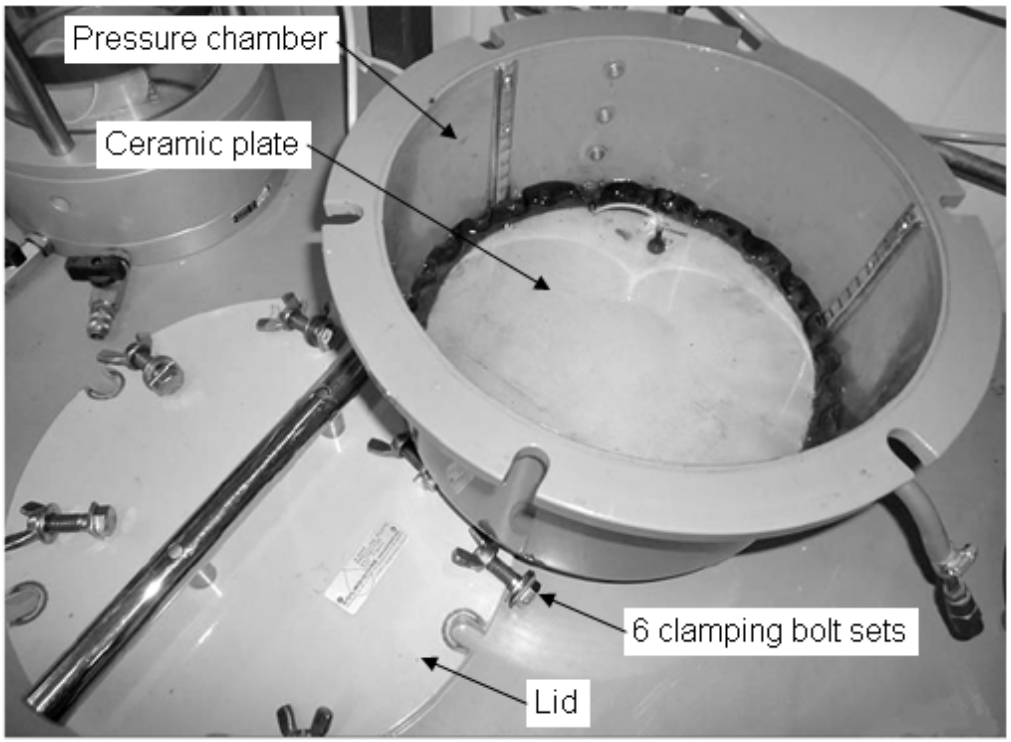

Figure 2.4 Pressure plate apparatus (Mendes, 2011)

The pressure plate apparatus normally consists of a pressure chamber and a saturated high air entry value (HAEV) porous ceramic disc (see in Figure 2.4). The soil sample is placed in good contact with the ceramic disc to allow the water flow. Once the pressure chamber is sealed, the water pressure is maintained at atmospheric or close to a zero value and the pore-air pressure is artificially increased of the atmospheric pressure to a reference value. Once the desired pore water and pore air pressure are achieved, the soil sample is left for equilibrium. Water is flow out from the soil sample through the HAEV ceramic disc during equilibrium and the amount of water expelled from soil can be measured to determine the water content that remains in the sample. Once the equilibrium of water flow achieved, the suction can be determined as the difference of pore-air and pore-water pressure (i.e., $u_a - u_w$). The process is repeated at different air pressure to impose different suction value, to establish the SWRC.

Cavitation is avoided by using an axis translation technique since the pore-air and pore-water pressure are maintained as positive values. However, the measurement range of this

technique is limited by the air-entry value of the porous stone (commonly 1500 kPa) and the maximum air pressure that can be allied in the pressure chamber.

2.3.2 Chilled-mirror technique

A chilled-mirror psychrometer measures the total suction of soil sample by determining the relative humidity using the chilled-mirror dew point technique. The most frequently used chilled-mirror device in the geotechnical engineering applications is known as the WP4 dewpoint potentiameter manufactured by Decagon Devices, Inc., as shown schematically in Figure 2.5. The soil sample fills about half the depth of a small container and is placed in the device under isothermal conditions in a sealed chamber. The measurement of total suction using the chilled-mirror device is based on the equilibrium between the water potential in the soil sample and the vapour potential in the air space above the soil sample in the sealed chamber. The closed chamber contains a mirror of which the temperature is precisely controlled by a thermoelectric cooler. An optical sensor is used to detect the exact point at which the condensation of the vapour first occurs on the mirror and the temperature at which condensation appears, referred to as a dewpoint, is recorded by the thermocouple attached to the mirror. The temperature of the soil specimen which is considered to be the same with the vapour temperature in the headspace is measured by an infrared thermometer. The relative humidity of the specimen is then computed from the dewpoint and the sample temperature. As the chilled-mirror psychrometer measures the relative humidity in terms of the dewpoint temperature, the temperature control is crucial. The temperature difference between the sample and the chamber should be small. An internal fan is employed to circulates the headspace to accelerate the equilibrium (Bulut and Leong, 2008).

The limitation of chilled-mirror dewpoint technique for low suction ranges (suctions less than 1000 kPa) is widely recognized. Bulut et al. (2002) tested the accuracy of WP4 instrument in total suction measurement by developing a characteristic curve on the relationship between the osmotic suction and the salt solution concentration and found that the readings scattered a lot once the osmotic suction falls below about 1000 kPa. Leong et al. (2003) compared the total suction measured by the WP4 device and the sum of the matric and osmotic suctions measured using the axis-translation method and pore fluid squeeze technique individually and found that the total suction measured by the

chilled-mirror technique is always higher than the sum of the matric suction and osmotic suction measured by other two techniques.

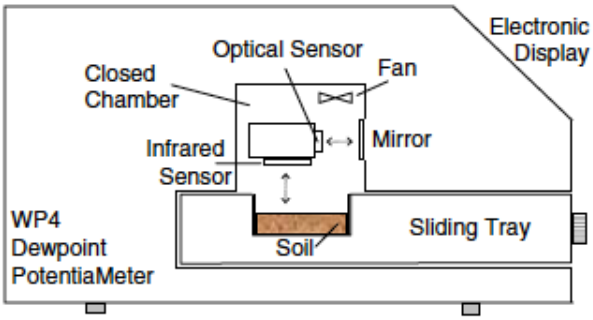

Figure 2.5 Diagram of the WP4 Dewpoint PotentiaMeter (Bulut and Leong, 2008)

2.3.3 High capacity tensiometer

Since the first high-capacity tensiometer developed by Ridley and Burland (1993) at Imperial College London, a number of devices have been developed by numerous authors using the same concept. Delage et al. (2008) provides a detailed review of the high suction tensiometers developed to date, as presented in Table 2.1.

Table 2.1 The proposed high-capacity tensiometers to date

Source	AEV of porous stone (MPa)	Pressure transducer measurement range (MPa)	Max positive pressure (MPa)	Max water tension (MPa)
Ridley and Burland (1993)	1.5	3.5	6	1.37
Ridley and Burland (1995)	0.5	4	4	0.74
	1.5	4	4	1.8
Guan and Fredlund (1997)	1.5	1.5	12	1.25
Meilani et al. (2002)	0.5	1.5	0.8	0.495
Tarantino and Mongiovì (2002)	1.5	4	4	2.06
Take and Bolton (2003)	0.3	1.5	1	0.53
Chiu et al. (2005)	0.5	1.5	0.7	0.47
Lourenço et al. (2006)	1.5	2	1	1.23
Mahler and Diene (2007)	0.5	0.5	0.6	0.8
	1.5	1.5	0.6	1.4

The main specifications of the tensiometers are summarized in Table 2.1. A high capacity tensiometer normally comprises a porous stone, a water reservoir and a ceramic force transducer or a strain gauge, which are enclosed in a metal housing (Figure 2.6). When the porous stone and the water reservoir are fully saturated, the pressure transducer of the

tensiometer measures at zero suction. When the tensiometer is in contact with a soil sample with a certain value of suction, the water in the tensiometer starts to be drawn towards the soil until an equilibrium is reached. The response of the pressure transducer is referred to the matric suction of the soil sample. The high suction tensiometers can be classified based on the air entry value of the porous stone or the form of construction. Nearly half of the tensiometers in Table 1 operate at the high suction range (up to 2000 kPa) while the remaining ones operate at lower suctions (up to 500 kPa).

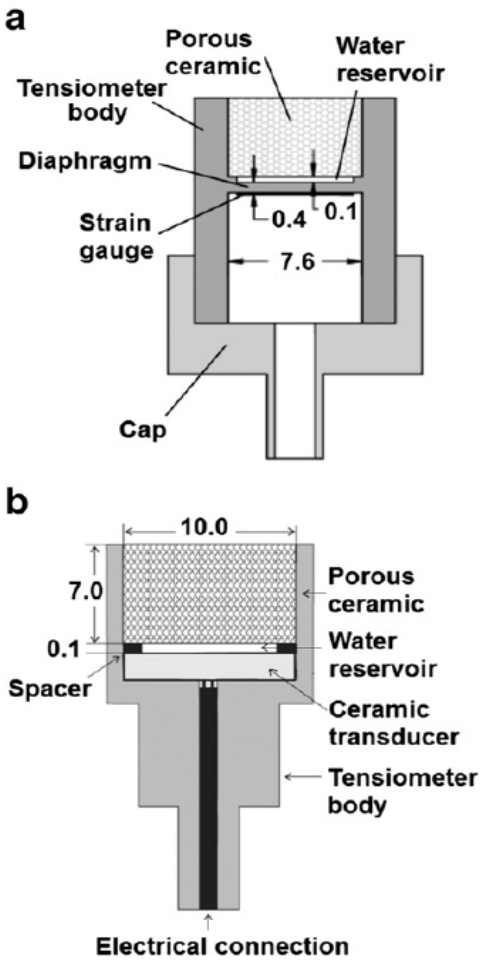

Figure 2.6 Two tensiometer designs (a) Tarantino and Mongiovi (2003); (b) Lourenço et al. (2006)

The construction of tensiometers varies in the air entry value and material of the porous stone, the size of water reservoir and the pressure transducer. Figure 2.6 shows examples of two designs: a tensiometer with a strain gauge attached on the diaphragm reported by Tarantino and Mongiovi (2003) and a tensiometer developed by Lourenço et al. (2006) in Durham university using a ceramic transducer. Low cost tensiometers have been

developed by Mahler and Diene (2007), using an acrylic body instead of the usual stainless steel.

2.3.3.1 Saturation

A good performance of a high capacity tensiometer relies on sufficient saturation to remove free air from the high air entry value (HAEV) ceramic plate and water reservoir, preventing cavitation at high suction. Cavitation in a tensiometer was the formation of vapour cavities in the water because of increasing tension induced by the negative pore water pressure to which the tensiometer was exposed. Furthermore, saturation is a process to remove the air within the ceramic stone and water reservoir of the tensiometer and refill the spaces with de-aired water.

2.3.3.2 Calibration

Once the tensiometer had been fully saturated from the saturation system, it needs to be calibrated before use. The calibration is carried out in the positive range and extrapolated to the negative range (Lourenço, 2008).

2.3.3.3 Advantages and disadvantages

As the tensiometer measures the matric suction directly, in both positive range and negative range, some errors related to indirect calibrations can be avoided (Toll et al., 2013). The small size of the tensiometer allows it to be properly used in both small-scale laboratory tests and the field experiments. With a good saturation and calibration process, tensiometers can provide reliable and accurate, and fast suction measurements.

The main disadvantages of using tensiometers are cavitation and drift in the calibration curve. The measurement range of the tensiometers is restricted by the air entry value of the porous stone and the working range of the pressure transducers be used. The drift in calibration curves of tensiometer is normally observed on tensiometers which have worked under negative pressures for a long period. This may cause some measurement errors in the low suction range. It is also important that the saturation process is time consuming for a tensiometer which is newly used or cavitated. Tarantino and Mongiovì (2001) found that the cyclic pressurisation and cavitation process can help to remove the air more completely from the tensiometer and reduce the time needed for saturation.

In previous studies, the SWRCs at low suction range (i.e. less than 1500 kPa) were usually obtained by techniques that measures matric suction, such as the axis translation technique (Fredlund and Morgenstern, 1977; Tarantino et al., 2000) and high capacity tensiometer technique (Ridley and Burland, 1993; Ridley and Burland, 1995; Tarantino and Mongiovì, 2001; Lourenço et al., 2006; Mendes, 2011; Toll et al., 2013). In the high suction range (i.e. greater than 1500 kPa), techniques that measures total suction are mainly used, such as the psychrometer technique (Campbell and Gardner, 1971; Rawlins and Campbell, 1986; Woodburn et al., 1993; Ridley and Wray, 1996) and chilled-mirror hygrometer (Gee et al., 1992; Leong et al., 2003; Tang and Cui, 2005; Agus and Schanz, 2006).however, there is no available technique for measuring soil matric suction over the entire moisture range (Delage et al., 2008; Pan et al., 2010). Most studies regarding the drying and wetting SWRCs for fine-grained soils have been carried out at the low suction range with limited studies performed on the high suction range (Agus and Schanz, 2006; Al-Mahbashi et al., 2018).

2.4 Shear strength of unsaturated soils

2.4.1 Shear strength equations

The shear strength of a soil plays a very important role in numerous engineering practices such as: the prediction and analysis of slope stability and the geotechnical designs. The conventional shear strength equation for saturated soils is based on the Mohr-Coulomb theory (Mohr, 1900) using the effective stress variable proposed by Terzaghi (1943), which is given as:

$$\tau = c' + (\sigma - \mu_w) \tan \phi' \qquad (2.14)$$

where:

τ = shear strength of soil

c' = the effective cohesion

$(\sigma - \mu_w)$ = effective stress of saturated soil

ϕ' = effective internal friction angle of saturated soil

Bishop (1959) extended the effective stress principle and proposed a shear strength equation for unsaturated soils:

$$\tau = c' + [(\sigma - u_a) + \chi(u_a - u_w)] \tan \phi' \quad (2.15)$$

where:

$(\sigma - u_a)$ = net normal stress of unsaturated soil

$(u_a - u_w)$ = matric suction of unsaturated soil

ϕ' = effective internal friction of soil at saturation

In 1960's, numerous of researchers (Jennings and Burland, 1962; Bishop and Blight, 1963; Matyas and Radhakrishna, 1968) realized that it is unsuitable and difficult to use a single stress state variable to describe unsaturated soil behaviour. Fredlund and Morgenstern (1977) suggested to use any two of the three stress state variables, i.e., $(\sigma - u_a)$, $(\sigma - u_w)$, and $(u_a - u_w)$ to describe the shear strength of unsaturated soils. A shear strength equation using $(\sigma - u_a)$ and $(u_a - u_w)$ as two independent stress state variables was proposed by Fredlund et al. (1978):

$$\tau = c' + (\sigma - u_a) \tan \phi^a + (u_a - u_w) \tan \phi^b \quad (2.16)$$

where ϕ^a is the angle of friction for changes in net normal stress, $(\sigma - u_a)$ and ϕ^b is the angle of friction for changes in matric suction, $(u_a - u_w)$.

In this equation, ϕ^a was assumed to be a constant value which is equal to the effective friction angle at saturation, ϕ'. In addition, ϕ^b was also assumed to be a constant value, which means that the Fredlund et al. (1978) equation assumed the shear strength to be a linear function of the matric suction. However, later studies showed that ϕ^a was not always be constant with changing matric suction (Delage, 1987; Toll, 1990; Toll and Ong, 2003) and ϕ^b was also varied as a function of matric suction (Escario and S´ez, 1987; Fredlund et al., 1987; Vanapalli et al., 1996; Toll and Ong, 2003).

Various shear strength equations have been proposed for predicting the shear strength of unsaturated soils. Guan et al. (2009) concluded the published equations for shear strength prediction of unsaturated soils as shown in Table 2.2.

Table 2.2 proposed shear strength equations for unsaturated soil (Guan et al., 2009)

Authors	Nature	Shear strength equations	Types of soil for the test data	Limits for the test data
Fredlund et al. (1978)	Fitting	$\tau = c' + (\sigma - u_a)\tan\phi^a + (u_a - u_w)\tan\phi^b$ (2.17)	Compacted sale, Boulder clay, Potters Flint and Peerless Clay	The test data is in a suction range less than 150 kPa
Vanapalli et al. (1996)	Prediction	$\tau = c' + (\sigma - u_a)\tan\phi' + (u_a - u_w)\left[\tan\phi'\left(\frac{\theta_w - \theta_r}{\theta_s - \theta_r}\right)\right]$ (2.18)	Fifteen types of soil published in literature (Vanapalli et al., 1996)	To predict the measured shear strength in the range of 0-200 kPa
Fredlund et al. (1996)	Fitting	$\tau = c' + (\sigma - u_a)\tan\phi' + [(u_a - u_w)\Theta^{\kappa}]\tan\phi'$ (2.19)	Decomposed tuff soil from Hong Kong	An additional soil parameter, κ is introduced
Öberg and Sällfors (1997)	Prediction	$\tau = c' + (\sigma - u_a)\tan\phi' + (u_a - u_w)\left[\tan\phi'(S)\right]$ (2.20)	Silts and sands	The equation uses degree of saturation *S* as an additional parameter dependent on SWCC
Bao et al. (1998)	Prediction	$\tau = c' + (\sigma - u_a)\tan\phi' + (u_a - u_w)(\zeta)\left(\tan\phi'\right)$ (2.21) $\zeta = \frac{\log(u_a - u_w)_r - \log(u_a - u_w)}{\log(u_a - u_w)_r - \log(u_a - u_w)_b}$	Nanyang Clay	The matric suction is in a range of 0-300 kPa
Khalili and Khabbaz (1998)	Prediction	$\tau = c' + (\sigma - u_a)\tan\phi' + (u_a - u_w)(\lambda')\left(\tan\phi'\right)$ (2.22) $\lambda' = \left\{\frac{(u_a - u_w)}{(u_a - u_w)_b}\right\}^{-0.55}$	Compacted Kaolin and Sand-Clay mixture	The matric suction is in the range 50-700kPa for Kaolin and 50-450 kPa for the Sand-Clay mixture
Tekinsoy et al. (2004)	Prediction	$\tau = c' + (\sigma - u_a)\tan\phi' + \tan\phi'(\psi_e + P_{at})\ln\left[\frac{\psi + P_{at}}{P_{at}}\right]$ (2.23)	Nanyang expansive soil, Glacial till, Notch Hill silt, Dhanauri clay	The matric suctions of the test data are all in a range of 0-500 kPa
Garven and Vanapalli (2006)	Prediction	$\tau = c' + (\sigma - u_a)\tan\phi' + [(u_a - u_w)\Theta^{\kappa}]\tan\phi'$ (2.24) $\kappa = -0.0016{I_p}^2 + 0.0975I_p + 1$	Twenty types of soil in literature (Garven and Vanapalli, 2006)	The matric suction is over a range from 0 to 1500kPa or lower based on the test data

All the shear strength equations for unsaturated soils were proposed in linear or non-linear approximations and were intended to describe the suction-induced shear strength in different approaches. A non-linear model is more realistic and suitable to predict the shear strength of unsaturated soils. The equations are all based on two frameworks: Bishop stress framework which is related to a part of the elastoplastic constitutive model and the Fredlund independent stress framework which is related to the soil water retention curve. Garven and Vanapalli (2006) evaluated six empirical equations using the shear strength data of twenty soils published and found that there was no single prediction equation that was suitable for all soil types. However, there is no doubt according to the literature that the prediction of shear strength of unsaturated soils significantly depends on the soil water retention curve. In other words, the shear strength is closely related to the matric suction for unsaturated soils.

2.4.2 Triaxial test for determining soil shear strength

One of the most common used methods to determine the soil shear strength in the laboratory is the triaxial test, of which the testing procedures are described in BS 1377-7: 1990 and BS 1377-8: 1990 (BSI, 1990d; BSI, 1990e).

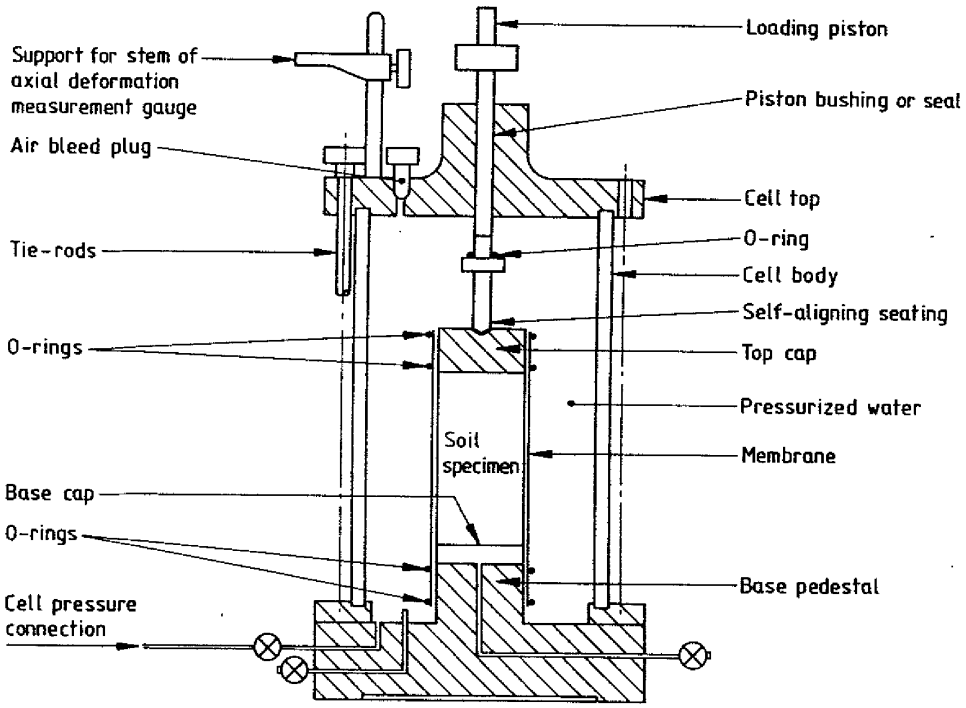

Figure 2.7 Typical apparatus of triaxial test (BSI, 1990d)

2.5 Climate change projections and its impact on engineered slopes

Climate change projections have suggested that in the further the UK will suffer more extreme weather (i.e., warmer, drier summers and wetter, milder winters with more intense rainfall invents) (CCRA, 2012; Watts et al., 2015). There is a great concern of how these projected changes in climate will affect the stability of the earth structures as the climatic changes are in close relation to the precipitation extremes that may contribute to the occurrence of landslides and slope failures (Huggel et al., 2012). In this subchapter, the background of climate change and the effects of a changing climate on the stability of engineered slope are reviewed.

2.5.1 Background

"Most of the warming observed over the last 50 years is likely to be attributable to human activities", stated by IPCC (the Inter-governmental Panel on Climate Change). A study of IPCC (2001) demonstrated that, since the industrial revolution, Carbon dioxide levels in the atmosphere have risen by over 30 percent in the world scale. Over the 21th century, the temperature of world is projected to rise by 0.3-1.7^{o}C under the lowest emission scenarios, and 2.6-4.8^{o}C for the highest emission scenarios (IPCC, 2014). The future climate has been predicted to be the mode of hotter drier summer and wetter winter with more intense rainfall (Jenkins and Lowe, 2003). Loveridge, et al. (2010) indicated that UK should suffer a drier summer by up to 10% -25%, and a 10% - 20% wetter winter in the year 2050. Similarly, the future scenarios utilised in BIONICS (Biological and Engineering Impacts of Climate Change on Slopes) project showed that climatic issue is likely to generate wetter winters in the north and west of UK and warmer summer particularly in the southeast, then produce much drier soils (Kilsby et al., 2009). Since the predicted climatic changes in temperature and precipitation are in close relation to the groundwater and pore-pressure fluctuations, a series of studies were set up to investigate the impacts of changing climate on the slope stability (Dehn et al., 2000). For example, Schmidt and Dikau (2004) established a GCM's (General Circulation Models) to predict the potential effect of climate change upon slope stability in UK. It is of great significance to understand the long-term effects of changing climate on the engineered soils and therefore the stability of engineered slopes.

2.5.2 Climate effects on slopes

Climate change has already been specified as an important natural change that has potential impact on engineering properties of engineered slope materials (Kilsby et al., 2009). Although the actual climate impact on the engineered infrastructures is still not fully investigated, the projected future climate scenarios have already shown the potential that the climate change will affect the precipitation and temperature and subsequently the soil water content and the mechanical behaviour of unsaturated soils (Schmidt and Dikau, 2004). The future climate scenario of drier summer and wetter winter is likely to contribute to the deformation in clay materials. Additionally, heavy precipitation and summer storm events are likely to induce the development of desiccation crack that contributing forward reduction of effective stress and other geotechnical parameters. "These changes subsequently lead to a degradation of engineered slope materials and have serious impact on slope stability" (Dijkstra and Dixon, 2010). There is sufficient literature evidence that increases in temperature and rainfall caused by climate change have an influence on the performance of engineered slopes. The increase in temperature and rainfall is likely to cause fluctuation of water content, and subsequently the crack development (Clarke and Smethurst, 2010). A key consequence resulting from the climatic change is deterioration in strength and pore water pressure of slope material due to continuous shrinking–swelling cycles and surface cracking (Kilsby et al., 2009). Previous studies have demonstrated that the engineered embankments failed by sliding many years after construction with reduced shear strength in the field much smaller than the estimated values determined from laboratory tests on compacted samples (Rogers and Wright, 1986; Glendinning et al., 2015; Gariano and Guzzetti, 2016). Therefore, it is very important to thoroughly understand the impacts of future climate on slope stability and the significance of research on monitoring and prediction methods.

2.5.3 Deterioration in soil mechanical properties under drying-wetting cycles

As mentioned above, the most direct impact of changing climate on engineered slopes is introducing more intensive fluctuations in soil water content, which are closely related to the hydraulic and mechanical properties of engineered soils (Glendinning et al., 2018). To understand the impact of climate change, in many previous studies, the hydraulic mechanical behaviour of soils, such as the soil water retention and shear strength behaviour, has been investigated through laboratory experiments under repeated drying

and wetting conditions. Rogers and Wright (1986) performed a series of direct shear tests on compacted Beaumont Clay specimens under drying and wetting processes and found that repeated drying and wetting can result in a significant decrease in the effective stress shear strength parameter. Goh et al. (2014) conducted a series of consolidated drained (CD) triaxial tests on three different sand-kaolin mixtures subjected to multiple drying and wetting cycles. Their results showed that both the water retention and shear strength behaviour changes with drying-wetting cycling, indicating a decrease in matric suction and shear strength at given water content as the number of cycles increased. Hen-Jones (2018) tested the undrained shear strength of two clays under two cycles of drying and wetting and showed that the undrained shear strength of soil reduced at the second cycle. Similar findings have been reported by a number of other previous studies demonstrating a deterioration in soil suction and strength properties (e.g. shear strength and tensile strength) driven by the successive drying and wetting activities (Stirling et al., 2014; Glendinning et al., 2015; Azizi et al., 2020; Stirling et al., 2020; Wen et al., 2020). All these studies demonstrated a deterioration in soil suction (water retention capacity) and strength properties associated with the microstructural changes drying and wetting cycles, with the most pronounced change occurring after the first cycle. The mechanism driving this deterioration was thought to be the microstructural changes associated with volumetric changes caused by cyclic swelling and shrinkage during moisture cycling. The micro-structure change of soil materials during drying-wetting cycles was investigated in previous study using the environmental scanning electron microscope (ESEM). The ESEM results suggested that the soil fabric and aggregates reconstructed and rearranged over time during drying and wetting cycles, results in deterioration in soil fabric with the development of micro-scale cracks and fractures (Hen-Jones et al., 2017; Stirling et al., 2020), as well as the changes in the pore size distribution (Azizi et al., 2020). Kong et al. (2018) analysed the pore size distribution of a clayey soil under multiple drying and wetting cycles using Nuclear magnetic resonance (NMR) relaxometry and found that the changes in SWRCs over drying and wetting cycles were quantitatively related to the pore size distribution. It has also been noticed that the drying and wetting cycles can cause reduction of the initial saturated water content, air entry value and therefore the water retention capacity.

It was realised that the soil deterioration strongly depends on the microstructure and volumetric changes driven by the repeated swelling-shrinking of clay materials during

drying-wetting cycles. The effect of drying and wetting cycles on soil swelling and shrinkage behaviour has also been investigated by a number of previous studies. Estabragh et al. (2015) investigated the volumetric behaviour of a clay mixture under cyclic drying and wetting through series of laboratory tests. Their results showed a hysteresis between the swelling and shrinkage curves (i.e. the relationships between void ratio and water content of soil for wetting and drying processes) and an evolution in the swell-shrink behaviour of soil over drying-wetting cycles, indicating a reduction in saturated void ratio over drying-wetting cycling. The results also showed that the hysteresis of the swell-shrink curves, in other words the change in volumetric behaviour, was most significant at the first drying-wetting cycle and decreased by cycles, and eventually reaching an equilibrium state after about four or five cycles. Similar findings has also been reported by other studies (Al-Homoud et al., 1995; Basma et al., 1996), which were thought to be due to the rearrangement and reorientation of the soil fabric and the destruction of the large elements. The volumetric behaviour of clays were found closely related to the clay content, index properties and shrinkage range (Izdebska-Mucha and Wójcik, 2013), and were further affected by the drying-wetting history and the as-compacted conditions under repeated drying and wetting cycles (Day, 1994).

As reviewed above, the soil deterioration driven by drying and wetting cycles has been evident by many previous studies. However, it should be noted that most of data for SWRC and strength properties under drying-wetting cycling were determined over the limited cycles or in a limited suction range. Data of SWRCs determined in both the high and low suction ranges and for multiple drying-wetting cycles are rarely found in the literature (Al-Mahbashi et al., 2018). It is of significant to obtain a more thorough understanding of the soil deterioration driven by the seasonal changing climate through laboratory and field testing and therefore the potential modelling approaches (Hen-Jones et al., 2017; Glendinning et al., 2018; Gunn et al., 2018; Stirling et al., 2020). This is crucial for more critically assessing the long-term geotechnical parameters.

2.6 Soil water content measurement methods

The gravimetric method is the only way to measure the soil water content directly. The gravimetric water content (GWC) of soil is defined as the water mass as a proportion of soil dry mass. The GWC can be directly determined through the soil mass measurements

before and after oven drying at 105^0C for 24h-48h (BSI, 1990a). During oven drying, the water is removed from a soil sample by evaporation with the amount of water removed being determined. The gravimetric water content, therefore, can be derived as:

$$w = \frac{m_{wet} - m_{dry}}{m_{dry}} \times 100\% \tag{2.25}$$

Where w is the gravimetric water content of soil, m_{wet} and m_{dry} are the soil sample mass before and after oven drying, respectively.

The gravimetric method provides direct measurement on soil water content. However, the method is time-consuming and the oven drying process damages the natural soil structure, making it difficult to be used in the field or provide continuous measurement on the soil water content. Nevertheless, since it is the most direct and actual measurement method of soil water content, the gravimetric method can be used to calibrate the data from all the indirect methods.

Indirect methods measure the water content through surrogate properties that are closely related to the soil water content with empirical relationships. Table 2.3 summarizes several of the indirect techniques available with the brief descriptions. In the following sections, the principles, advantages and disadvantages of several widely used indirect water content measurement methods will be reviewed.

Table 2.3 Indirect methods for determining the soil water content (Evett et al., 2008)

Method	Surrogate Measurement	Explanation
Neutron moisture meter	Count of slow neutrons around a source of fast neutrons	A radioactive source emits fast neutrons (5 MeV), which lose energy as they collide with other atoms, in particular hydrogen. The surrogate is the concentration of slow neutrons. Since the only rapidly changing source of hydrogen in the soil is water, θ_v can be calibrated vs. the count of slow neutrons.
Thermal sensors	Heat conductivity or heat capacity of the soil	A pulse of heat is generated and the subsequent rise or fall in temperature of adjacent soil is measured over time. Soil is a poor conductor of heat, and water a good one, so the amount of heat or rate of heat transmission is closely related to θ_v.
Time domain reflectometer (TDR)	Travel time of an electromagnetic pulse	A fast rise time electromagnetic pulse is injected into a waveguide inserted into or buried in the soil. The time required for the pulse to travel along the metal rods of the waveguide is determined by the bulk electrical permittivity of the soil. The θ_v is a major factor influencing the bulk permittivity (BEC). True TDR involves capture of a waveform and analysis to find the travel time of the highest frequency part of the pulse.
Campbell FDR	Repetition time for a fast rise time electromagnetic pulse	See TDR sensors; same, except reliance on reflected pulse reaching a set voltage rather than waveform analysis causes the method to be more influenced by BEC and temperature.
Capacitive sensors	Frequency of an oscillating circuit	An oscillating current is induced in a circuit, part of which is a capacitor that is arranged so that the soil becomes part of the dielectric medium affected by the electromagnetic field between the capacitor's electrodes. The θ_v influences the electrical permittivity of the soil, which in turn affects the capacitance, causing the frequency of oscillation to shift.
Conductivity sensors (e.g., granular matrix sensors and gypsum blocks)	Electrical conductivity of a porous medium in contact with the soil	An alternating current voltage is placed on two electrodes in a porous material in contact with the soil, and the amount of current is a measure of the conductivity and amount of water in the porous material between the electrodes. These are used for estimation of soil water tension (suction), not θ_v.
Tensiometers	Matric and gravitational soil water potential components	Capillary forces retaining water in the soil pores are connected through the soil water to water in a porous cup connected to a tube filled with water. This generates a negative pressure within the tube, which can be measured with a vacuum gauge. These are used for estimation of soil water tension (suction), not θ_v.

2.6.1 Neutron probe

The neutron probe detects the thermal neutrons to determine the water content of soil. The probe employs a fast neutron source being installed on the surface or lowered in an access tube. When the fast neutrons collide with the hydrogen nucleus in the water, the

neutrons slow down since they lose much of their energy. The detection of slow neutrons returning to the probe allow the estimate of amount of hydrogen present, giving a measure on the soil moisture. The neutron probe is relatively easy to use and can provides robust and accurate measurements on soil water content (<1%). Disadvantages of using neutron probe include the high costs, the risk with radioactive material, and the specific calibration for the probe (Muñoz-Carpena et al., 2004; Robock, 2015). In addition, the neutron probe works well for the deep profiling of underground (Robinson et al., 2003a) but becomes inaccurate near surface since the neutron scattering is most imprecise near the soil surface (Evett et al., 1993).

2.6.2 Dielectric methods

In addition to the neutron probe technique, the dielectric methods determined the volumetric water content by measuring the dielectric constant (or the bulk permittivity) of soil ε_a. The dielectric constant can be determined by measuring the velocity of an electromagnetic wave travelling through the soil (Topp et al., 1980). Since the permittivity of water (ε_a =81) is distinct from the permittivity of air (ε_a =1)and soil matrix (ε_a =2 to 5), the bulk permittivity of soil is closely related to the volumetric water content (Topp et al., 1980; Blonquist et al., 2005). Topp et al. (1980) proposed an empirical calibration relationship of soil dielectric constant and volumetric water content for mineral soils, which is expressed as:

$$\theta = -5.3\times10^{-2} + 2.92\times10^{-2}\,\varepsilon_a - 5.5\times10^{-4}\,\varepsilon_a^{\,2} + 4.3\times10^{-6}\,\varepsilon_a^{\,3} \qquad (2.26)$$

The empirical calibration equation (2.26) is widely used as the default calibration for the commercial dielectric type instruments. However, this empirical equation is a universal calibrating relationship for mineral soils independent with the soil type and complex densities of natural soils. A soil specific calibration is required for the high organic content soils and those expansive soils who have strong volumetric changes during drying and wetting.

According to the sensor outputs, the dielectric devices can be divided into three different types: the time domain reflectometry (TDR), the frequency domain reflectometry (FDR) and the amplitude domain reflectometry (ADR).

2.6.3 Time domain reflectometry (TDR)

2.6.3.1 Introduction

TDR is one of the most accurate and reliable measurement techniques on estimating the soil volumetric water content (Topp et al., 1980; Robinson et al., 2003a; Huisman et al., 2006). TDR technique was first used to detect discontinuities in the transmission lines, thus it was so called 'cable tester' in the telecommunication industry (Jones et al., 2002). In 1970s, Topp et al. (1980) used the TDR technique with coaxial transmission lines to determine the volumetric water content of different mineral soils. They found there was a strong relationship between the permittivity measured by TDR and volumetric water content of soil and proposed an empirical equation which is given by Equation (2.26). Topp equation allows the volumetric water content of the soil to be estimated from permittivity measurements using TDR technique as well as other dielectric-based methods. The empirical equation by Topp et al. (1980) has been verified by numerous authors using many different types of soils (Topp et al., 1982; Smith and Patterson, 1984; Topp and Davis, 1985; Drungil et al., 1989; Grantz, 1990).

In addition to determining the apparent permittivity, the TDR technique is able to measure the bulk electrical conductivity of soil samples. Dalton et al. (1984) first suggested the use of TDR to determine soil bulk electrical conductivity from the attenuation of the TDR signal voltage. Alternative approaches have been proposed for the simultaneous measurements of both apparent permittivity and electrical conductivity of soil by using TDR (Dalton et al., 1984; Dasberg and Dalton, 1985; Topp et al., 1988). However, the thin-sample approach by Giese and Tiemann (1975) has been suggested to be the most effective method of determining BEC of soil using TDR among other approaches (Nadler et al., 1991; Topp et al., 2000; Lin and Tang, 2007). Heimovaara et al. (1995) proposed that the load resistance measured by TDR consisted of the sample resistance and the cable resistance. However, the theory was suggested to be incomplete by comparing the measured and optimised cable resistance (Huisman and Bouten, 1999). In consequence Castiglione and Shouse (2003) proposed an improved solution for calibrating the ER measurement of the TDR method. These efforts promoted calibrating methodology for the TDR probes to obtain a more accurate measurement of soil bulk EC.

Over the years, the development of manufactures in data acquisition systems and computer-operated multiplexers have made TDR one of the standard techniques to monitor the soil water content in the field (Baker and Allmaras, 1990; Topp et al., 2003).

2.6.3.2 Measurement principles of TDR

Principle of the permittivity measurement

The TDR device propagates high-frequency electromagnetic signals into its coaxial waveguides, normally consisting of two or three stainless steel prongs (Figure 2.8), and measures the propagation time that takes for the signal to travel along the transmission lines (Evett et al., 2008). The reflection of a signal that involves a change in voltage is received by the TDR system. The common way to express the reflection of the signal is to use a reflection coefficient, ρ_u, which is given by:

$$\rho_u = \frac{V_i - V_o}{V_0} \tag{2.27}$$

where V_i is the measured voltage of the soil sample (V) and V_o is the output voltage of the TDR system (V).

The velocity of the signal travelling through the waveguides of TDR probe is a function of refractive index (i.e. square root of the apparent permittivity), $\sqrt{\varepsilon_a}$, of soil and can be determined from the travel length (i.e. the length of waveguides) and the travel time (Topp et al., 1980).

$$v = \frac{c}{\sqrt{\varepsilon_a}} \tag{2.28}$$

and

$$v = \frac{2L}{t} \tag{2.29}$$

where c is the velocity of light in free space (ms^{-1}), Δt is the time for the electromagnet signal to travel along the waveguides (s) and L is the length of the waveguides (m). The equations (2.28) and (2.29) can be rearranged and simplified to be written in terms of a ratio between an apparent length and actual length of the TDR probe, which is given as:

$$\sqrt{\varepsilon_a} = \frac{L_a}{L} \tag{2.30}$$

where $L_a\ (m)$ is an apparent length equal to $\frac{c\Delta t}{2}$. The apparent length can be observed and determined by analysing the waveform of the TDR measurement plotting in terms of the reflection coefficient vs. the apparent length, as shown in Figure 2.8. The apparent length of measurement is defined as the distance between the two points that the reflections of signal occur at the start and the end of the probe rods. The two reflection points at the start and the end of probe rods have been marked in the waveform in Figure 2.8. Equation (2.30) can thus be used to determine the apparent permittivity using TDR (Robinson et al., 2003a).

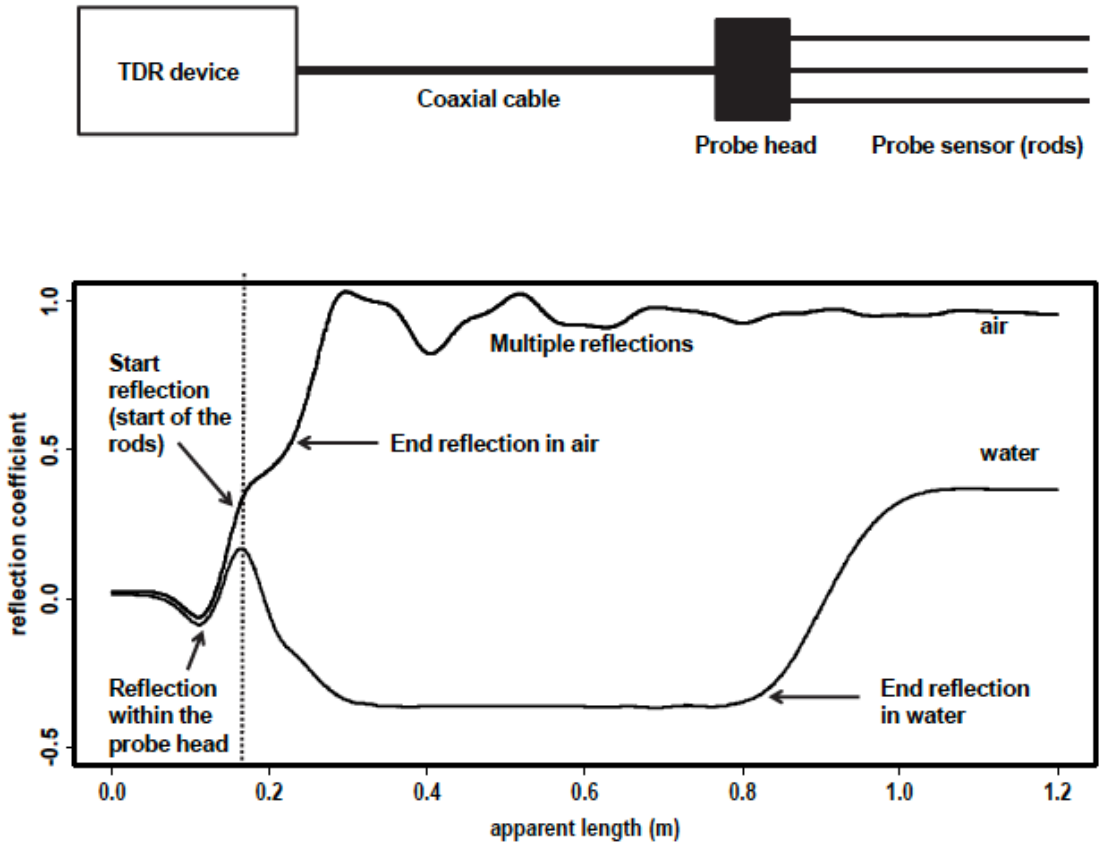

Figure 2.8 Schematic of the TDR equipment and the waveforms of TDR measurements in air and in water (Curioni, 2013)

Principle for bulk electrical conductivity (BEC) measurement

In a TDR measurement, the bulk electrical conductivity, σ_a of soil is correlated to the attenuation of the propagating signal, resulting in a lower level out the state of the reflection coefficient at long apparent distance (Dalton et al., 1984). According to the thin

sample approach proposed by Giese and Tiemann (1975), the BEC of soil measured by TDR can be expressed by equation (2.31):

$$\sigma_a = \frac{1}{Z_c} \times \frac{Z_0 c \varepsilon_0}{L} \times \frac{1 - \rho_\infty}{1 + \rho_\infty} \tag{2.31}$$

where σ_a (Sm^{-1}) is the bulk electrical conductivity, Z_c (Ω) is the output impedance of TDR system (typically ≈ 50Ω), ε_0 is the electric constant equal to $8.854 \times 10^{-12} Fm^{-1}$, Z_0 (Ω) is the characteristic impedance of the probe, L (m) is the physical length of probe and ρ_∞ is the measured reflection coefficient at long distance. The equation (2.31) can be simplified by introducing a probe constant, K_P (m^{-1}) giving by equation (2.32) to be expressed as equation (2.33):

$$K_P = \frac{Z_0 c \varepsilon_0}{L} \tag{2.32}$$

$$\sigma_a = \frac{K_P}{Z_c}\left(\frac{1 - \rho_\infty}{1 + \rho_\infty}\right) \tag{2.33}$$

Where K_P is the geometric constant of TDR probe which can be measured experimentally by immersing the probe in solutions of known ER (Jones et al., 2002). Equation (2.31) is proposed assuming that there is no loss in the reflection coefficient in the system. However, anything between the start points of reflection occurring and the probe head results in attenuation of the reflection coefficient in the practice. With the loss in the system, the reflection coefficient of the open circus would reduce to less than 1 whilst the reflection coefficient of the closed circus would tend upwards. In order to account for the system dependant attenuation, Castiglione and Shouse (2003) suggested an approach to correct the reflection coefficient:

$$\rho_{corr} = 2\left(\frac{\rho_u - \rho_o}{\rho_o - \rho_c}\right) + 1 \tag{2.34}$$

Where ρ_{corr} is the corrected reflection coefficient for use instead of ρ_∞ in equation (2.33), ρ_u is the uncorrected reflection coefficient measured at long distances, ρ_o is the reflection coefficient of the open circus and ρ_c is the reflection coefficient of the close circus. With calibrating the probe constant, K_P and output impedance, Z_c, the bulk EC of soil can be calculated by applying ρ_{corr} measured by TDR to equation (2.33).

2.6.3.3 Applications of TDR

In last few decades, the establishment of dielectric theory and the success of high-frequency measurement of dielectric constant (permittivity) have prompt TDR to become a practical technique for measuring the permittivity of porous media. Since the late 1970s, the use of TDR techniques has extended to geosciences for estimating soil water content, because the apparent permittivity of soil is strongly dependent on volumetric water content (Robinson et al., 2003a). Empirical and dielectric mixing models are two different approaches used to relate dielectric permittivity to volumetric water content for the calibration of the TDR method. Empirical equations are determined directly from the functional relationships that fit the experimental data points, normally expressing water content as a polynomial function of dielectric permittivity, such as equation (2.26) by Topp et al. (1980), without consideration of any physical justifications. The dielectric mixing models consider soil as a multiphase mixture of dielectric components (i.e. solids, water and air), and therefore relates its bulk dielectric permittivity to the individual permittivity and volume fractions of the dielectric constituents (Tinga et al., 1973; Roth et al., 1990). The empirical equation for mineral soils has been widely used since it does not require the determination of additional parameter, whereas soil-specific calibrations are suggested for the determining of VWC for organic soils and clays, which bind a large amount of water (Jones et al., 2002). In addition to estimate the soil water content from the apparent permittivity, TDR was used to estimate soil bulk electrical conductivity (BEC) from its signal attenuation. As the signal propagates along the TDR rods buried in the soil, the energy of the applied signal attenuated in proportion to the electrical conductivity. The proportional decrease in signal voltage is closely related to the bulk conductivity of soil (Jones et al., 2002). The development of multiplexing and advanced data acquisition system allowed the simultaneous measurements of multiple TDR probes for the field testing (Heimovaara and Bouten, 1990; Herkelrath et al., 1991; Topp et al., 2003). The TDR techniques have been used in many studies for soil water content and BEC measurements in the laboratory and field tests for agricultural research and slope stability monitoring (Evett et al., 2008), over a wide range of soil types including frozen soils (Patterson and Smith, 1981; He et al., 2016). Jacobsen and Schjonning (1995) summarised various empirical equations and suggested that Topp's equation might be the first choice if an accuracy of $\pm$ 0.02~0.03 (VWC) was acceptable. Curioni (2013) calibrated the TDR probes rigorously follow the methodologies reported by Heimovaara

(1993) and Robinson et al. (2003b) and evaluated the performance of the well-calibrated probes with reference solutions with known permittivity and electrical conductivity. The results of this study suggested that TDR can achieve a good level of the measurement of apparent permittivity and BEC with an accuracy of 2% and 3%, respectively, and a precision of approximately 2% for both parameters. However, the study also reported that the accuracy of TDR reduced to up to 10% when the measurements were taken on materials in dry conditions, which have low permittivity and BEC. Similar phenomenon was pointed out in previous studies and was thought to be due to the air gaps around the TDR rods caused by installation or shrinkage of soils during drying (Topp et al., 1982; Asquith, 2015). In addition to perform as a less expensive and more accurate tools for soil water content and BEC estimation, the TDR techniques were also used as a proxy of other soil properties such like specific surface area and water retention properties (Jones et al., 2002). Much efforts have been paid in previous studies to relate the electromagnetic properties to the geotechnical properties, as it was make great potential of using geophysical methods and remote sensing to describe the underground geotechnical information (Thomas et al., 2010a). TDR has also been used in research with respect to relate the electromagnetic property to the geotechnical properties, such as liquid limit, linear shrinkage property (Thomas et al., 2010a), dry density (Thomas et al., 2010b) and specific surface area (Peplinski et al., 1995). Furthermore, TDR techniques were used for providing reference measurements of apparent permittivity, conductivity, or water content in geophysical surveys, such as electrical resistivity tomography (Koestel et al., 2008; Schwartz et al., 2008) and ground penetration radar (Huisman et al., 2003; Curioni, 2013).

2.6.4 Frequency domain reflectometry (FDR)/capacitance

In addition to the TDR technique, there are some other dielectric type devices available for measuring the permittivity of soil with different principles, such as the FDR and ADR probes. FDR and capacitance probes measure the soil dielectric constant using two or more plates or rods as capacitors that are embedded into the soil. For FDR, the dielectric constant is determined by measuring the resonant frequency of the circuit (composed by the capacitors and the soil as the dielectric) when applying an oscillating charge into the soil. In the capacitance method, the dielectric constant is determined by measuring the charging time which is related to the volumetric water content of the soil.

FDR and capacitance techniques provide accurate and robust water content measurements and the costs of these types of sensors are relatively lower than TDR probes. However, the measurements are affected by the soil bulk density, solution conductivity and potential air pockets around the capacitors. A soil specific calibration is also needed for these probes while dealing with different types of soil (Dean et al., 1987; Muñoz-Carpena et al., 2004).

2.6.5 Impedance/amplitude domain reflectometry (ADR)

The amplitude domain reflectometry determines the dielectric constant of soil by measuring the electrical impedance of the soil medium. The oscillator in the probe propagates an electromagnetic signal with a fixed frequency through the transmission line, and the amplitude of the voltage standing wave produced on the transmission line is measured to determine the impedance of the soil medium. The impedance of soil is composed by two parts: the electrical conductivity and the dielectric constant. The effect of conductivity can be removed by using an appropriate frequency (commonly 100MHz). The ADR probe is much cheaper than the other dielectric probes and has similar performance as TDR and FDR (Nakashima et al., 1998). However, the ADR probe is also affected by the soil conditions and requires soil specific calibration (Muñoz-Carpena et al., 2004).

2.7 Electrical resistivity methods

2.7.1 Introduction

The electrical resistivity method is used in the investigation of horizontal and vertical discontinuities in the electrical properties of the ground. It is routinely made at the surface of the earth to investigate the shallow subsurface conditions (Sharma, 1997).

Electrical resistivity methods use direct currents or low-frequency alternating currents, which can avoid dielectric conduction, to investigate the electrical properties of the earth (Reynolds, 2011). In the most commonly used resistivity method, an artificially generated current is introduced into the ground, which can cause potential differences due to the anomalous geological conditions and inhomogeneity within the earth, and the resulting potential differences are measured at the surface (Kearey et al., 2002). In 1912,

Conrad Schlumberger used the resistivity method for the first time in field experiments in Normandy (Sharma, 1997).

As the electrical resistivity method is a non-intensive and low-cost technique that can provide measurements of soil water content in a large field scale (Hassan, 2014), it has great potential to investigate the characteristics of the water content of engineered soils, and subsequently the soil water retention behaviour, and consequently the shear strength behaviour of engineered soils.

2.7.2 Electrical resistivity of earth materials

Electrical resistivity is a physical property of a material that describes the ability to resist the current flow within it. It is defined as the resistance between opposite faces of a unit cube conductor. For a conductor of resistance R (ohm), length L (m) and uniform cross-section area A (m^2), its resistivity ρ is expressed as:

$$\rho = \frac{RA}{L} \tag{2.35}$$

The SI unit of resistivity is ohm meter (Ω m). The reciprocal of resistivity is termed conductivity, σ_b, which is measured in Siemen per meter (S/m).

The electrical conduction is caused by the movement of electrically charged particles through a transmission medium. Electrical current is driven in most rocks mainly by the movement of ions in pore water, since most mineral grains in rocks are insulators (Sharma, 1997; Kearey et al., 2002). The electrical conduction is, therefore, mainly electrolytic in most rocks. As a result, the electrical resistivity property of a rock is mainly controlled by the porosity and pore water content (Bryson, 2005; Friedman, 2005) . However, in water-bearing rocks, the lithology and geologic age affect slightly on resistivity, since these two factors tend to control the porosity, pore water content and salinity of rocks (Keller, 1966). Nevertheless, the temperature also affects the resistivity as it affects the mobility of ions present in the water filling the pores (Zhou et al., 2015).

2.7.3 Basic theory of electrical resistivity (ER) methods

In a homogeneous conductor, the relationship between current I, resistance R and potential differences ΔV can be expressed by Ohm's law:

$$\Delta V = RI \tag{2.36}$$

Substituting R using equation (2.4) into equation (2.3), the resistivity ρ can be written as:

$$\rho = \frac{\Delta V}{I}\frac{A}{L} \tag{2.37}$$

Considering let the length of the conductor in equation (2.5) tend to zero and its resistivity is uniform within it, the equation (2.5) can be written as:

$$-\frac{\partial V}{\partial L} = \frac{\rho I}{A} = \rho i \tag{2.38}$$

Where $-\partial V/\partial L$ represents the potential gradient associated with current through the conductive element in volt m^{-1} and i is the current density per unit cross-section area in A m^{-2}.

Now consider a semi-infinite, homogeneous conducting medium of uniform resistivity with a single current source of strength, $+I$ enter at point C on its surface (Figure 2.1a). The current will travel away radially from the original point C, and the equipotential surfaces will be uniformly distributed over hemispherical shells within the medium. At a distance r from the current source C, the area of hemispherical surface is $2\pi r^2$, then the current density i can be expressed as:

$$i = \frac{I}{2\pi r^2} \tag{2.39}$$

Combining equation (2.6) and (2.7), the potential gradient associated with current can be written as:

$$-\frac{\partial V}{\partial r} = \frac{\rho I}{2\pi r^2} \tag{2.40}$$

The potential V_r at distance r can be obtained by integration:

$$V_r = \frac{\rho I}{2\pi r} \tag{2.41}$$

In engineering practice, four-electrode method is most commonly used in resistivity determination, since the contact issues can be minimized via this electrode configuration (Keller, 1966). Current is injected into the ground by one pair of electrodes (C1 and C2); potential differences are measured with the second pair of electrodes (P1 and P2) at ground surface (Figure 2.9b).

From equation (2.9), the potential difference between P_1 and P_2 is expressed as:

$$\nabla V = V_{P1} - V_{P2} = \left(\frac{\rho I}{2\pi C_1 P_1} - \frac{\rho I}{2\pi C_2 P_1}\right) - \left(\frac{\rho I}{2\pi C_1 P_2} - \frac{\rho I}{2\pi C_2 P_2}\right) \tag{2.42}$$

$$\nabla V = \frac{\rho I}{2\pi}\left(\frac{1}{C_1 P_1} - \frac{1}{C_2 P_1} - \frac{1}{C_1 P_2} + \frac{1}{C_2 P_2}\right) \tag{2.43}$$

Rearranging equation (2.11), it is:

$$\rho = K\frac{\nabla V}{I} \tag{2.44}$$

Where K is the geometric factor depends on the electrode configuration.

The text above demonstrates the basic theories of electrical resistivity methods.

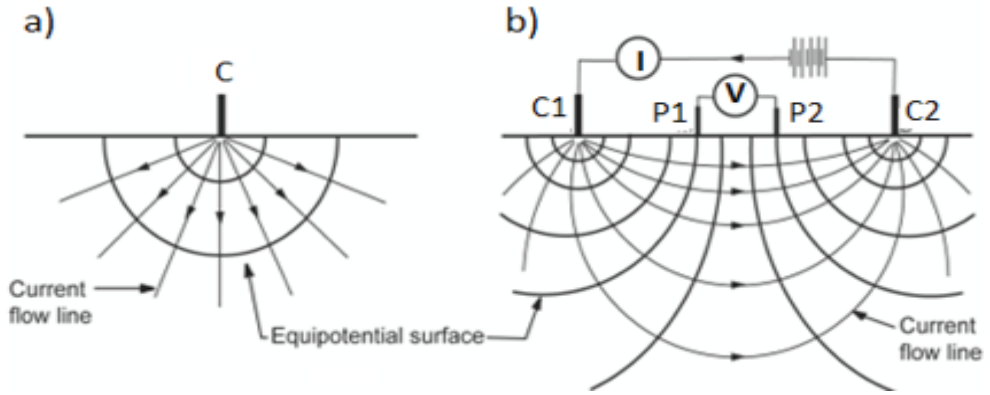

Figure 2.9 The current flow and potential distribution of a semi-infinite and homogeneous medium (a) a single current source (b) four-electrode method (Hassan, 2014)

2.7.4 Point/one-dimensional measurement of ER methods.

In a laboratory scale, the resistivity of soil can be measured by either two-electrode or four-electrode systems. Normally a two-electrode system injects current flows using only two electrodes (two metal plates) from two ends of a regular shaped specimen and the potential difference is measured between the same pair of electrodes (ASTM, 2005). A Miller soil box method (ASTM, 2001) is a modified two-electrode method that introduces an additional pair of inner electrodes for potential measurement. In the system, the outer two pins (metal plates) are used for injecting current into the soil and the inner pair are used for potential difference measurement (see in Figure 2.10). Although the soil box system has four electrodes, it is still using the same principle that the traditional two-electrode method uses. The resistivity can be determined according to equation 2.45, where A is the cross-sectional area of the current flow and L is the spacing between two inner electrodes.

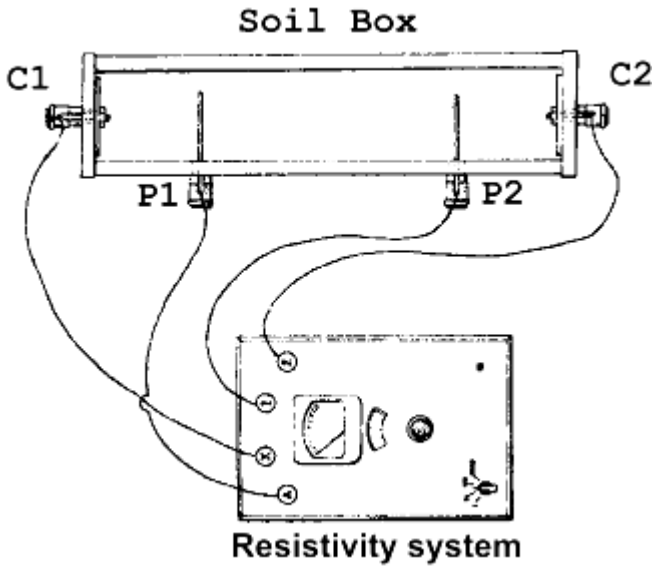

Figure 2.10 Typical apparatus for Miller soil box (ASTM, 2001)

A conventional four-electrode resistivity measurement system normally consists of a resistivity meter, four electrodes (i.e., one pair for injecting current into the soil and another pair for the potential measurements) and cables for connecting the system. The resistivity meter has two essential components: a direct or low-frequency current source for current generation and a potential measuring unit (Loke, 2001; Samouëlian et al., 2005). In a resistivity system, the electrodes are inserted into the soil in specific arrays, from where the geometric factor K can be defined.

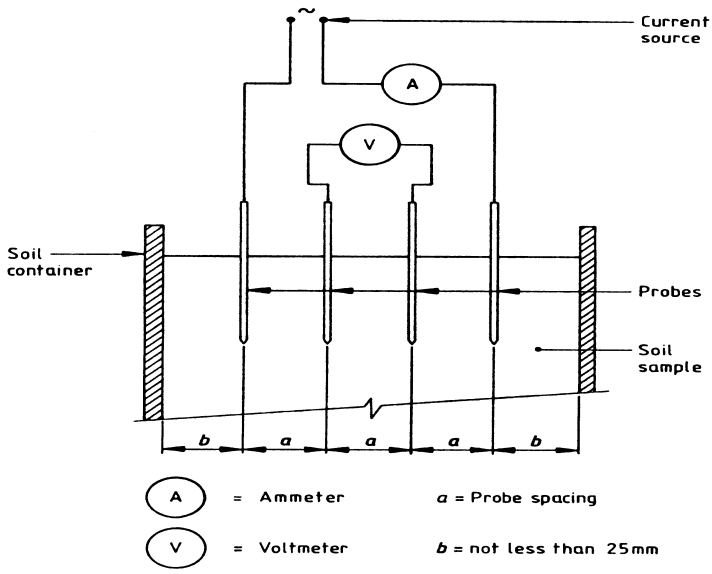

Figure 2.11 Testing apparatus of the four-electrode resistivity system using Wenner array (BSI, 1990b)

Figure 2.11 shows the typical testing set up for a four-electrode resistivity system using Wenner array. The detailed testing procedures for this method are stated in BSI (1990b) and ASTM (2001). In this method, four metal electrodes are inserted into the soil specimen with a constant spacing a. Current I is injected to the soil though the outer two electrodes and is measured by an Ammeter in series and the voltage difference ∇V is measured between the two inner electrodes by a Voltmeter. The geometric factor K can be determined from the configuration of the array that:

$$K = \frac{2\pi}{\left(\frac{1}{C_1P_1} - \frac{1}{C_2P_1} - \frac{1}{C_1P_2} + \frac{1}{C_2P_2}\right)} = 2\pi a \tag{2.46}$$

and the resistivity can be calculated using equation 2.29.

The use of two-electrode methods requires good contact between the metal plate and the surfaces of the soil specimen as a poor contact decreases the actual cross-sectional area of the current flow and raises high contact resistance. In addition, the continuous direct current applied in a two-electrode system will cause an unreversed oxidation-reduction reaction in the metal electrodes, which causes the orientation of ions, referred to as polarization (Keller, 2017). The arrangement of four electrode methods minimises the contact issues and the polarization problems (Gupta and Hanks, 1972; Campanella and Weemees, 1990; Beck et al., 2011).

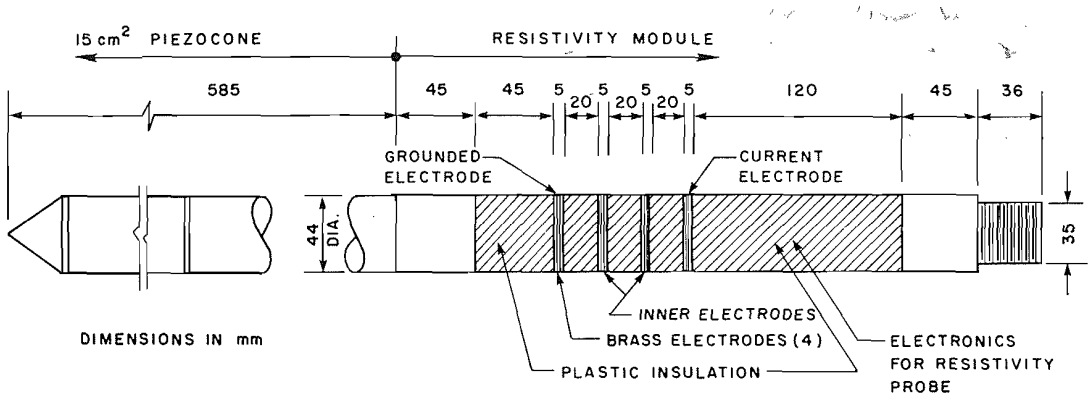

Figure 2.12 Diagram of resistivity piezocone using linear four-electrode arrangement (Campanella and Weemees, 1990)

Numerous resistivity probes have been developed based on the four-electrode arrangement to adapt to the needs of resistivity measurements on different soil types, sizes and shapes. In addition to the standard Wenner testing systems described in ASTM (2001) and BSI (1990b), the most widely used resistivity probing systems are normally designed based on the linear electrode arrays (e.g. Dipole-Dipole, Wenner and Schlumberger). Campanella and Weemees (1990) proposed a resistivity piezocone (Figure 2.12), in which a four-electrode resistivity module is embedded at the back of the piezocone. The four electrodes are made of brass and are arranged in a linear array in constant spacing. Similar devices have also been reported in numerous literature, e.g. Peixoto et al. (2010), Davies and Campanella (1995), Cai et al. (2013).

In addition to the conventional linear arrangements, Habberjam and Watkins (1967) suggested a non-linear array of which the four electrodes are in a square configuration (Figure 2.13). Two adjacent electrodes (C) are used as current dipoles and the other two (P) are used as potential dipoles. There are two main advantages of this square configuration, firstly, the configuration makes all the measurement pairs to be close together, allowing the probe to be adapted to smaller specimens; and secondly, the configuration allows measurements to be taken from two perpendicular directions, which reduces the orientation effect.

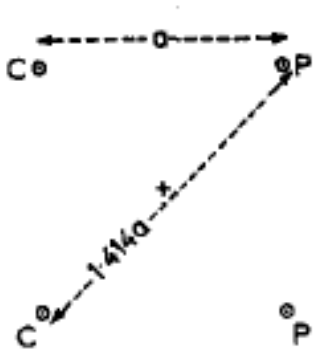

Figure 2.13 square configuration of four-electrode method (Habberjam and Watkins, 1967)

More recently, Munoz-Castelblanco et al. (2011) developed a square configuration resistivity probe to investigate the resistivity behaviour of a local unsaturated soil in a triaxial apparatus while the soil sample is subjected to a drying and wetting process. The probe is constructed by four metal electrodes embedded in a silicone body. Since the electrodes are flat with the contact surface of the silicon body, it is difficult to maintain good contact between the electrodes and soil. A slurry paste of clay is required to improve the contact; therefore, a specific calibration is needed due to the use of wet paste. Using the same arrangement, Hassan (2014) developed a square array resistivity probe to investigate the resistivity characteristics of a sandy clay under drying and wetting among the relationships between soil resistivity and geotechnical properties (e.g. water content, dry density and void ratio). The probe used a similar design to Munoz-Castelblanco et al. (2011), whereas the electrodes were made of finer steel wires, the ends of which protrude from the probe body to form four prongs that can be inserted into the soil specimen (Figure 2.15).

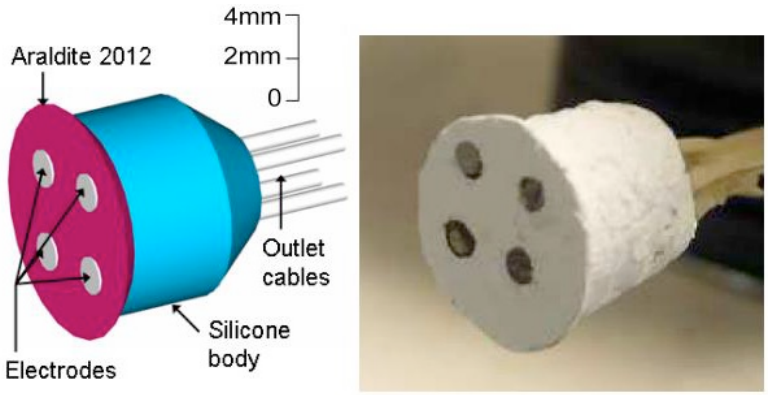

Figure 2.14 four-electrode resistivity probe in square configuration (Munoz-Castelblanco et al., 2011)

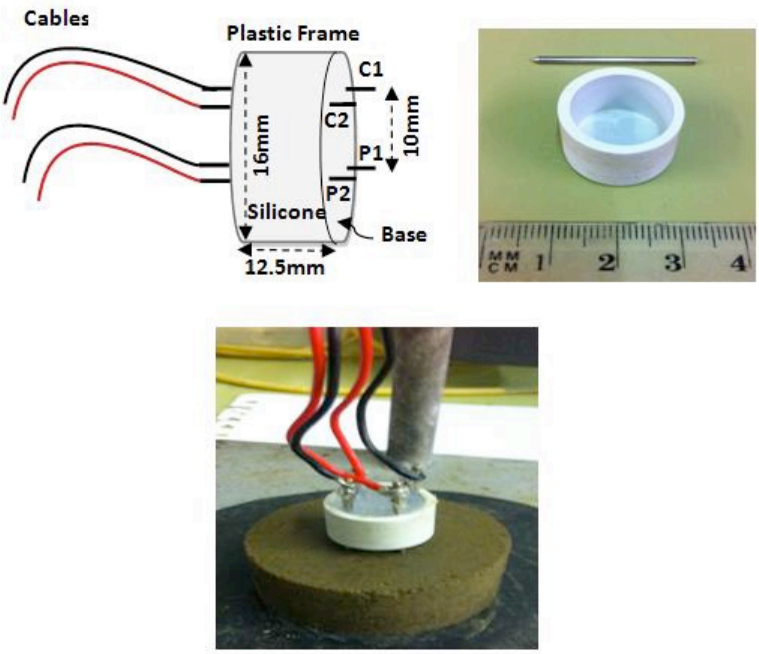

Figure 2.15 square configuration resistivity probe developed by Hassan (2014).

2.7.5 Electrical resistivity tomography (ERT)

Electrical resistivity tomography (ERT) technique is one of the active geophysical methods in engineering practices for surveying the subsurface geotechnical information using electrical resistivity as a proxy, which is widely used in landslide investigation and slope stability monitoring (Samouëlian et al., 2005; Perrone et al., 2014). The ERT technique can provide two-dimensional (2D), three-dimensional (3D) and four-dimensional (4D) imaging of the subsurface resistivity distribution using multi-electrode arrays.

2.7.5.1 Apparent resistivity pseudo-sections for a 2D ERT

In a typical 2D ERT survey, numbers of electrodes are installed into the ground surface in a regular spacing along a line (Figure 2.16). The measurements are operated at different stages by increasing the inter-electrode spacing from a single-spacing stage. In the first stage, each single resistivity value is measured using a fixed array (i.e. the array of electrode A, B, M and N shown in station 1), and the measurement array, referred to as 'station' in the Figure 2.16, will be rolling along the line to complete the total profile of resistivity values for the stage. The inter spacing between the electrodes is increased to

extend the investigation depth and the measurement process is repeated until the maximum spacing is reached.

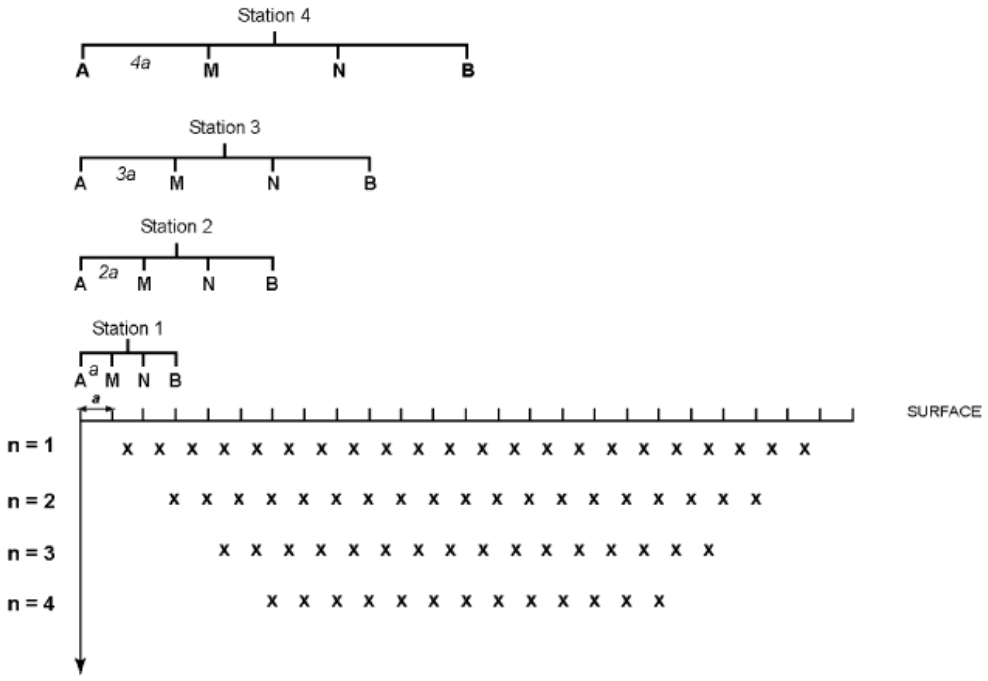

Figure 2.16 Diagram of a typical pseudo-section for a 2D ERT survey using Wenner array. (Samouëlian et al., 2005)

It is crucial to understand that the measured resistivity values represent an apparent resistivity, which is not the true resistivity for the heterogeneous subsurface (Sharma, 1997; Slater et al., 1997). It should also be noted that this electrode spacing-dependent investigation depth is a pseudo-depth in the pseudo-section, but not the actual investigation depth (Loke, 2004). In conventional resistivity interpretation for a dipole-dipole array, the measured apparent resistivity data point is placed at the intersection of two 45 degree lines starting from the centre of the current and potential dipoles respectively (Hallof, 1957). Another method is to place the horizontal position of the data point at the centre of the quadrupole and the vertical position of the data point at a "pseudo depth", which is the median depth of investigation of the electrode array used in the survey (Edwards, 1977). The median depth is dependent on the sensitivity values or the Fréchet derivative of the resistivity array. All the sets of measurements are, hence, gathered to map a 2D pseudo-section, in which an approximate resistivity distribution of the subsurface is displayed.

2.7.5.2 Configuration and sensitivity of resistivity arrays

A resistivity array defines the specific positions of the four electrodes (i.e., current pair and potential pair) during the measurement. The resolution, sensitivity and depth of ERT measurement data are affected by the electrode array been used (Seaton and Burbey, 2002). The most frequently used array configurations are shown in Figure 2.17 along with their electrode arrangements and the geometric factors. The geometric factor K differs from different arrays. Hesse et al. (1986) pointed out that the use of combination of multiple measurement arrays can help to understand more features of the testing material and get better interpretation.

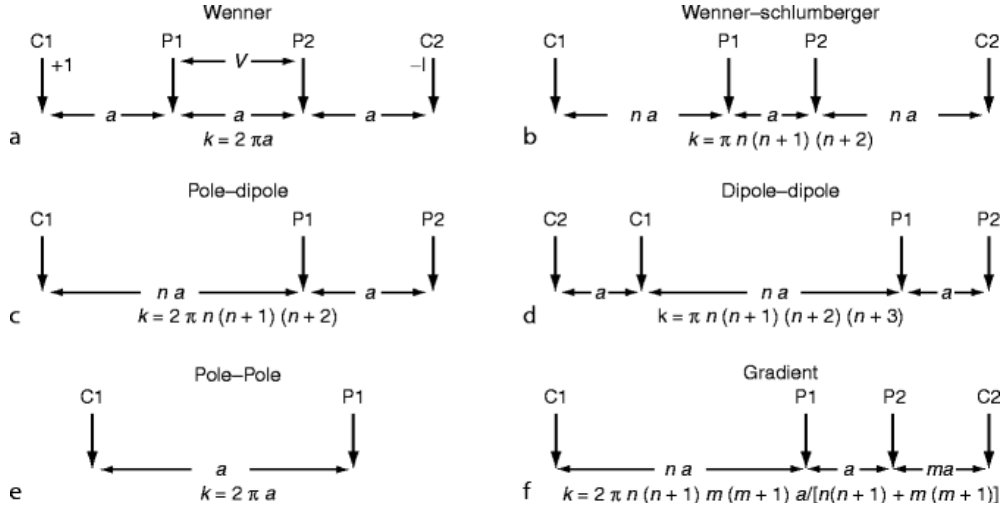

Figure 2.17 Typical array configurations for ERT (Loke et al., 2011)

Figure 2.18 shows the sensitivity patterns for different resistivity arrays. The sensitivity value represents the degree to which a change in the resistivity of a fraction of the subsurface will influence the potential measured by a particular array (Loke, 2001). The sensitivity function is derived mathematically from the Fréchet derivative for a homogeneous half-space (McGillivray and Oldenburg, 1990), and is given by:

$$F_{3D}(x,y,z) = \frac{1}{4\pi^2}\frac{x(x-a)+y^2+z^2}{[x^2+y^2+z^2]^{1.5}[(x-a)^2+y^2+z^2]^{1.5}} \qquad (2.47)$$

Where, a is the electrode separation in the pole-pole array.

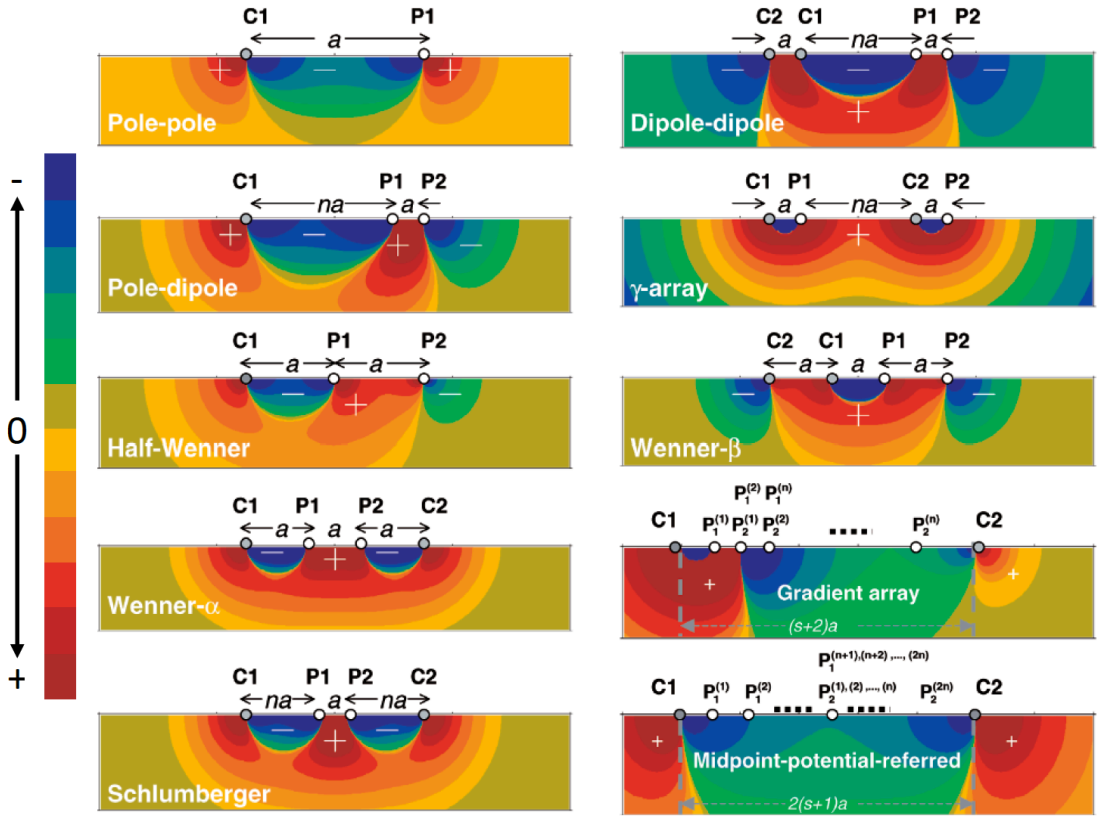

Figure 2.18 The sensitivity patterns for different electrode arrays (Dahlin and Zhou, 2004)

2.7.5.3 3D-ERT data

The 3D ERT provides subsurface electrical information in a spatial basis, which is more accurate in describing the heterogeneities of the property information in the complex subsurface of the earth (Loke, 2001; Aizebeokhai, 2010). A three-dimensional ER imaging can be obtained from reconstruction of a series of parallel 2D ER imaging to map the spatial resistivity distributions. Chambers et al. (2002) emphasized that for a heterogeneous subsurface, 2D profiles from at least two perpendicular orientations are require for mapping the 3D ERT model. Additionally, an alternative method for mapping 3D resistivity imaging is using the square configuration proposed by Habberjam and Watkins (1967). They reported that the use of square configuration reduces the orientation effect in resistivity measurement, comparing with using the co-linear arrays.

2.7.5.4 4D ERT data

The 1D,2D and 3D resistivity imaging demonstrate the resistivity distribution in the subsurface at a specific time of the measurement. ERT techniques of adding time series to the collected data are so called “time-lapse” or “4D” data sets. 4D ERT typically refers

to a 3D data set with multiple time steps, while the time lapse method can also be used in analysis of data sets of any dimension (1D, 2D, and 3D) with multiple time steps. The time-lapse inversion methods (LaBrecque and Yang, 2001; Daily et al., 2004) can be performed using ERT data sets in which the time series between the collected data sets are treated as a variable in the inversion process. Moreover, another common method is to conduct individual inversions each time step in the time lapse sequence, and subsequently establish difference models (e.g., percentage changes or difference ratios) between the inversion results (Whiteley et al., 2019). Time-lapse ERT data can provide information on spatial variations in the resistivity in the subsurface overtime. Time-lapse ERT methods have grown rapidly and have been widely used in the field of monitoring the landslides since the interrelationship between the soil resistivity and water content (Drahor et al., 2006; Chambers et al., 2014; Gunn et al., 2015; Wilkinson et al., 2016).

2.7.6 Applications of ER methods

2.7.6.1 The use of ERT in multiple engineering disciplines

The ERT technique has been used in many engineering disciplines, since a wide range of material changes are accompanied with the changes in resistivity. For example, the ERT has been used in geological characterisation (Sass, 2007; Hirsch et al., 2008; Hsu et al., 2010; Chambers et al., 2012) for identifying the subsurface geological variations. It is used as an efficient tool to monitor the frozen ground (Hauck et al., 2003; Hilbich et al., 2011; Rosset et al., 2013), and for monitoring the CO_2 storage and immigration (Kiessling et al., 2010; Schmidt-Hattenberger et al., 2013). The 2D ER survey has also been utilized for detecting the urban caves (Antonio-Carpio et al., 2004; Santos and Afonso, 2005; Gambetta et al., 2011) and sinkholes (Dobecki and Upchurch, 2006; Carbonel et al., 2014; Kaufmann, 2014) near the ground surface.

2.7.6.2 ERT for slope monitoring and landslide investigation

Recently, the development of automated multi-electrode resistivity systems has significantly accelerated the speed of resistivity measurements. These multi-electrode systems make it possible for the complex multiple-electrode arrays to be managed using computer-controlled resistivity meter, of which the switching units allow any four-electrode combination to be selected. The latest multi-channel systems also allow numbers of potential electrode pairs to be measured at the same time, letting the

acquisition process to be rapid (Samouëlian et al., 2005). Gunn and Ogilvy (2010) developed a fully automated resistivity system, ALERT-ME (Automated Time-Lapse Electrical Resistivity Tomography), which can be operated remotely, providing 24h monitoring (Figure 2.19). The system has been used to monitor the groundwater movement of an embankment while the subsurface soils are subjected to a seasonal drying and wetting.

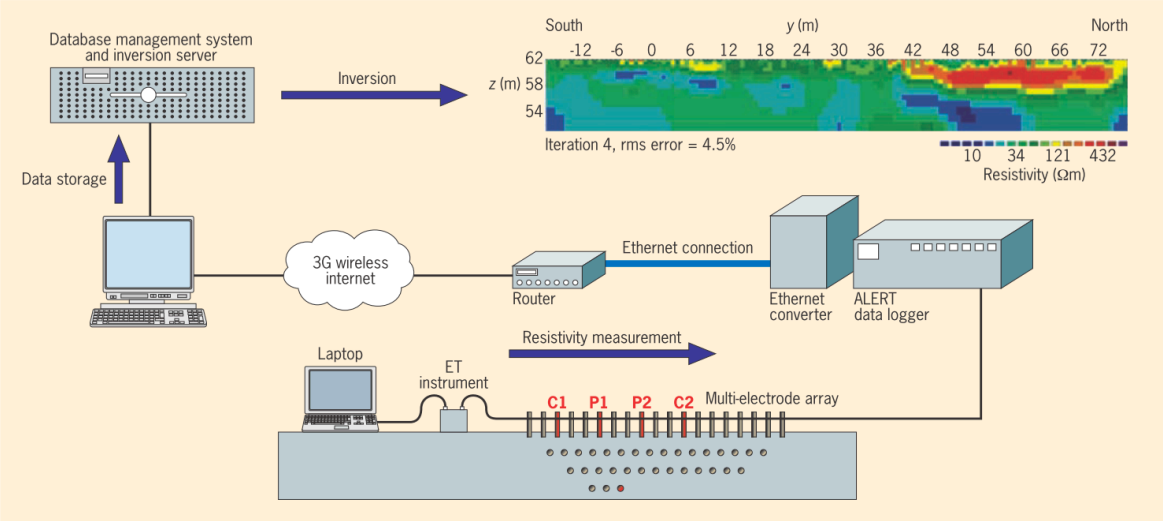

Figure 2.19 The ALERT-ME system developed by British Geological Survey (BGS) (Gunn et al., 2010)

The ERT data should always be analysed associated with the local geology and can help to verify the geotechnical model of the investigation site. Figure 2.20 shows 2D ERT cross-sections for two profile lines of a landslide site in North Switzerland, along with the geotechnical model for one of the profile lines obtained from the direct penetration tests (Friedel et al., 2006). The ERT model shows good agreement with the geotechnical model referring to the subsurface geological information of the slope. A similar study conducted by Perrone et al. (2008) on a clay slope in Italy, used 2D ERT to construct the boundary between bedrock and clay formation, again, an agreement was shown between the resistivity model and the geotechnical model based on borehole data (see Figure 2.21). Both studies indicate the ability of ERT for providing subsurface geotechnical information.

Since 2000's, a large number of studies with respect to the applications of 2D and 3D ERT for landslide investigation and slope stability monitoring have been published. The studies covered comprehensive landside types involving complex landslides (Gallipoli et al., 2000; Lapenna et al., 2003; Naudet et al., 2008; Ogusnsuyi, 2010), translational or

rotational landslides (Godio and Bottino, 2001; Meric et al., 2005; Lee et al., 2008; Hibert et al., 2012; Shan et al., 2014), debris, earth flows or shallow landslides (Demoulin et al., 2003; Schmutz et al., 2009; Chambers et al., 2011; Carpentier et al., 2012; Ravindran and Prabhu, 2012) and the rockslides (Godio et al., 2006; Heincke et al., 2010; Pánek et al., 2011).

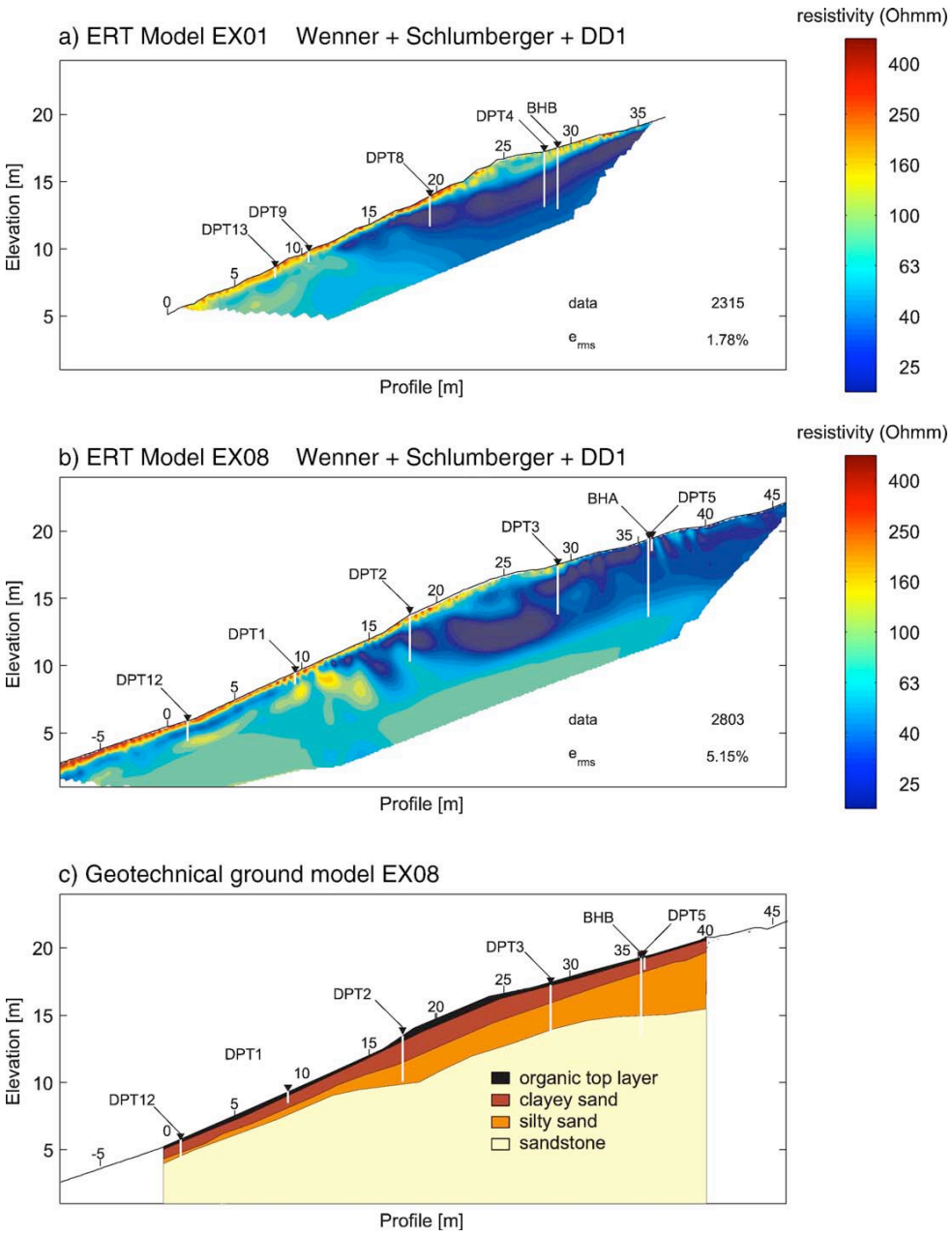

Figure 2.20 2D ERT model based on the combination of Wenner, Schlumberger and Dipole-Dipole array data collected from two profile lines: (a) cross-section EX01, (b) cross-section EX08; and (c) 2D geotechnical model obtained from direct penetration tests (DPT) for profile EX08. (Friedel et al., 2006)

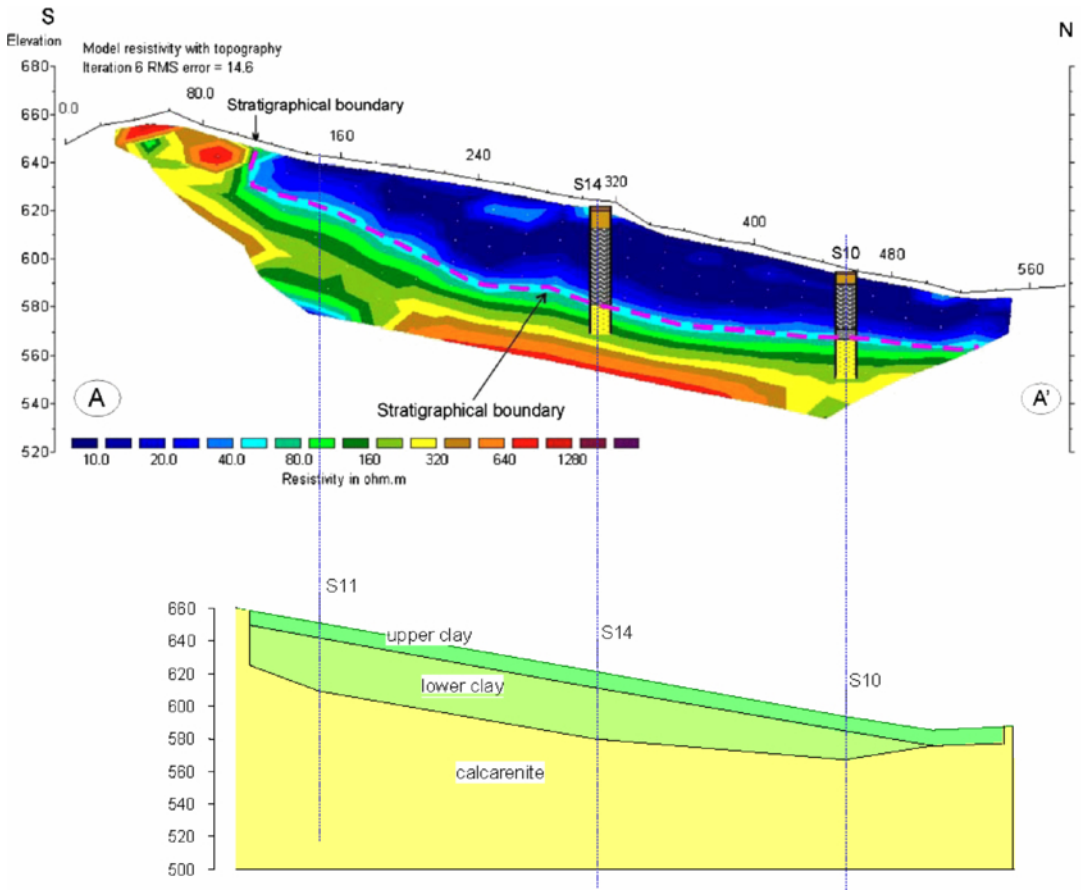

Figure 2.21 Geotechnical model for a clay slope in Italy, generated from the 2D ERT survey and borehole data. (Perrone et al., 2008)

The 2D ERT survey can provide basic geological information of the subsurface soils, help to reconstruct the geotechnical model of the investigated slope, to identify the geometry and formation boundaries of the landslide body, to detect the possible failure surface and the fracture location, and to estimate the groundwater saturation and storage in an interested cross-section in the site (Perrone et al., 2014). Otherwise, series 2D ERT data can be used to reconstruct the 3D ERT model, providing a volumetric information of resistivity variations in the subsoil, which is very similar to that obtained from the 2D ERT, but in a spatial basis. Bichler et al. (2004) investigated the Quesnel Forks landslide in British Columbia, Canada using 3D ERT technique. In this study, a total of ten 2D ERT profiles, from two perpendicular directions, were gathered to reconstruct the 3D ERT diagram that was covering the whole investigated area, using the grid-based approach (see in Figure 2.22). From the 3D imaging, the rupture surface and separating boundaries between the sliding materials and the undisturbed strata, which are indicated by low resistivity portions, can be identified. Drahor et al. (2006) used similar approach to reconstruct the 3D ERT model from parallel and perpendicular 2D ERT cross-sections

in a graphical way (Figure 2.23), and successfully detected the failure surface of the landslide and the presence of a fault in the investigated area.

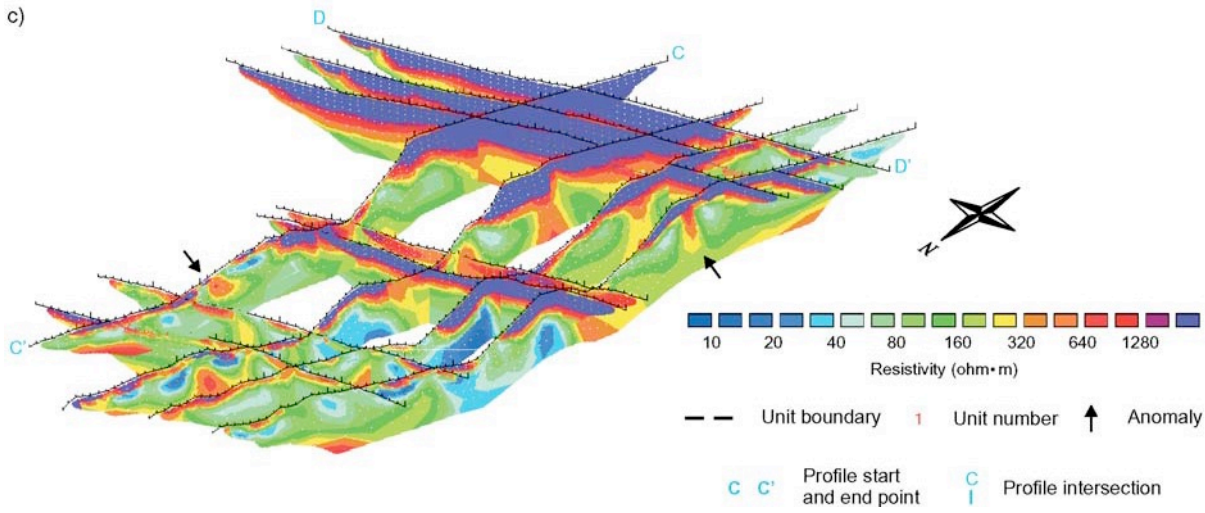

Figure 2.22 3D ERT diagram for the Quesnel Forks landslide constructed from two perpendicular 2D ERT data sets (Bichler et al., 2004).

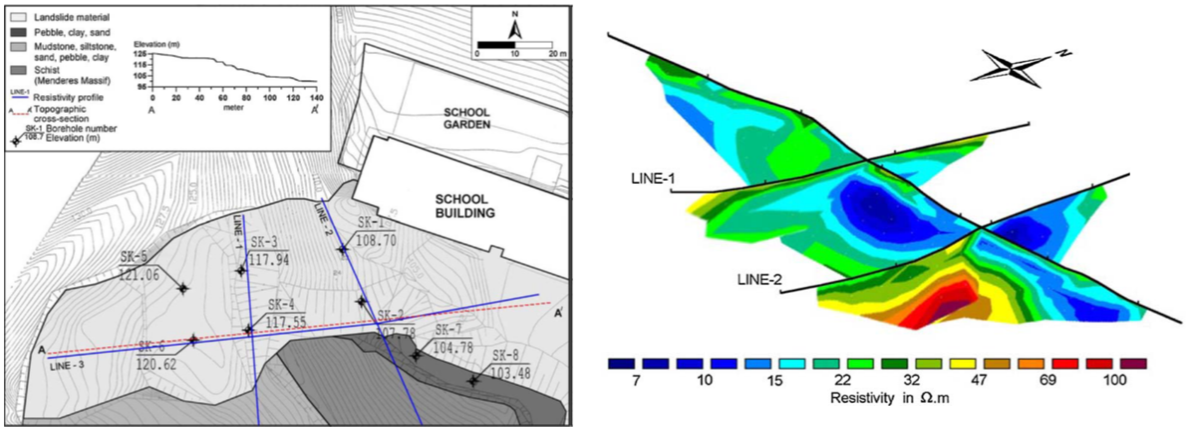

Figure 2.23 Local geological map of a landslide site in Turkey and the 3D resistivity diagram. (Drahor et al., 2006)

However, the 2D and 3D ERT only provide static electrical information of the subsurface soils. More recently, the developments in time-lapse ERT methods allow the change of resistivity in both space and time to be displayed. Most of the studies involving time-lapse ERT are aimed at identifying the groundwater movement and distribution within the slope subsurface (Whiteley et al., 2019). All of these studies were based on either 2D or 3D ERT model with additional time series variable. Chambers et al. (2009) used the ALERT system to investigate an active landslide at a site near Malton, North Yorkshire, UK. In the study, 2D time-lapse ERT method was employed to investigate the hydraulic

changes in the subsoil of the landslide (see Figure 2.24). From the percentage change in resistivity between two time series 2D profiles, the near-surface fissures, moisture accumulation zones and the evaporation boundary can be identified.

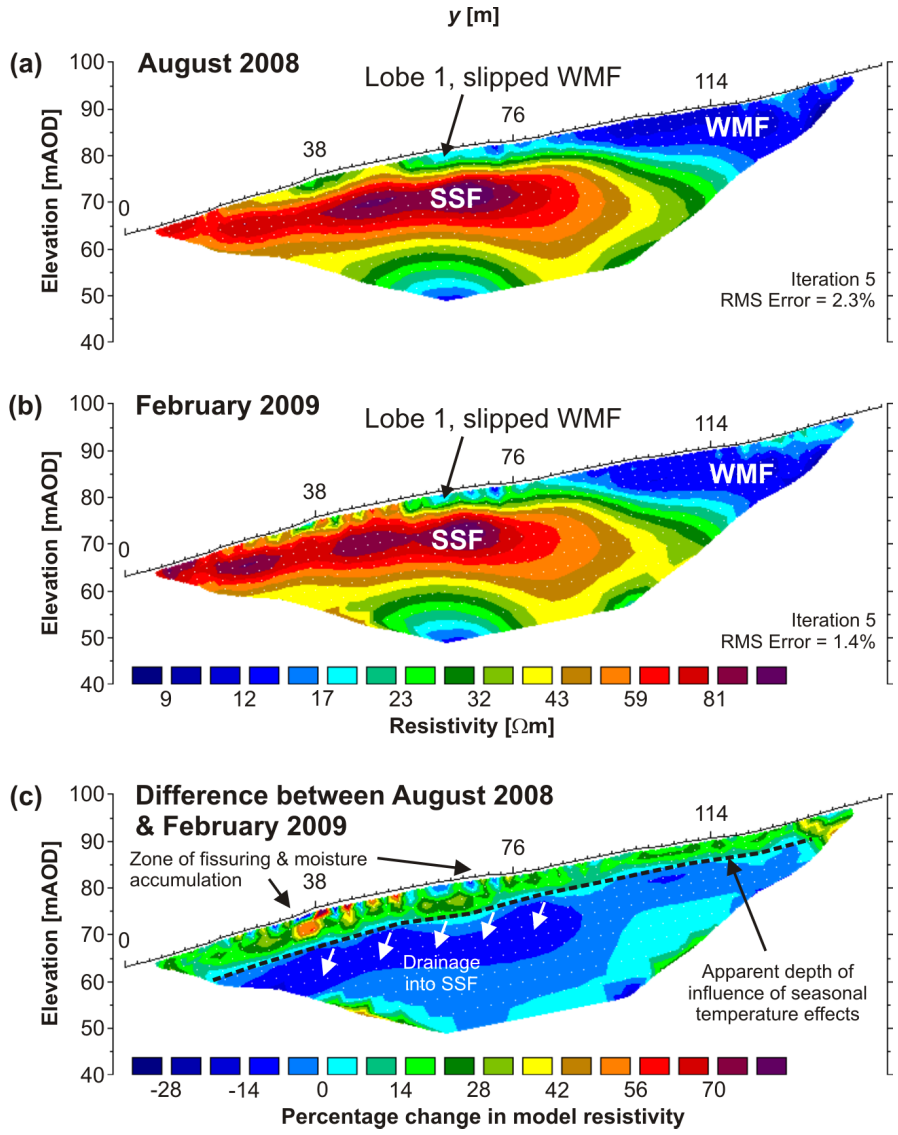

Figure 2.24 2D time-lapse resistivity results (a) August 2008 (b) February 2009 and (c) differential resistivity image (Chambers et al., 2009)

Uhlemann et al. (2017) employed 3D time-lapse method to image the hydrological processes in the Hollin Hill landslide in North Yorkshire, UK. In this study, the electrode movements in the sliding material has been considered and taken into account to the inversion models to eliminate the possible artefacts in the electrode configurations (Wilkinson et al., 2016). In addition, the resistivity data were converted to moisture content data by fitting with a Waxman-Smits model (Waxman and Smits, 1968), which was established based on the experimental data. Figure 2.25 shows the time-lapse

volumetric images of moisture content data, which presents the hydrogeological variations in the landslide body. Both the shallow and deeper moisture dynamics were imaged to be assessed incorporating with the local lithological model. The shallow moisture behaviour involves the seasonal infiltration activities in winter and the near surface moisture decreasing during summer, whereas the deep moisture dynamics are related to the regional ground water table and the drainage path from upper mudstone to the underneath sandstone formation. Additionally, the crack development during the reactivation period of the landslide and the formation of ponds during post-reactivation were captured from the 4D time-lapse imaging.

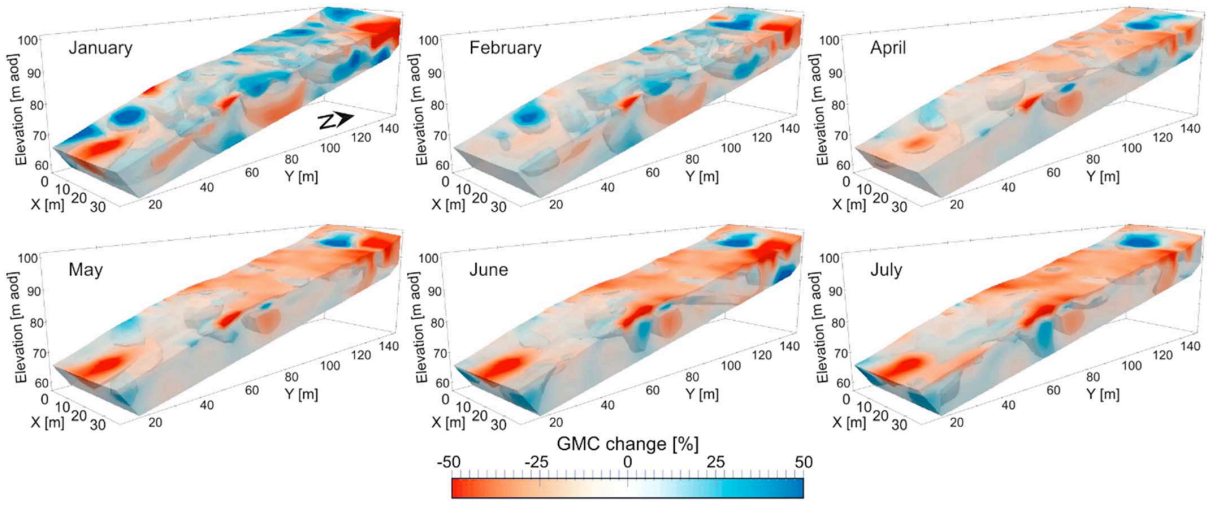

Figure 2.25 3D gravimetric moisture content (GMC) images extrapolated from a 3D time-lapse ERT model (Uhlemann et al., 2017).

A similar study undertaken by Hen-Jones (2018) employed both 2D and 3D time-lapse ERT to investigate the hydrogeology and hydraulic changes in the subsurface of a research embankment (Hughes et al., 2009) at Nafferton Farm in Northumberland. The ERT data was converted to 2D and 3D GMC images using the same geotechnical-geophysical transformation approach. Furthermore, the GMC data derived from ERT profile was subsequently converted to a suction distribution diagram (Figure 2.26) by fitting a Van Genuchten model (van Genuchten, 1980) through the drying and wetting SWR data obtained from laboratory experiments. The ERT-derived data (i.e., GMC and suction data converted from ERT measurements) were compared with the data that were directly measured from the point measurement sensors. The results suggested that resistivity can be well-used as a water content indicator if appropriate proxy relationships between resistivity and water content were established. However, the author pointed out

that the estimated soil suction from ERT-derived data showed limited quantitative agreement with the suction values measured by the point sensors. This may be attributed to the differential in between the laboratory and in-situ SWR behaviour, since the SWRC properties (e.g., AEV, shape, saturated water content, hysteresis) vary from many factors such as the as-compacted conditions and volumetric changes. In this case, the laboratory-derived proxy relationships (i.e., SWRCs) that are more representative of the field condition, are required for the application of estimating soil suction using ERT-derived data. Additionally, the abilities of 3D ERT to capture crack development and the rapid infiltration activities from heavy precipitation were identified through the time-lapse surveying.

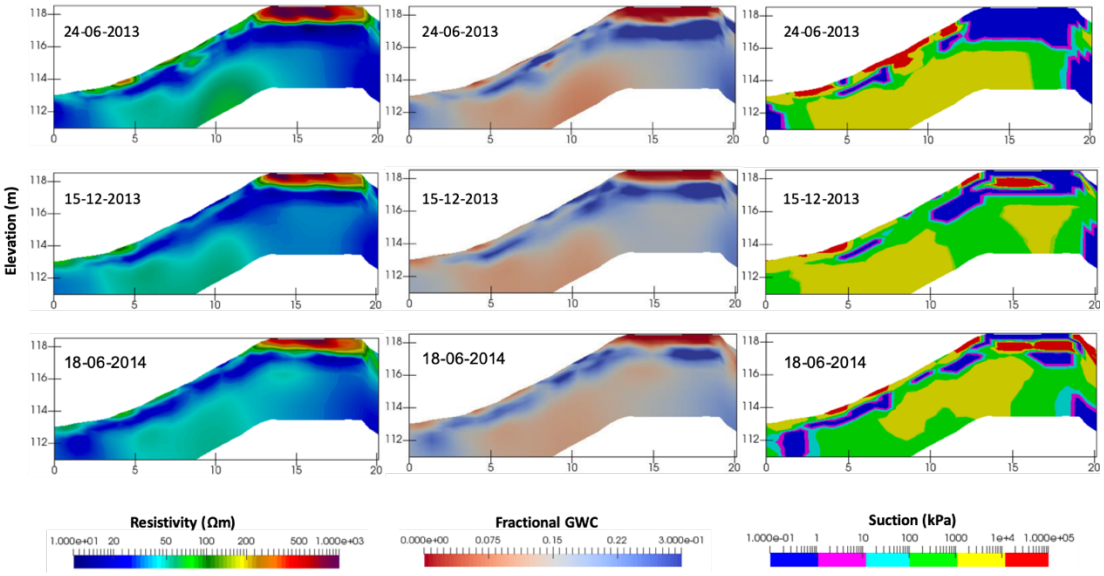

Figure 2.26 Time-lapse 2D ERT profiles and the converted GWC and suction images, modified from Hen-Jones (2018).

However, in most of these previous studies, ERT data have been successfully used to qualitatively describe the relative changes in soil resistivity and water content, whereas limited data were found to provide quantitatively measurements that can be compared to the reference measurements from other techniques. Future work to investigate the potential use of ERT data for quantitatively describing the soil water content and other geotechnical properties through laboratory and field tests is very important (Gunn et al., 2018; Hen-Jones, 2018).

2.8 Chapter summary

The literature review presented in this Chapter forms the background knowledge of the thesis. It can be summarised as follows:

The future climate is going to be hotter, drier summers and milder, wetter winters with more intense rainfalls in the UK according to the climate change projections. Such a change in atmospheric conditions will make the soils in the engineered slopes subjected to more frequent cyclic drying and wetting and influence the soil properties related to the slope stability.

Many factors may be involved in the failure of slope, but the rainfall-induced suction and shear strength changes are likely to be the important roles, especially relevant for the low permeable and expensive clays that widely spread in the UK. The seasonal water content changes result in deterioration in soil suction (i.e. negative pore water pressure) and hence the effective stress which controls the shear strength of the slope soils. Soil suction can be determined from the soil water retention curves, which are hysteretic between drying and wetting paths. As the soil water retention capacity deteriorated over time driven by the seasonal water fluctuations, the relevant strength parameters determined from laboratory tests have gradually become unreliable for the long-term stability assessment of the engineered infrastructure (Glendinning et al., 2018; Stirling et al., 2020). So that the determination of soil water retention behaviour for engineered soils under effect of drying-wetting cycles can help to understand the long-term shear strength behaviour of the soils. However, the suction measurements are limited in low or high suction ranges due to restriction of measurement techniques (Al-Mahbashi et al., 2018). SWRC data are rare for expansive soils over both the low and high suction range under repeated drying and wetting cycles. Since the soil deterioration is closely related to the microstructure change due to cyclic swelling-shrinking behaviour of clays, which is controlled by the soil type and drying-wetting history, the data of soil water retention and shear strength characteristic curves determined over a more completed water content (suction) range may contribute to an improved understanding of soil deterioration. Determination of SWRCs over a wide range of suction (water content) can be performed using the combination of different techniques (Agus and Schanz, 2006; Delage et al., 2008).

The real-time monitoring of soil water content using remote sensing and the geophysical methods is aneffective tool for predicting the potential slope failures and assessing the slope stability (Glendinning et al., 2018; Gunn et al., 2018; Tang et al., 2018a). Point moisture sensors are widely used in the laboratory and field moisture determinations, but only provide point measurement. As the electrical resistivity of soil is closely related to the soil water content, the ERT-based slope monitoring system has now been developed to monitor the water content changes in the engineered slopes associated with the laboratory determination of the interrelationships between the soil resistivity and water content (Chambers et al., 2014; Hen-Jones et al., 2017). In most of these previous studies, ERT data have been successfully used to qualitatively describe the relative changes in soil resistivity and water content, whereas the comparable data for quantitative assessment are very limited. Further work to quantitatively describe the geotechnical properties using ERT techniques has important implications for monitoring and early prediction of the slope stability (Hen-Jones, 2018). Additionally, the effect of repeated drying and wetting cycles on resistivity behaviour needs to be more fully understand in order that the ERT data can be effectively used to indicate water content of soils. Further work is needed for determining the interrelationships between soil moisture and resistivity and the effect of seasonal water content changes on their relationships.

Considering this context, the identified gaps of knowledge are described as follow:

- Deterioration of soil suction (i.e. negative pore water pressure) and strength property driven by drying-wetting cycles has been identified in previous study, but it still needs to more fully understood by investigating the SWR behaviour and shear strength behaviour of engineered soils subjected to multiple cycles of drying and wetting conditions.

- SWRC data are rare for clays over both the low and high suction range under repeated drying and wetting cycles. Determination of SWRC and shear strength data over a more completed water content (suction) range through laboratory experiments is needed to get a more thorough understanding of soil deterioration. The determination of SWRC over the entire water content range can be achieved by combination of different suction measurement techniques.

- ERT data have been successfully used to qualitatively describe the relative changes in soil resistivity and water content, whereas limited data were found to provide quantitatively measurements that can be compared to the reference measurements from other techniques. Future work to investigate the potential use of ERT data for quantitatively describing the soil water content and other geotechnical properties through laboratory and field tests is very important.

- Further work is needed for determining the interrelationships between soil moisture and resistivity and the effect of seasonal water content cycling on their relationships in order that the ERT data can be effectively used to indicate water content of soils.

3 Methodology

3.1 Introduction

This chapter describes the principles, procedures and techniques used in the experiments to achieve the objectives stated in Introduction Chapter. The methodology consists of three parts that represent three laboratory-based experiments:

a) Investigation of soil properties using point sensors in a box lysimeter.
b) Laboratory investigation of soil property relationships under drying-wetting cycles.
c) Investigation of geotechnical-geophysical relationships in a lysimeter with a 1.2-m diameter.

3.2 Investigation of soil property relationships using different devices in a soil box lysimeter

3.2.1 Introduction

In this laboratory programme, a glacial till material obtained from the BIONICS (Biological and engineering impacts of climate change on slopes) embankment (Hughes, 2009) were compacted into a plastic box using dynamic compaction to obtain a dry density and water content close to nature conditions. Four different water content sensors and four suction measurement devices were installed in the soil to measure hydraulic and electrical properties under cyclic drying and wetting processes. The soil properties measured in this programme included volumetric water content, pore-water pressure, conductivity (the reciprocal of resistivity).

3.2.2 Construction and materials of soil box lysimeter

The remoulded BIONICS glacial till materials was compacted into a cubic container to construct the soil box lysimeter. Four different water content sensors and four suction measurement devices were installed in the soil to measure hydraulic and electrical properties. Figure 3.4 shows a three-view drawing of the construction of soil box lysimeter along with the locations of the testing devices. To perform measurements in similar soil conditions during drying and wetting, the devices were placed at the same

depth of the soil sample and were expected to locate close enough. For these purposes, an 84L (610 mm × 390 mm × 355 mm) cubic plastic box was used as the soil container in this test. The size of the container was considered appropriate because the volume of such a container was large enough to accommodate all the instruments and arranges them at the same depth based on the measurement volume of the instruments. It is also a suitable size for observing the cracking behaviour on the surface of the sample and leaving enough depth for the instrument to avoid the influence of surface cracks on the instruments during drying and wetting. 103 kg of BIONICS materials were compacted into the box to form a 210-mm height soil sample. The details of the BIONICS glacial till material can be found in subchapter 3.3.2. The sample was initially compacted at 25% gravimetric water content (GWC) which was wet of optimum water content of 15.4% (as shown in Table 3.2) and representative of the saturated water content used for describing the SWRC of BIONICS materials in numerous previous studies (Glendinning et al., 2018). To determine the SWRC in the whole suction range, the initial dry density of 1.6 Mg/m^3 was targeted to achieve a near saturated initial condition. Various commercial moisture and water potential measurement devices were arranged at half the depth of the soil sample, as shown in Figure 3.3, to monitor the electrical and hydraulic changes.

3.2.3 Soil water content and suction measurement devices

Various point sensors were employed in this experiment to measure the water content, suction, and bulk electrical conductivity/ resistivity of the soil sample under drying and wetting cycles. The instruments used in this experiment are as follows:

- Two 5TE sensors and MPS (1,2 and 6) sensors from Decagon Devices.
- An Ml2x probe from Theta Probe.
- A CS640 time domain reflectometry (TDR) probe from Campbell Scientific Inc.
- A TDR probe developed in the ROBUST project, which is referred to 'TDR-R' probe in this thesis.
- A high capacity tensiometer (HCT) made in Durham University.

The TDR probes, 5TE sensors and ML2x probe measure the apparent permittivity (i.e., square root of the permittivity/dielectric constant) using time domain, frequency domain and amplitude domain techniques, respectively. Decagon MPS (1,2 and 6) sensors and tensiometer were used to estimate matric suction of soil sample. Additionally, The TDR

probes the 5TE sensors could also provide the measurements of the soil bulk electrical conductivity. Figure 3.1 shows the pictures of the point sensors employed in this experiment.

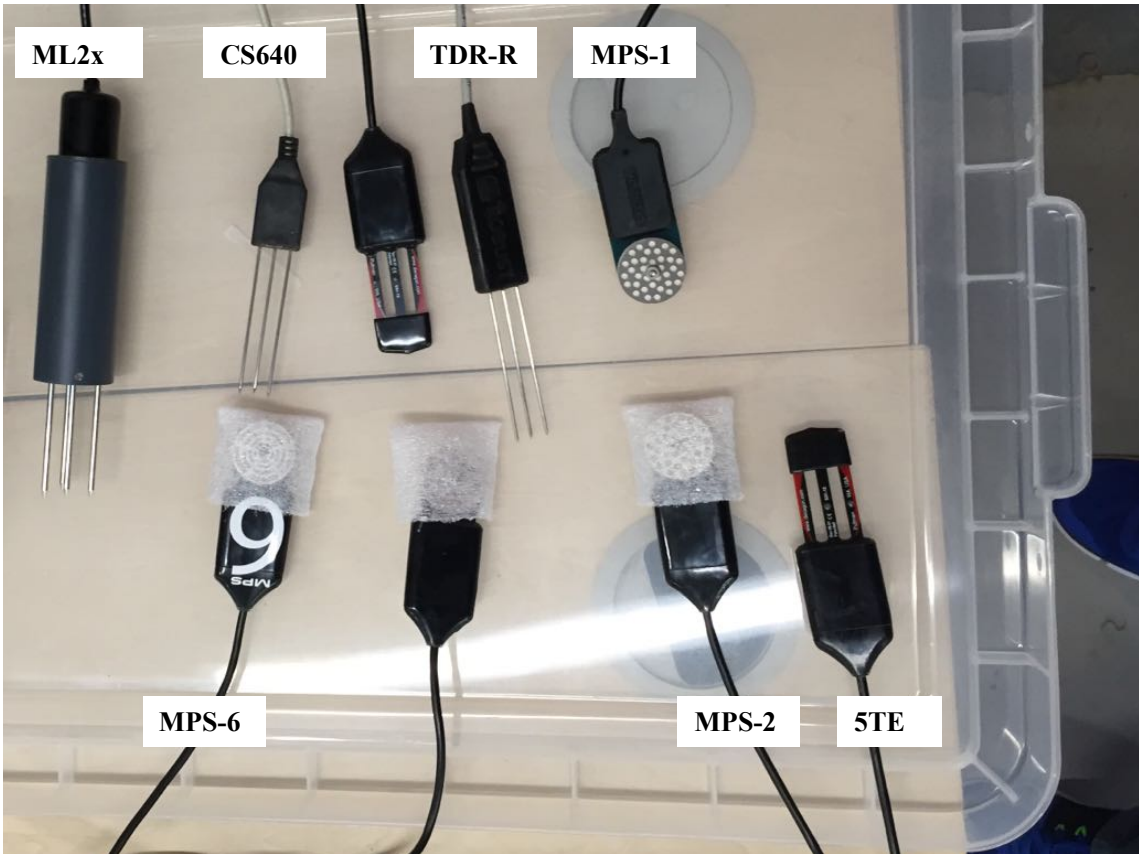

Figure 3.1 Pictures of the instruments used in this experiment.

3.2.3.1 Specifications

Table 3.1 shows the specifications of the point sensors employed in this experiment. The specification information of these sensors was referred to Decagon Devices (2016), Delta-T Devices Ltd (2009), Campbell Scientific Inc. (2017) and J.D. Asquith (2015).

Table 3.1 Specifications of point sensors used in soil box

Sensor type	Property measured	Range	Resolution	Accuracy
5TE	VWC	0 to 100% VWC	0.08% VWC	±3% VWC
	Bulk conductivity	0 to 23 ds/m	0.01 ds/m	±10% from 0~7ds/m
	Temperature	-40 ℃ to 60 ℃	0.1 ℃	±1 ℃

ML2x	VWC	5 to 60% VWC	0.1% VWC	±2% VWC
TDR probe	VWC Bulk conductivity	0 to 100% VWC 0 to 5 ds/m	- -	- -
MPS-1	Pore water pressure	-10 to -500 kPa	0.1 kPa	-
MPS-2 & MPS-6	Pore water pressure Temperature	-9 to -100,000 kPa -40 ℃ to 60 ℃	0.1 kPa 0.1 ℃	- ±1 ℃
Tensiometer	Matric suction	up to 1,500 kPa	0.1 kPa	-

3.2.3.2 Calibrations of decagon sensors

MPS-1, 2 and 6 sensors were using factory calibration built in to the EM50 datalogger.

Two 5TE sensors were calibrated with the soil specific calibrations and the calibration results are presented in subchapter 4.2.1.

3.2.3.3 Calibration of ML2x probe

The ThetaProbe ML2x probe measures volumetric water content θ_v by measuring the apparent dielectric constant ε based on the certain relationship between them proposed by Topp et al. (1980):

$$\sqrt{\varepsilon} = a_0 + a_1 \times \theta_v \quad (3.1)$$

where a_0 and a_1 are two coefficients related to the soil type.

The ML2x probe responds sensitively to the changes in dielectric constant ε of the soil, and it converts these changes to a voltage output V (ThetaProbe ltd., 1999). The relationship between these two properties can be expressed as follows:

$$\sqrt{\varepsilon} = 1.07 + 6.4V - 6.4V^2 + 4.7V^3 \quad (3.2)$$

Therefore, the calibration process is to determine the coefficients a_0 and a_1. For mineral soil, a_0 and a_1 are suggested to be 1.6 and 8.4, respectively. Combining the equations

1and 2, the final calibration relationship between voltage output V of ML2x probe and volumetric water content θ_v shows a non-linear curve (as shown in Figure 3.2), and is written as

$$\theta_v = -6.309 + 7.619\times10^{-2}V - 7.619\times10^{-5}V^2 + 5.59\times10^{-8}V^3 \qquad (3.3)$$

However, a soil specific calibration was established for ML2x probe based on the relationship between the sample VWC and the dielectric constant response of the probe to be compared with the default empirical calibration and is presented in subchapter 4.2.1. The result suggests that a soil specific calibration is necessary for the ML2x probe to provide more accurate readings of VWC for the glacial till material.

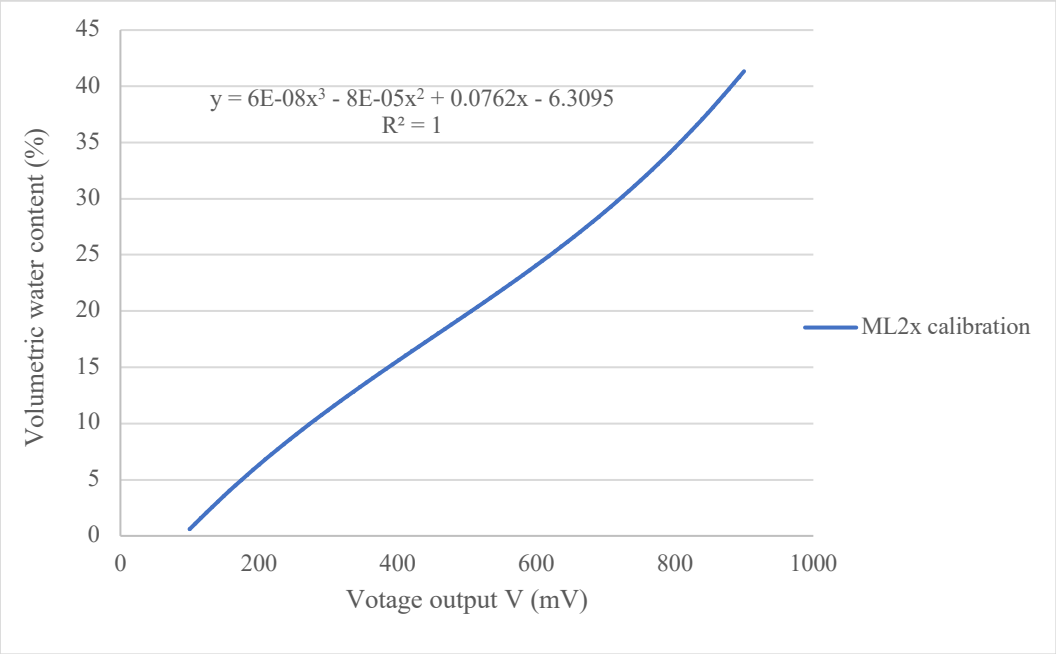

Figure 3.2 Calibration curve of ML2x probe

3.2.3.4 Saturation and calibration of a high-capacity tensiometer

Saturation

A good performance of a high capacity tensiometer relies on sufficient saturation to remove free air from the high air entry value (HAEV) ceramic plate and water reservoir, preventing cavitation at high suction. Cavitation in a tensiometer is the formation of vapour cavities in the water as a consequence of increasing tension induced by the negative pore water pressure to which the tensiometer is exposed.

Furthermore, saturation was carried out to remove the air within the ceramic stone and water reservoir of the tensiometer and refill the spaces with de-aired water. The detailed procedures are stated below:

1. The tensiometer was inserted into a sealed stainless-steel saturation manifold.
2. A vacuum was applied to the saturation manifold to remove any air from the tensiometer and inner space of the manifold.
3. The de-aired water was refilled into the saturation manifold using a pump during vacuuming to saturate the tensiometer's ceramic stone and water reservoir.
4. The saturation manifold was then pressurised to 1 MPa using a pressure controller to further remove the present air within the tensiometer. At least a two-week pressurisation period was needed for a new tensiometer undergoing its first saturation and for a tensiometer that was dry or long from cavitation. A shorter saturation period – normally 2 days – was used for a freshly cavitated tensiometer.

Calibration

Once the tensiometer had been fully saturated from the saturation system, it was calibrated before use. The calibration was carried out in the positive range and extrapolated to the negative range as performed by Lourenço (2008).

The calibration process involved 1) stepping down the pressure in the saturation manifold from 1,000 kPa to 200 kPa at an interval of 200 kPa using a pressure controller, 2) recording the voltage response output by the embedded force transducer and 3) stepping up the pressure in the manifold back from 200 kPa to 1,000 kPa and recording the voltage output to check for hysteresis.

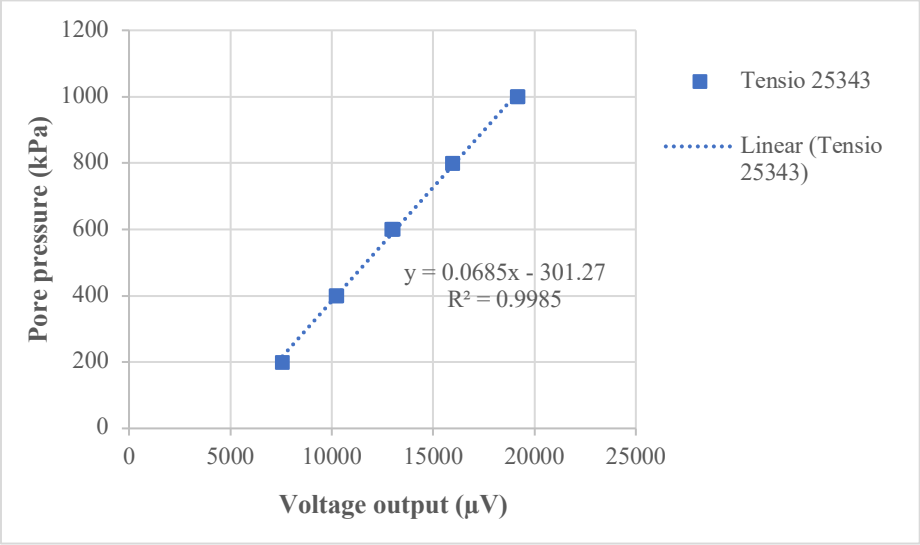

Figure 3.3 Calibration relationship between the pressures allied to the manifold and the voltage output of the force transducer.

Figure 3.3 shows the calibration curve of the tensiometer – number 25343 – used in this programme. It indicates a linear relationship between the pressure allied to the tensiometer and the voltage response of the tensiometer's force transducer. An R-squared value equal to 1 indicates perfect fitting by the calibration points with the linear regression mode. However, the tensiometers whose R^2 values are closely approaching 1 are also considered to be reliable in measurements of suction, such as the one used in this programme.

3.2.3.5 Installation of sensors

The probes and sensors were installed into the soil horizontally at half the depth of the sample in an arrangement as shown in Figure 3.4. Once the third layer of soil was compacted into the plastic box, soils were trimmed from the sample surface at the designated sensor locations using a small shovel to create rectangular potholes that were slightly larger than the sensor sizes.

For the two TDR probes and Theta-probe (ML2x), installation method is directly inserting the coaxial rods of probes into the soil sample horizontally from the lateral wall of the potholes. The process was carried out carefully and slowly to avoid any deviation of probe's rods and contact with hard materials.

Other sensors that do not have long and fine rods (5TEs and MPS-1, 2 & 6), were first coated with bulk soils to maintain good contact between the soil and the sensor prongs

(or the ceramic sensor heads), then placed horizontally in the potholes, letting the sensors lied on the pothole base. The soils cut out were than backfilled to the potholes.

The tensiometer was installed with assistance from a plastic guide through a Poly Vinyl Chloride (PVC) tube. Wet soil paste was used as slurry at the face of the tensiometer to ensure good contact between the probe and the soil.

Once the devices were all buried in the potholes, the soil was filled back up to level the surface. The back-filled soils were compacted more slightly and carefully upon the sensors using a 0.5kg round PVC bar, considering that the large compaction effort may cause large change in the density of the surrounding soils and shake the underneath sensors. The cables of the devices were passed through the holes drilled on the wall of the plastic box and connected to data loggers.

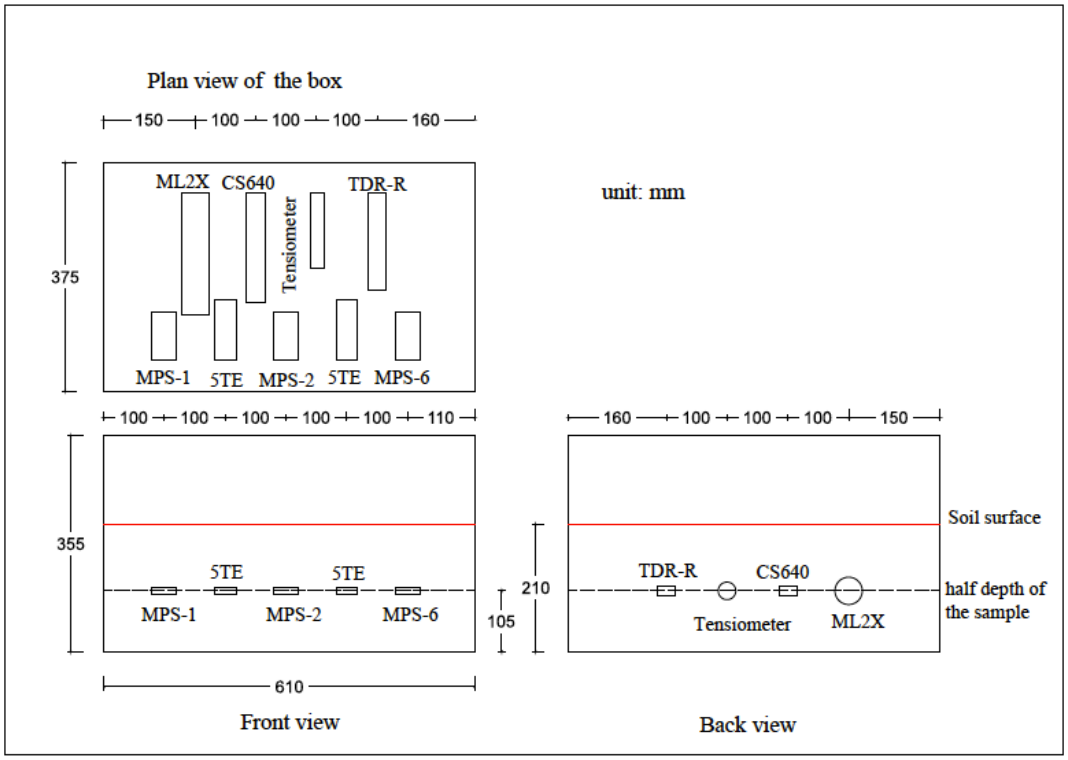

Figure 3.4 The plan view and side views showing the construction of the soil box lysimeter and the employed devices

3.2.4 Sample preparation

The original BIONICS soil was remoulded in the laboratory to achieve an initial water content of 25% and an initial dry density of 1.6 Mg/m^3. By calculation, 103 kg of remoulded soil was required.

The soil sample preparation methodologies adopted are as follows:

1) The soil was air dried at room temperature.
2) The soil was crushed using a crushing machine and sieved through a 2 mm sieve to remove large particles.
3) The sieved material was sealed in a plastic container to equalise for 24 hours, and samples were taken to measure the residual water content.
4) 105 bags – each containing 1kg of soil – were prepared to mix with rainwater.
5) Soil was mixed with water using Hobart rotary mixing machine to achieve the target gravimetric water content (GWC) of 25%.
6) All the mixed soil was sealed in plastic bags and left to equalise for at least 24 hours before compaction.

3.2.5 Compaction

The dynamic compaction was used in this experiment for compacting soil materials into the cubic box container manually by using a 5 kg hammer. Considering that relatively large volume of soil needed to be compacted, compacting all the soils in one time was not applicable as it would make the upper part of the compacted sample denser than the lower part. The decision was thus made to compact the sample by five layers in order to get a more uniformly compacted sample. Consequently, 103 kg of soils were divided into five equal parts to be compacted into the soil box. The layered compaction may still cause some vertical anisotropy in the density of sample as extra compaction efforts would be applied to the lower layers during compaction of upper layers. However, the influence of extra compaction effort on the lower layers was thought to be not significant in this test since a near saturated as-compacted condition was targeted.

Five horizontal lines were marked at inside wall of box from the base in an interval of 42 mm to indicate the upper limit of each layer during compaction. 20.6 kg of soil for each layer was weighed out and evenly distributed in the soil box. A plastic sheet was then placed over the soil to maintain the water content and to prevent the wet soil from sticking to the hammer. The soil was manually compacted using a 5 kg metal hammer, with a 120mm square base and a long handle. The hammer was dropped along the inside wall clockwise with a constant drop height 150 mm and evenly covered the whole compaction area. For each layer, the soil was evenly compacted until the mark-line was reached. Once the third layer was compacted, soil was cut off from the positions of each sensor to allow

them to be installed, the installation process of the sensors has been stated in section 3.2.3.5.

Considering that the TDR probe as well as other sensors need a seating time for allowing the settling of the soil around the rods/sensor heads to get good contact (Lane and Mackenzie, 2001), the compacted sample was left for a period of approximately one month before commencing the test.

3.2.6 Drying and wetting cycles

The soil sample was subjected to a cyclic drying and wetting process after compaction so that the effects of extreme weather (seasonal water content changes) on soil property relationships could be investigated. In this experiment, three drying and wetting cycles were achieved for the glacial till sample in a period of 28 months.

3.2.6.1 Drying process

Once the compaction was completed, the soil sample was covered by a plastic sheet at the top to allow moisture in the soil to reach equilibrium. When the readings of the sensors became stable, the plastic sheet was removed, and the sample was exposed to the air for drying until a residual water content of approximately 5% was achieved. However, in practice the water loss in soil sample became fairly slow when the VWC went down to approximately 13-15% (corresponding to about 7% GWC), as shown in Figure 4.2, the sample was not allowed to dry to an exact value of 5% GWC due to the time limitation. The drying processes ended up at approximately 14% VWC, 15% VWC and 20% VWC respectively for the first, second and third drying process.

3.2.6.2 Wetting process

Once the drying process had been completed, the soil sample was irrigated by water spray from the surface for wetting. The surface of the sample was fully covered by four thin cotton towels during wetting to ensure that the water could infiltrate evenly and slowly into the soil sample from the surface. The set-up of box lysimeter was weighing by a loadcell to monitor the mass change of the soil sample throughout the experiment. Results showed that 17.51kg water had been lost from the soil sample in the first drying period of 181 days, yielding a mean evaporation rate at approximately 0.4 mm per day. To give the sample a similar wetting rate to that of the drying and considering the presence of

evaporation simultaneously during the wetting period, the sample was recharged by water spray at an intensity of about 0.8 mm per day (double of the drying rate), meaning in an average of approximately 180 ml water was sprayed to the soil sample per day for wetting.

3.2.7 Data gathering

The devices from Decagon Devices (5TEs, MPS 1, 2 & 6) were logged by the EM50 data logger manufactured by Decagon Devices Inc.

The tensiometer and ML2x were connected to the MSL data logger and received by the TRIAX system (Toll,1999).

3.3 Laboratory investigation of soil property relationships under drying-wetting cycles

3.3.1 Introduction

In this testing programme, soil properties of three engineered clay materials were measured through laboratory tests to investigate the soil property interrelationships under successive drying and wetting conditions. The water content, suction, shear strength and electrical resistivity of the soil material were simultaneously measured using 38-mm diameter triaxial samples which subjected to drying and wetting cycles. Materials tested in this study comprised BIONICS glacial till, London Clay, and Hollin Hill Clay. The soil suction was measured using Decagon WP4C water potentiameter; the resistivity was measured using a four-point resistivity probe; and the undrained shear strength was determined through the British standard undrained unconsolidated (UU) triaxial test. The details of the methodologies used in this testing programme are presented in the following sections.

3.3.2 Testing materials

To investigate the soil property interrelationships of engineered soils under drying and wetting conditions, three representative clay materials were tested. The following soil materials were tested in this study:

1) **BIONICS glacial till**

The material collected from a research embankment in Nafferton Farm, Northumberland, Northeast of England, which is a part of the Biological and engineering impacts of climate change on slopes (BIONICS) project. The fill materials of BINOICS embankment was Durham lower boulder clay, sourced from the east of Durham city, UK (Hughes et al., 2009). Testing showed the material is a sandy clay of intermediate plasticity (plastic limit 19.5%, liquid limit 41.7% and plasticity index 22.2%), according to Figure 3.5 and Figure 3.6. The X-Ray Diffraction (XRD) analysis for the sub 2 μm fraction of the BIONICS materials suggested the clay mineral assemblages of BIONICS material composed of variable amounts of illite/smectite (percentage mean of 49 %), chlorite/smectite (mean of 5 %), illite (mean of 19 %) and kaolinite (mean of 26 %). The non-clay minerals found in the sub-2 μm fractions were quartz and lepidocrocite (Hen-Jones, 2018). This type of boulder clay is representative of UK transport infrastructures as it is typical of over 60% of the British Isles (Hughes et al., 2009).

2) Hollin Hill material

The material, which is derived from Whitby Mudstone Formation (Upper Lias Group), collected from the surface flow of the Hollin Hill landslide (Chambers et al., 2008). Results of the particle size distribution (PSD) test and Atterberg limit test suggested that the Hollin Hill material was a silty clay material of high to very high plasticity (plastic limit 31.1%, liquid limit 71.2% and plasticity index 40.1%). Results of mineralogy from XRD analysis showed the Hollin Hill material (surface flow) composed of variable amounts of illite-smectite (33.4%), kaolinite (21.6%), Mica (16.2%), quartz (18.4%), Albite (5.4%) and microcline (4.8%) (Merritt, 2014). The Hollin Hill clay is a representative material in the research for the landslides in UK. Approximately 50% of all landslides in Yorkshire occurred within the Lias Group. Particularly, the Whitby Mudstone Formation, which outcrop at Hollin Hill was the most prone to landsliding in North Yorkshire (Foster et al., 2007).

3) A weathered London Clay

The London Clay tested in this study sourced from a quarry site in Colchester, Essex, UK. The PSD test and Atterberg limit test suggested that the London Clay used in the study

was a silty clay of very high plasticity (plastic limit 28%, liquid limit 77% and plasticity index 49%). The soil presented a clay content of 56%, and a specific density of 2.72. The sub-2-μm clay mineral XRD analysis indicated that the Colchester London Clay samples have mean clay mineral assemblages of 44% smectite, 18% illite, 13% chlorite and 24% kaolinite, and small amount of quartz (Kemp and Wagner, 2006). The London Clay is an important type of fissured stiff clay deposited in the Tertiary, which is widely underlying in south-east of England, including most area of London (Nishimura, 2006).

These three clay materials are all representative soils in the geotechnical engineering practice, which are in close relation to UK infrastructures or geological hazards. Additionally, the three clay materials have different clay contents varies from 27% to 56% and have different plasticity of intermediate to very high plasticity. One of the objectives of this thesis is to investigate the soil property behaviour under effect of the drying and wetting cycles. A significant feature of expansive clay materials driven by the cyclic drying and wetting processes is the volumetric swelling and shrinkage behaviour. Since the swelling-shrinkage behaviour of clays is generally believed to correlate to the plasticity and clay content (Izdebska-Mucha and Wójcik, 2013; Widomski et al., 2018), the three soils, which were representative of different clay contents and different plasticity , were meaningful to be investigated.

3.3.2.1 Particle size distribution (PSD)

For all three types of soils, the materials of which had passed the 2mm sieve were used to make the 38mm diameter triaxial specimens (76mm in height). The particle size distribution (PSD) curves for the three soil materials are shown in Figure 3.5. The PSDs for the Glacial till and the London Clay were determined following the procedures described in BS 1377: Part 2 (BSI, 1990). The PSD data for Hollin Hill Clay material was obtained from the internal engineering geological report for the Lias Group produced by British Geological Survey (BGS) (Hobbs et al., 2012). From Figure 3.5, the glacial till, Hollin Hill Clay and London Clay have clay contents of 27, 40 and 56% respectively. The silt contents for the same types are 35, 52 and 36% respectively, indicating all the three materials have high clay and silt particle concentrations. The sand contents for the same types of soil are 38, 8 and 8% respectively. The PSD results show that the glacial till tested in this study is a sandy clay whilst the London Clay and Hollin Hill Clay are the silty clays.

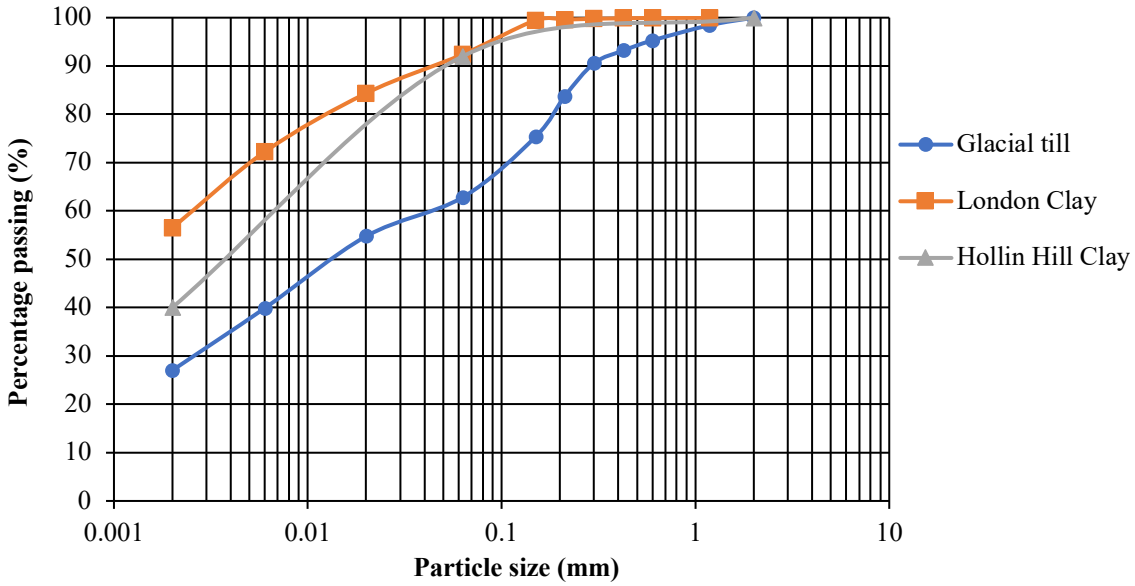

Figure 3.5 Particle size distributions (PSD) for the glacial till, London Clay and Hollin Hill Clay. The PSD data for Hollin Hill Clay is obtained from the Engineering Geological report for Lias Group by British Geological Survey (Hobbs et al., 2002).

3.3.2.2 Plasticity index

The results of Atterberg limits determined by cone penetrometer method for the liquid limit and the rolled thread method for the plastic limit following the BS 1377: Part 2 (BSI, 1990a) are presented on a Casagrande Chart in Figure 3.6. In the Casagrande chart, the A-line separates the claylike materials (plotted above the A-line) from silty materials (plotted below the A-line), and the B-line shows the upper limit for general soils. Testing of the materials suggested that the BIONICS glacial till, London Clay and Hollin Hill Clay are intermediate plasticity, very high plasticity, and high to very high plasticity clays, respectively. The results indicated that the three selected materials were representative of clay materials from a wide range of plasticity. A summary of index properties for the three soils are shown in the Table 3.2.

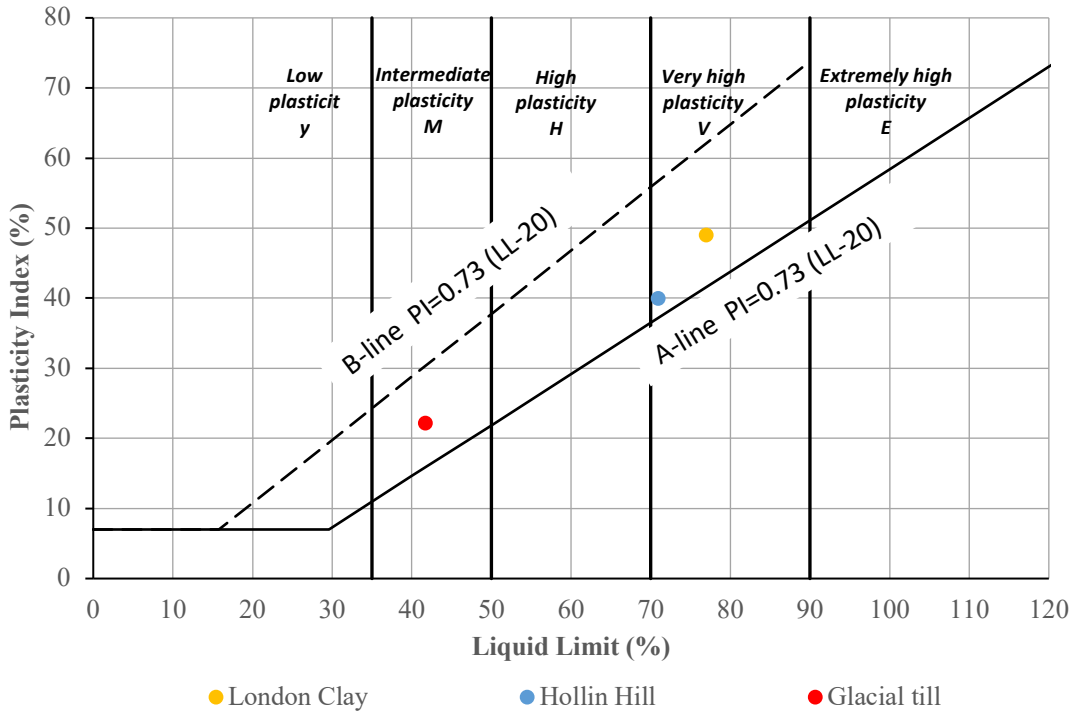

Figure 3.6 Results for Atterberg limit tests for Glacial till, London Clay and Hollin Hill materials, according to BS 1377: Part 2 (BSI, 1990a). A-line shows the boundary of clay (above) and silt (blow), whereas B-line shows the upper bound of general soils.

3.3.2.3 Compaction tests

Compaction curves were obtained for BIONICS material and London Clay by the BS light (Proctor) compaction test (BSI, 1990c), using a mechanical compaction machine with a 2.5kg hammer. The compaction tests were performed for determining the maximum dry density (MDD) and correspondent optimum water content (OMC) for the material under the certain compaction effort. In engineering practice, compaction of earth structures is suggested to be performed close to the optimum water content to give the materials the best performance. The compaction results of BIONICS material and London Clay are presented in Figure 3.7 and Figure 3.8 respectively, suggesting that the MDD and OMC for BIONICS soil are 1.81 Mg/m^3 and 15.5%; the MDD and OMC for London Clay are 1.40 Mg/m^3 and 30.1%. For Hollin Hill material, the compaction test was not conducted in this study due to insufficient soils. However, the historical data has shown that the MDD and OMC for Whitby Mudstone Formation (at Hollin Hill) are 1.71 Mg/m^3 and 15.4%, respectively (Hobbs et al., 2002).

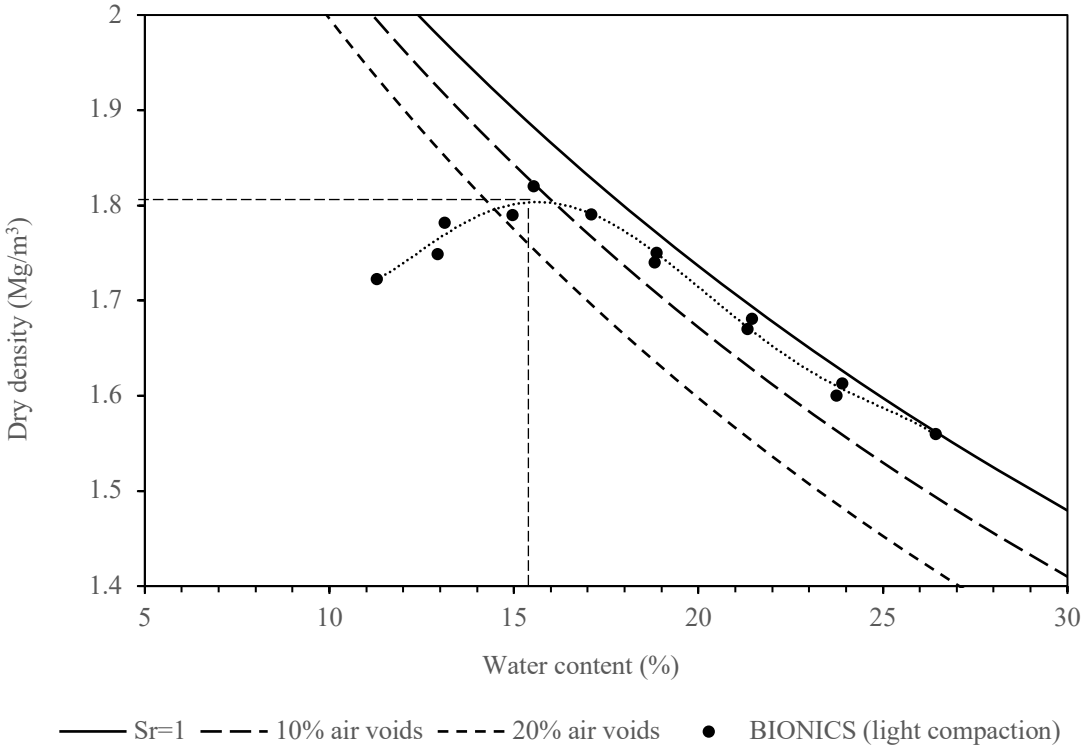

Figure 3.7 compaction curve for BIONICS glacial till material along with the air voids lines. (after Hen-Jones, 2018)

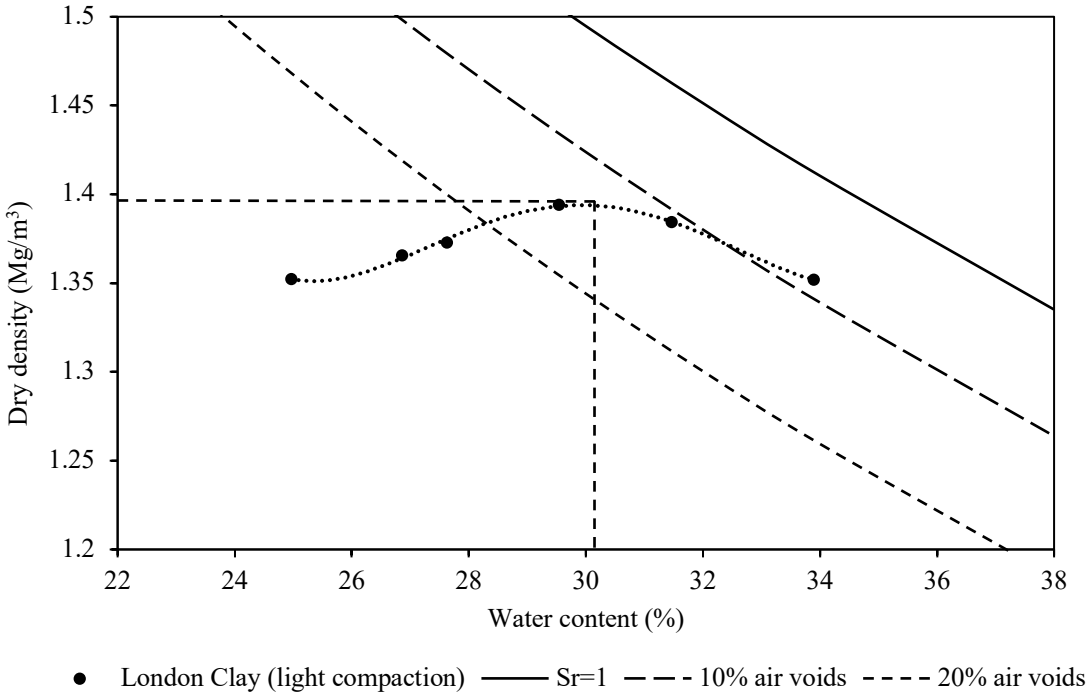

Figure 3.8 compaction curve for London Clay along with the air voids lines.

Table 3.2 Summary of the index properties of soils tested in this study

Index property			
Soil type	Glacial Till	London Clay	Hollin Hill Clay
Maximum dry density (Mg/m^3)	1.81	1.40	1.71
Optimum moisture content (%)	15.5	30.1	15.4
Plastic limit (%)	19.5	28	31.1
Liquid limit (%)	41.7	77	71.2
Plasticity index (%)	22.2	49	40.1
Specific gravity (Mg/m^3)	2.66	2.72	2.65

3.3.3 Sample preparation

One of the important purposes of this testing programme was to measure the soil properties (i.e., water content, suction, resistivity, and shear strength) simultaneously on the same soil specimen, in order that the property relationships can be directly established from the measurements. To achieve this purpose a large number of specimens are required to be arranged at multiple water content stages within the drying and wetting cycles. Considering the efficiency and for saving the time of making sample and testing, quick undrained triaxial tests using samples with relatively small size (38mm diameter) was chosen for determining the undrained shear strength, resistivity and suction of the soils. The use of small size samples was known to give more variability than samples of larger size (e.g., 50mm and 100mm). For this reason, three repeated samples were prepared and tested at each water content stage to reduce the variability due to the sample size.

Sample preparation procedures are stated in this section using glacial till as an example. In order that the soil property relationships can be compared between different sample size, the initial conditions for the small triaxial specimens used in this testing programme

are mostly the same as for the box lysimeter sample to keep the consistency in as-compacted condition.

Bulk soil was first air dried to a residual condition and then crushed by a crushing machine with a plate spacing of 3 mm. The large gravel pieces were removed from the materials before crushing. The crushed material was passed through a 2-mm sieve to remove large particles and stones, and the material was then mixed with water using a large mixer to achieve an initial GWC of 25%. The wet bulk soil that was made was sealed in plastic bags and left to reach equilibrium for at least 24 hours. For each specimen, 173.5 g of soil was statically compacted into a standard 38-mm triaxial mould (see in Figure 3.9) to achieve an initial dry density of 1.6 Mg/m^3 and a porosity of 0.38, which corresponds to approximately a 96% degree of saturation.

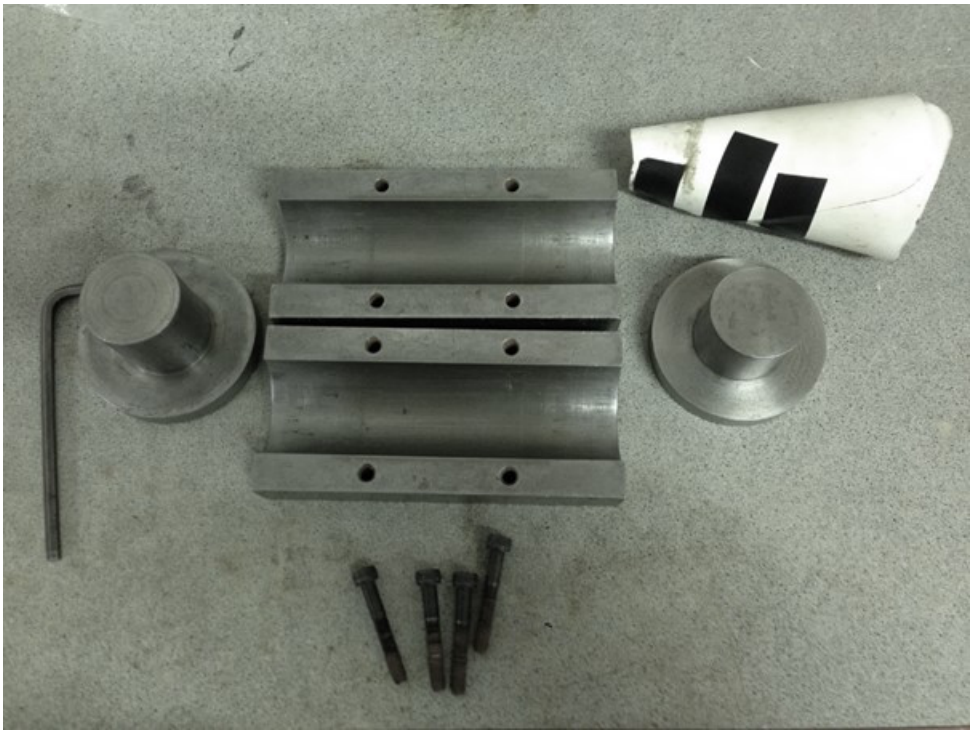

Figure 3.9 A 38-mm triaxial sample mould with a funnel (top right) for adding the soils

The sample-making procedures are as follows:

1) An amount of 173.5 g of soil was weighted out and divided into five equal parts.
2) Silicon grease was applied to coat the inner wall of mould for decreased friction between the soil and mould.

3) Each portion of soil was added into the mould through a home-made funnel (shown on the top right in Figure 3.9), and roughly compacted Using a small steel hammer to be slightly higher than one fifth of the depth of the mould.
4) The surface of the soil was scarified after each layer to improve interlocking between layers.
5) Once the last layer was completed, caps were installed on the two ends of mould, and the mould was statically compacted by a hydraulic compaction machine for at least five minutes.
6) The caps were removed, and the soil sample was pushed out slowly.

Once a specimen was made, it was wrapped in a plastic film and left to equalise for at least 24 hours before testing.

3.3.4 Drying and wetting cycles

The soil samples were subjected to repeated drying and wetting cycles, in order to investigate the soil property relationships under the seasonal moisture change, for the reasons reviewed in subchapter 2.5. The drying and wetting processes for the triaxial specimens are described in this section using glacial till material as an example. The drying and wetting processes for London Clay and Hollin Hill specimens are mostly the same as for glacial till material but started with different as-compacted conditions and numbers of drying-wetting cycles as shown in Table 3.3. The London Clay samples were prepared at 30% GWC with an initial dry density of 1.40 Mg/m^3 in accordance with its maximum dry density (MDD) and optimum water content (OMC). The BIONICS material and Hollin Hill Clay were prepared at 25% and 24% GWC, respectively, which were wet of optimum representative of the in-situ conditions in accordance with the previous studies using these materials (Glendinning et al., 2018; Hen-Jones, 2018).

Testing of the first drying and wetting cycle has been frequently investigated in the previous research and is not sufficient for investigating the long-term changes in the soil property relationships due to seasonal drying and wetting cycles. However, the two-cycle testing is still not sufficient as this is not able to make clear about the tendency of the changes in soil property relationships. For these reasons three-cycle testing is considered suitable herein for more thoroughly understanding the effects of repeated drying -wetting on the soil property interrelationships.

Table 3.3 Drying and wetting of three types of soil

Soil type	Initial GWC (%)	Initial dry density (Mg/m^3)	Residual GWC (%)	Number of dry and wet cycles
Glacial till	25	1.6	≈ 5	3
London Clay	30	1.40	≈ 6	2.5
Hollin Hill	24	1.61	≈ 4	1

For glacial till which is the most concerned soil in the study, 3-cycle was chosen. For London Clay, the initial condition was chosen based on the optimum water content and maximum dry density from BS light proctor compaction. For Glacial till and Hollin Hill material the initial condition was representative for the field condition.

In total, 183 specimens with 38mm diameter were made using Glacial till and subjected to three full drying and wetting cycles at different GWC stages. In one drying/wetting path, 33 specimens were distributed into 11 GWC stages from 5% to 25% with an interval of 2% GWC. Table 3.4 shows target water content stages of six drying and wetting paths (three drying and wetting cycles). For each water content stage, three repeated soil samples were prepared for repeated tests to reduce the variability due to the small sample size and ensure the reliability and repeatability of the tests.

Table 3.4 Water content (WC) stages of three drying and wetting cycles for the Glacial till material

WC stages / Cycle No.	1	2	3	4	5	6	7	8	9	10	11
1st drying	25%	23%	21%	19%	17%	15%	13%	11%	9%	7%	5%
1st wetting	25%	23%	21%	19%	17%	15%	13%	11%	9%	7%	←
2nd drying	→	23%	21%	19%	17%	15%	13%	11%	9%	7%	5%
2nd wetting	25%	23%	21%	19%	17%	15%	13%	11%	9%	7%	←
3rd drying	→	23%	21%	19%	17%	15%	13%	11%	9%	7%	5%
3rd wetting	25%	23%	21%	19%	17%	15%	13%	11%	9%	7%	←

For drying, the specimens were unwrapped, labelled, and placed in large trays to be air-dried (as shown in Figure 3.10).

Figure 3.10 The 38mm diameter triaxial soil specimens air-drying on the bench

For the wetting process, a humidifying chamber was used (Figure 3.11,Figure 3.12). The chamber was constructed in an 84L insulated box with two mist makers immersed in the water to produce mist. The soil specimens were placed above the water level supported by a steel grate. A plastic clapboard was placed on the grate above the mist makers to prevent the water splashing to the specimens. Before wetting, the target mass of each sample was calculated according to the target GWC shown in Table 3.4, and the soil sample was regularly weighed with an electronic scale during wetting process to control the GWC. Once the samples were wetted by the mist produced in the chamber to the target GWCs, they were then wrapped by the cling films for at least 24 hours for equilibrium before testing.

The significance of this cyclic drying and wetting process is to simulate the impact of cyclic moisture changes caused by extreme weather and to investigate how it influences the behaviour of soil suction, shear strength and resistivity.

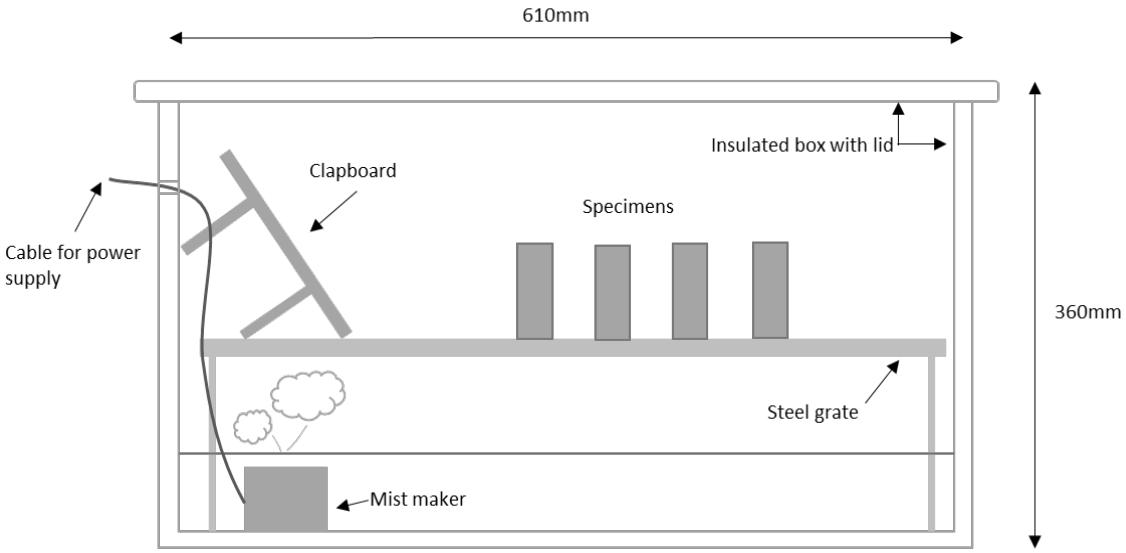

Figure 3.11 Schematic of the humidifying chamber

Figure 3.12 Humidifying chamber used to wet soil samples in this study

3.3.5 Laboratory testing methods

Once the sample was prepared, the resistivity was measured for each sample using a four-point resistivity probe prior to the triaxial test, as stated later in section 3.3.5.1. The soil sample was then put into the triaxial cell to measure the undrained shear strength through the unconsolidated undrained (UU) triaxial test. A piece of soil specimen was then sliced from the triaxial sample after the triaxial test to measure the soil suction using WP4C potentiameter (procedures see in section 3.3.5.3). Three repeated samples were tested for each water content stage of the drying and wetting cycles.

3.3.5.1 Resistivity measurement using a four-electrode resistivity probe

The square four-electrode probe developed in Durham University (Hassan, 2014) was used to measure electrical resistivity properties. The probe consists of four stainless steel electrodes with an inter electrode spacing, a, of 10 mm, and it is capped by a PVC frame with a diameter of 16 mm and a depth of 12.5 mm as shown in Figure 3.13. Silicone was filled within the frame between the electrodes to avoid interference between them.

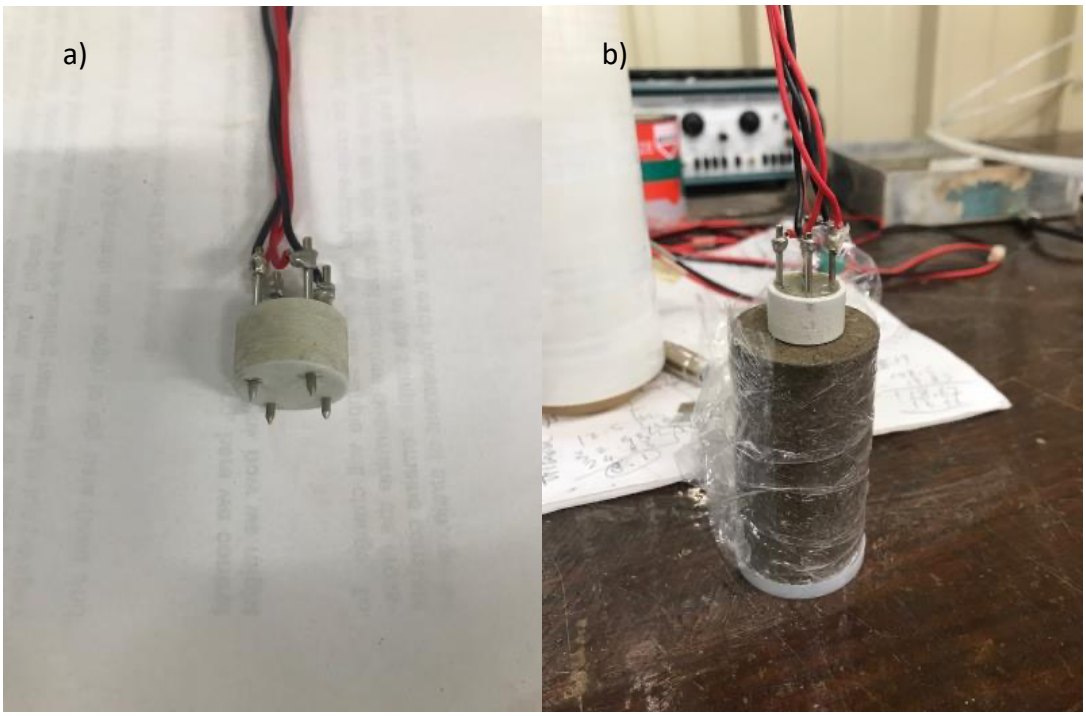

Figure 3.13 a) Four-electrode resistivity probe used for measuring soil resistivity; b) resistivity probe being installed on the soil sample

During the measurement, one pair of electrodes was connected to a low-frequency (95 Hz) AC power source for injecting current into the soil sample; another pair of electrodes

was used for potential measurement. A reference resistor, R_0 = 20 Ω, was connected in series to calculate the current of the circuit (see in Figure 3.14).

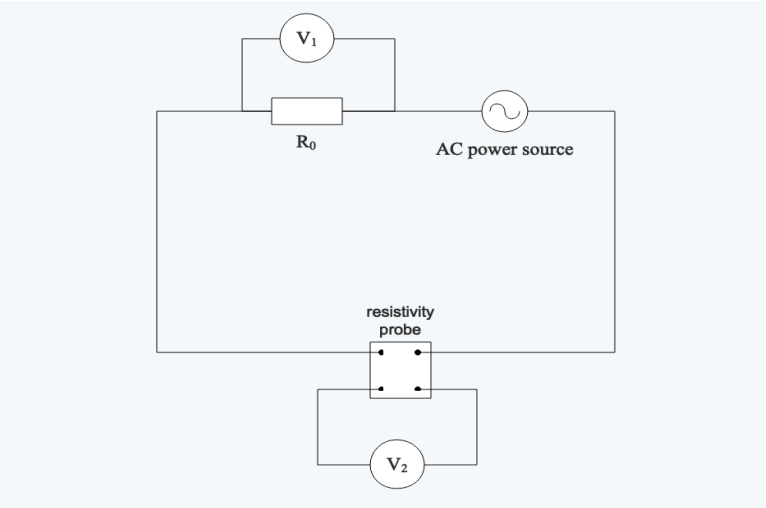

Figure 3.14 The circuit for measurement of resistivity using the square four-electrode resistivity probe

The resistivity can be determined using equation (2.44) associated with the readings of the two voltage meters (V_1 and V_2), which is expressed as:

$$\rho = K\frac{\Delta V}{I} = K\frac{V_2}{V_1/R_0} \tag{3.4}$$

The geometric factor, K can be simply calculated by equation (2.46):

$$K = \frac{2\pi}{\left(\frac{1}{C_1P_1} - \frac{1}{C_2P_1} - \frac{1}{C_1P_2} + \frac{1}{C_2P_2}\right)} = \frac{2\pi a}{2-\sqrt{2}} = 0.1073 \tag{3.5}$$

However, the theoretical equation (2.46) can only be used in an ideal condition that the measured sample should have a simi-infinite surface and to make point contact with the electrodes. Hence the resistivity probe was calibrated to determine the geometric factor K.

The Hanna EC meter manufactured by Hanna Instrument was employed for calibrating the resistivity system. The EC meter was firstly calibrated using three standard solutions of known conductivities (84 µS/cm, 1413 µS/cm and 12.88 mS/cm) produced by Hanna Instrument. To calibrate resistivity measurements over a sufficiently large range, samples of rainwater and distilled water were collected, as well as three solutions mixed from Hanna standard solution and distilled water. Table 2.1 shows the calibration results of the

resistivity system. The resistivity of samples was obtained by calculating the reciprocal of the conductivity values measured by Hanna EC meter. The apparent resistance measured by resistivity system was determined from the readings of two voltmeters (V_1 and V_2).

Table 3.5 Calibration results of four-point resistivity meter

specimens	conductivity (μS/cm)	resistivity (ohm.m)	V1 (mV)	V2 (mV)	apparent resistance (ohm)
distilled water	4.09	2444.99	0.38	445.46	23507.12
rainwater1	29.30	341.30	2.66	446.92	3360.30
rainwater2	30.10	332.23	2.99	476.03	3184.15
solution1	38.80	257.73	3.95	468.61	2372.71
84 μS/cm solution	84.00	119.05	8.18	467.30	1142.54
solution2	156.10	64.06	13.40	389.85	581.87
solution3	737.00	13.57	56.00	362.48	129.46
1413 μS/cm solution	1413.00	7.08	116	381.41	65.76

The calibration curve between resistivity and measured apparent resistance was shown in Figure 3.15. The geometric factor, K was equal to the slope of the line ($K = 0.104$), which was different to the value determined using theoretical equation. Hence the resistivity of soil samples can be measured using the resistivity probe by applying equation (3.4).

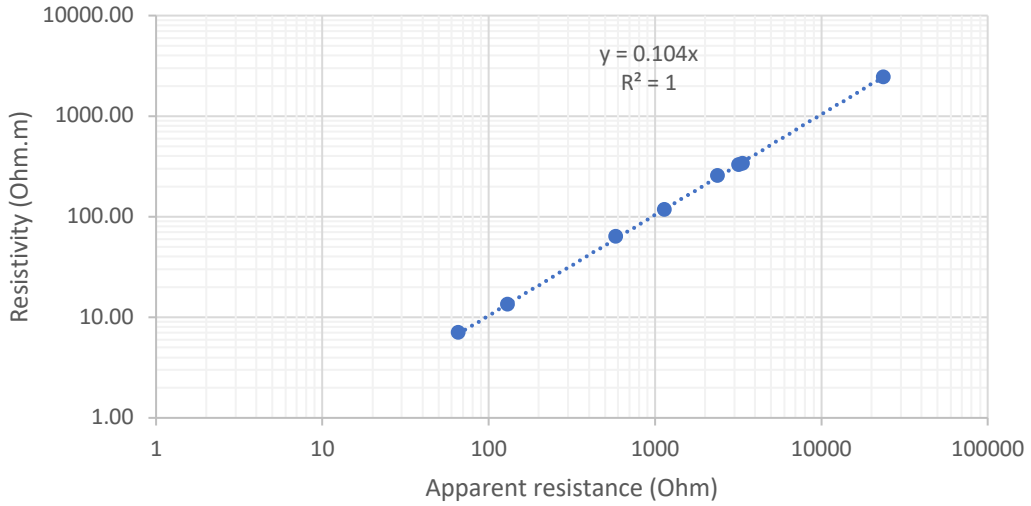

Figure 3.15 Calibration line for the four-point resistivity meter.

3.3.5.2 Undrained unconsolidated triaxial test

The undrained shear strength of specimens was determined through unconsolidated undrained triaxial test (UU test) using a triaxial compression apparatus. The testing processes followed the procedures described in BS 1377-7:1990 Chapter 8 (BSI, 1990d). All the specimens were compressed at a uniform strain rate of 1 mm/min. The UU test is typically used to determine shear strength of low permeability soils for a shallow foundation or other engineering infrastructures. For the UU triaxial test, a constant confining pressure of 100 kPa was applied to the soil sample, which represents the field condition with a soil depth of about 5m at which the soils were collected.

3.3.5.3 Suction measurement

Total suction measurement by WP4C PotentiaMeter

A small cylindrical sub-sample, normally with a thickness of 2-3 mm and a diameter of 3cm, was sliced off from the original triaxial specimen after triaxial testing to take a suction measurement using the WP4C water potential meter (manufactured by Decagon Devices), as shown in Figure 3.16.

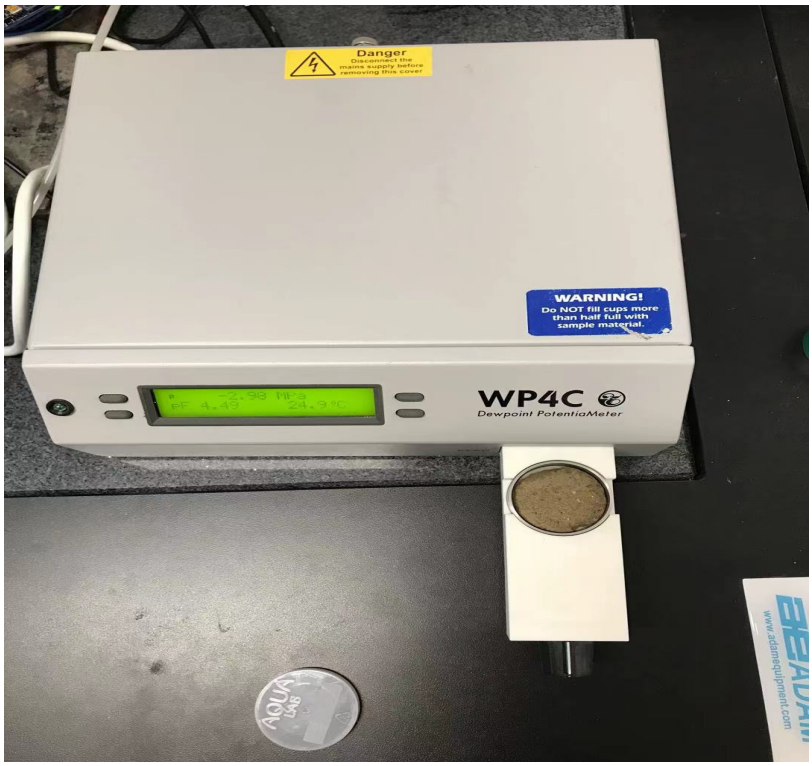

Figure 3.16 WP4C PotentiaMeter manufactured by Decagon Devices

The WP4C uses the chilled-mirror dewpoint technique to measure the water potential (total suction) of samples. It is suitable for the measurement of total suctions up to 100 MPa, whereas it has limited accuracy in the wet end of the suction range. It has an accuracy of 0.05 MPa in the suction range of 0 to 5 MPa, which results in an accuracy of ±5% of the reading at 1MPa and ±50% of the reading at 0.1 MPa. (Decagon Devices Inc., 2015).

Matric suction measurement by Durham SWRC apparatus

The dewpoint method derived by the WP4C is not able to measure the suction accurately in the wet end of suction range, especially where the suction is lower than 1MPa as discussed above. An alternative method was proposed to measure the soil water retention curves (SWRCs) for the wet moisture (low suction) range using the Durham SWRC apparatus (Toll *et al.*, 2015). The apparatus can provide continuous measurements of water content, suction and volume change. The apparatus is made up of a PVC fame placed on an electronic balance to measure the specimen mass, and hence determine the water content (Figure 3.17a). Four horizontal and two vertical linear variable differential transformers (LVDTs) are fixed on the frame to measure the volume change of the sample during drying and wetting so that the volumetric water content could be determined. The matric suction of sample was determined using a Durham high capacity tensiometer placed beneath the sample. A soil slurry was applied between the soil sample and the tensiometer to aid the contact. SWR data was determined for both drying and wetting paths using the apparatus for the BIONICS glacial till material. For the drying process, the sample was exposed to the air for drying; whilst for the wetting process, a clear plastic plate was placed over the soil sample to prevent evaporation, and four injectors were used to add water to the sample trough the holes in the plastic plate (Figure 3.17b).

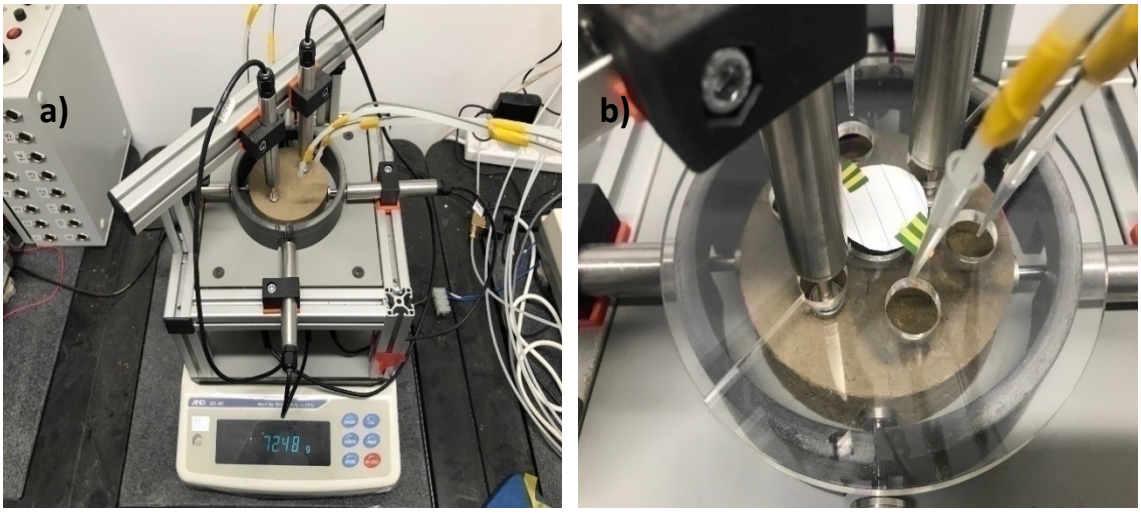

Figure 3.17 The Durham SWRC apparatus for measuring the soil water retention (SWR) data using the tensiometer: a) the overlook of the apparatus and b) an enlarged picture showing the sample condition during wetting

3.3.5.4 Water content measurement

The gravimetric water content (GWC) of each soil sample was determined following the procedure described in BS 1377:Part 2:1990 (BSI, 1990a). The remaining soil sample was placed in a small tray, and the mass of both the tray and the wet sample was measured by a digital scale before sending them into a 105 ℃ oven. After heating for at least 24 hours, the dry mass of the sample was weighed, and the GWC can be calculated. For each sample, only a small piece of soil was sliced off (with 2-3 mm thickness) for testing the suction by WP4C. All the remaining samples were put into the oven to measure the GWC. Therefore, the GWC measured can be treat as the average value of whole sample. Before testing, all samples were wrapped in cling film and left for at least 24 hours for water equilibrium. The GWC was thought to be consistent in the samples.

3.4 Investigation of geotechnical-geophysical relationships in a large cylindrical lysimeter

3.4.1 Introduction

A lysimeter allows soil to be segregated from its surroundings, and to some extent, it is closer to the natural conditions in site. The lysimeter test lies somewhere between field testing and the small-scale laboratory experiments.

The BIONICS glacial till materials were compacted into a large lysimeter to simulate a more representative scale that is closer to a field condition than the small-scale laboratory testing. The volumetric water content and suction were measured using TDR probes and high-capacity tensiometers from different depths and locations. Electrical resistivity tomography (ERT) was employed to map the distribution of resistivity of the soil over time, as well as to map the water content distributions based on the proxy relationship between the resistivity and water content obtained from the small-scale laboratory tests using the triaxial samples stated in section 3.3.

3.4.2 Structure of the lysimeter

The lysimeter in this experiment was a cylindrical soil container made of black Poly Vinyl Chloride (PVC) material with an inner diameter of 1.2m and a height of 1.5m (as shown in Figure 3.18). Four columns of instruments were buried into the lysimeter at six different layer depths of 0.05 m, 0.2 m, 0.35 m, 0.5 m, 0.7 m and 0.9 m respectively (see in Figure 3.19). In each layer, there were four TDR probes and four tensiometer ports that arrayed in pairs at an insertion depth of 0.17 m to measure the volumetric water content and suction, and there were 16 stainless steel electrodes, which were evenly spaced around the circumference of the lysimeter wall to measure the resistivity (Figure 3.20).

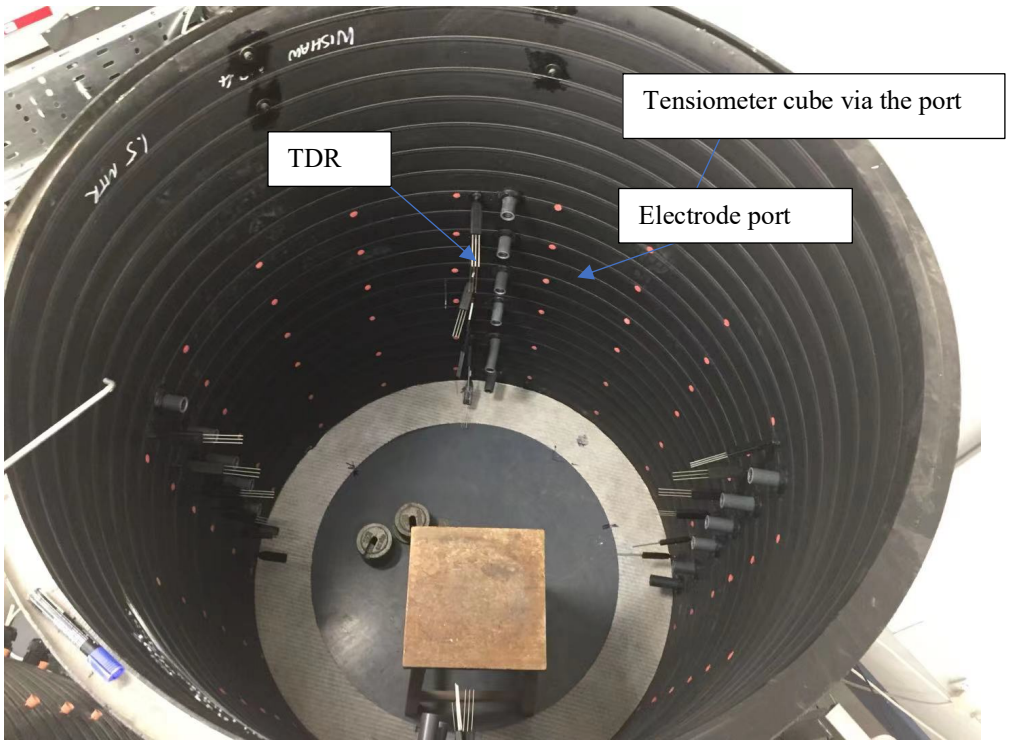

Figure 3.18 The cylindrical soil lysimeter with a diameter of 1.2m and a height of 1.5m, and the arrays of instrument ports for settling tensiometer, TDR probes and ERT electrodes.

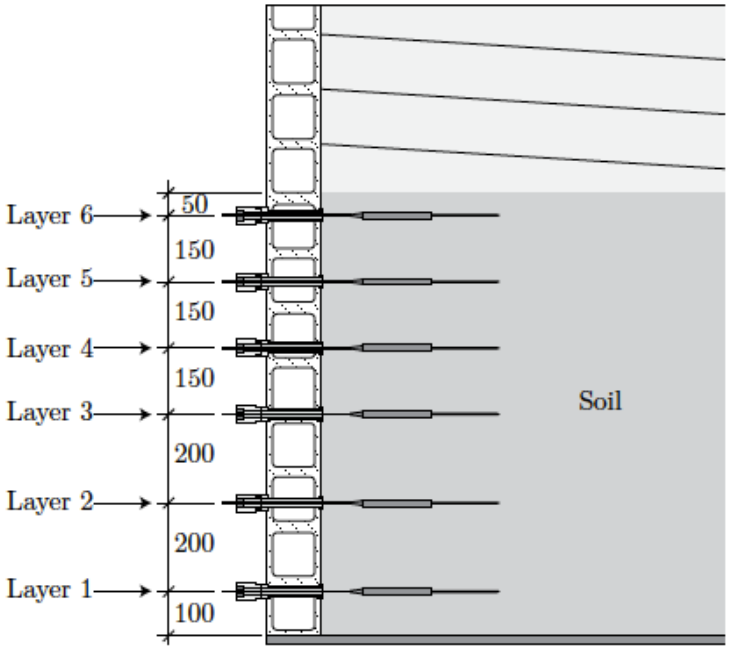

Figure 3.19 Diagram of vertical port positioning (after Asquith, 2015)

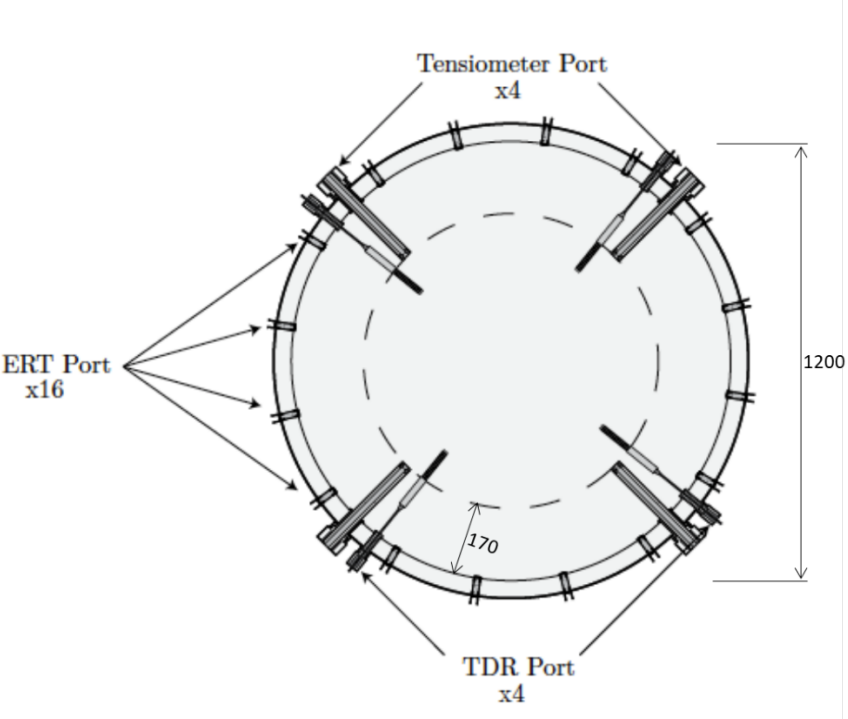

Figure 3.20 Diagram of horizontal port positioning (after Asquith, 2015)

3.4.3 Sample preparation

All the soil collected from the site was dried out to residual and tamped to small clumps using a 5-kg metal hammer. The soil clumps were then passed through a 10-mm sieve to remove rocks and other large particles. The passed materials were separated into 100-kg batches and stored in plastic bins. Samples were taken from each batch to calculate the residual water content and to determine the amounts of water needed to reach a target water content of 22%. Each batch of soil was then mixed with water in a large paddle mixer. Once all the batches were mixed, the remoulded soil was stored in dumpy plastic bags, well-sealed and left to reach equilibrium before use.

3.4.4 Filling the lysimeter

The filling process involves weighing out the certain amount of soils, the compaction of soils in the large lysimeter and scarifying the surface of each sub-layer to improve the connections between layers.

The prepared material was filled into a lysimeter in 50 equal layers to form a large soil sample with a height of 1 m. For each layer, the thickness was 20 mm, and the soil was compacted to an initial dry density of 1.65 Mg/m^3. Soil was compacted manually using a 5-kg tamper with a square base of 120 mm by 120 mm.

Before filling the lysimeter, a trial compaction test was performed to determine the compaction effort required to fill the lysimeter. The test was conducted in a rigid plastic box with a base area of 365 mm by 263 mm and a hight of about 250 mm. The inside box was marked using a mark pen at every 20 mm height intervals from the base, consistent with that of one compaction layer in the lysimeter. The quantity of soil needed for each 20 mm layer, which can be determined from the target dry density and the water content, was weighed and filled into the container for compaction. By compacting the soil to 20mm height, adjusting the falling height and the number of blows, the appropriate falling height and the number of blows were determined to be 150mm and about 39 times. The results were then scaled up to the large lysimeter size. The results suggested that 460 blows per layer with a 150-mm drop height were appropriate to achieve the target initial dry density in the large lysimeter.

The lysimeter was also marked at every 20 mm from the base to a height of 1 m. For each layer, the soil was compacted in four quarters. The filling method for one layer is as follows:

1. The soil for one layer was weighed out and divided equally into four parts.
2. The first three parts of soil was distributed evenly into the first three quarters of the lysimeter using a coarse rake.
3. A plastic sheet was placed on one quarter, and the person compacting stood on the sheeting whilst distributing the final bucket evenly in the last quarter.
4. The heights around the circumference were checked against each of four series of wall markings that indicate layer heights every vertical 20 mm.
5. Any anomalies were distributed whilst trying to minimise the amount of raking, as this causes separation of the larger soil particles from the smaller ones.
6. For each quarter layer, 115 tamps were applied with 150-mm drops whilst the person compacting preferentially stands on compacted soil.
7. Using a trowel, the circumference of the lysimeter was navigated, sliding the trowel flat against the soil to remove any lip forming against the side wall.
8. Soil cuttings were distributed where appropriate, gauged using the markers on the side walls.
9. The process continued by covering the soil with a plastic sheet once more and repeating 115 tamps per quarter of the lysimeter.
10. The plastic sheeting was then be removed, and the final 115 tamps were applied over the entire surface of the lysimeter.
11. All but the last layer was scarified to aid in interlocking between layers.

After each layer, the level of the surface was assessed to check whether more soil needed to be distributed into some sections over others to maintain a flat surface area during the filling process. Once the last layer was filled, the surface of the sample was flattened.

3.4.5 Installation of instruments

Once the soils have been filled into lysimeter reaching the instrument layers at 0.1, 0.3, 0.5, 0.65, 0.8 and 0.95m height from the bottom, respectively. The instruments employed in the lysimeter tests were set up according to the procedure described below.

For TDR probes, the installation method involved trimming soils out from the installation positions to create four potholes to allow the insertion of the TDR probes and inserting the rods directly into the soil from the potholes (as shown in Figure 3.21). The process was carried out carefully and slowly to avoid the deviation of probe's waveguides and the contact with hard materials. After installing the TDR probes, the soils cut out were filled back to the potholes.

The tensiometer was installed with assistance of a plastic guide through a PVC tube. The PVC tubes for guiding the insertion of the tensiometers were buried into the soil sample following the same procedures with TDR installation. After the compaction was completed, tensiometers were inserted into the PVC tube until touching the soil sample. Wet soil paste was used as slurry at the head surface of the tensiometer to ensure good contact between the probe head and the soil.

Once the compaction has been completed, 64 electrodes were installed to lysimeter via the electrode ports on the upper four instrument layers. The electrodes (as shown in Figure 3.22) are 20cm stainless-steel rods with a diameter of 0.8cm, with 5cm and 7cm threaded at the two ends, respectively. The electrodes were installed by screwing the long thread head into the soil sample via the electrode ports with an insertion length of about 5cm. Considering that the shrinkage of soil during drying may break the contact between the soil and the electrode, a threaded head was designed to embed the electrode more firmly in the soil, thereby improving the contact between the soil and the electrode. The shorter threaded end (5cm) was designed to fix the copper cable to the electrode with two hex bolts. The 8cm smooth section on the electrode is reserved to allow the movement of electrode due to the shrinkage and expansion of the soil during drying and wetting cycles. A completed set up of one instrument column on lysimeter is shown in Figure 3.22 (right).

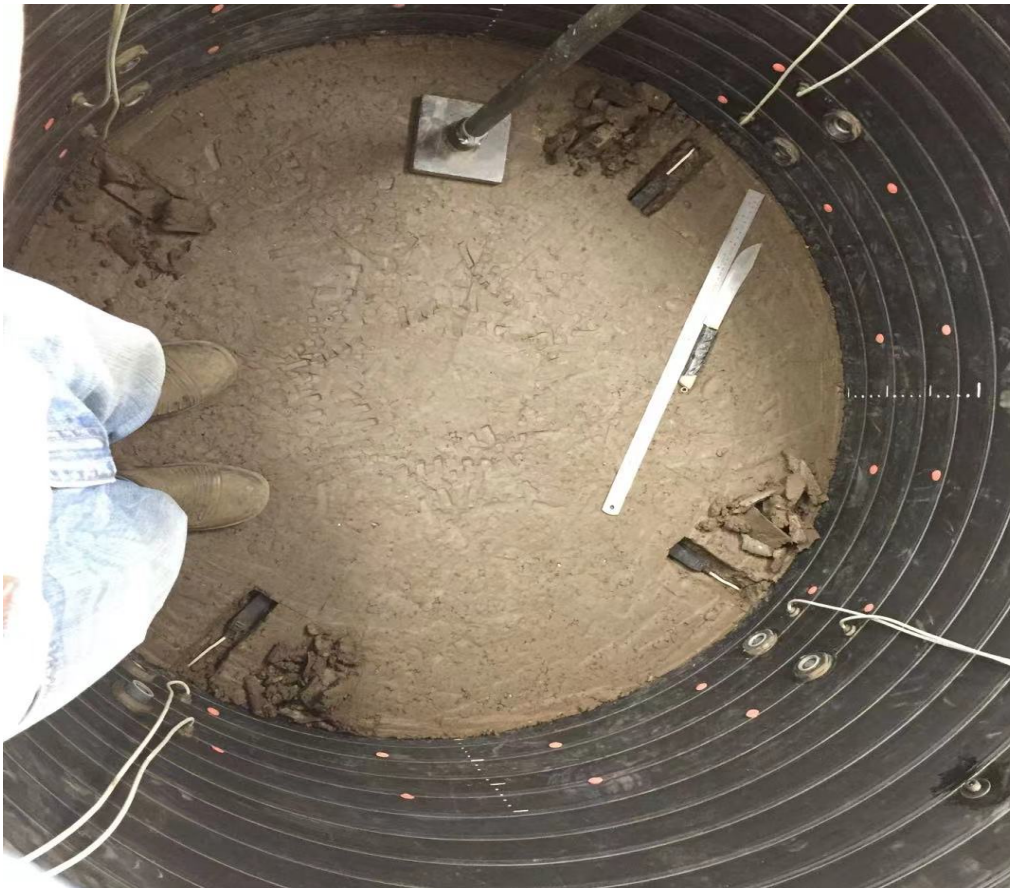

Figure 3.21 TDR probes installed in lysimeter sample from the trimmed potholes

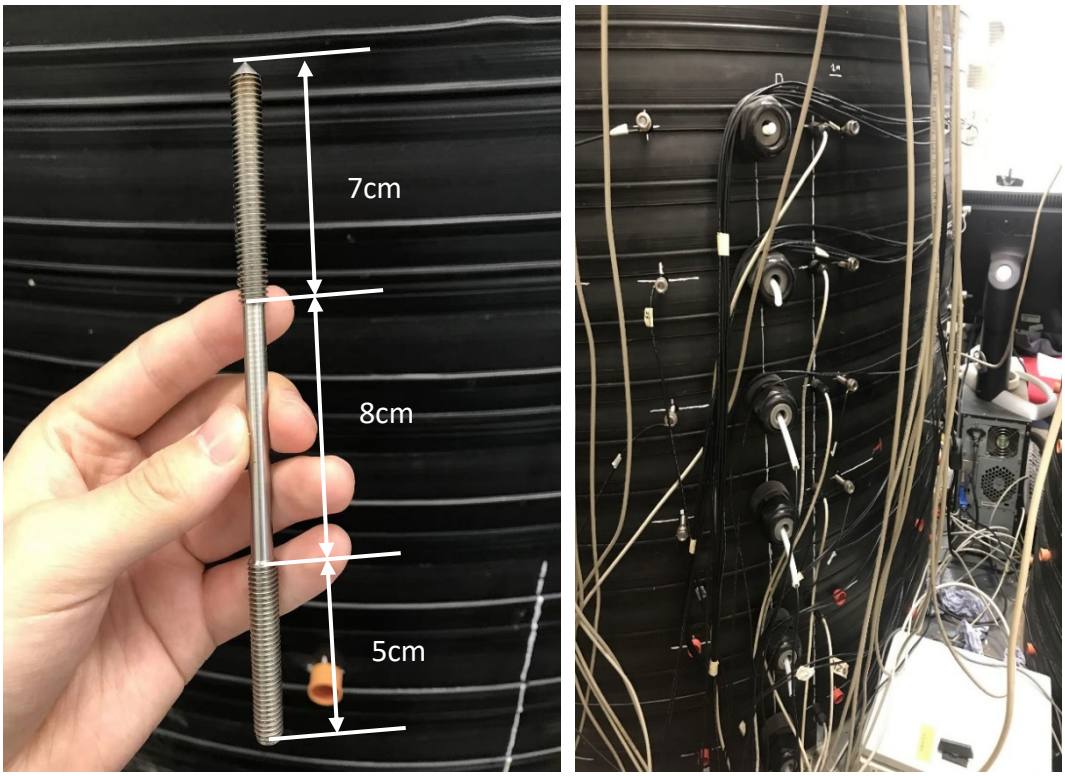

Figure 3.22 The diagram of stainless-steel electrode with dimensions for ERT measurements (left) and the completed set up of one instrument column on lysimeter (right).

3.4.6 High capacity tensiometers

Eight tensiometers were employed in this laboratory programme due to a shortage of available tensiometers. Six of them were installed in a column to obtain a full vertical data profile. The other two tensiometers were initially installed to the near-surface layer (layer 6) to provide a parallel comparison with the main measurement column and were moved down stepwise to the lower layers when their readings approached the cavitation point. The saturation and calibration processes for the tensiometers are described in section 3.2.3.4.

3.4.7 Time domain reflectometry system

Twenty-four TDR probes were calibrated and installed in the lysimeter to measure the volumetric water content and soil bulk conductivity.

Once the compaction of the lysimeter was completed, the TDR probes were connected to the SDMX50SP multiplexers, which were controlled by the TDR100 switching box. The TDR100 was then connected to the computer though serial port and controlled by the TRIAX software which was designed for data acquisition of TDR measurement (Asquith, 2015). The command signals can be delivered to the TDR100 by the computer via the software to control the switching between twenty-four probes and perform time-lapse measurements using TDR probes.

The raw data received from the TDR probes were analysed by the Waveform software (Asquith, 2015) to calculate the relative dielectric permittivity and then converted into volumetric water contents.

3.4.8 Irrigation system

An automated irrigation system was set up on the large lysimeter for sample wetting, as shown in Figure 3.23. During the wetting period, a PVC lid with a square hole in the centre was fixed over top of the lysimeter to reduce the evaporation of soil sample. A Tee-tube was placed on the lid with the short edge inserted into the lysimeter via the hole on the lid. An irrigation sprinkler was fixed at the base of the Tee-tube and with its water supply pipe passing through and out of the Tee-tube, down to the computer-controlled water pump. The pump was powered by a programable power supply, of which the pulse-on time and output power can be controlled by the computer. While working, the

rainwater was pumped from a water container placed outside the lysimeter through water supply piping and was sprayed radially to the sample surface by the sprinkler fixed above the centre of sample surface. The irrigation was run 4 times a day with an intensity of 650mL per minute and lasted for 30 seconds each time, meaning a total of 1.15 mm of rain was applied to the lysimeter sample per day. This irrigating rate was chosen based on two considerations: firstly, allow the soil sample to be wetted efficiently; and secondly, avoid pooling on the sample surface.

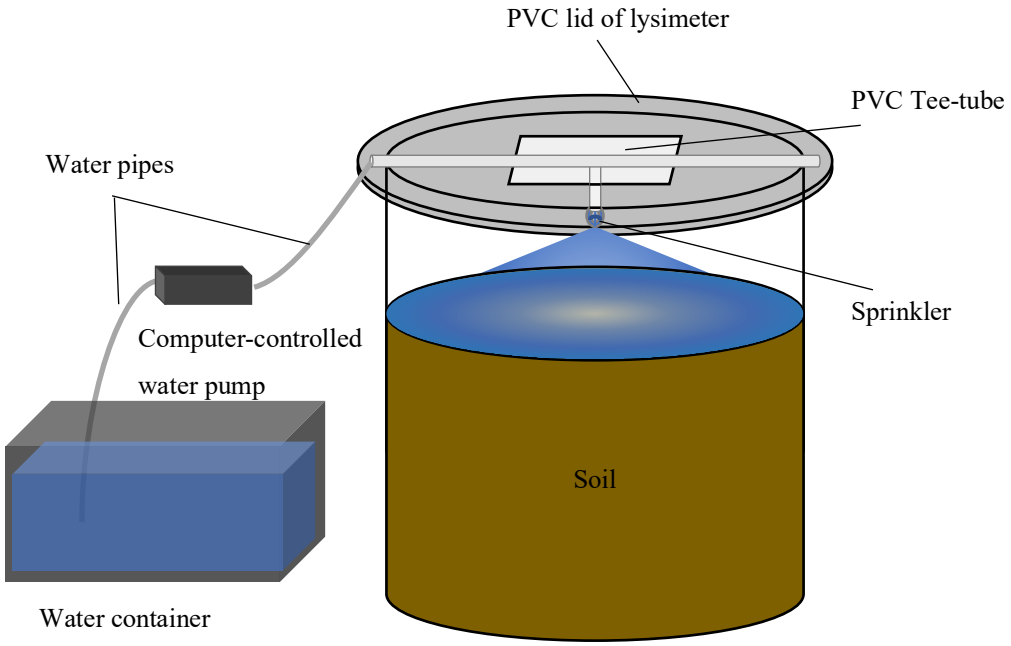

Figure 3.23 Schematic diagram of irrigation system for large lysimeter test

3.4.9 Electrical resistivity tomography system

3.4.9.1 Instrumentations

A multiple-channel resistivity system was used for data collection (see in Figure 3.24). The system consisted of the following:

- A Supersting R8 resistivity meter manufactured by Advanced Geosciences, Inc. (AGI) that provides accurate output current and allows one to take measurements from eight potential pairs at the same time.

- An AGI multi-electrode switching box that allows Supersting to automatically control and switch between 64 electrodes during resistivity surveys.
- A 12-V leisure battery for the power supply.

Due to the capacity of the switching box, only 64 electrodes on the upper four layers of the lysimeter were used in the ERT system. The electrodes were made of stainless steel, with 5-mm thread heads to be screwed into the soil through the ERT ports. The outer ends of the electrodes were connected to the switching box through copper cables and multi-pin connectors.

Figure 3.24 A multi-channel resistivity system used for ERT

3.4.9.2 Resistivity arrays

The measurements were taken following the predefined resistivity arrays that were read by the SurperSting resistivity meter with command files. The inversion results were generally obtained with the 4x16 electrode geometry based on the upper four electrode rings installed on the lysimeter. For each electrode ring, a circular dipole-dipole

configuration was chosen to take resistivity surveys and generate survey files for ERT inversion. For each measurement array, a fixed electrode pair (A and B) was selected as the current injection dipole (see in Figure 3.25), while the other electrodes were selected as potential pairs (M and N) for potential measurements. The potential dipoles were paired by adjacent electrodes and shifted anticlockwise around the electrode ring. After seven potential pairings of M and N electrodes providing 180° coverage, the current pair was shifted anticlockwise by one electrode along the electrode ring, and the potential measurements were repeated as stated above. The arrays were repeated until the current dipole covered the whole electrode ring. Reciprocal measurements were taken for each normal measurement to check the data quality.

The command files defining the sequences of the ERT measurements were created and uploaded to the resistivity meter to control its measurements. The Supersting automatically ran measurements following the designed sequences of the resistivity arrays which were written into the command files and recorded the data in its built-in memory storage.

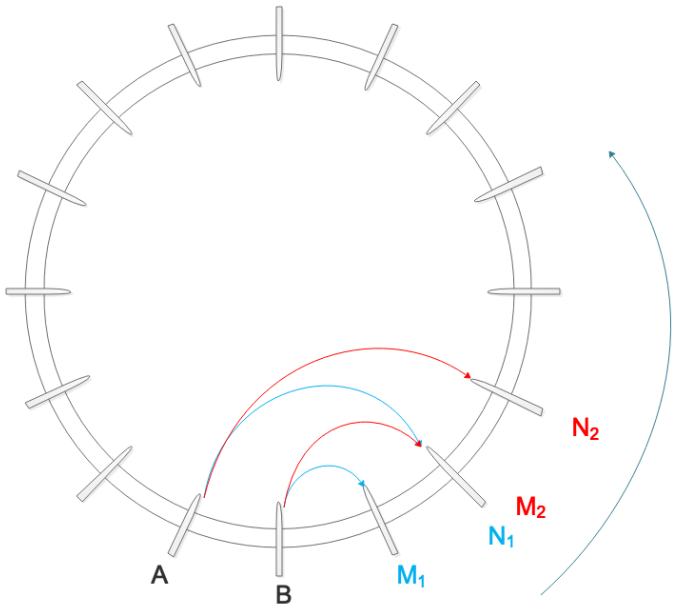

Figure 3.25 Circular dipole-dipole configuration with the current injection dipole at electrodes A and B, and the potential measuring dipole at electrodes M and N

3.4.9.3 Pre-processing of the raw data

The Supersting resistivity meter operated the resistivity surveys following the resistivity arrays defined in the command files, and it saved the data in stg. file format, which

included the date/time of measurement, the V/I (apparent resistance of measurement), and the xyz coordinates of the A, B, M and N electrodes.

Pre-processing of the raw data was done to rearrange the data into the required format to create input files for ERT modelling. The detailed procedures are as follows:

- Defining the electrode IDs of A, B, M and N electrodes for each measurement point by correlating the IDs to the electrode coordinates.
- Correlating the reciprocal measurements to each corresponding normal measurement and calculating the reciprocal errors.
- Removing large errors in data, of which the reciprocal errors were greater than 5%.
- Rearranging the processed data and writing them into the required format for modelling.

3.4.9.4 Error analysis for ERT measurements

Accurate determination of measurement errors is important to reduce misinterpretation in the inverse modelling of ERT measurements (LaBrecque et al., 1996). Measurement noise decreases resolution of the inverted model. Incorrect noise estimation results in gross smoothing of the structure (noise overestimation) or artefacts (noise underestimation). The measurement error can be caused by factors such as (1) poor contact between the soil and the specific electrode, (2) random errors associated with the measurement device and (3) occasional error related to background and environmental noise.

Stacking (repeated tests) is a method of noise quantification to check the data quality of ERT measurements. An alternative measure is the 'reciprocal error', defined as,

$$e_r = R_n - R_r \tag{3.6}$$

where R_n is the resistance of normal measurements and R_r is the resistance of reciprocal measurements. The reciprocal error, e_r is the difference between resistances of normal and reciprocal measurements, indicates the data noise. The reciprocal error can detect errors that may not be apparent from repeated checks. In the inverse modelling of ERT, the reciprocal errors were used to identify bad measurements and to estimate error level for the inversion. The inversion used a simple Gaussian error model in which the

magnitude of reciprocal error |e| increases with the magnitude of measured resistance |R| according to,

$$|e| = a + b|R| \tag{3.7}$$

Error models were created for ERT data at each time point to identify the error levels of the measurements. Figure 3.26 shows the error model produced for ERT data collected on date 15/02/2019. It shows that the magnitude of the reciprocal error |e| increases with the magnitude of the measured resistance |R|. For this individual ERT measurement, the data noise of 0.0086 (0.86%) was determined from the error model. In inverse modelling of the ERT data, an estimated system error of 2.5% was added to the reciprocal errors to obtain the error level for the inversion such that the error parameter for the inversion of ERT data collected on 15/02/2019 was 3.36%.

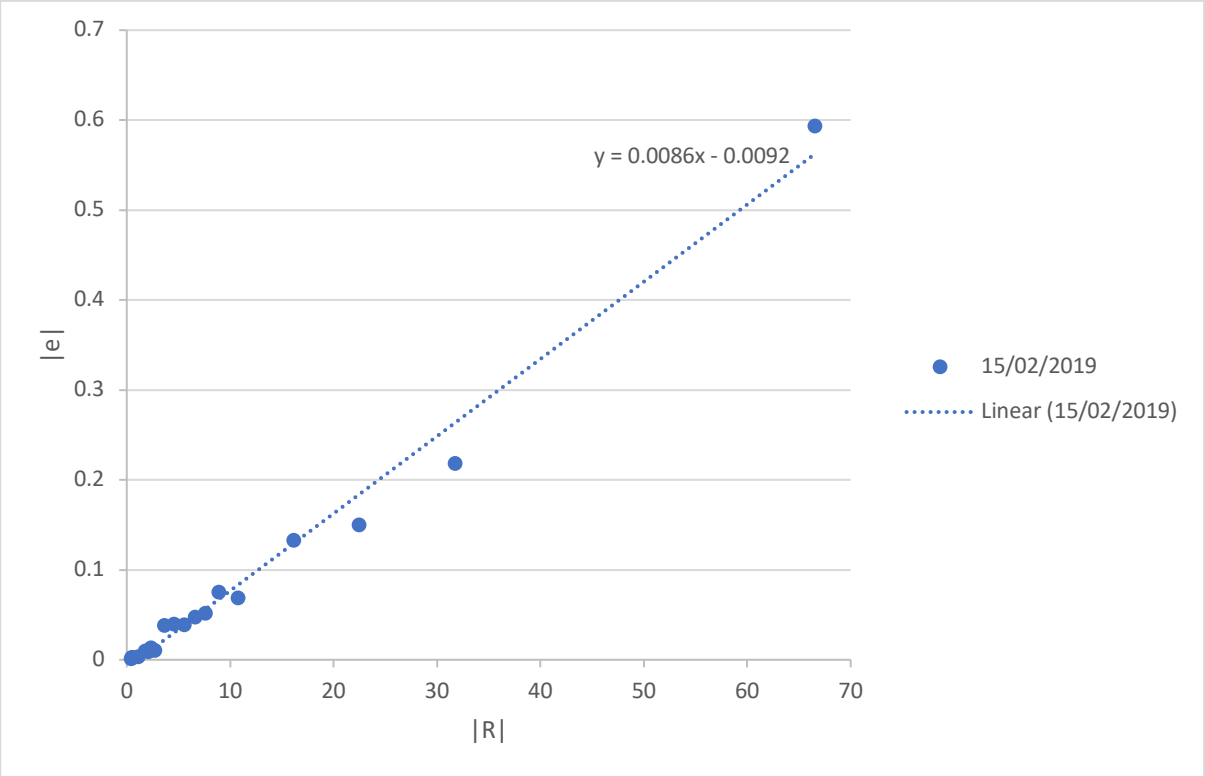

Figure 3.26 Error model for the ERT data of 15/02/2019

3.4.9.5 Electrical resistivity tomography modelling

The ERT data modelling was achieved using an open-source code, E4D (https://e4d.pnnl.gov/), described in Johnson et al. (2010). This E4D code is a 3D

modelling and inversion code for ERT data that allows forward modelling, numerical inversion and time-lapse 4D inversion to be achieved.

Three running modes in E4D were used to establish the 3D and 4D resistivity tomography of the lysimeter sample:

1) ER mesh generation Mode (Mode 1 as defined in the E4D user guide): A mesh generation mode was used to create the finite element mesh (FEM) for the ERT forward and inverse modelling, based on the lysimeter sample geometries and the electrode locations.
2) An ER static inversion mode (Mode 3 in the E4D user guide) was used to perform electrical resistivity inversion for the starting ERT measurement data.
3) An ER time-lapse inversion mode (Mode 4 in the E4D user guide) was used to undergo inversions for multiple time-lapse surveys based on the resistivity solution of the baseline ERT data.

3.4.9.6 3D and 4D ERT inversion methods using E4D

The large lysimeter test had ran for a period of nine months over one drying and one wetting period from 20 September 2018 to 20 May 2019. A total of 36 survey files in weekly intervals were produced for doing the time-lapse inversions. For each survey file, 200 apparent resistance readings were obtained from the upper four layers following the circular dipole-dipole configurations as mentioned in section 3.4.7.2. Once the ERT survey files were produced, the survey created for the starting date 20/09/2018 was set as the baseline survey data. A real resistivity inversion was done for the baseline data using the ER static inversion mode (Mode 3) in E4D to obtain the 3D real resistivity solution for the baseline. Once the baseline resistivity solution was made, the time-lapse inversion Mode (Mode 4) in E4D was used to produce the real resistivity solutions for the series of ER surveys obtained from the large lysimeter test. The time-lapse inversion was conducted using time-lapse smoothness constraints and using the baseline solution as the reference.

3.5 Chapter summary

In order that the aim of the project can be achieved, three phases of laboratory-based experiments have been conducted as stated below.

In the first phase, several point measurement sensors were employed for estimating the soil water content, electrical resistivity and suction on a cubic glacial till sample during cyclic drying and wetting in a controlled environment.

In the second phase, soil electrical resistivity, suction and shear strength were determined by a four-electrode resistivity probe, WP4C soil water potentiameter and Unconsolidated Undrained triaxial tests on 38mm diameter triaxial specimens made of three different types of soil.

In the third phase, a 3D time-lapse electrical resistivity tomography (ERT) method was employed to map the real-time resistivity changes in a 1.2m diameter cylindrical lysimeter; point sensors were also used to provide water content and suction measurements on different depths within the lysimeter. In establishing the interrelationships between the electrical and the geotechnical properties, the spatial geotechnical information (i.e., the water content and suction distributions) within the large lysimeter sample could be converted from the ERT-derived resistivity data.

4 Results

4.1 Introduction

In order that the aim of the project can be achieved, three phases of laboratory-based experiments have been conducted to investigate the soil property interrelationships under repeated drying and wetting cycles. In the first phase, SWRCs and resistivity-water content relationships were determined for a cubic soil tank using different point sensors. In the second phase, soil electrical resistivity, suction and shear strength were determined by a four-electrode resistivity probe, WP4C soil water potentiameter and Unconsolidated Undrained (UU) triaxial tests on 38mm diameter triaxial specimens made of three different types of soil. In the third phase experiment, spatial resistivity distributions were measured for soil sample in a 1.2m diameter cylindrical lysimeter using time-lapse electrical resistivity tomography (4D-ERT) method; point sensors were also used to provide reference measurements of water content, resistivity and suction on different depths within the lysimeter.

In this chapter, results from the three phases of experiments are presented separately followed by a comparison of the soil property relationships between the results obtained in different phases.

4.2 Box lysimeter results

The aims of the box lysimeter testing were to:

- Compare the performances of different point sensors for soil water content and suction measurements.
- Investigate the relationships between soil water content, pore water pressure, and resistivity and how the relationships change over cycles of drying and wetting.
- The experiment was designed to achieve three complete drying and wetting cycles. However, it stopped at the midway point of the third wetting path due to time limitations. This section shows how the soil property relationships between water content, pore water pressure and resistivity evolve over cycles of wetting and drying.

4.2.1 Sensor calibrations

All the moisture sensors used in this experiment determine the Volumetric water content by measuring the dielectric constant/permittivity, ε_a of soil medium using different principles, i.e., the TDR probes, 5TE sensor and ML2x probe measure the apparent dielectric permittivity using time domain, frequency domain and amplitude domain techniques respectively. The sensor responses relate to the soil permittivity and then need to be converted into volumetric water contents based on the calibration relationship between the apparent permittivity and the VWC of the soil. The widely used factory-default calibration for these permittivity type moisture sensors is the empirical equation with respect to the relationship between the apparent permittivity and the VWC proposed by Topp (1980). However, the default calibration is only the universal relationship between ε_a and VWC independent of the soil type. The effect of dry density and soil matrix permittivity varying from different soils should have been considered when correlating apparent permittivity to the water content (Malicki and Walczak, 1999). A soil specific calibration is, therefore, required for clays to reach a higher accuracy for research purposes as the dry density of the clay changes by the variation of the water content during drying and wetting.

Figure 4.1 shows the calibration relationships between the refractive index (i.e. square root of apparent permittivity) and volumetric water content for the sensors. With respect to the ability of the empirical equation to estimate the volumetric water content of the soil, the soil specific calibrations are compared with the empirical Topp's mineral equation. The results can be observed to have close linear relationships between the apparent permittivity measured by the sensors and the sample volumetric water content. As can be seen that the calibration lines of TDR probes are better fitted with the Topp's equation, especially the CS640 probe, whereas the other two types of sensors show distinct deviations from the empirical equation. It is noted that the two 5TE sensors show different calibration lines, implying that a soil specific calibration is required for each specific sensor when using the 5TEs.

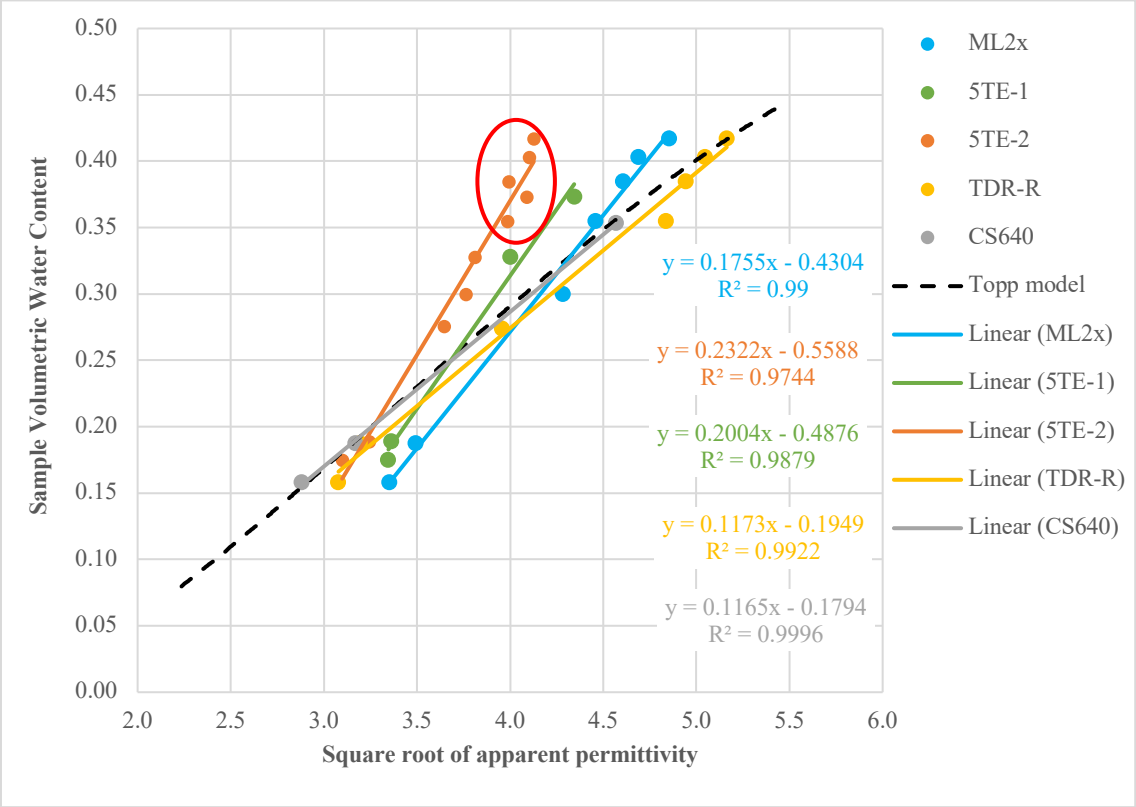

Figure 4.1 Calibrations of moisture sensors between square root of the apparent permittivity $\sqrt{\varepsilon_a}$ and VWC. The red circle in the figure shows a steeper tendency than the normalized trend line for 5TE 2 with data points over 35% of VWC.

4.2.2 Property changes over time

4.2.2.1 Volumetric water content

Figure 4.2 presents the time series volumetric water content (VWC) data obtained from five different water content sensors, in which there are two Decagon 5TE sensors used at different locations in the box lysimeter as shown in Figure 3.3 (in section 3.2.3.5). All the volumetric water content values are converted from the permittivity measurements using the soil specific calibrations of the sensors as presented in Figure 4.1. All the sensors show degrees of the VWC variability while the soil sample subjected to cyclic drying and wetting and the five sensors show differences in the VWC measurements.

Overall, the TDR-ROBUST (TDR-R), 5TE-1 and ML2x sensors approximately agreed to each other in the data span. However, the readings of the TDR-R probe and the ML2x probe show higher values than those of the 5TE-1 sensor in between 32% and 40% VWC in the first drying process due to the insufficient calibration for 5TE-1 over 30% VWC. In accordance with the calibration line of 5TE-1 in Figure 4.1(green line), the calibration points of the 5TE-1 sensor generally follow a linear relationship while the VWC is below

35%, whereas there are insufficient data points to fix the calibration for VWC measurement over 35%. However, from the calibration line for 5TE-2 (orange line in Figure 4.1), it can be seen that the trend of calibration points over 35% VWC becomes steeper than the normalized calibration line of 5TE-2 (marked by the red circle in Figure 4.1), implying that the response of 5TE sensor shows lower sensitivity in apparent permittivity measurements over 35% VWC, which may cause the less accuracy of 5TE sensor in VWC measurements over 35%. In the range of 32% to the residual water content on the first drying process, the 5TE-1 and TDR-R shows strong agreement in the VWC measurements and show higher values than the ML2x probe. In the second and third drying processes, the VWC measured by TDR-R probe is higher than that of 5TE-1 and further higher than that of ML2x, the possible reason for this may be due to the air pockets between soil and the sensor prongs caused by compaction and sample drying. The effects of entrapped air will be discussed later in this section.

As can be seen Figure 4.2, at the starting point of the experiment, the VWC readings of TDR-R and ML2x are around 38%, while the readings of 5TE-1 and 5TE-2 are both at around 35%, and the reading of CS640 is at about 28%. The gravimetric water content (GWC) and the dry density of the soil sample are initially made at around 23% and 1.63 Mg/m^3 respectively, which correspond to a VWC at approximately 37.5%. The TDR-R and ML2x probes, and therefore, provide the most reasonable readings in VWC at the starting point.

It can also be seen in Figure 4.2 that there are instant jumps in VWC measurements for the CS640, 5TE-2 and ML2x probes (marked by the red circles) occurring at the wet ends. This provides evidence of the existence of the entrapped air pockets between the sensor prongs and the surrounding soils. When the soil was becoming saturated approaching the wet ends, the irrigated water infiltrated and filled the air gaps, causing the sudden increases in the VWC measurements of the sensors, as parts of the sensors were directly surrounded by the water. However, the issue is more serious for the 5TE-2 sensor and CS640 probe than the ML2x. The poor contact between the sensor prongs and the soil for 5TE-1 and CS640 also led to an underestimation of VWC when the soil was unsaturated, since parts of the sensor prongs were in direct contact with the entrapped air, resulting in a low value in permittivity measurements.

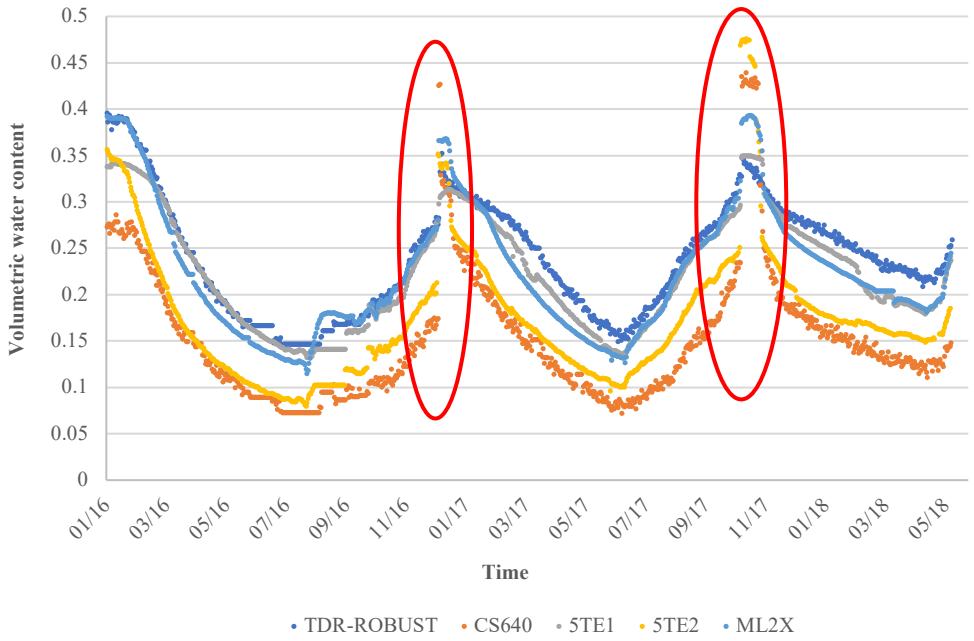

Figure 4.2 Time series volumetric water content data measured by four different sensors in the soil box lysimeter. The red circles show instant jumps in VWC measurements for the CS640, 5TE-2 and ML2x probes.

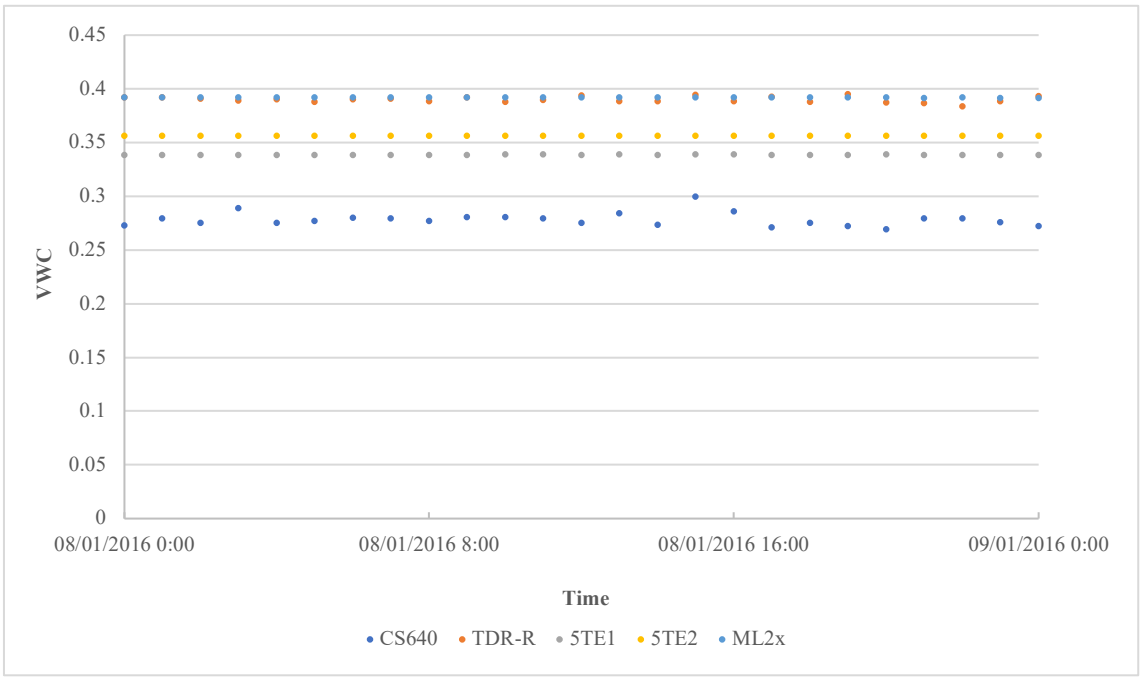

Figure 4.3 VWC data obtained by the five point sensors for the date 08/01/2016 at a measurement interval of one hour.

The variability of determining the VWC using point sensors can be seen from Figure 4.2. Compared with other sensors, the data obtained by TDR probes gave greater variability when measuring the VWC of sample. Data of one day before the test started was collected for investigating the variability of results obtained by the point sensors. Figure 4.3

presents the hourly VWC data for the date 08/01/2016obtained by the five point sensors. The data sets show the measurements of VWC before the start of the test, where the VWC values should be constant.

Table 4.1 The mean value and standard deviations (S.D.) of hourly VWC data for date 08/01/2016.

Property	CS640	TDR-R	5TE1	5TE2	ML2x
Mean	0.2784	0.3900	0.3384	0.3566	0.3919
S.D.	0.0063	0.0026	0.0002	0.0000	0.0002

Table 4.1 shows the mean values and standard deviations (S.D.) of the one-day data sets for the five sensors. The standard deviations given clearly represent the variability of sensors in determining the VWC in the period. The results suggest that the CS640 probe has the greatest variability in VWC measurement with a bias of two standard deviations, denoted ±1.26% VWC. The TDR-R has a comparatively greater variability in the measurement with a bias of two standard deviation, denoted ±0.52% VWC. The 5TE sensors and Theta probe (ML2x) have relatively smaller variability in VWC measurements that the bias introduced is less than ±0.04% VWC.

4.2.2.2 Pore water pressure

Figure 4.4 shows the time series pore water pressure (PWP) data collected by three different versions of Decagon MPS water potential sensors and the Durham high capacity tensiometer. It can be seen that all of the sensors show agreements in the range of around -300 to 0 kPa and separation occurs when the PWP continues to decrease in the first drying path. The reading of the MPS-2 sensor shows high consistency with the tensiometer all the way down to -1151 kPa, where the tensiometer cavitated and goes down to about -3000 kPa at the dry end of the first drying path. The reading of the MPS-1 sensor keeps constant after reaching a value of around -430 kPa, which is close to the measuring limit (-500 kPa according to its user manual) of it. The MPS-6 sensor was considered damaged or improperly installed because it gave lower readings in suction (i.e. negative pore water pressure) estimation compared to the MPS-2 and the tensiometer.

From Figure 4.2 and 4.3, It can be seen that the readings the PWP obtained by the MPS-2 sensor at the dry ends of three drying and wetting cycles are -3042 kPa, -2190 kPa and -1883.7 kPa respectively, which indicate a reduction in suction (negative pore water pressure) at the dry ends by cycles. While the VWC readings from the TDR-R probe at

the three driest points are 15%, 14.9%, and 21.3% respectively, where the driest water contents for the first and second cycle are very close and lower than that of the third cycle. It can also be seen that the 21.3% VWC corresponds to a PWP of about -1942 kPa on the second drying path in accordance with the same time point. This might indicate a reduction in suctions of the soil sample at given VWCs from the initial drying path to the subsequent drying path.

The readings of VWC measured by TDR-R at the wet ends (referring to the zero suction points) of three drying-wetting cycles are approximate 40.0%, 36.4%, and 36.0% respectively. This might indicate a reduction in saturated VWC from the initial drying path to the main drying path and the consistency of saturated VWCs in the following cycles.

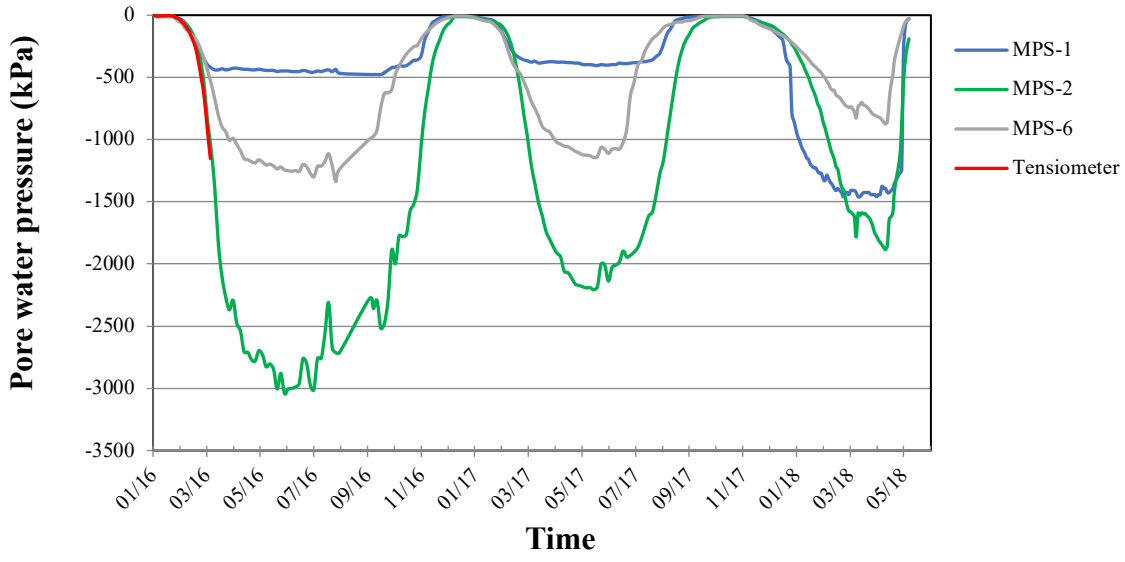

Figure 4.4 Time series pore water pressure data measured by four different sensors in the soil box lysimeter.

4.2.2.3 Resistivity

The TDR probes and 5TE sensors measure the bulk conductivity of soil. The bulk resistivity value is reciprocal to the bulk conductivity value. Figure 4.4 shows the time series data of electrical resistivities obtained from the TDR-R, CS640, 5TE-1 and 5TE-2 sensors. Overall, the data from the TDR-R and 5TE-1 sensors show strong agreement with each other in the whole data span, whereas the readings taken by the CS640 are higher than the readings taken by the former two sensors. The resistivity data taken by 5TE-2 shows large division with others that it is much higher than the readings taken by

the other three sensors. Again, it is due to the poor contact issue mentioned above. The 5TE sensor measures the bulk conductivity of soil by using two stainless steel screws (installed on two of the sensor prongs) as the two electrodes (i.e., positive and negative electrodes). When the soil is unsaturated, the entrapped air, especially around the two screws, cause poor contact between the electrodes and the soil medium, dramatically reducing the electrical conductivity between the two electrodes. At the wet ends, when the soil is reaching a saturated condition, the water fills the air gaps, causing the sudden jumps in conductivity (drops in resistivity) readings of 5TE-2 (see in Figure 4.4). The results suggest that the saturated resistivity is about 20 Ωm for the initial sample, 17 Ωm after one drying-wetting cycle and 13-17 Ωm for the sample after two drying and wetting cycles. The decreases in saturated soil resistivity during cyclic drying and wetting might be attributed to the changes in soil fabric and micro-structures during repeated drying and wetting processes. Results in section 4.3.5 illustrate the volumetric changes of clays over successive drying and wetting cycles, the void ratio of Glacial till switched to lower values over cycles. It has been proven that there is a positive correlation between soil void ratio and soil resistivity at a given water content (Hassan, 2014), which may imply that the decrease in saturation resistivity over cycle is the result of a decrease in the void ratio. is a result of decrease in the void ratio. In addition, the cracking and deterioration in clays at the micro-scale due to drying and wetting cycling have been observed in many previous studies using ESEM imaging (Hen-Jones, 2018; Azizi et al., 2020; Stirling et al., 2020). Hen-Jones (2018) suggested that the development of micro-cracks lead to an increase in soil resistivity at low water contents and a decrease in resistivity approaching saturation, since these cracks cause more discontinuity in soil medium at low water content and become more conductive bridges when they were filled with water at high water content.

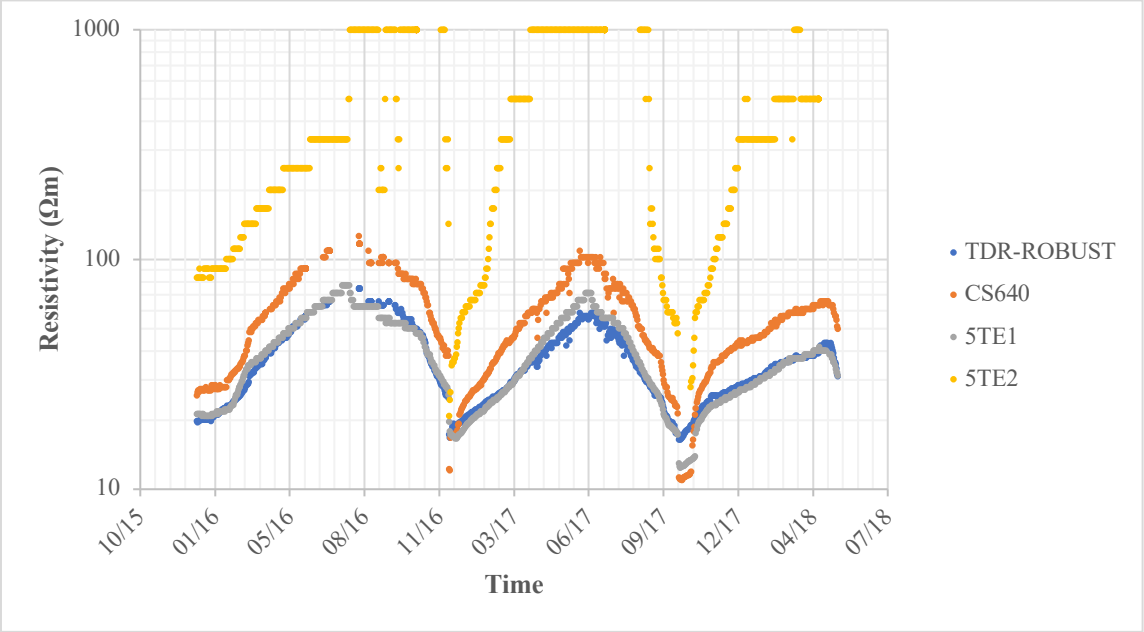

Figure 4.5 Time series resistivity data measured by three different sensors in the soil box lysimeter.

The variability of results can be observed in the resistivity measurements of the four sensors in Figure 4.5. In order to assess the accuracy of the sensors in resistivity measurement, hourly data of one day before the start of the test was collected to investigate the variability in determining the resistivity using the four-point sensors as shown in Figure 4.6.

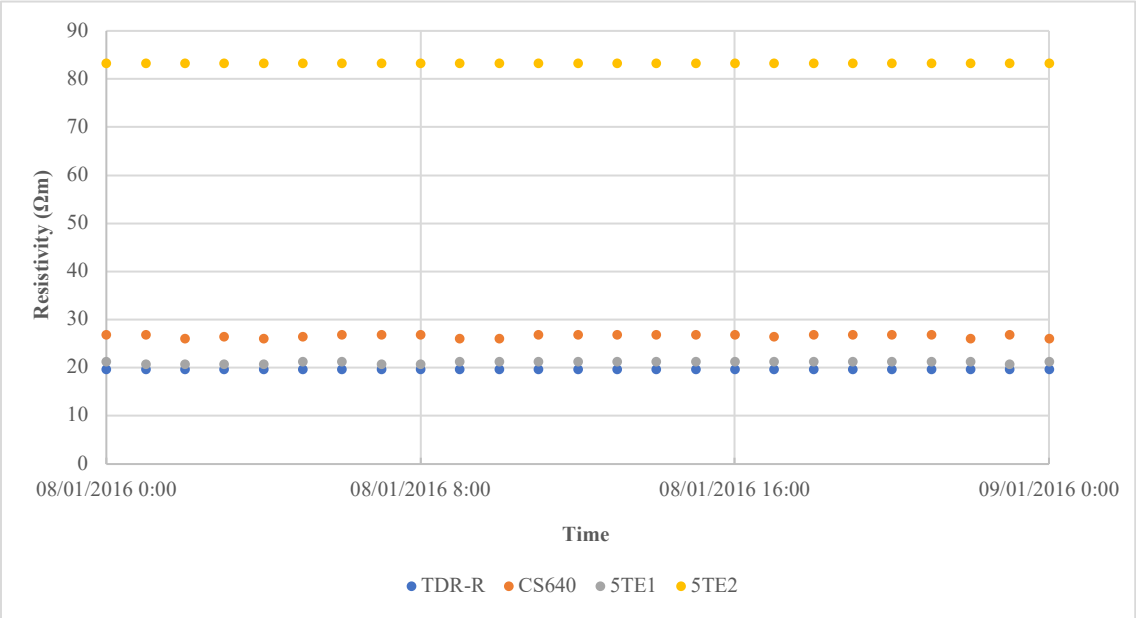

Figure 4.6 Resistivity data obtained by four point sensors for the date 08/01/2016 at a measurement interval of one hour.

Table 4.2 presents the mean values and standard deviations of the resistivity data obtain by the four point sensors on date 08/01/2016. The standard deviations clearly represent the variability of measurement results from the four sensors. The results suggest that CS640 has the greatest variability in resistivity measurement with a bias of two standard deviations, ±0.74Ωm, denoted percentage variability of ±2.78% of resistivity. The 5TE-1 has a variability in resistivity measurement with a bias of ±0.4Ωm, denoted percentage variability of ±1.89% of resistivity. The measurements of TDR-R and 5TE2 sensors are relatively consistent without significant variability.

Table 4.2 The mean values and standard deviations (S.D.) of hourly resistivity data for date 08/01/2016.

	TDR-R	CS640	5TE1	5TE2
Mean (Ωm)	19.76	26.63	21.15	83.33
S.D.	7.25×10^{-15}	0.37	0.20	5.80×10^{-14}

4.2.2.4 Data at the end of the experiment

The box lysimeter experiment was terminated in May 2018. The overlying soils above the sensors were carefully removed from the box using a soil shovel. For each sensor, one soil sample was collected locally from the surrounding soil to test on the gravimetric water content. Additionally, three intact soil samples were taken near the instrument layer using a cutting ring to estimate the average dry density of the soil sample from the GWC and the volume measurements at the end of the experiment. The final VWCs of the soil samples around each of the sensors were estimated from the GWC and dry density values to compare with the final records of the sensors. Table 4.1 shows a comparison between the VWC results measured by the sensors at the end of the experiment and the VWCs estimated from the gravimetric and the dry density data. It can be seen that the reading of TDR-R probe is closest to the estimated value, whose percentage error is 1.61%. The Ml2x and 5TE-1 also provide relatively accurate readings, whereas the readings of 5TE-2 and CS640 have large differences from the estimated values. However, the dry density of the final sample in Table 4.3 was estimated from the average of the three regular shape soil samples. The actual dry density may vary among the surrounding soils of each sensor due to the heterogeneities of water content within the soil sample.

Figure 4.5 shows the sensor locations and the gravimetric water content results of the surrounding soils for each sensor. The results indicate that the gravimetric water contents

are heterogeneous within the soil sample at different locations. The GWC is shown to be higher at the edges than that in the centre. This might be due to the water flowing down from the gaps between the soil edges and the lysimeter wall and wet the soil at the edges prior to the centre. In addition, it can be seen that the 5TE-2 sensor is situated very close to the ML2x and the CS640 probe, especially the ML2x. This close location may cause interference between these sensors which affects the VWC measurements resulting in the abnormal readings of 5TE-2 and CS640. However, the sensors were used to conduct an interference test after they were removed from the box. The results of this check did not show any clear evidence of interference.

Table 4.3 Data for the final point of box lysimeter experiment

Device	GWC (%)	Estimated average dry density (Mg/m^3)	VWC (%) estimated from GWC and dry density data	VWC (%) read by the sensors	percentage error	Suction (kPa)
5TE-1	15.85	1.74	27.58	24.59	10.84%	
5TE-2	16.06	1.74	27.94	20.69	25.96%	
Tensiometer	16.51	1.74	28.73	n/a		
MPS-1	17.98	1.74	31.29	n/a		38.00
MPS-2	16.31	1.74	28.38	n/a		77.00
MPS-6	17.64	1.74	30.69	n/a		35.60
Ml2x	17.03	1.74	29.63	24.96	15.77%	
TDR (ROBUST)	15.73	1.74	27.37	26.93	1.61%	
TDR (CS640)	16.22	1.74	28.22	17.40	38.35%	

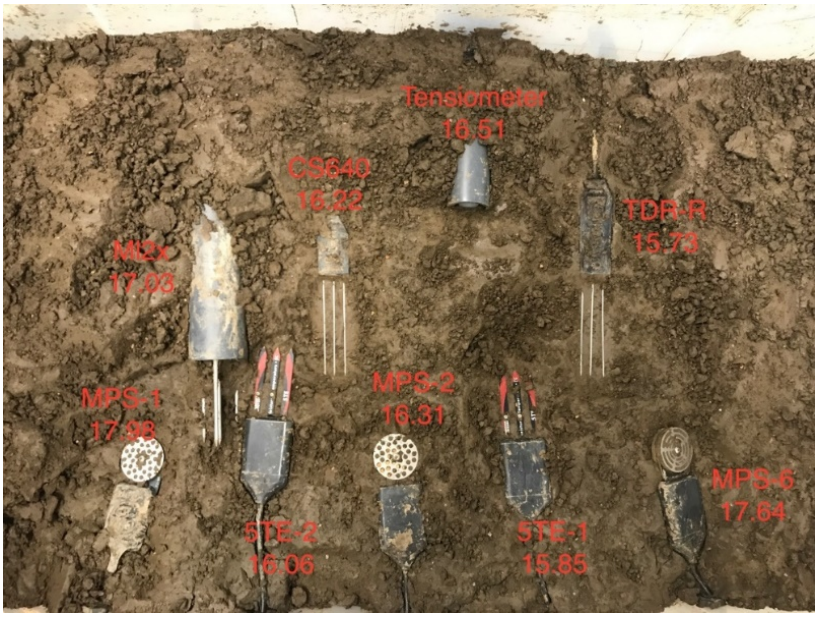

Figure 4.7 A photograph of device layout in the soil box lysimeter showing the sensor locations and the gravimetric water content results of the surrounding soil for each sensor.

In summary, heterogeneities in water content and suction were detected in the soil box (the 54L soil sample in this experiment). The point measurement sensors can provide abnormal measurements due to many uncertainties. In order that the sensors can be used properly, soil-specific calibrations are essential.

4.2.3 Soil property relationships

4.2.3.1 Soil-water retention curves (SWRCs)

In the previous sections, the time series pore water pressure, volumetric water content and electrical resistivity data were presented. In this section, the data are presented as soil water retention curves (SWRCs), which combine the pore water pressure and water content data at each time point. The SWRC is produced based on the VWC and suction data obtained from TDR-R and MPS-2 sensors respectively as these devices were considered to have the greatest accuracy during the calibration exercise. Figure 4.6 presents the SWRCs of the soil sample under three drying and wetting cycles. In Figure 4.6a it can be seen that in the first drying and wetting cycle, the VWCs on the drying path are higher than those on the wetting path corresponding to the same suction values, clearly demonstrating a hysteresis between drying and wetting. The saturated VWC drops from about 39.5% at the beginning of the first drying path (initial VWC as a compacted

condition) to approximately 35% at the end of the first wetting path. Figure 4.6b presents the SWRCs of the soil sample for the second drying-wetting cycle, again there is a hysteresis between the drying and the wetting path that demonstrates a higher VWC on the drying path than that of the wetting path corresponding to the same suction. However, the hysteretic behaviour of SWRCs is less significant in the second cycle than in the first cycle. In addition, the hysteresis is shown to be insignificant at the top and bottom portions of the drying-wetting loop and the sample was wetted back to about 35% VWC at the wet end of the second cycle wetting path. Figure 4.6c shows the SWRCs of soil samples for the third cycle. The same hysteretic behaviour is detected in the third cycle. The wetting stage of the third cycle was not completed due to time limitations.

Figure 4.7 illustrates combining SWRC data for all the three drying-wetting cycles. It can be seen that the suction value at a given water content in the first drying path is higher than that in the second drying path and further higher than that in the third drying path, indicating a deterioration in the suction of soil sample as the number of drying-wetting cycles increases.

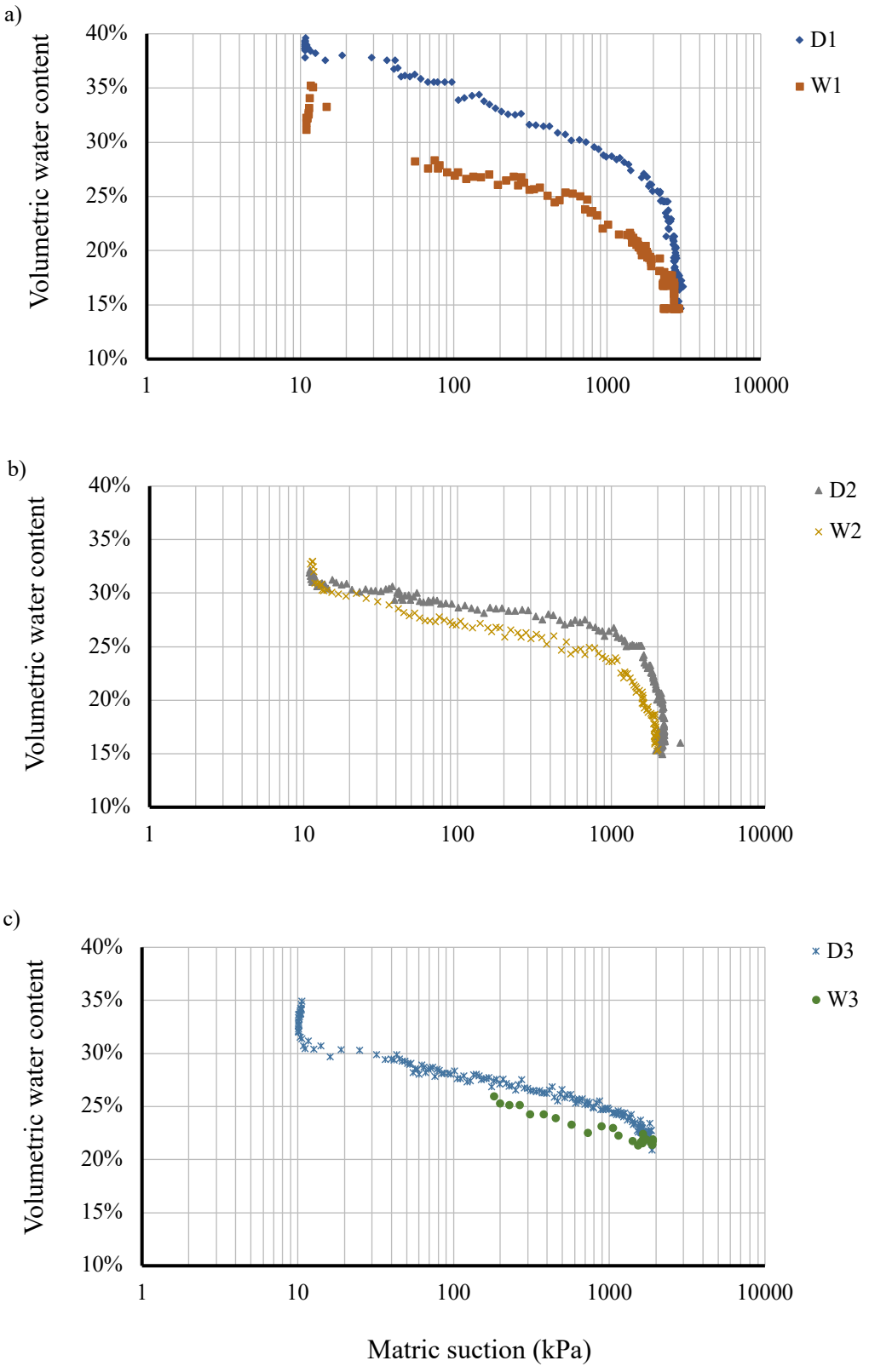

Figure 4.8 SWRCs for glacial till material under drying and wetting (a) the first cycle (b) the second cycle (c) the third cycle

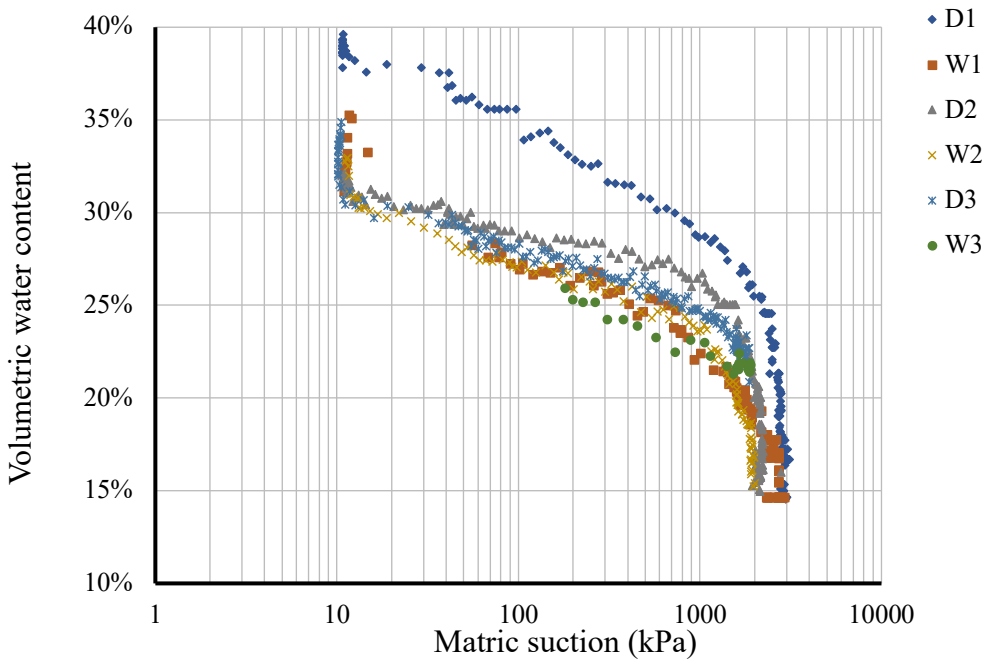

Figure 4.9 SWRCs of glacial till under drying and wetting for the box lysimeter sample

4.2.3.2 Resistivity-water content relationships under drying and wetting

The relationships between electrical resistivity and volumetric water content under cyclic drying and wetting for the box lysimeter sample are presented in Figure 4.8. Overall, the soil resistivity increases with decreasing water content. In the first drying-wetting cycle (see Figure 4.9a), the resistivity increases from 20 Ωm to 74.6 Ωm during drying and then decreases to 17 Ωm during wetting. It can be seen that the resistivities in the wetting path show higher values than in the drying path when the VWC of the sample is over 26% and lower values than in the drying path when the VWC is under 26%. The same situation can be seen in the second and the third drying-wetting cycles. This may be due to 1) the different volumetric (shrinking and swelling) behaviour of clays during drying and wetting, which cause the differences in soil's degree of saturation between drying and wetting at given VWCs and the resistivity of soil is more closely related to the degree of saturation than to the VWC; 2) the development of micro-cracks during drying processes, as the air in the cracks reduce the conductivity of soil in the dryer condition and the water in the cracks increase the conductivity of soil in the wetter condition.

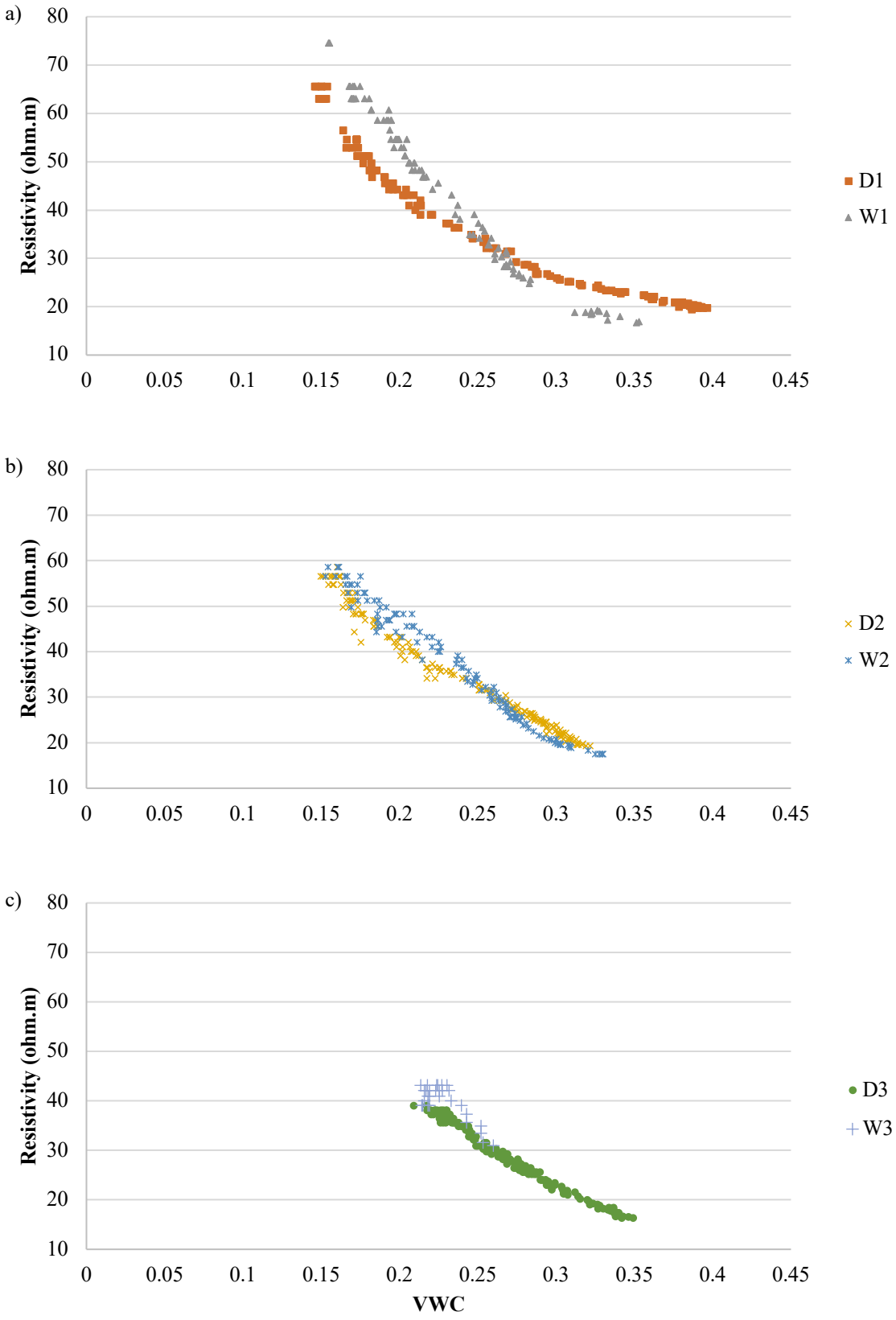

Figure 4.10 Resistivity-volumetric water content relationships of glacial till under drying and wetting for box lysimeter sample: a) the first cycle; b) the second cycle: c) the third cycle.

4.3 Triaxial sample experiment results

In this section, testing results obtained using the 38 mm diameter triaxial specimens according to the methods stated in subchapter 3.3 are presented. In the triaxial sample testing programme, soil properties including water content, suction, resistivity and undrained shear strength were measured using triaxial samples made of three different soil materials. The interrelationships between the measured properties for these soils such as the SWRC, strength water content relationship and resistivity water content relationships are presented.

4.3.1 Soil water retention (SWR) behaviour

A series of soil water retention curves (SWRCs) are presented in this section to understand the soil water retention behaviour of the three different types of soil (i.e., glacial till, London Clay and Hollin Hill clay).

For all three types of soil, the total suctions were measured on small pieces of sample (cylinder with a diameter of 30mm and a thickness of 2mm) that were sliced off the triaxial samples (after triaxial testing) using the Decagon WP4C water potential-meter. An additional SWRC measurement was conducted using the tensiometer apparatus to determine the cyclic SWRCs for the glacial till material in low suction ranges (less than 1000 kPa). Since the osmotic suction takes a large proportion of the total suction in the low suction range (normally < 1000 kPa) and a very minor proportion in the higher suction range (> 1000 kPa), the total suction data of which the values are greater than 1000 kPa are also representative for the matric suction. As a result, a full range data set for the SWRCs was made in a combination of data measured by the tensiometer apparatus for the low suction range (<1000 kPa) and data measured by the WP4C for the high suction range (>1000 kPa). All the measured suction data were fitted with the Fredlund and Xing (1994) model and the obtained SWRCs are presented using volumetric water content (VWC).

4.3.1.1 Total suction SWRCs

The total suction SWRCs for glacial till material determined using the WP4C potential meter are shown in Figure 4.11. SWR data for three drying and wetting cycles are presented for the glacial till material. Generally, the total suction SWRCs are interpreted

as logarithmic functions as to the relationships between total suction and volumetric water content and all the curves fall within the range of suction approaching residual water content at high suction values and the air entry pressure at low suction values. The total suction grows rapidly as the soil samples desaturate. In the first drying path, the total suction increased from about 100 kPa to around 40,000 kPa when samples were dried from a saturation VWC of about 40% to a residual VWC of about 5%. In the first drying and wetting cycle, an obvious hysteresis can be detected between the drying and wetting path, which indicates a higher volumetric water content on the drying path than that on the wetting path at a given suction value. It can be seen that the SWRCs for the following two cycles are all enveloped in between of the first drying and wetting curves. The SWRCs for the second and the third drying-wetting cycles are less hysteretic than in the first cycle. Comparing the first and the second drying curves, it can be seen that the total suction on the first drying path is higher than that on the second drying path at a given VWC value, indicating a deterioration in suction from the first to the second drying path.

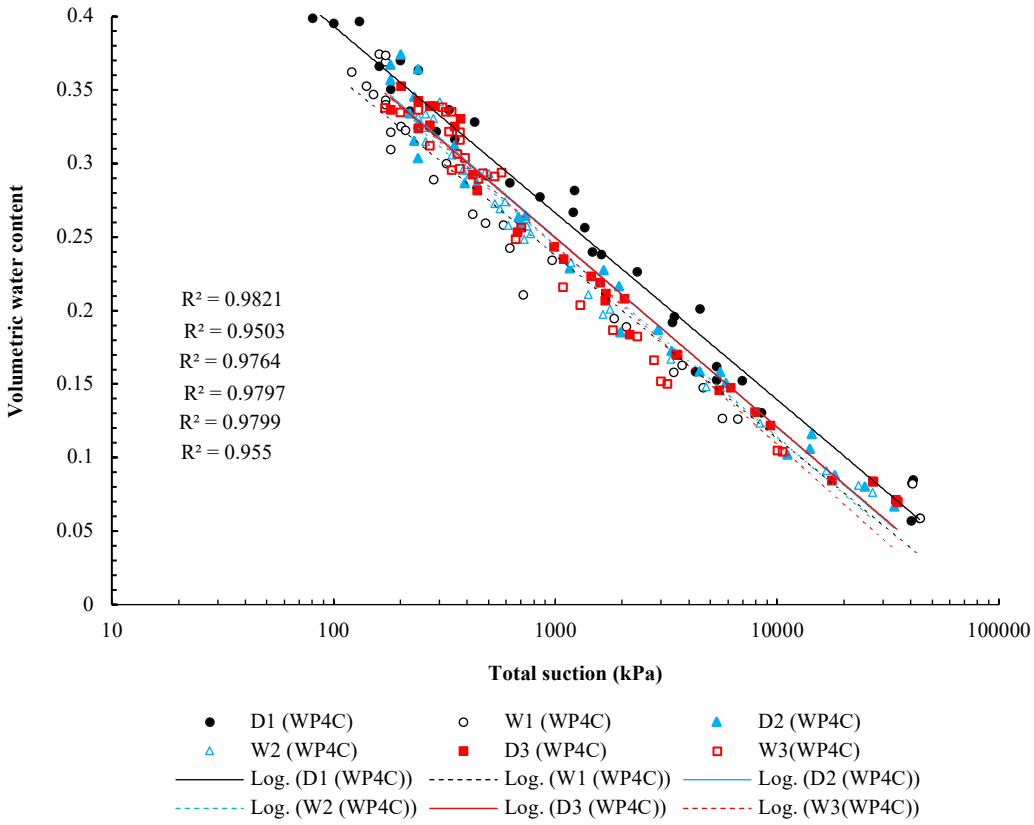

Figure 4.11 Soil water retention curves of the glacial till for cyclic drying and wetting. The suction values are presented using total suction measured by the WP4C potential meter. 'D1' and 'W1' represent the first drying path and the first wetting path.

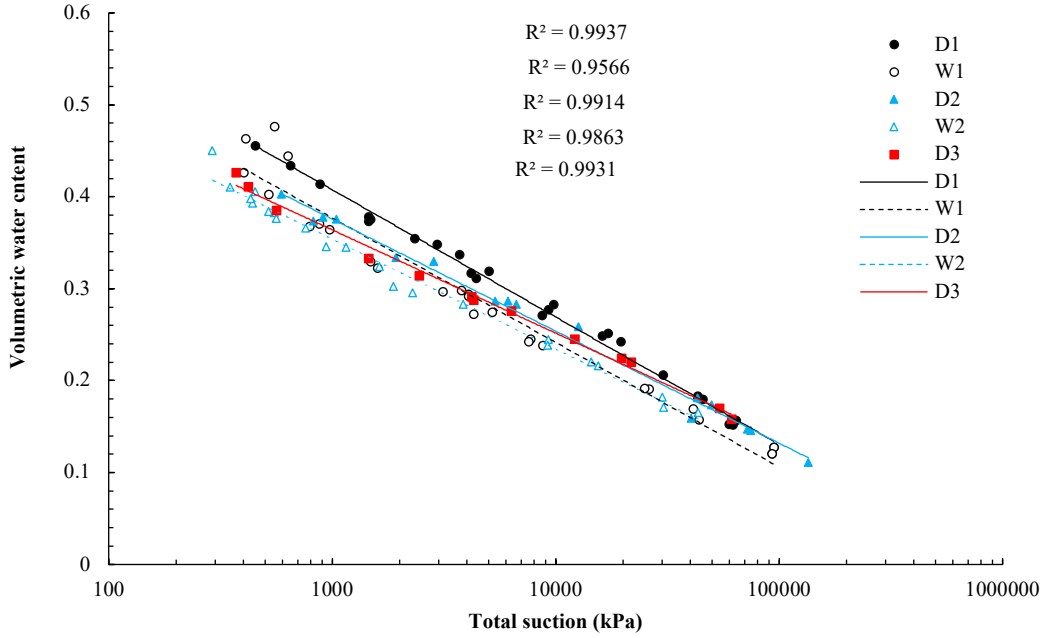

Figure 4.12 Soil water retention curves of the London Clay for cyclic drying and wetting. The suction values are presented using total suction measured by the WP4C potential meter.

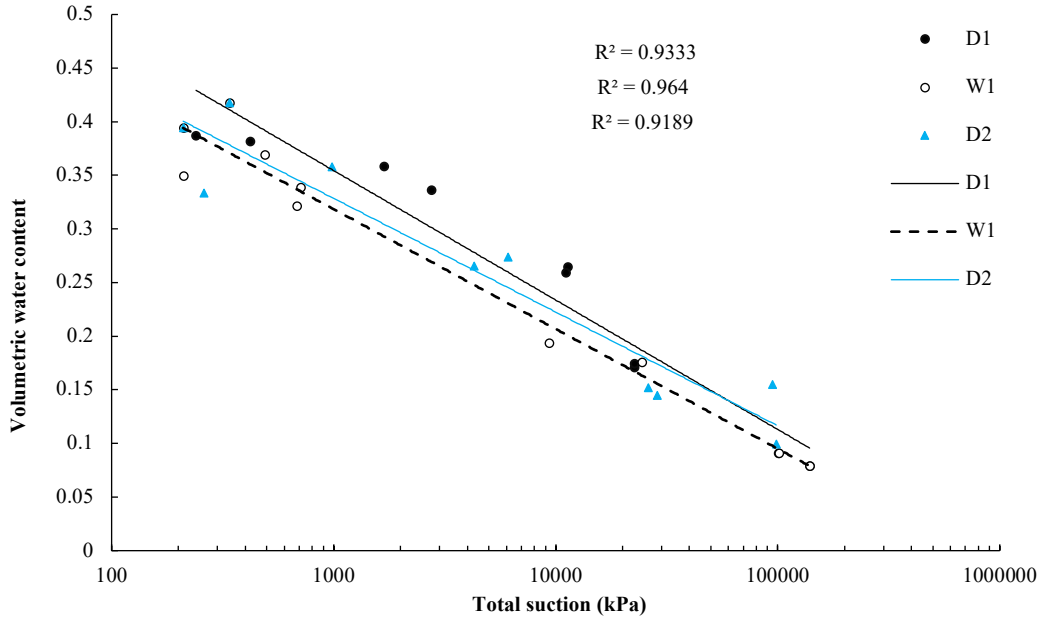

Figure 4.13 Soil water retention curves of the Hollin Hill Clay for cyclic drying and wetting. The suction values are presented using total suction measured by the WP4C potential meter.

The total suction SWRCs for London Clay and Hollin Hill Clay under cyclic drying and wetting are presented in Figure 4.12 and Figure 4.13 respectively. In Figure 4.12, the same hysteresis between drying and wetting paths is found in the London Clay's SWRCs

during the first and the second drying-wetting cycles. The deterioration in total suction can also be detected between the drying curves as the number of cycles increases. The SWRC data for the Hollin Hill are more scattered as shown in Figure 4.13, this may be due to some operation error during the experiment. It must state that the tests on Hollin Hill samples was conducted with the assistant of an undergraduate student, Anna Brooks. More variability in Hollin Hill data may be resulted from the different operating procedures during testing. However, the hysteresis and deterioration in the total suction SWRCs can also be evident in the fitting curves to the Hollin Hill data.

4.3.1.2 Matric suction SWRCs

The total suction values measured by WP4C can only substitute matric suctions when the values are greater than about 1000 kPa where the osmatic suctions make up only a minor proportion. In order that the soil water retention curves can be made on a wider range, a series of soil water retention data were measured using tensiometer apparatus to cover the measurements in low suction range (<1000 kPa). Parts of the data obtained using the dewpoint method (WP4C) are selected to cover the measurements in high suction range (>1000 kPa). By combining these two sets of data a full range SWRC data set with respect to the matric suction was determined. The widely used SWRC models proposed by van Genuchten (1980) and Fredlund and Xing (1994) were used to fit experimental data obtained in the laboratory, hereafter referred to as the VG model and the FX model, respectively. Figure 4.14 shows experimental data of SWRCs for the Glacial till during the first drying and wetting cycle along with the best-fit curves for both the VG and the FX models. The R-squared values of the regression models show that both the VG and the FX models have a good fit to the measured data, whereas the FX model performs better than the VG model in describing the drying SWRC data. As can be seen in Figure 4.14 that discrepancy could be found between the VG and the FX fitting curves at the wet end, where the suction values were less than approximately 300 kPa. The VG SWRC was flatter than the FX fitting curves in the low suction range and overestimated the VWC values in the suction range between 10 to 300 kPa on the drying path. It can also be observed that the VG fitting curves demonstrated higher VWC values than the FX fitting curves in the high suction range with suction values greater than 10 MPa. To be concluded, the FX model performed better than the VG model since it provided more flexible fit to the experimental data obtained in this study. It may be due to that the VG equation

(Equation 2.11) related the two fitting parameters m and n through the fixed relationship $m = 1 - 1/n$. This reduces the flexibility of the fitting model. More accurate results can be obtained using FX model which leaves m and n parameters with no fixed relationship (Fredlund and Xing, 1994). Therefore, the SWR data of Glacial till under multiple drying and wetting cycles were fitted with the FX model hereafter to produce the SWRCs in this thesis.

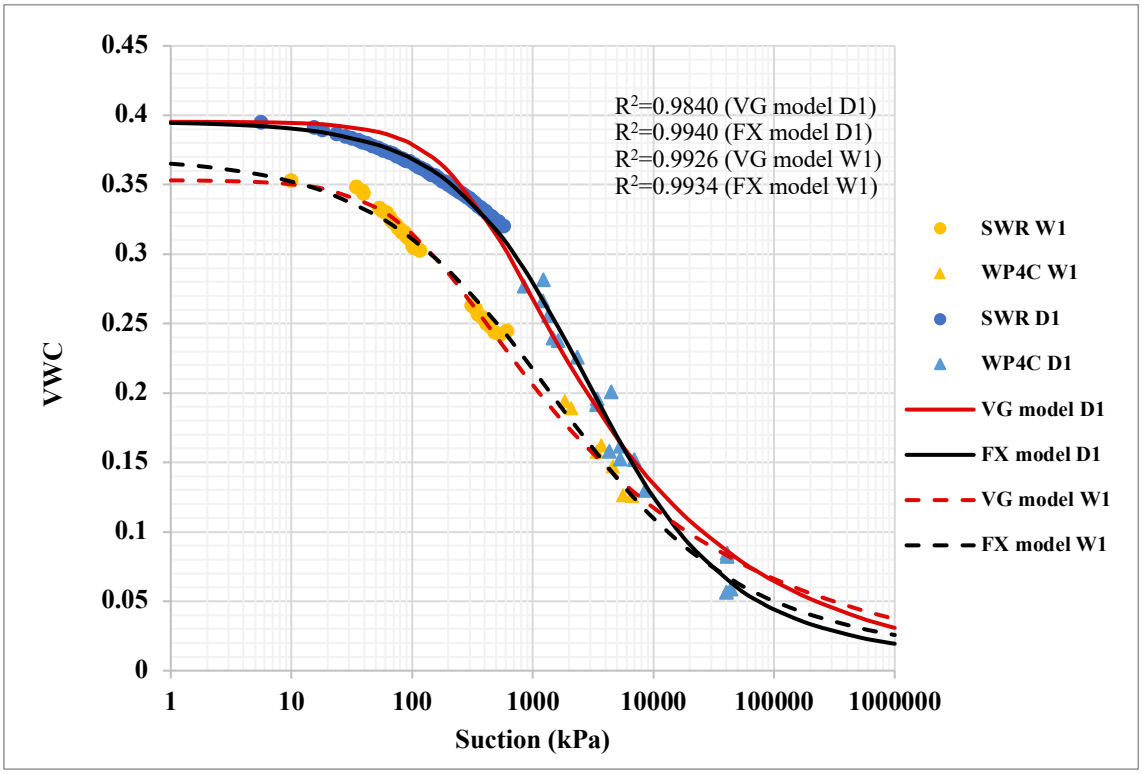

Figure 4.14 Curve fits for the van Genuchten (VG) and the Fredlund and Xing (FX) models with SWRC data for the Glacial till during the first drying and wetting cycle.

SWRCs for Glacial till under cyclic drying and wetting were produced using Fredlund and Xing (1994) model as shown in Figure 4.15. Generally, in one drying and wetting cycle, the VWCs of drying path show higher values than that of the wetting path at given suctions. Distinct hysteresis can be found between the primary drying and wetting paths, whereas the hysteretic behaviour gradually decreased as the number of cycles increased. It can be seen that VWC of the first-cycle drying path is higher than those of the subsequent cycles and the saturated VWC gradually drop down by cycles at the wet end of the drying curves. The saturated volumetric water content at the beginning of the first drying path is shown to be about 39% and dropped to around 34% when the second drying path started, and subsequently dropped to about 32.5% while the third drying path started, indicating a deterioration in suction as the number of drying-wetting cycle increases.

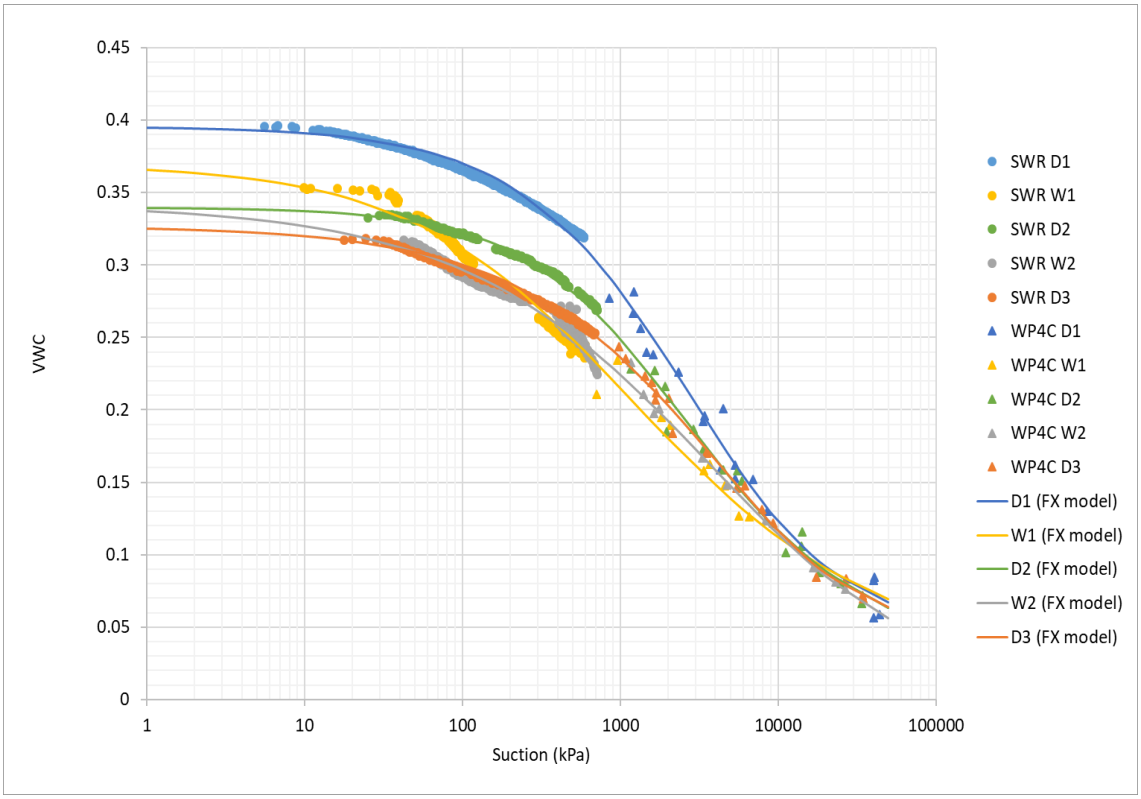

Figure 4.15 Soil water retention curves for glacial till under three cycles of drying and wetting obtained using tensiometer apparatus for wet range (SWR) and dew point potentiometer for dry range (WP4C) along with the best fitting curves based on Fredlund and Xing model

The SWRCs for three continuous drying paths are presented using the degree of saturation as moisture proxy in Figure 4.16 where the air-entry values (AEVs) were also determined based on the curves. It shows that the air-entry value of the glacial till material at the first drying path was determined to be close to 610 kPa, whilst the AEVs for the drying paths of the second and the third cycle were about 500 and 400kPa, respectively. It means the air entry value of glacial till material gradually decreased by cycles as the number of drying-wetting cycles increased.

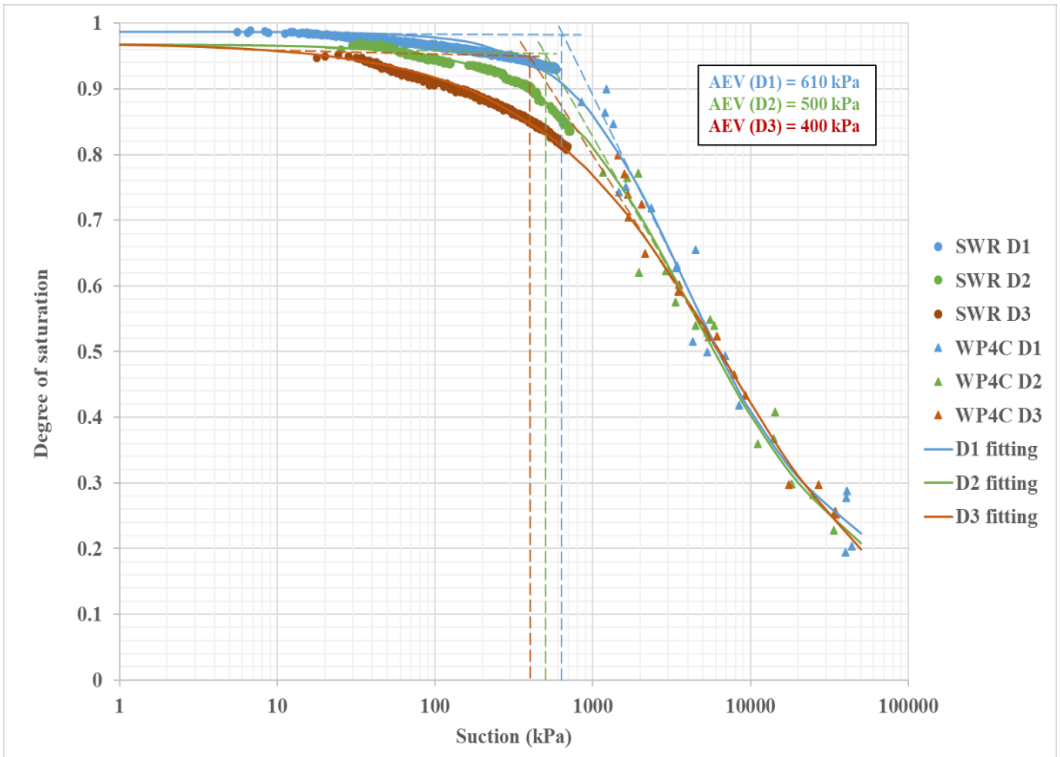

Figure 4.16 Degree of saturation versus matric suction SWRCs obtained from compacted glacial till material by tensiometer and WP4C potential meter for three drying paths. Air entry values for the three drying paths are determined based on the Fredlund and Xing (1994) fitting models.

Figure 4.17 shows the comparison between the total and matric suction SWRCs determined for the first drying and wetting cycle of glacial till material. The total suction was measured using WP4C and the matric suction was determined using the combination of the tensiometer apparatus and WP4C. It can be seen that both the drying and wetting curves in a wet moisture range from continuous measurements using tensiometer are in good connection with the data points of total suction in a dryer range measured by the WP4C potentiometer, indicating the SWRCs can be successively determined over the whole soil moisture range by the combination of these two methods. However, for the wet end, the total suctions measured by WP4C show higher values than the matric suctions measured by tensiometer as the osmatic suction of soil is more pronounced in low moisture range.

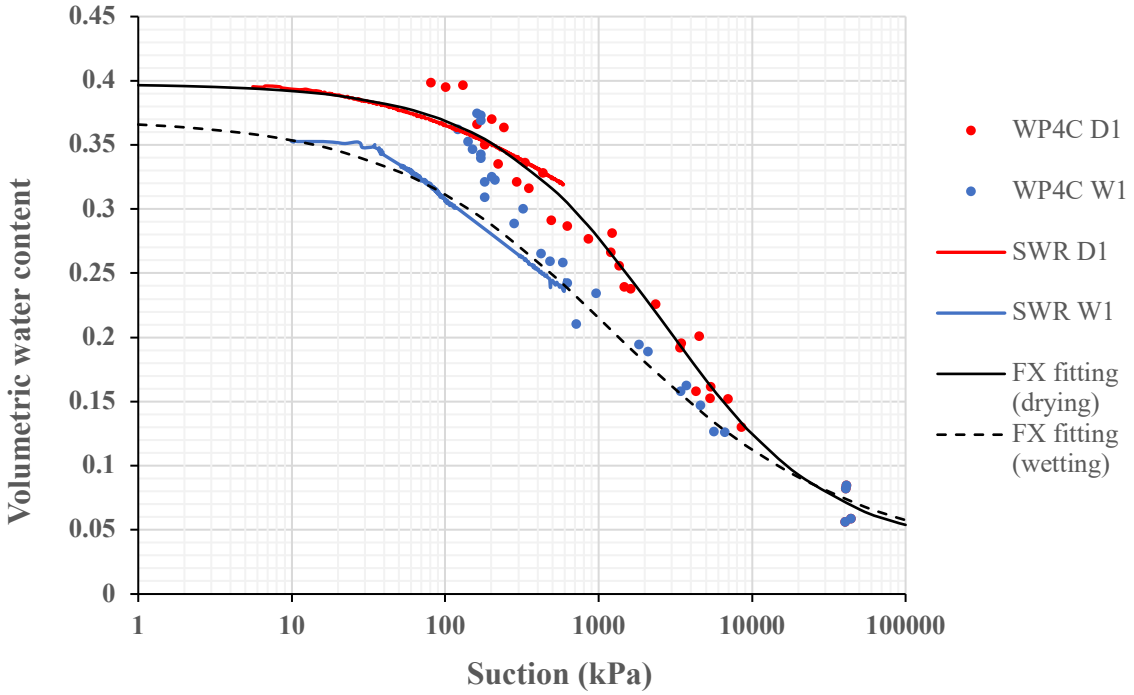

Figure 4.17 A comparison of SWRCs between total suction and matric suction measured for the glacial till material in the first drying and wetting cycle with total suction obtained by WP4C and matric suction obtained by the combination of tensiometer and WP4C.

4.3.2 Shear strength-water content relationships

The undrained shear strengths of soil samples were determined through the undrained unconsolidated (UU) triaxial test following the procedures described in BS 1377-7:1990 Chapter 8 (BSI, 1990). The shear strength results of the three soils under drying and wetting cycles are presented in this section.

4.3.2.1 BIONICS material

The relationships between the undrained shear strengths C_u and the gravimetric water contents w for the glacial till under three drying and wetting cycles are presented in Figure 4.18 by different cycles separately. As shown, the C_u-w characteristic curves are interpreted as logarithmic functions within the water content range between residual water content to nearly saturation. The undrained shear strength increases as the specimens are dried out from the initial water content and decreases as the specimens are wetted back.

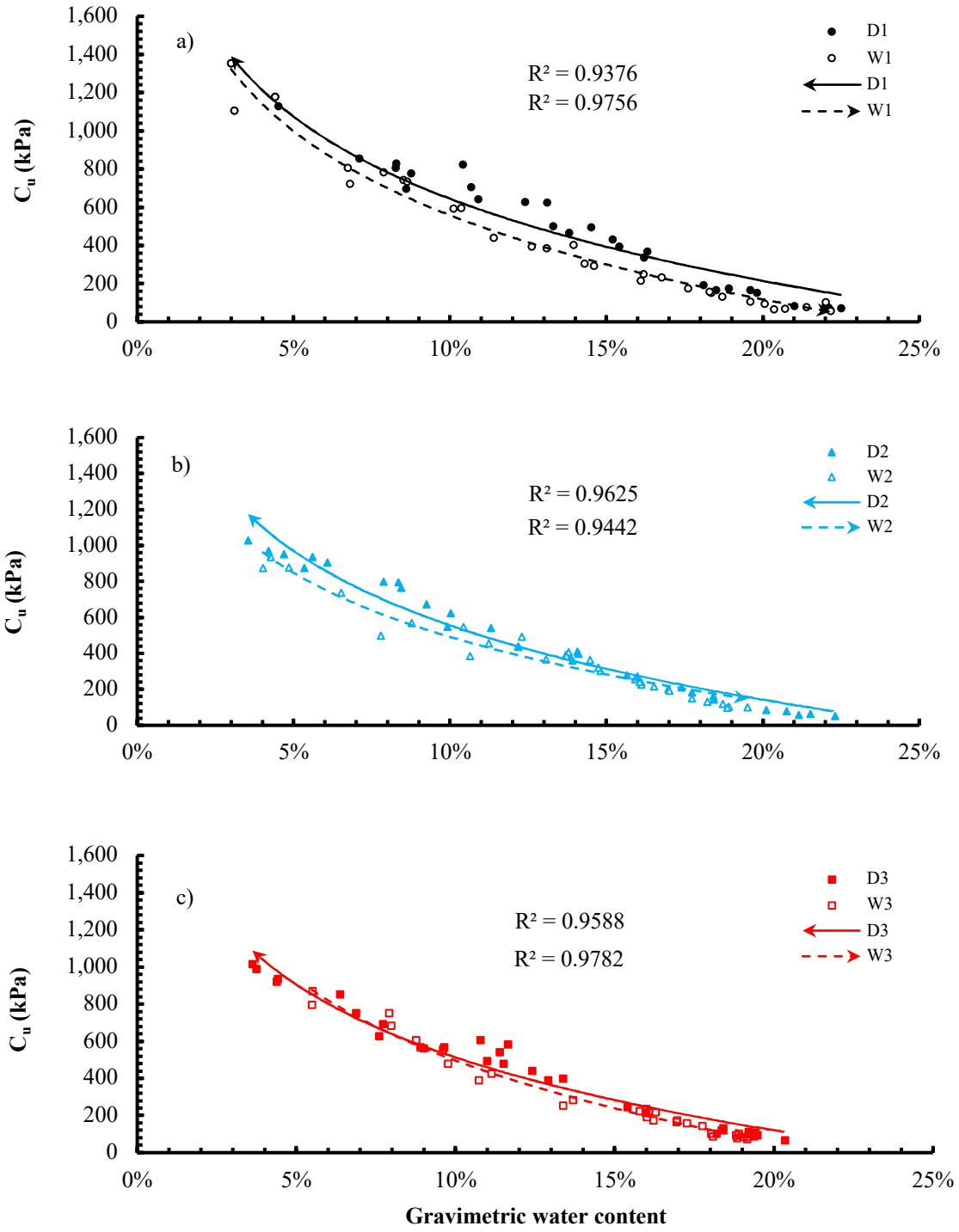

Figure 4.18. Undrained shear strength, C_u - water content (gravimetric) relationship of the glacial till for three drying-wetting cycles: a) the first drying-wetting cycle, b) the second drying-wetting cycle, c) the third drying-wetting cycle.

Hysteresis can be found between the drying and wetting path of the C_u-w relationship, for all the drying-wetting cycles. The specimens exhibit higher shear strength values in the drying path than in the wetting path at a given water content, although these converge at

two ends of the loops. This behaviour relates to the hysteresis between the drying and wetting of the soil water retention behaviour, the lower suctions of the wetting path might result in the lower suction-induced shear strengths, causing the reductions in wetting path shear strengths. However, the hysteretic relationship between C_u and w may also be influenced by micro-scale cracking or the volumetric changes (swelling and shrinking) of the clay material during cyclic drying and wetting.

Figure 4.19 presents the shear strength – gravimetric water content relationships for the drying paths of the three drying-wetting cycles in the glacial till. The data shows a deterioration in shear strength while the number of drying and wetting cycles increases, which might be due to the micro-scale crack development. However, the deterioration is shown to be more significant between the first and the second cycle than between the second and the third cycle. This can be explained as the initialization of the main cracks normally occurs in the first drying path while the soil is subjected to successive drying and wetting (Stirling al et., 2015); or it could also be linked to relatively large porosity changes driven by the shrink-swell action causing changes to the SWR relationships between different drying-wetting cycles.

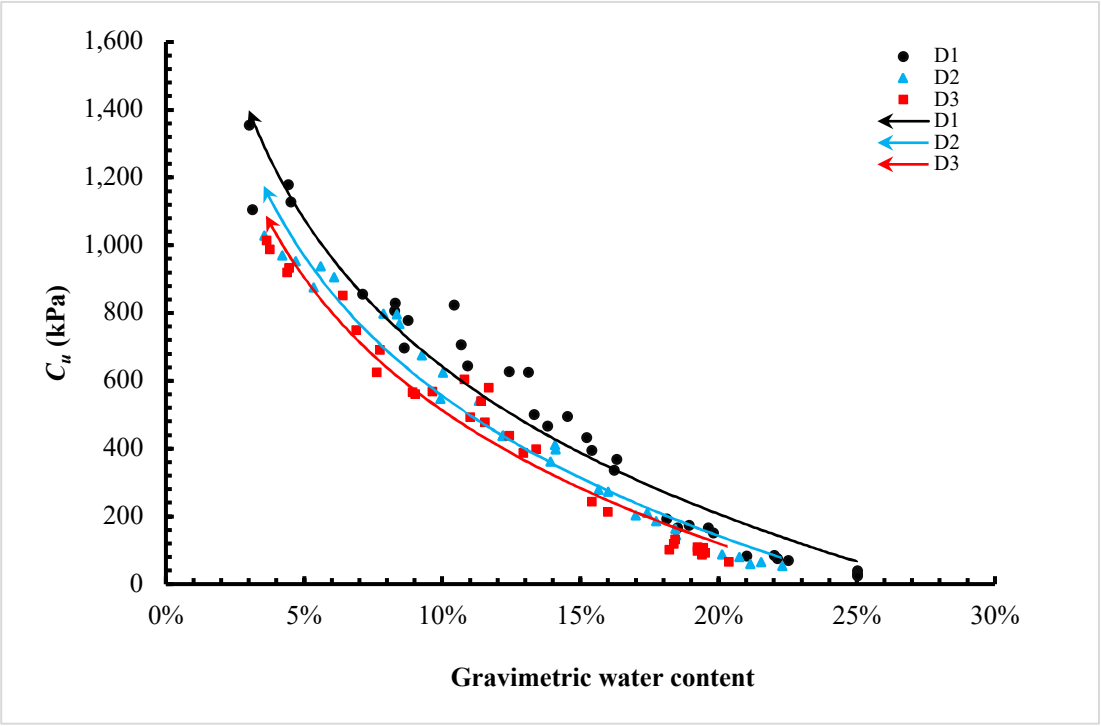

Figure 4.19 Comparison of the C_u-w relationships between the drying paths of the three cycles for glacial till

However, it must be noticed that describing the shear strength changes using GWC as the water content proxy does not take the volumetric changes into account. The shear strength data are also plotted against volumetric water content (VWC) and degree of saturation (S_r), showing in Figure 4.20 and 4.20, respectively. The shear strength against VWC and S_r plots also show a hysteresis between drying and wetting in each drying-wetting cycle due to hysteretic soil water retention behaviour. The reduction in shear strength at a given VWC or S_r as the number of drying-wetting cycle increases also indicates the deterioration in soil fabric due to the development of cracking.

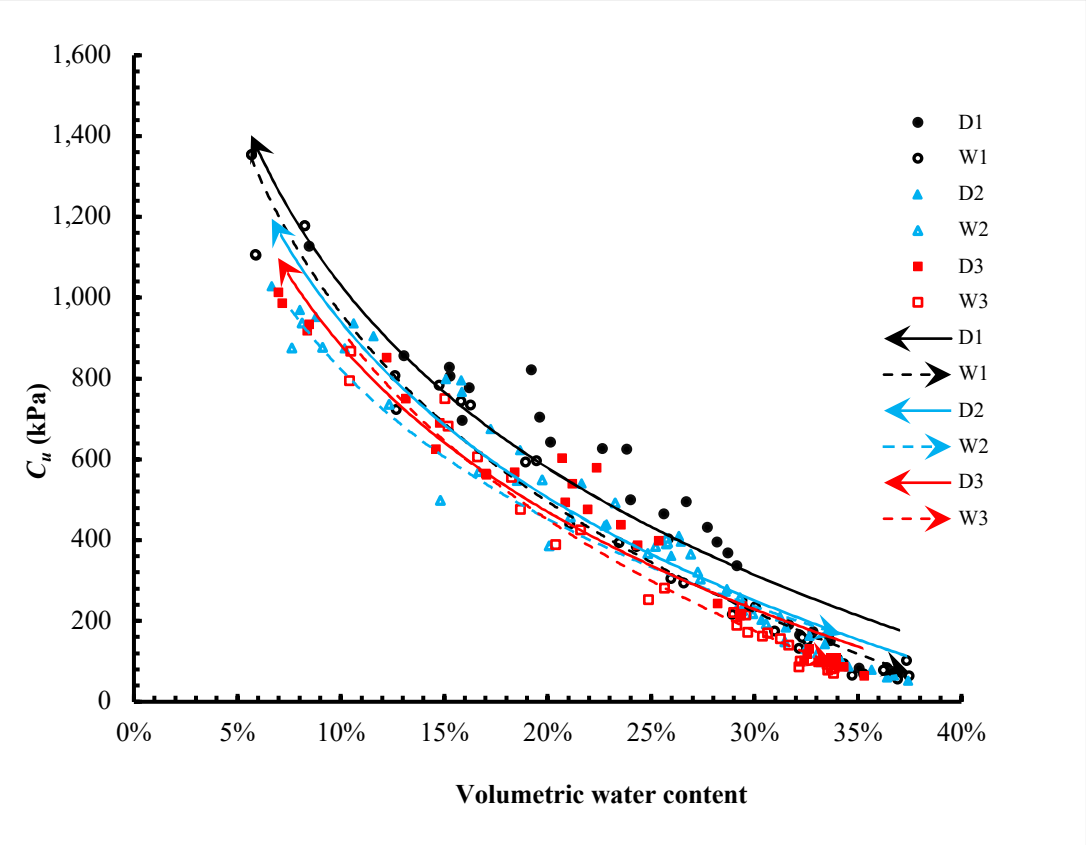

Figure 4.20 Relationships between undrained shear strength and VWC for glacial till for three drying-wetting cycles

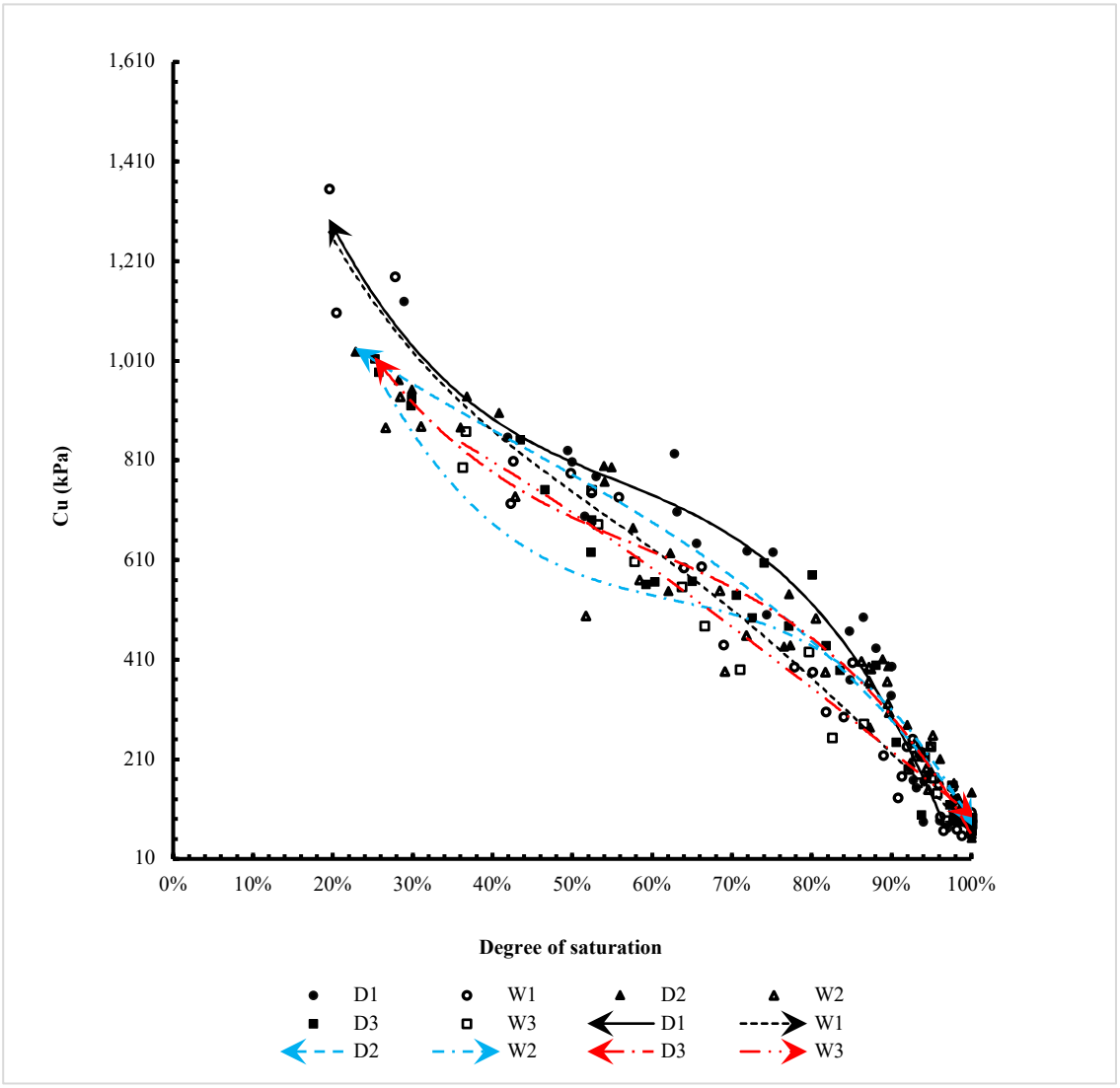

Figure 4.21 Relationships between undrained shear strength and degree of saturation for glacial till for three drying-wetting cycles

4.3.2.2 London Clay

Figure 4.22, 4.21 and 4.22 present the relationships between undrained shear strength against GWC, VWC, and degree of saturation for the London Clay specimens under successive drying and wetting, respectively. From the gravimetric water content plot (Figure 4.22) it can be seen that the C_u of specimens increase with the decreasing water content. Hysteresis between drying and wetting paths can be detected for the first and second cycle, however, for the third cycle, only the drying experiment has been done. The shear strengths in the first cycle drying path show higher values than the second cycle drying path at given water contents, while the shear strengths of third drying path lie somewhere in between of the first and second paths. Again, the gravimetric plot does not count the effect of dry density (and other volumetric changes of clay material under

drying and wetting), so that the volumetric water content and S_r plots are presented in Figure 4.23 and 4.23 respectively. The undrained shear strength data against VWC and S_r indicate that the C_u increases with decreasing VWC and desaturation during drying and vice versus during wetting. Hysteresis in shear strength behaviour between drying and wetting is evident again in the data. Comparing the three drying paths, the drops in shear strengths at given VWC and S_r from first to following drying-wetting cycles imply the deterioration in strength property of London Clay as the number of drying-wetting cycle increases.

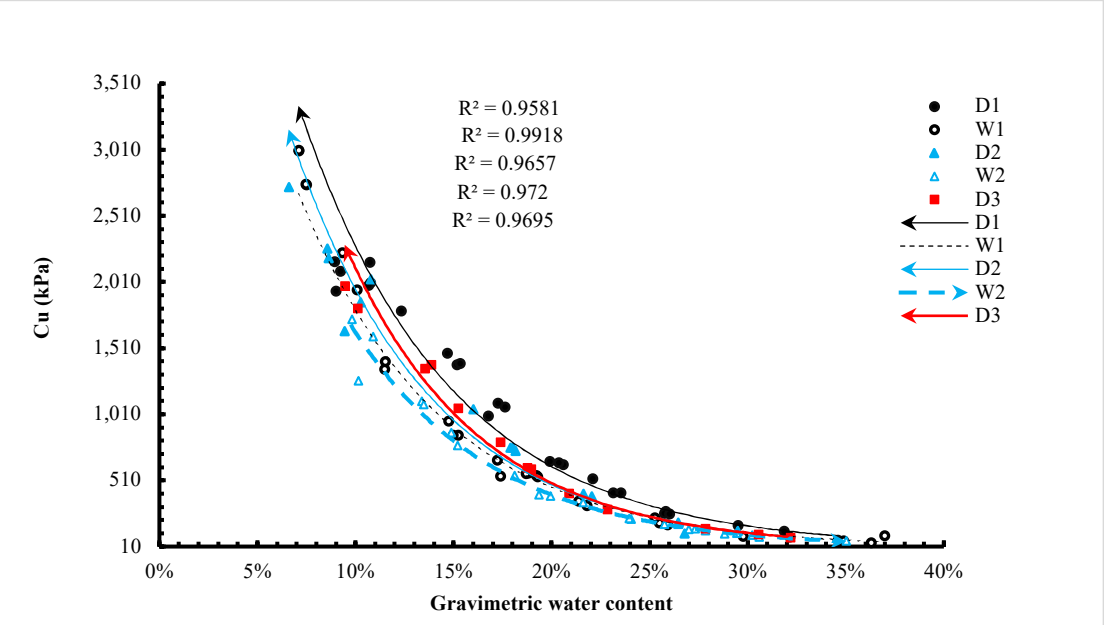

Figure 4.22 Shear strength-GWC relationships for London Clay under cyclic drying and wetting

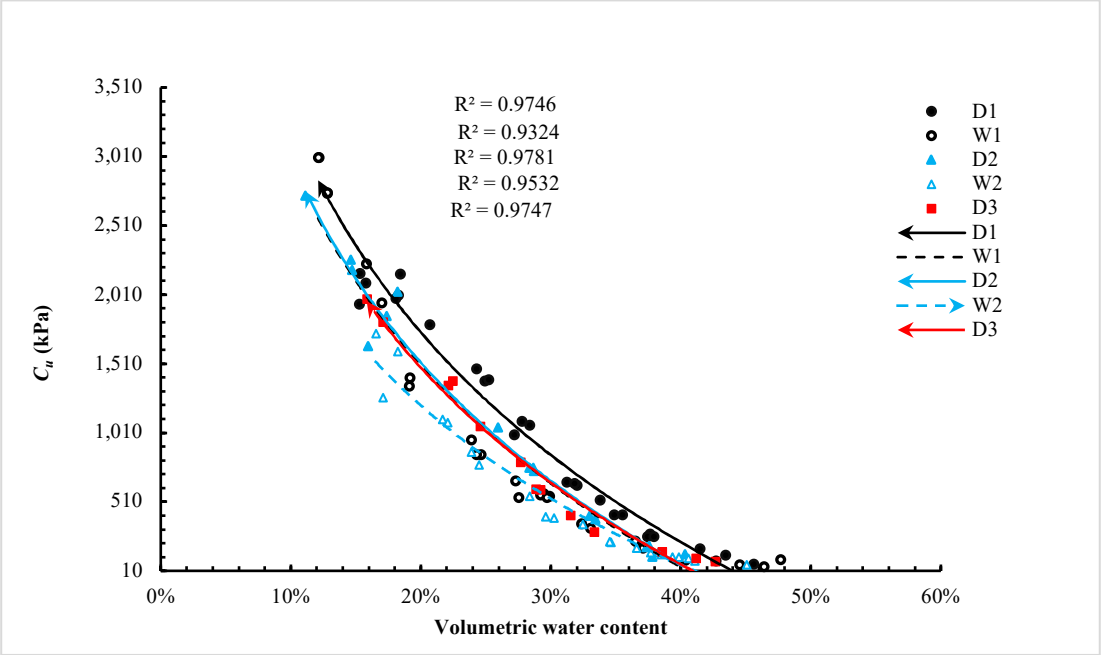

Figure 4.23 Shear strength -VWC relationships for London Clay specimens under cyclic drying and wetting.

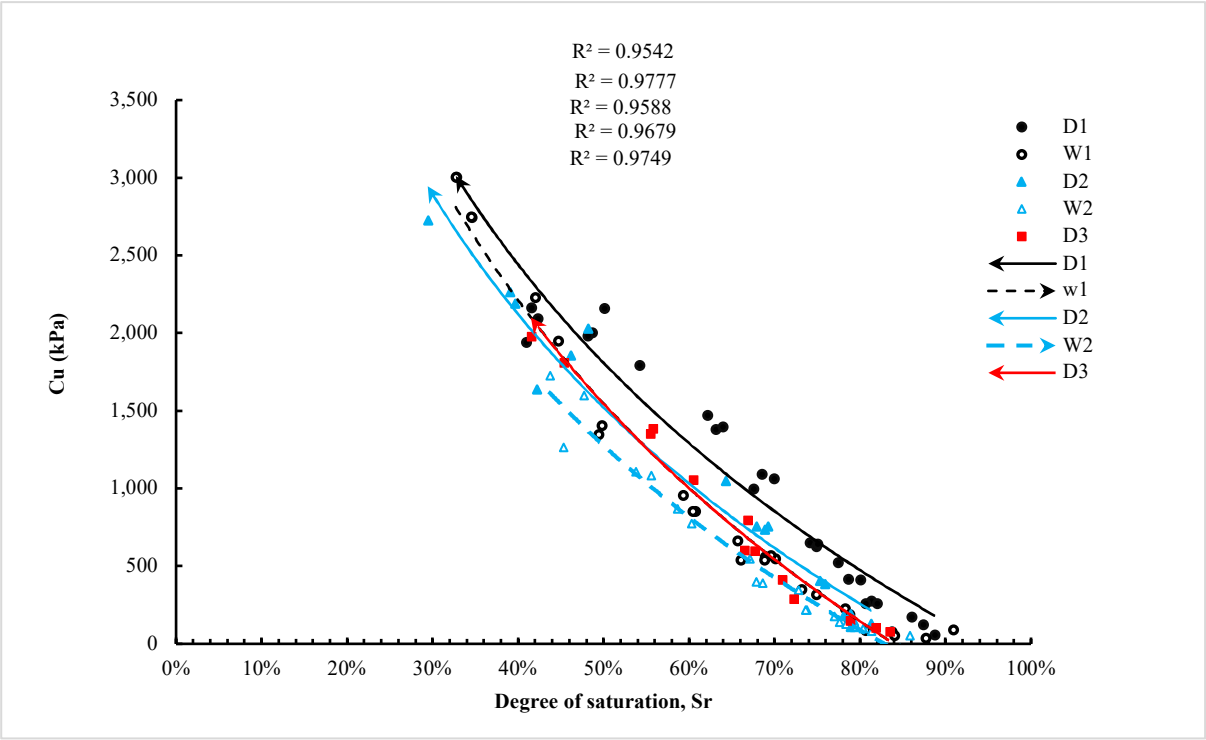

Figure 4.24 Shear strength - degree of saturation relationships for London Clay under cyclic drying and wetting.

4.3.2.3 Holin Hill Clay

Figure 4.25, 4.25 and 4.26 present the undrained shear strength data as a function of the GWC, VWC, and degree of saturation, respectively. Once again, the data suggests that

there is a hysteresis between the drying and wetting path of C_u-soil water content relations. The undrained shear strengths of Hollin Hill specimens on the second drying path are lower than those on the first wetting path, strongly proving that the reduction in shear strength from the first to second drying path is not entirely due to the hysteric soil water retention behaviour, the deterioration in soil fabric is evident.

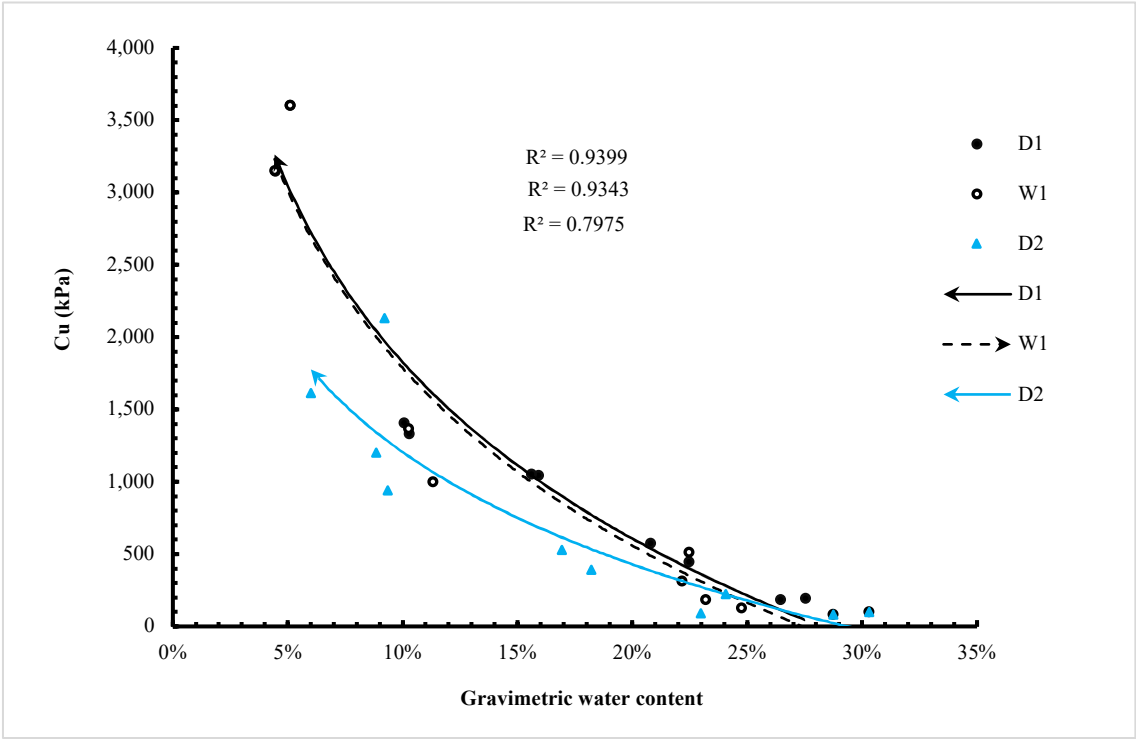

Figure 4.25 Relationship between undrained shear strength and GWC for Hollin Hill material under cyclic drying and wetting.

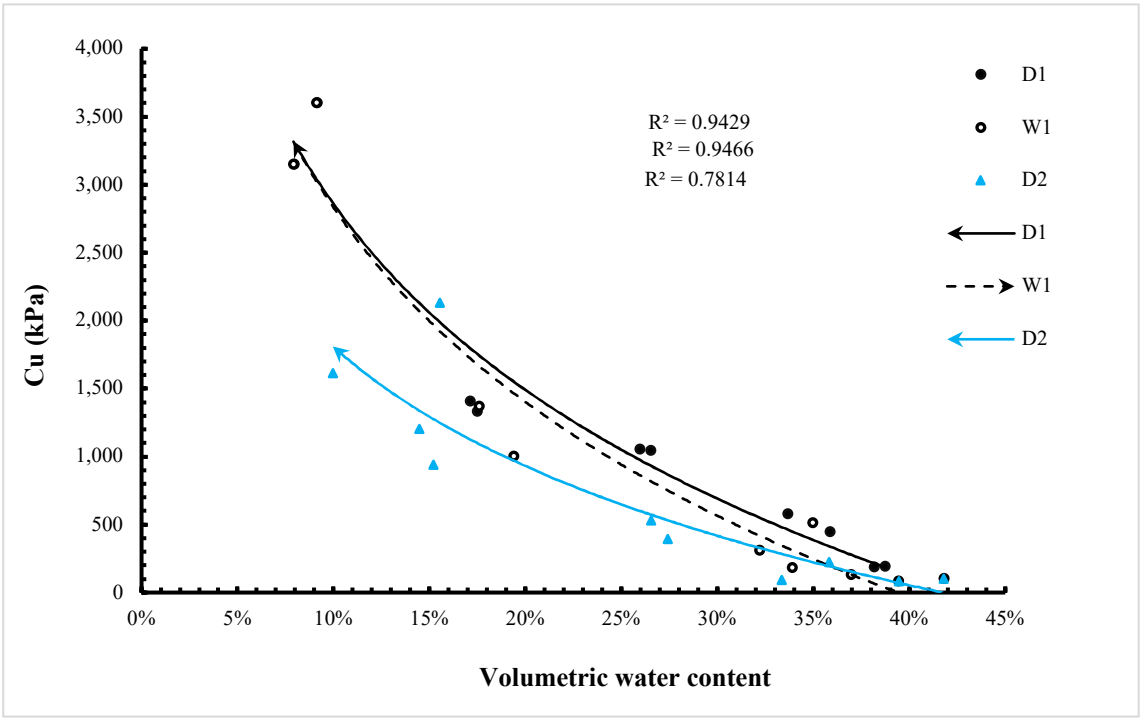

Figure 4.26 Relationship of undrained shear strength and volumetric water content for Hollin Hill material under cyclic drying and wetting.

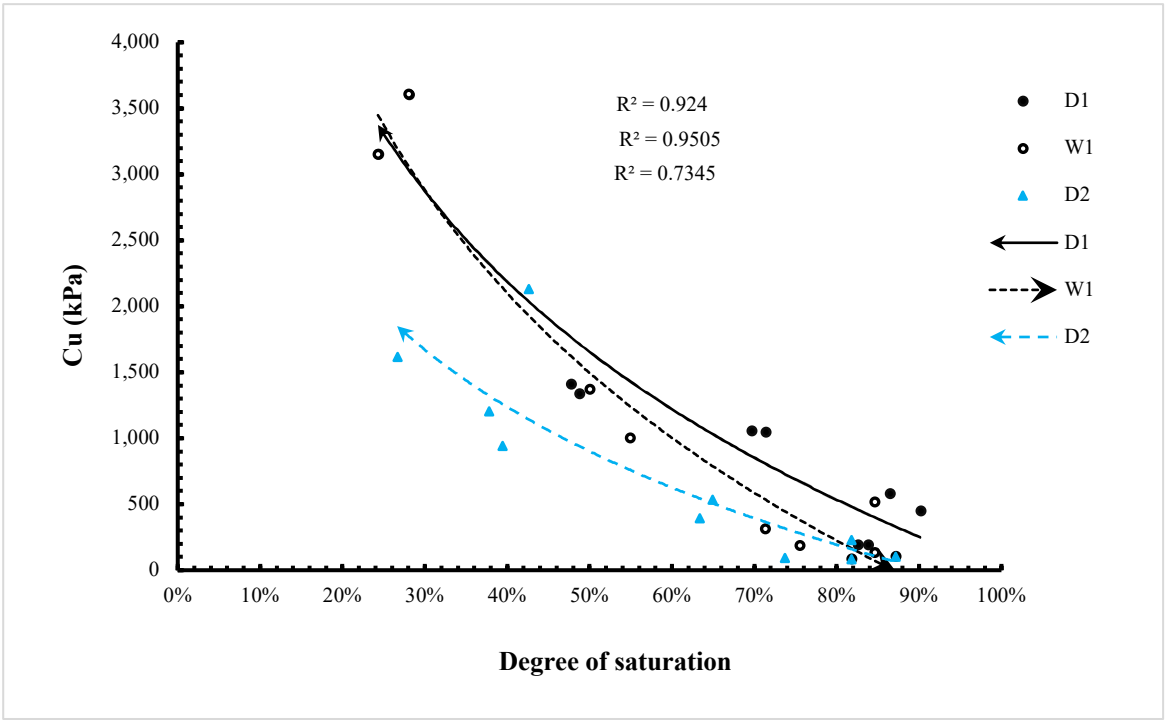

Figure 4.27 Relationship between undrained shear strength and degree of saturation for Hollin Hill material under cyclic drying and wetting.

4.3.3 Shear strength – suction relationships

Figure 4.28 shows the data of undrained shear strength C_u as a logarithmic function of the soil suction for specimens of glacial till at three drying paths. It can be seen that the C_u increases rapidly to about 600 kPa with the growing suction and then increases gradually thereafter as the specimens are dried out. All the drying stages exhibit a drop in shear strength at a given suction with increasing number of drying-wetting cycles.

Figure 4.29 and 4.29 present the C_u-total suction relationships of drying paths for the London Clay and Hollin Hill Clay specimens, respectively. The data also suggest a rapid increase in C_u of London Clay and Hollin Hill Clay specimens up to about 800 kPa and 500 kPa respectively with growing suction, in a low suction range. The shear strength then increases slower with growing suction in the higher suction range. The drops in shear strength from previous to next drying path at a given suction can also be observed in the London Clay and Hollin Hill Clay data. These suction-independent deterioration in shear strength from successive drying and wetting can be addressed and might be due to the development of micro-scale cracks during the drying process.

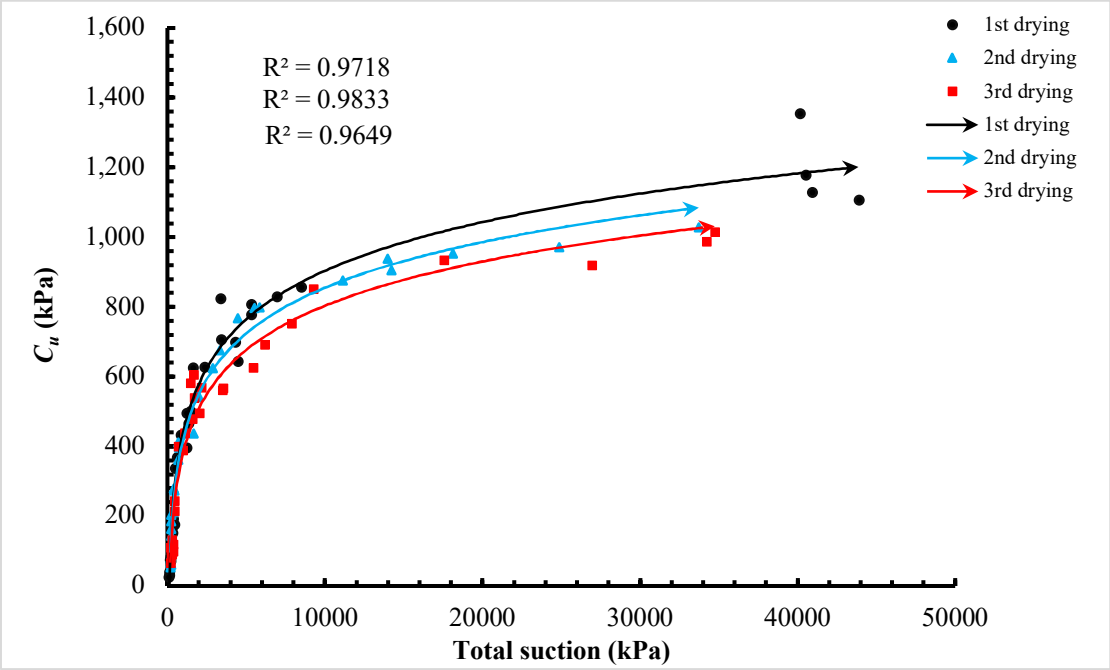

Figure 4.28 Undrained shear strength against total suction relationships during drying of three drying-wetting cycles for the glacial till specimens.

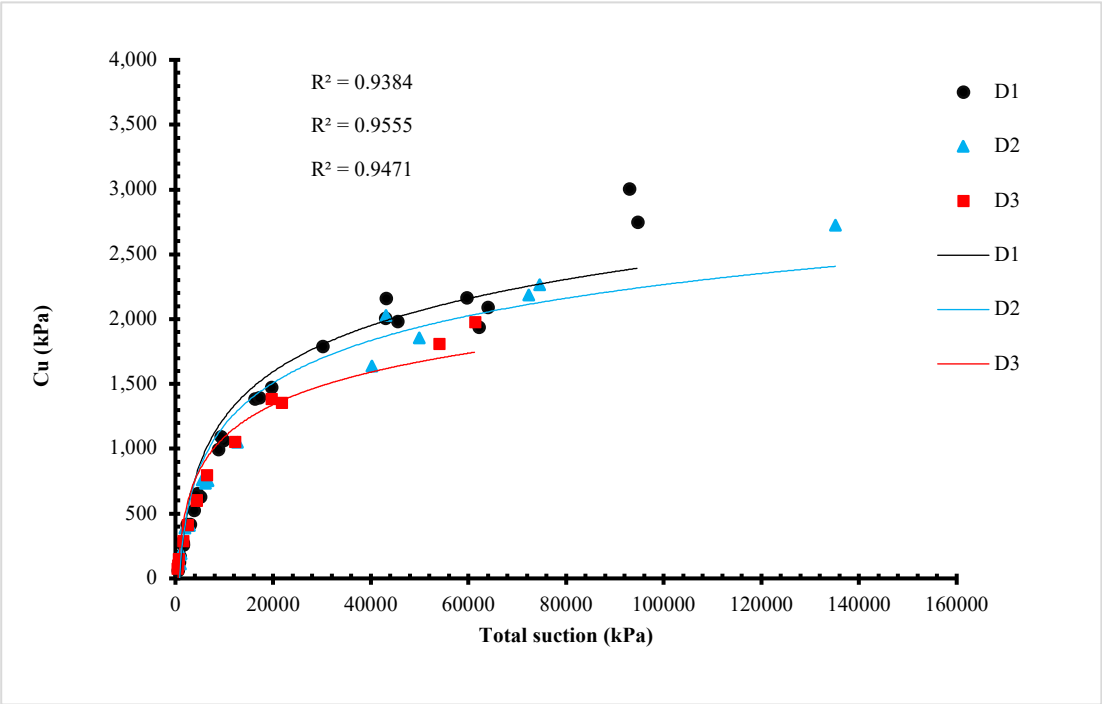

Figure 4.29 Undrained shear strength against total suction relationships of three drying paths for London Clay

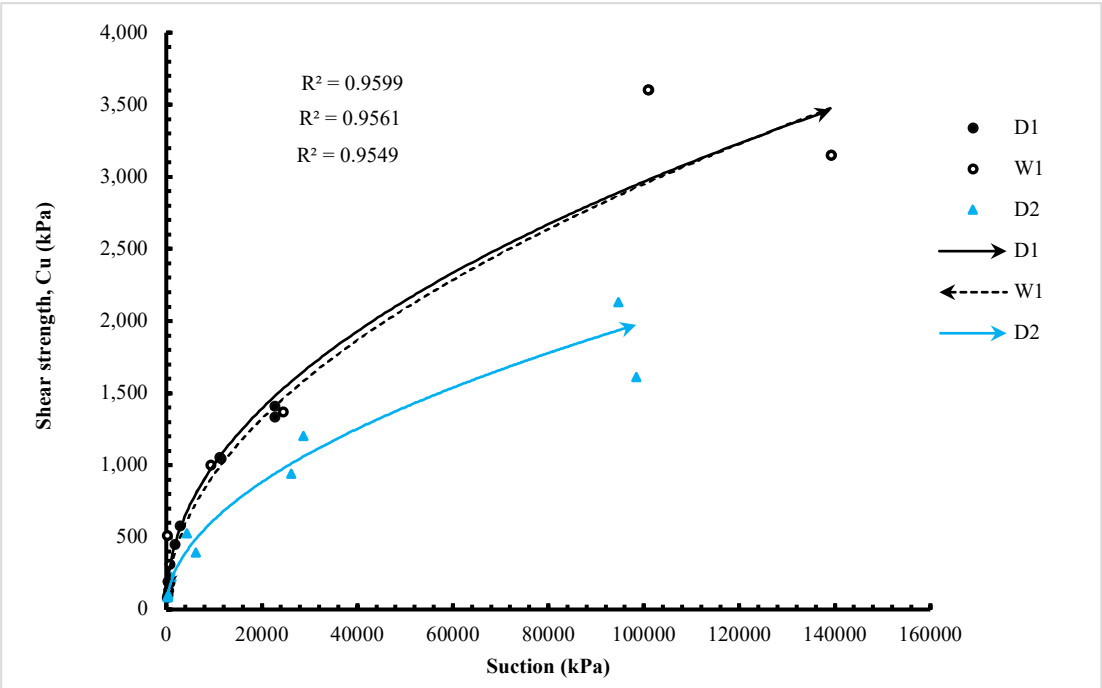

Figure 4.30 Undrained shear strength against total suction relationships of two drying paths for Hollin Hill Clay.

4.3.4 Resistivity-water content relationships

4.3.4.1 Glacial till

Figure 4.31 illustrates the relationships between electrical resistivity and degree of saturation for glacial till under three cycles of drying and wetting. In general, data sets from all the drying and wetting paths established an inverse power relationship between resistivity and degree of saturation, the resistivity increases as the degree of saturation decreases in a testing S_r range of 20% to 100%. In much previous research, similar relationship was presented between soil resistivity and water content from laboratory tests performed on Clay materials (Hassan, 2014; Merritt, 2014; Hen-Jones, 2018). The resistivity values increase slowly from full saturation to a S_r of about 70% from about 20 Ωm to 30~40 Ωm and grow more dramatically to a residual S_r of about 20%.

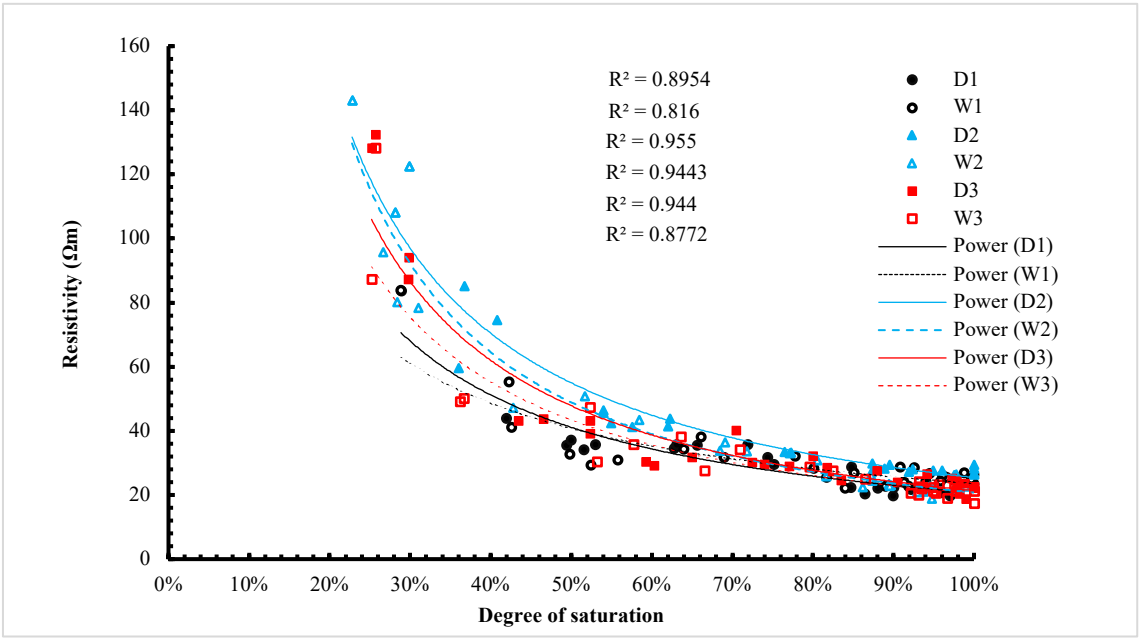

Figure 4.31 Resistivity -water content relationships for the glacial till under three drying-wetting cycles.

It should be noticed that, in general, the relationships between resistivity and degree of saturation for different drying-wetting cycles and drying/wetting paths do not display a consistent trend. According to the trends of resistivity changes shown in Figure 4.31, the resistivities in drying path at a given S_r are a little higher than those in the wetting path within the same drying-wettting cycle. This might be due to the development of micro-cracks during drying processes, as the micro-cracks interrupt the continuities of fluid water and block the current flows within the soil specimen, resulting in higher resistivities.

In Figure 4.31, it can also be seen that the resistivities show higher values in the second drying-wetting cycle than in the first and the third cycles, and the resistivities from the third drying-wetting cycle are lying between the first and second cycles. This implies that the resistivity is affected by multiple factors while the clay material being subjected to a successive drying and wetting, the volumetric changes of clays due to swelling and shrinking should also be considered except the water content changes and cracking.

4.3.4.2 London Clay

The relationships between electrical resistivity and degree of saturation for London Clay specimens under cyclic drying and wetting process are presented in Figure 4.32. It can be seen from the trend lines that the resistivity has an inverse power relationship with the degree of saturation for all the drying and wetting paths. Hysteresis is not found between the first drying and wetting path for the London Clay resistivity data, whereas the data shows little hysteresis between drying and wetting path for the second cycle. However, this hysteric behaviour in drying and wetting resistivities may result from the inconsistency in crack development of the individual soil specimens. An increase of soil resistivity at given S_r with the increasing number of cycles is evident from the results, indicating a deterioration in soil fabric due to crack development.

The relationships between electrical resistivity and degree of saturation for London Clay specimens under cyclic drying and wetting processes are presented in Figure 4.33. The second drying path establishes a higher resistivity value than the first drying path in the dry range, which indicates an increase in resistivity when subjected to a cyclic drying and wetting due to crack development.

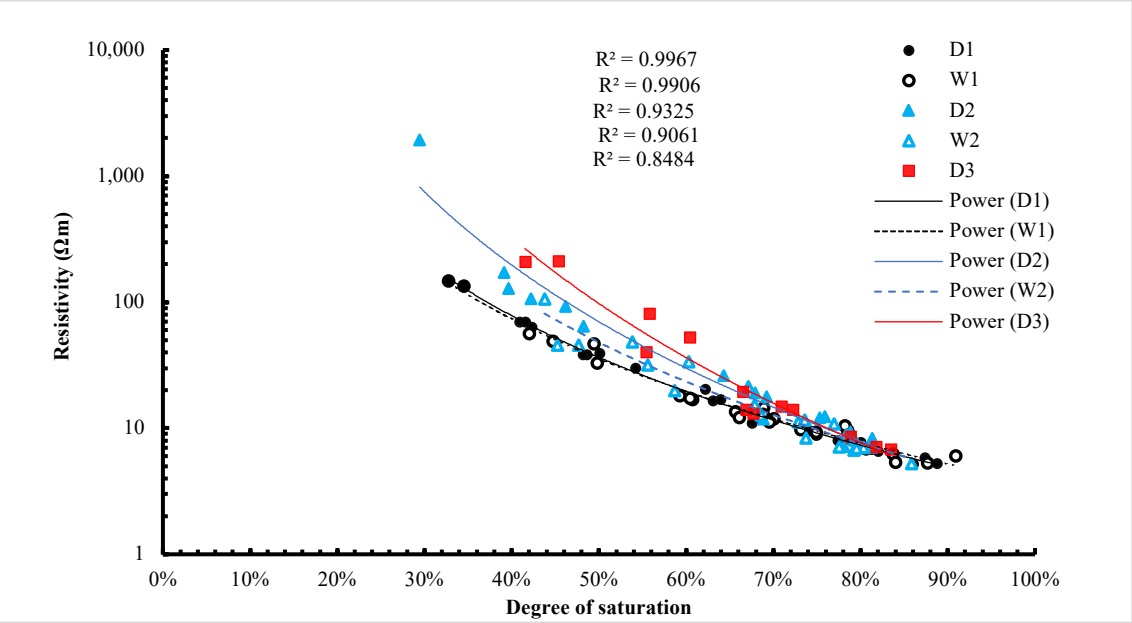

Figure 4.32 Resistivity- degree of saturation relationships under cyclic drying and wetting for London Clay specimens.

4.3.4.3 Hollin Hill Clay

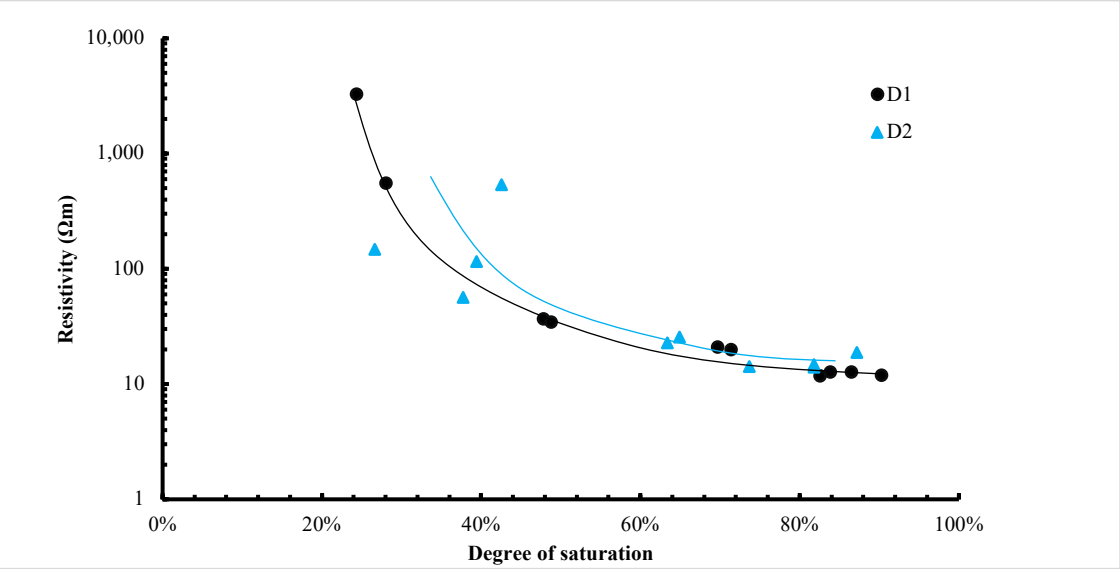

Figure 4.33 Resistivity-Sr relationships for Hollin Hill specimens under drying and wetting.

4.3.5 Shrinking-swelling curves

The volumetric changes of clays during successive drying and wetting induce variations in dry density and void ratio, which have an impact on the soil property behaviour. It has been proved that for given water content, a higher dry density (corresponding to a lower void ratio) results in a lower resistivity for the glacial till material (Hassan, 2014). The changes in void ratio also affect the behaviour of soil suction and suction induced shear

strength as they are related to the pore size of soil. The pore size and pore size distribution have been proved to affect SWRC (Fredlund & Xing, 1994; Vogel & Roth, 2001).

4.3.5.1 Glacial till

Figure 4.34shows the shrinkage and swelling curves for glacial till under drying and wetting cycles. In the first cycle drying path (see in Figure 4.34a), the void ratio of the specimens decreased from 0.68 at 25% GWC until reaching a shrinkage limit of 0.42 at around 12% GWC, then stays constant to the dry end. In the wetting path, the void ratio of specimens keeps constant until wetted to about 13% GWC and then decreases to 0.58 at a saturated water content of about 22%. It can be seen in Figure 4.34b that the glacial till specimens in the second cycle were wetted from an initial void ratio of 0.59 at 22% GWC to a shrinkage limit of 0.4 void ratio at 12% GWC. For the second wetting path, the void ratio remains constant before being wetted to about 13% GWC and increases to 0.53 at 20% GWC. In the third drying-wetting cycle, the shrinkage curves of drying and wetting are nearly reaching equilibrium, the specimens are dried from an initial void ratio of 0.53 at 20% GWC to a shrinkage limit of around 0.38 void ratio at about 13% GWC before drying out to the residual and then be wetted back by the same path to a void ratio of 0.5 at 19.5% GWC.

In order that the changes in soil void ratios for the glacial till under cyclic drying and wetting can be presented more clearly, trendlines of shrinkage curve data from all the three drying-wetting cycles are combined and shown in Figure 4.35 with the data points removed. A hysteretic relationship is shown between soil water content and void ratio, for the repeated drying-wetting cycles. For all three drying and wetting cycles, hysteresis between the drying and wetting paths can be found, showing that the specimens following a drying path exhibit higher values of void ratio for a given water content than those following a wetting path. However, the hysteresis is more significant in the first cycle and becomes less significant as the number of drying-wetting cycle increases, and convergence is almost reached in the third cycle. It can also be seen that the relationship between void ratio and water content for glacial till changes as the number of cycles increases. Both the secondary and tertiary drying paths exhibit a drop in void ratio from the previous drying path, indicating a change in swelling and shrinking behaviour of the soil material under repeated drying-wetting cycles.

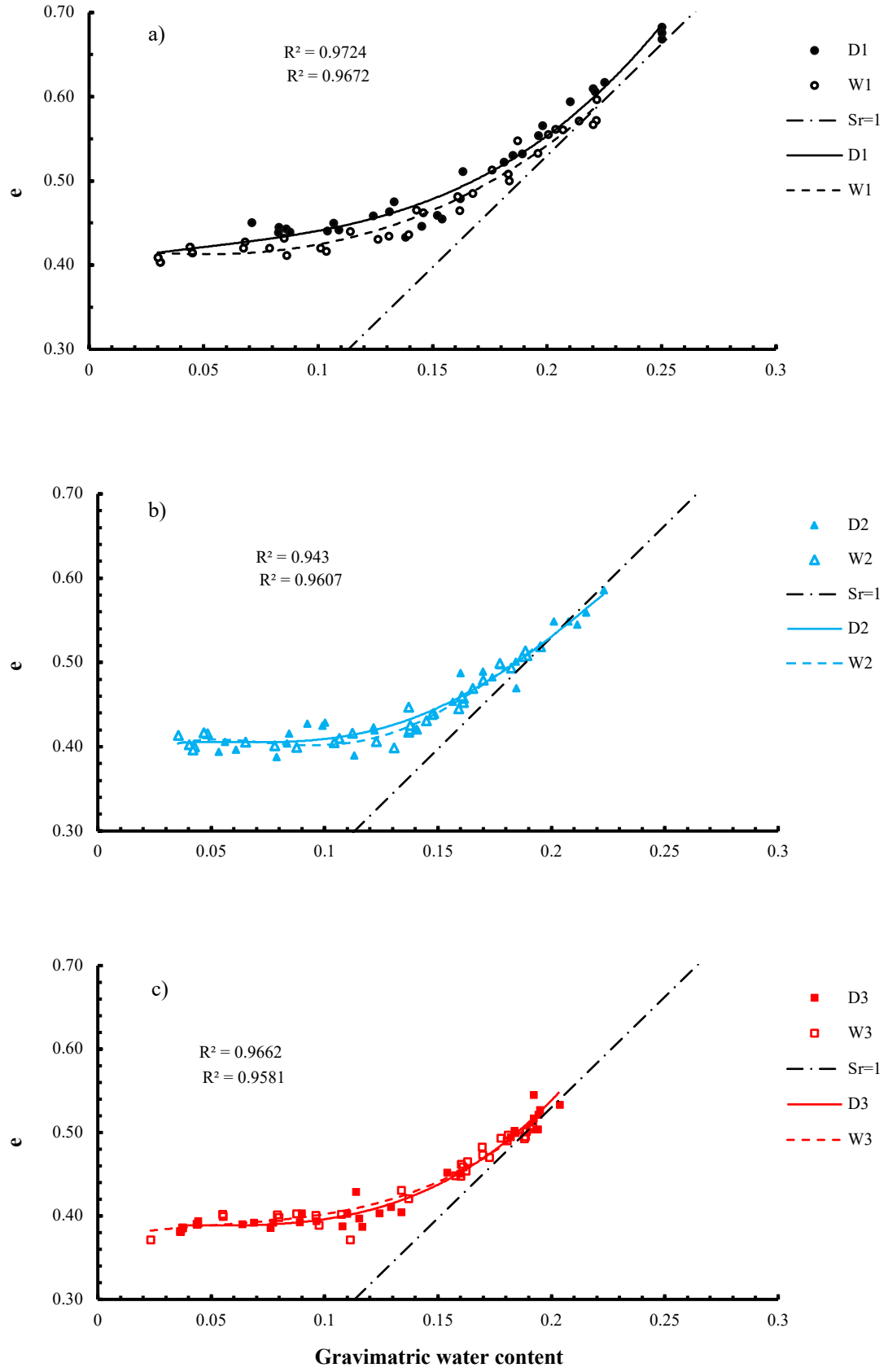

Figure 4.34 Shrinkage curves of glacial till under three cycles of drying and wetting: a) the first cycle, b) the second cycle, c) the third cycle.

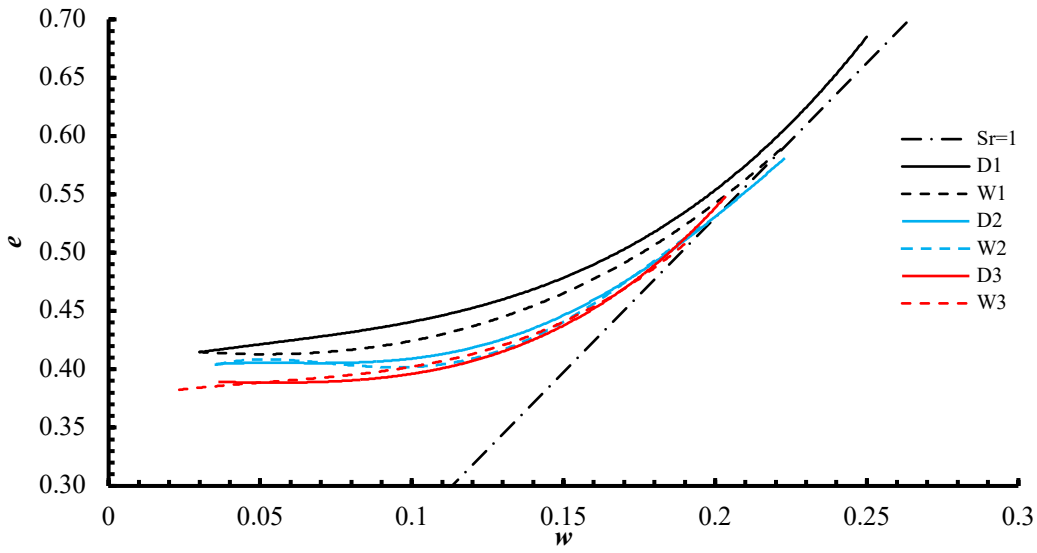

Figure 4.35 Shrinkage curves of glacial till material for three drying and wetting cycles.

4.3.5.2 London Clay

Shrinkage and swelling curves for London Clay specimens under repeated drying and wetting cycles are presented in Figure 4.36 by individual cycles, along with the saturation line of 80% and 100%. The shrinkage curve for the third drying path is presented accompanying the second wetting curve as the tests were ended by the end of the third drying. All the London Clay specimens were statically compacted to an initial condition of 1.41 Mg/m^3 dry density and 30% GWC, corresponding to the optimum water content and maximum dry density obtained from the proctor test. This gives the London Clay specimens an initial degree of saturation at about 86%, which is different from the full saturation initial condition for the glacial till specimens. The specimens for the first cycle drying path were either dried to residual or wetted to fully saturation to get a more complete understanding of the shrinking-swelling behaviour (see in Figure 4.36a).

It can be seen that the shrinkage limits for the three drying-wetting cycles are 0.59, 0.60 and 0.61 respectively. Hysteresis can be observed between the shrinkage (drying) and swelling (wetting) curves in the first and second drying-wetting cycle and convergence is achieved between the second cycle wetting and third cycle drying path, implying that the soil particles and fabric are re-structured while going through a repeated drying and wetting from the as-compacted condition. This restructuring process of soil affects the shrinking and swelling behaviour, i.e., volumetric changes, and finally the soil reaches an

equilibrium condition after certain cycles of drying and wetting. It is noticed that the void ratio on the wetting path at a given water content is higher than that on the drying path in a drying-wetting cycle before the equilibrium is achieved, indicating an increase in void ratio with the increasing number of drying-wetting cycles.

In order that the changes in soil void ratios for the glacial till under cyclic drying and wetting can be presented more clearly, trendlines of shrinkage curve data from all the three drying-wetting cycles are combined and shown in Figure 4.37 with the data points removed. Hysteresis is found between the drying and wetting paths in both the primary and secondary drying-wetting cycles, showing that the void ratios of specimens following a wetting path for a given water content have higher values than those following a drying path. This shows a contrasting trend to the glacial till of changes in void ratio-water content relationships under repeated drying and wetting.

4.3.5.3 Hollin Hill Clay

Shrinkage and swelling curves for Hollin Hill Clay under drying and wetting are presented in Figure 4.38, along with the saturation line of 80% and 100%. The results suggest that the void ratio of Hollin Hill Clay at shrinkage limit is about 0.48 for the first cycle and 0.60 for the second cycle. Similar to the London Clay data, the void ratio of Hollin Hill Clay shows the higher value on the wetting path than on the drying path at a given water content, exhibiting an increase in void ratio as the number of drying-wetting cycle increases.

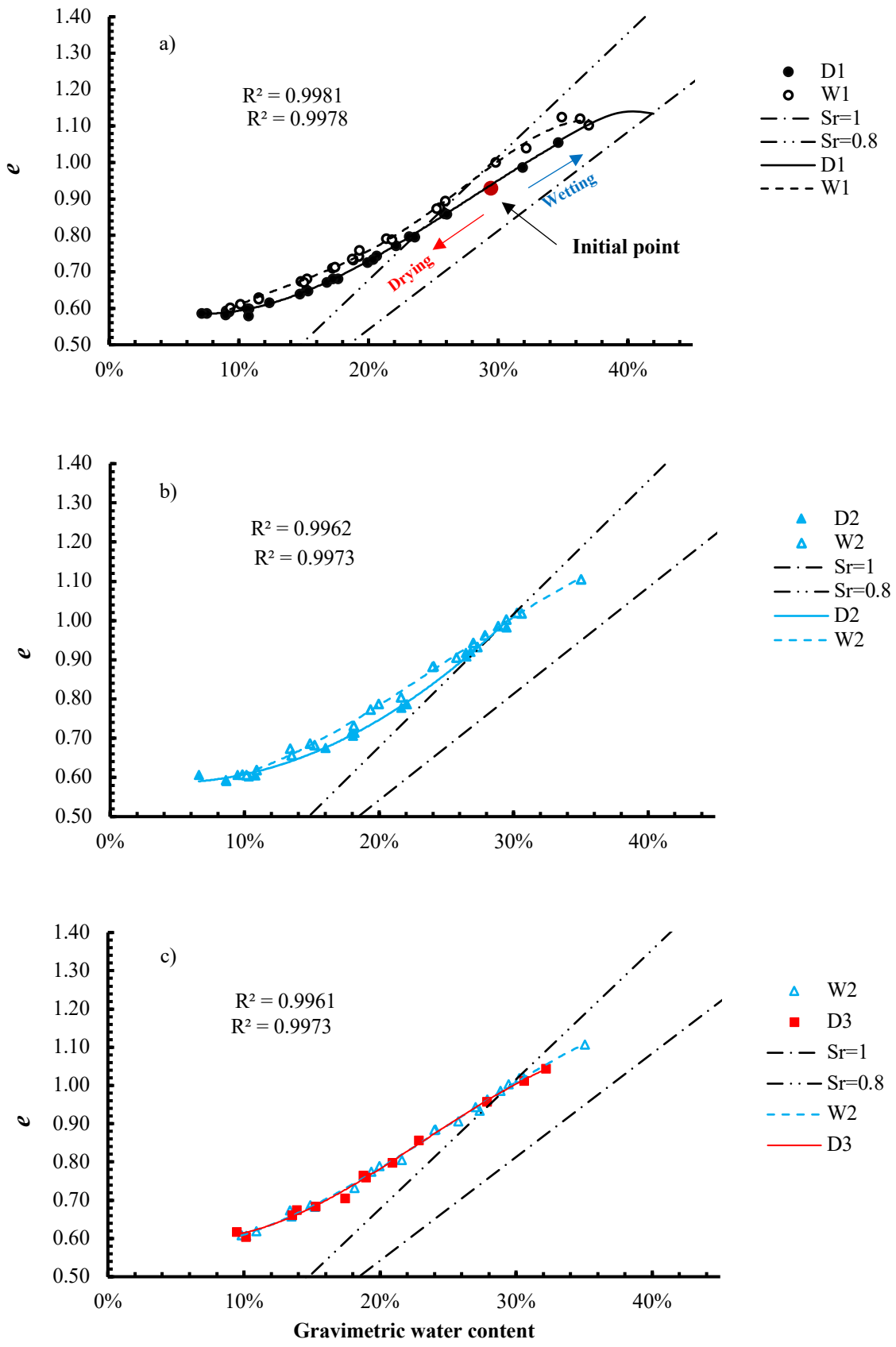

Figure 4.36 Shrinkage curves of London Clay specimens under three cycles of drying and wetting: a) the first cycle, b) the second cycle, c) the third cycle.

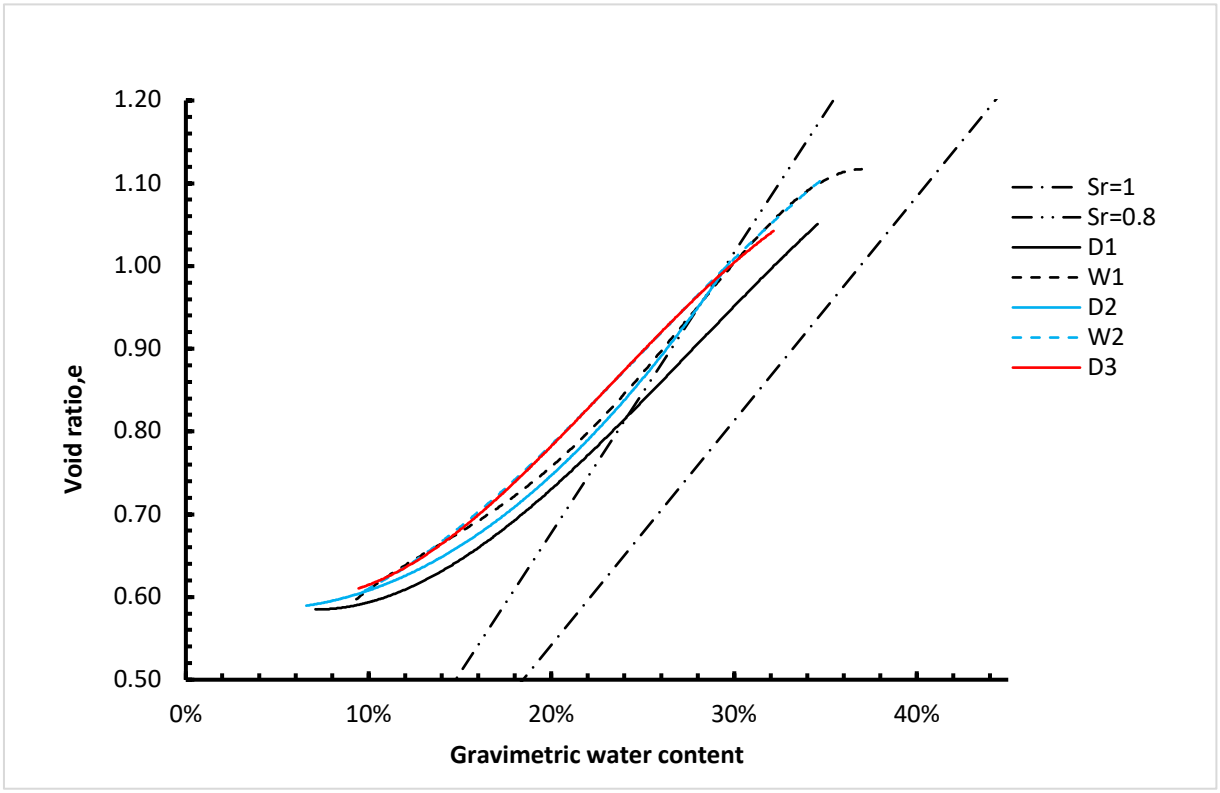

Figure 4.37 shrinkage and swelling curves for London Clay under repeated drying-wetting cycles

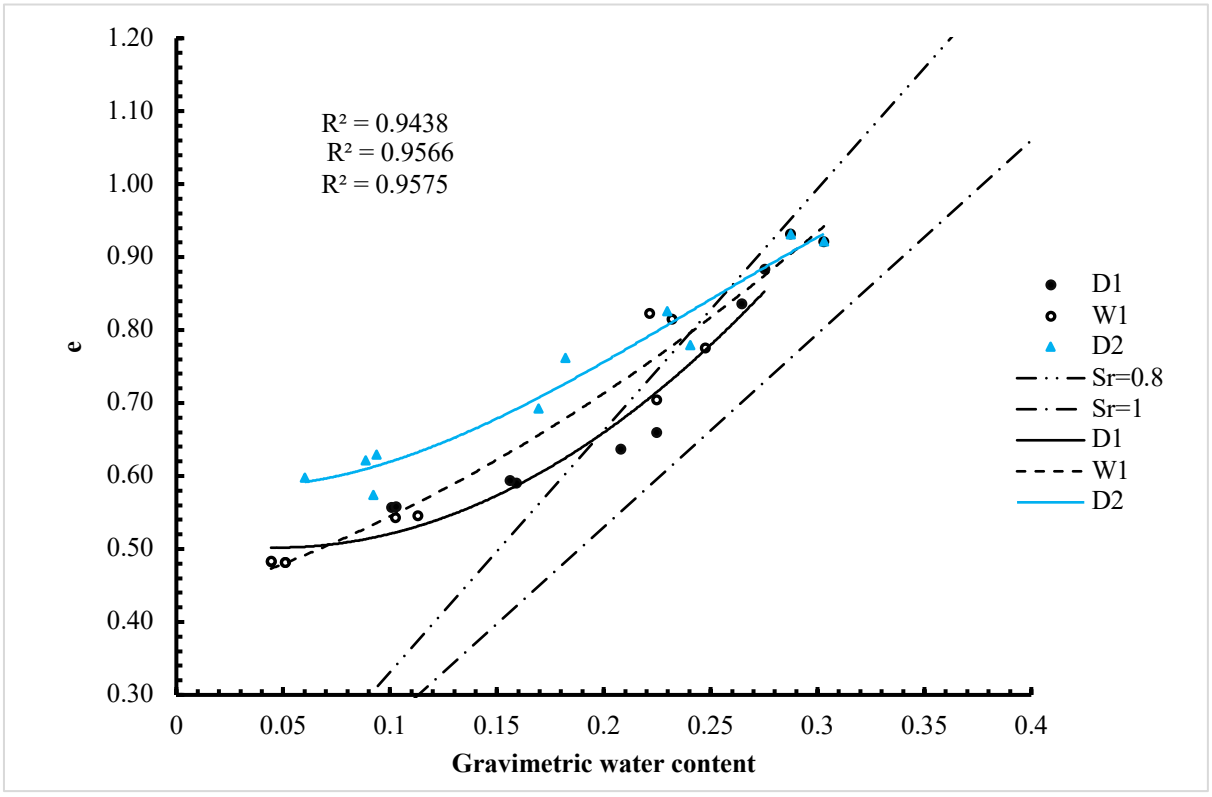

Figure 4.38 Shrinkage curves for Hollin Hill Clay under cyclic drying and wetting

4.4 Results of large lysimeter test

4.4.1 Introduction

In this subchapter, the results from nine months of testing the lysimeter containing the glacial till material are presented.

4.4.2 Water contents

The water contents were measured the Time Domain Reflectometry (TDR) probes buried within the lysimeter at certain depths and applying the specific calibration determined in subchapter 4.1.1.

Within the lysimeter, four columns of instrumentation were labelled as columns A, B, C, and D in an anticlockwise order around the circumference of the lysimeter as shown in Figure 4.40. In each instrumentation column, there were 6 device layers vertically distributed and were numbered 1 to 6 from the bottom to the top as shown in Figure 4.39.

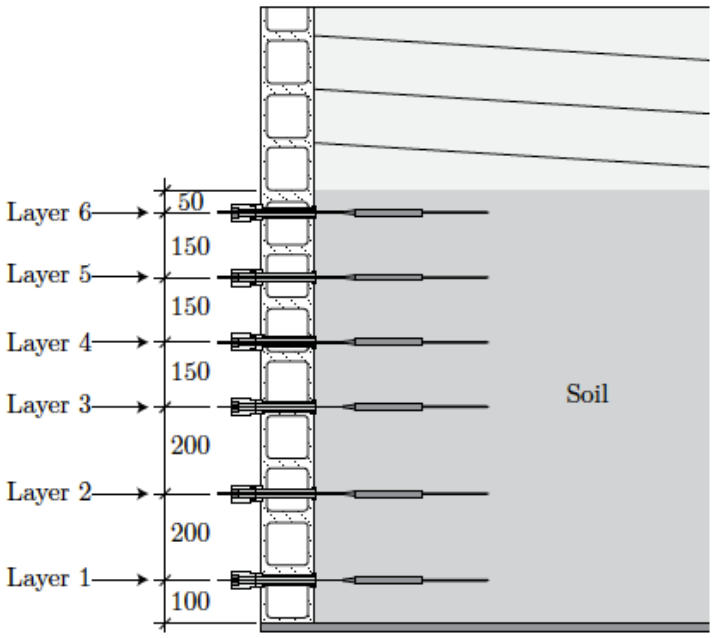

Figure 4.39 Diagram of the vertical arrangement of instrument layers in the lysimeter

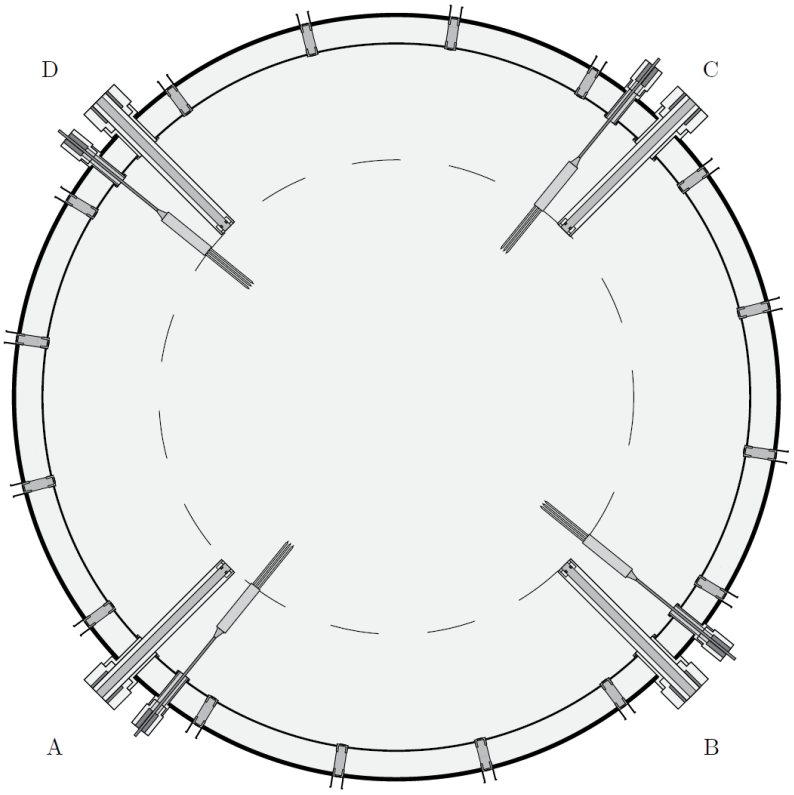

Figure 4.40 Diagram of horizontal instrument arrangement for one layer in the lysimeter, the locations of A, B, C, D columns are highlighted

Figure 4.41 shows the initial distribution of volumetric water contents (VWC) with depth for the lysimeter sample measured by TDR probes on the starting date 20th September 2018. It can be seen that there was a broad agreement as the VWCs lay between 34% to 40% excluding those of column B and C at 0.5m depth (layer 3), which present relatively lower water contents. The lysimeter had an estimated initial bulk volumetric water content of 36.2% based on the estimated initial dry density and gravimetric water content of the bulk soil in the lysimeter, whilst the TDR probes provided an average initial VWC of 36.1%, which is fairly close to the estimated value. However, the TDR probes on the instrument port B3 (column B, layer 3), C3 (column C, layer 3) and D2 (column D, layer 2) exhibited large deviations in VWC estimation from the other probes in the same depth as marked by the red dash line circles in Figure 4.41. This can be due to either: 1) underestimating in VWC by TDR probes caused by the poor contact between the probe prongs and the surrounding soils or the entrapped air between the probe prongs; 2) the different as-compacted conditions of the surrounding soils of these specific probes due to the uneven compaction efforts that might be applied in some specific areas during the compaction, as the soils were manually compacted using a tamper.

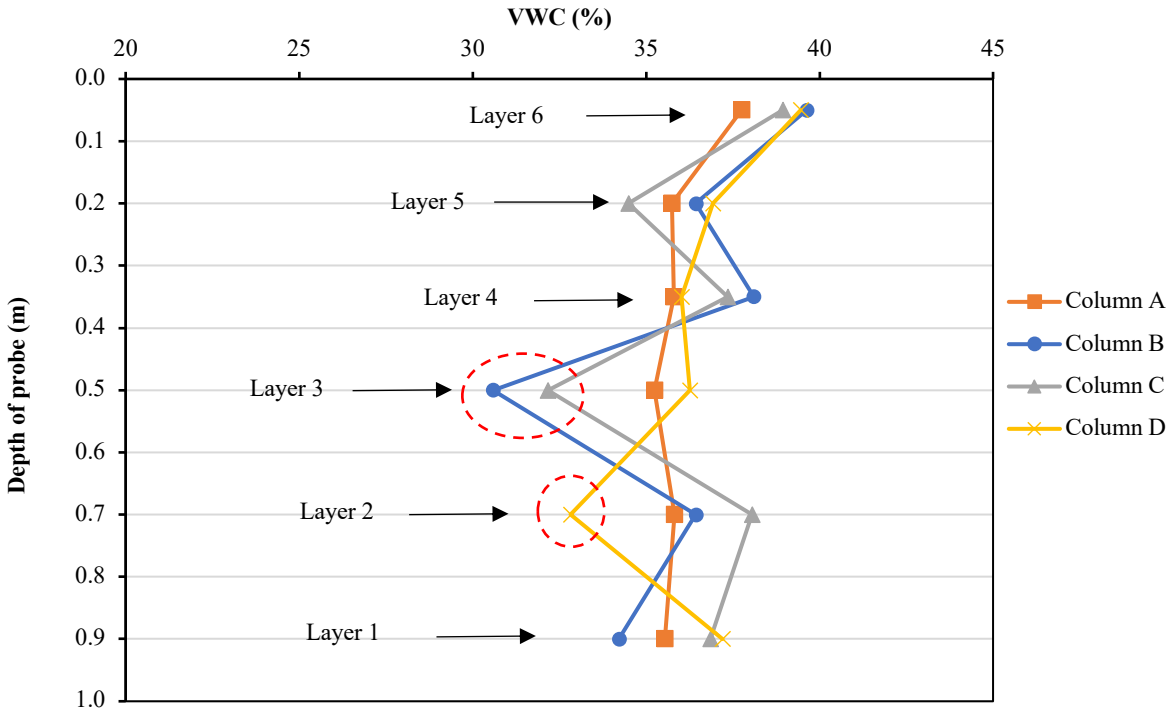

Figure 4.41 Initial vertical distributions of volumetric water content for lysimeter using TDR probes. The red dash line circles marked the large deviation data points at layer 2 and 3.

4.4.2.1 Drying period

The time series VWC data for four instrument columns of lysimeter are presented in Figure 4.42, 4.43, 4.44 and 4.45 separately, indicating the VWC variations in the lysimeter with depth for the drying period from 20th September 2018 to 14th February 2019 followed by a wetting period until 24th May 2019. Each figure illustrates VWC data from six TDR probes installed at layers 1 to 6 referred to different depths as shown in Figure 4.39.

Across the four figures, there is a general trend for the near-surface probes in layer 6 to have the greatest decrease rate in water content during the air-drying period and the drying rate becomes slower as the burial depth of the probe increases. However, the two TDR probes on ports C3 (soil column C, layer 3) and D2 (soil column D, layer 2) were deemed to be not functioning as they provide anomalous readings. It can be seen in the Figures that the water contents measured by the layer 6 (near-surface) probes showed an immediate decrease from the starting of the drying process and the water contents measured in the layer 5,4 and 3 started showing the decreasing trends after about 3 days, two weeks and three weeks, respectively. In the layer 1 and 2, it takes much longer time

for the probes to response to the drying activity. The water contents at the bottom two layers started to decrease at approximately 50 days after the beginning of the drying. It can also be noticed that the drying rates of layers 3 and 4 probes became slower and tended to remain constant with the bottom two layers while the desaturation of the bottom two layers started. This can be explained as the water started to drain from the bottom into the middle layers of lysimeter once the air entry value of soils in the bottom layers was reached, the inter-movement of water between the bottom and middle layers occurred.

4.4.2.2 Wetting period

After a drying period of nearly five months, the near-surface layer (layer 6) was observed to be dried out according to the steady readings by the TDR probes. Since the time required for the lysimeter sample to be dried out to the bottom would be extremely long, the wetting process for the lysimeter sample was started on 14th February 2019. An automated irrigation system, as mentioned in subchapter 3.4.8 , was used to wet the sample from the top surface by providing an intensive water spray.

It can be seen in Figure 4.42, 4.43, 4.44 and 4.45 that for all the columns the water contents in layer 6 increased instantly when the wetting started. Layer 5 wetted slowly as irrigation was applied to the lysimeter and the wetting rate gradually increased over time. The water contents in the lower layers took longer to begin to wet. This can be explained due to the time required for the wetting front to pass deeper into the lysimeter.

Another observation with layer 6 is the different wetting behaviour within the soil columns while the layer was wetted to between 30% - 32% of VWC. It can be seen that the columns A and B in Figure 4.42 and 4.43 show an abrupt increase in water content after being wetted to 30% and 32% respectively, whereas the columns C and D show this upward trend more slowly. This was explained as the water pooled above columns A and B in preference to C and D due to unevenness of the sample surface. A similar abruptly rising tendency in VWC was also found in layers 4 and 5 on soil column A. This can be explained as a consequence of water infiltrating the vertical cracking developed during drying and wetting along the instrument line for the column A as the soil column became more heavily saturated.

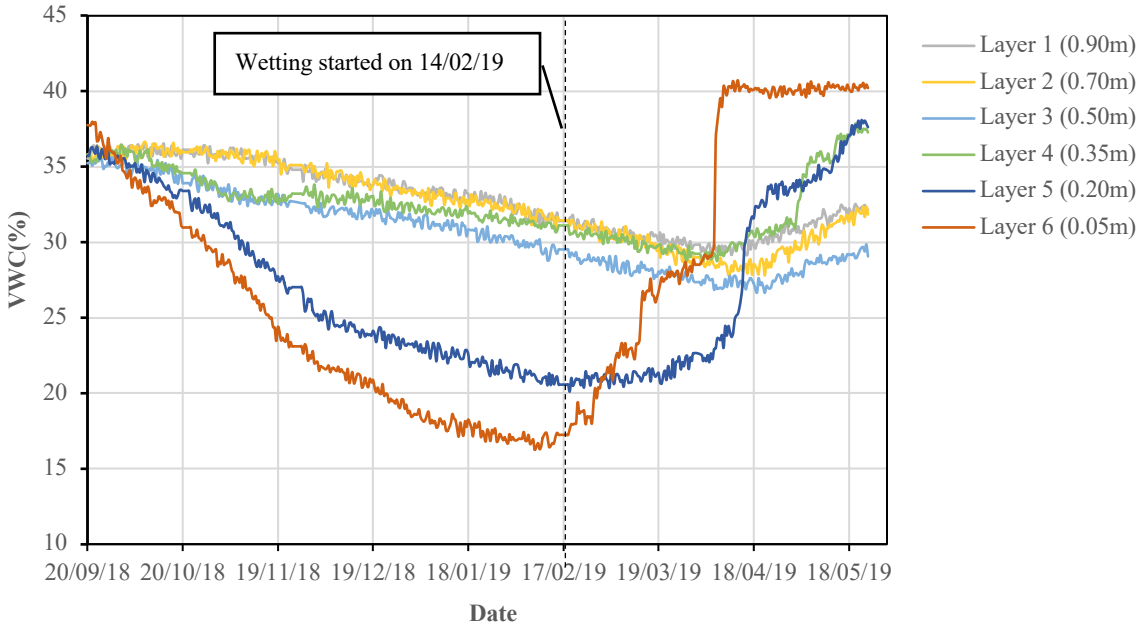

Figure 4.42 In time Volumetric water contents measured by TDR probes at different depth for lysimeter Column A

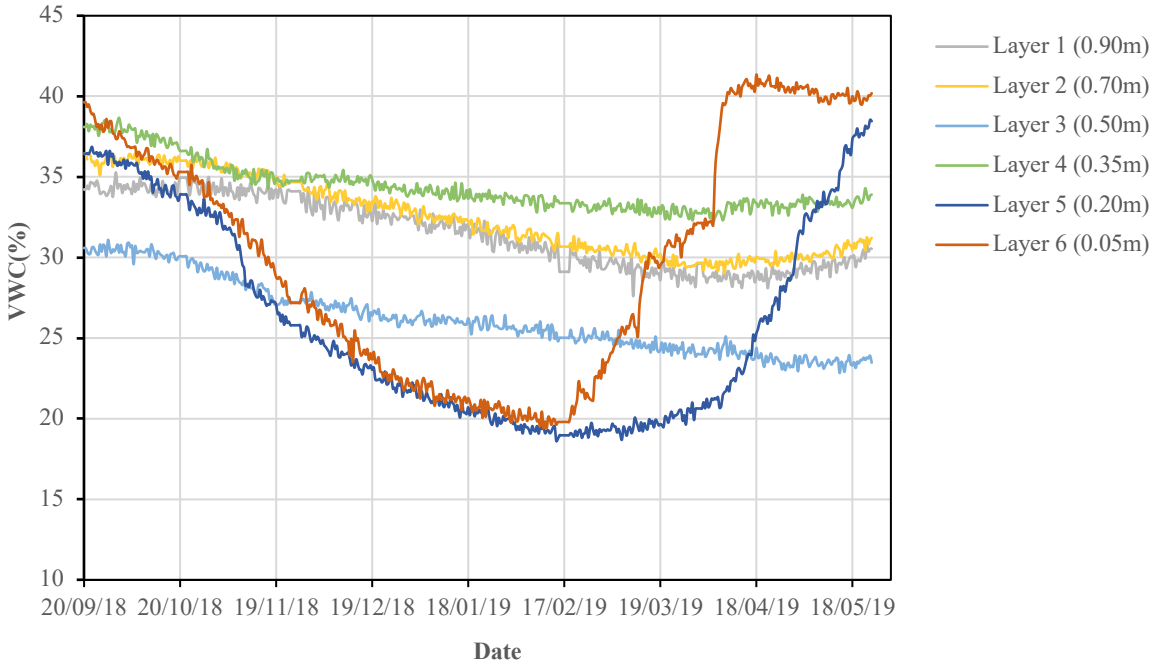

Figure 4.43 In time Volumetric water contents measured by TDR probes at different depth for lysimeter Column B

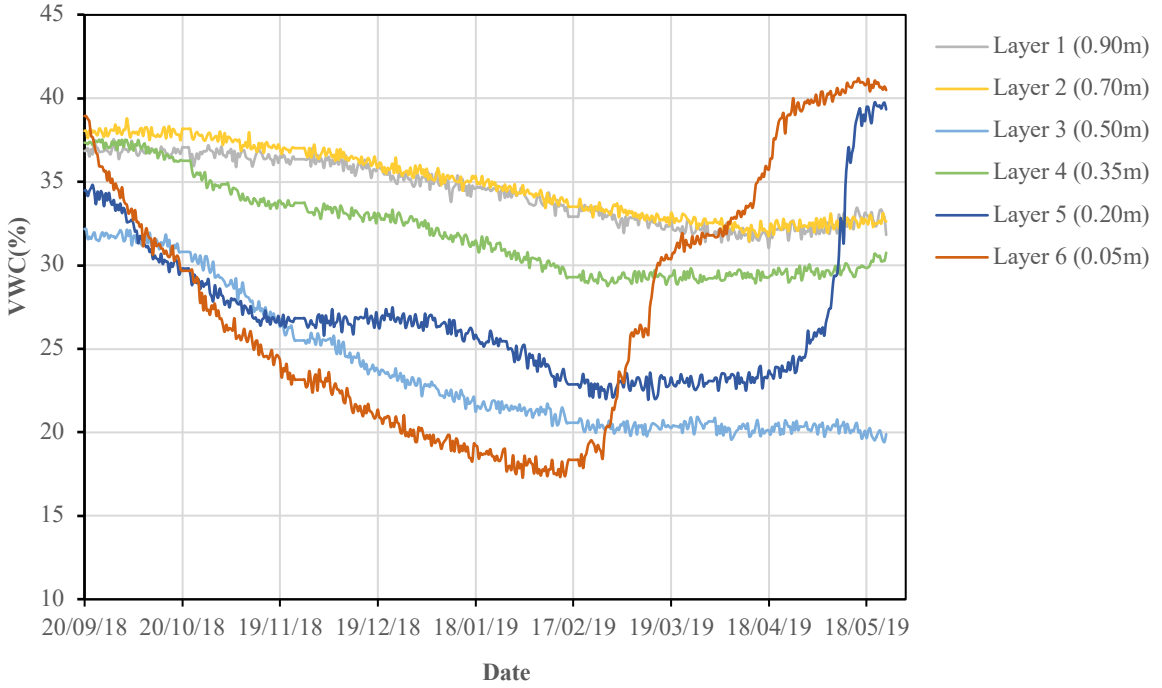

Figure 4.44 In time Volumetric water contents measured by TDR probes at different depth for lysimeter Column C

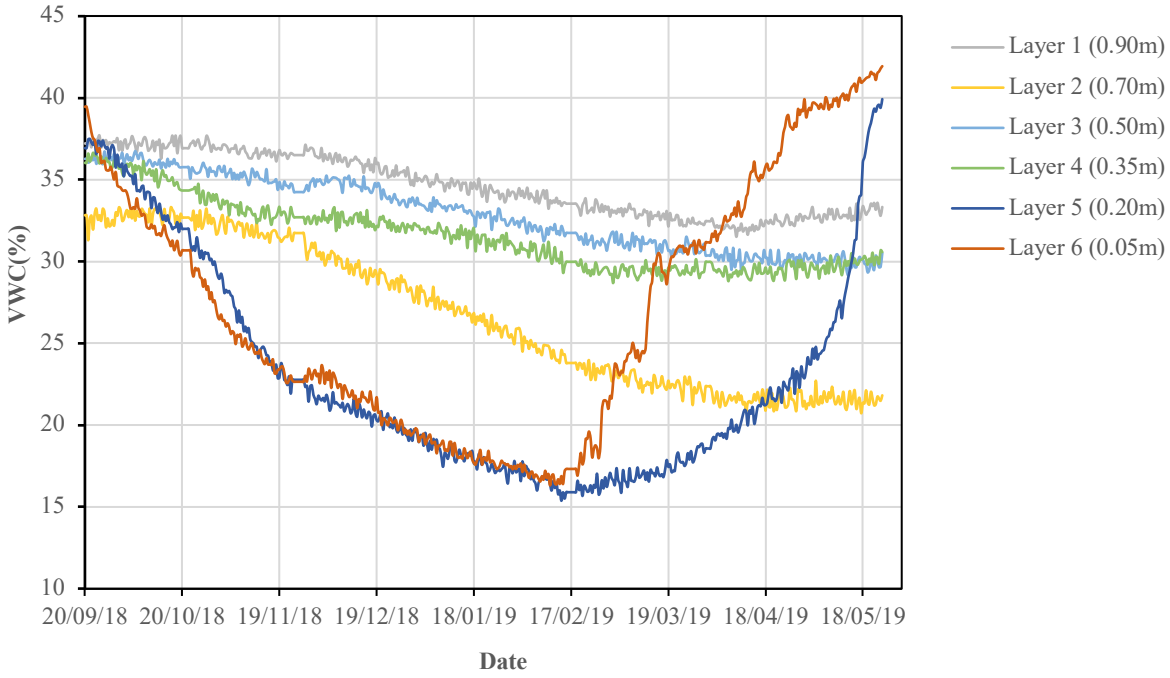

Figure 4.45 In time Volumetric water contents measured by TDR probes at different depth for lysimeter Column D

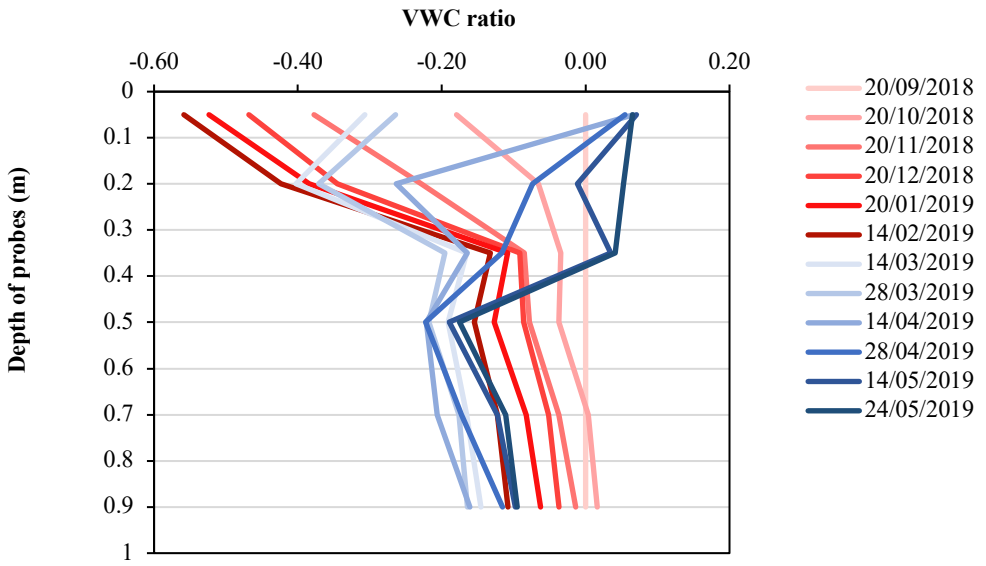

Figure 4.46 Volumetric water content ratio profiles with depth for the lysimeter Column A during the drying period (from 20/09/2018 to 14/02/2019, labelled by red polyline) and the wetting period (from 14/02/2019 to 24/05/2019, labelled by blue polyline).

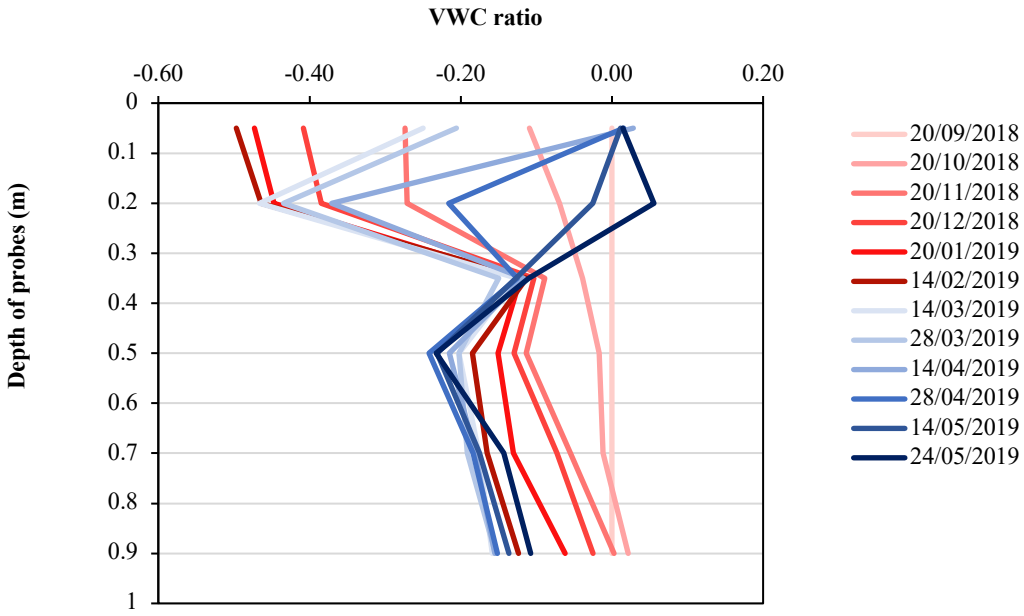

Figure 4.47 Volumetric water content ratio profiles with depth for the lysimeter Column B during the drying period and the wetting period.

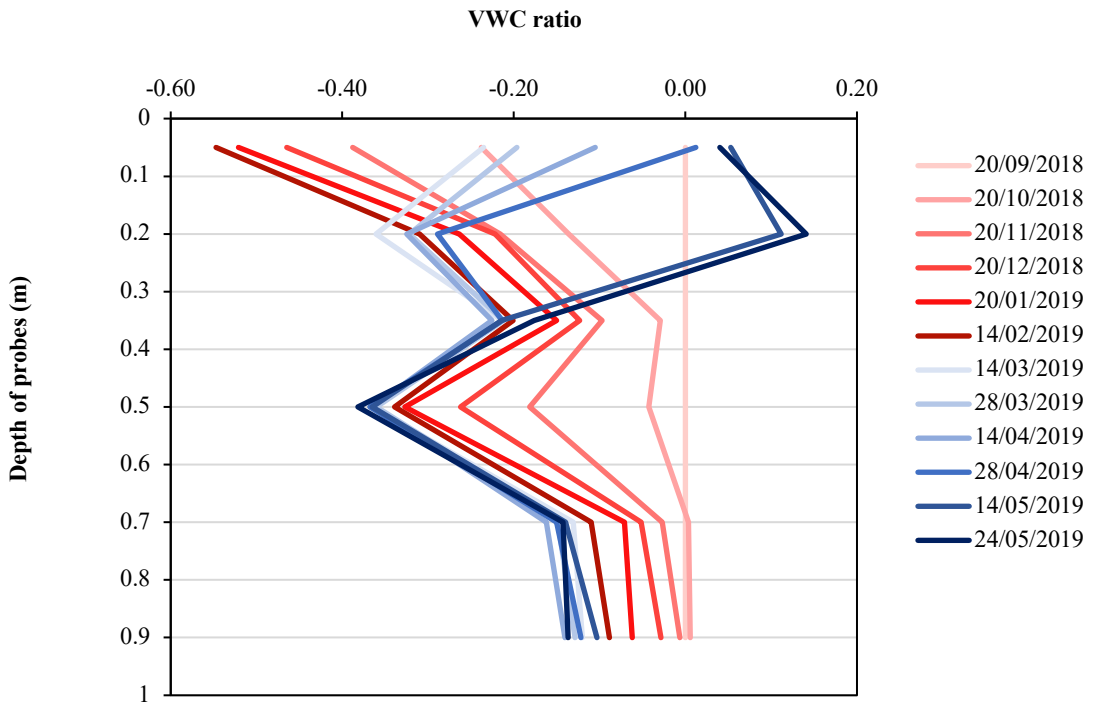

Figure 4.48 Volumetric water content ratio profiles with depth for the lysimeter Column C during the drying period and the wetting period.

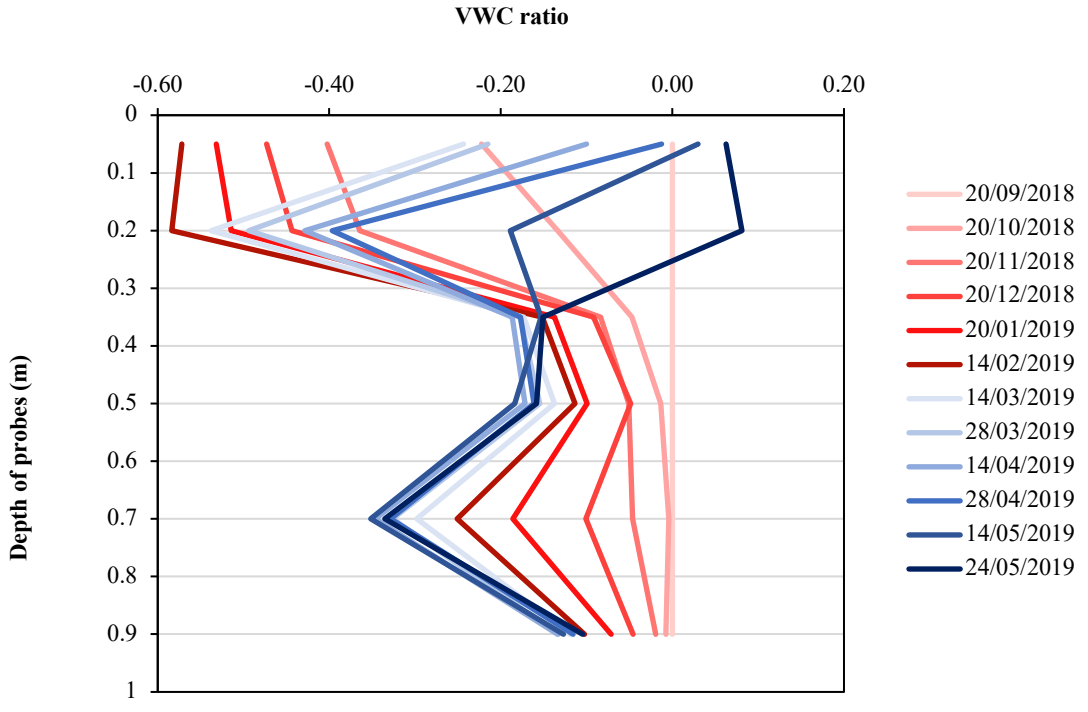

Figure 4.49 Volumetric water content ratio profiles with depth for the lysimeter Column D during the drying period and the wetting period.

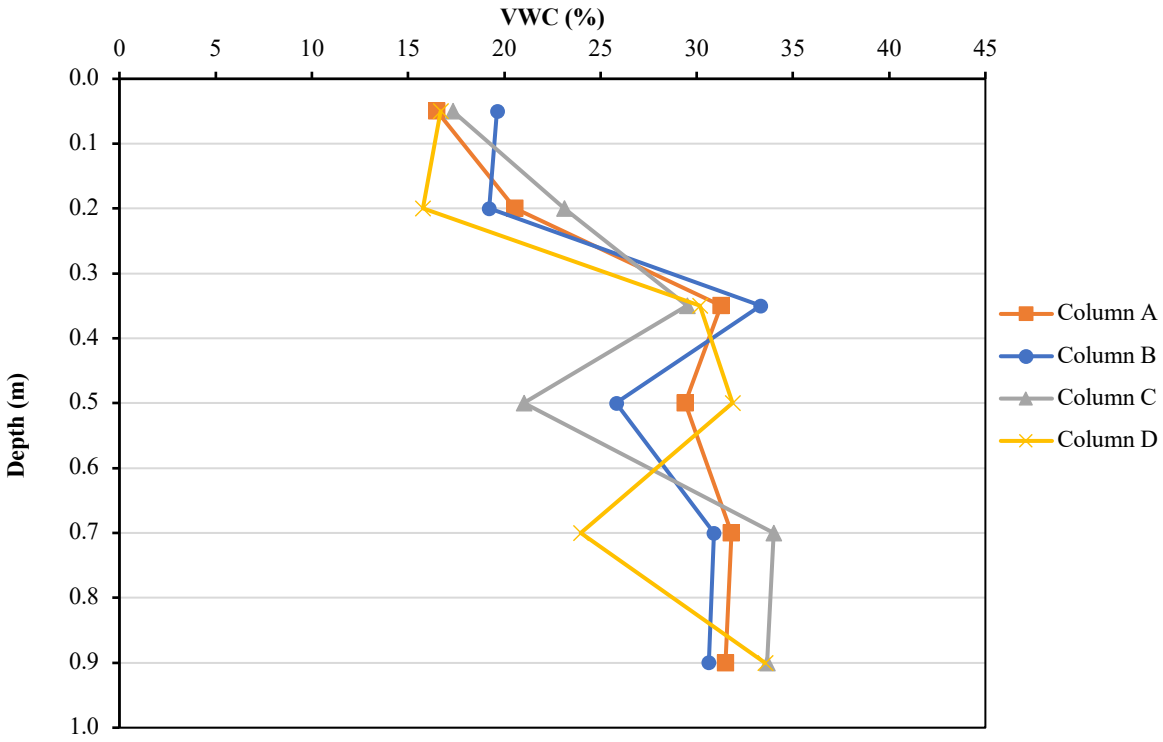

Figure 4.50 Vertical VWC distribution in lysimeter for the date 14th of February 2019 before wetting applied

4.4.3 Pore water pressure

The pore water pressure in the lysimeter was determined using the high capacity tensiometers described in chapter 3. Due to the limited number of available tensiometers in the laboratory, it was unrealistic to make full use of the total 24 tensiometer ports on the lysimeter. Therefore, eight tensiometers were used in the drying period, six of them were used to make measurements covering a whole vertical instrument column (soil column D) on the lysimeter and the other two probes were initially installed into the two ports on the column A and C in layer 6 to provide comparative measurements. The two tensiometers were then moved down to the next lower depth once the measured suction was approaching the cavitation point of the tensiometer.

Figure 4.51 presents the pore water pressure profiles of lysimeter for the drying and wetting periods. It was undesirable to let a tensiometer to be cavitated as it takes weeks for a cavitated tensiometer to be re-saturated and a recalibration is also required. However, most of the tensiometers used in the drying period cavitated before reaching a negative pore water pressure (PWP) at -800 kPa, and half of them cavitated before achieving a negative PWP at -500 kPa as shown in Figure 4.51. This can be explained by the poor contact issue caused by the shrinking of soil during drying even a guide tube was used to

aid the contact between the tensiometer and the soil. It may also be caused by the insufficient saturation process, which makes the entrapped air left in the water reservoir of the tensiometers, leading to a reduction of cavitation point. During the drying period, a maximum suction measurement of about 1400 kPa was achieved by the tensiometer installed on the port A6.

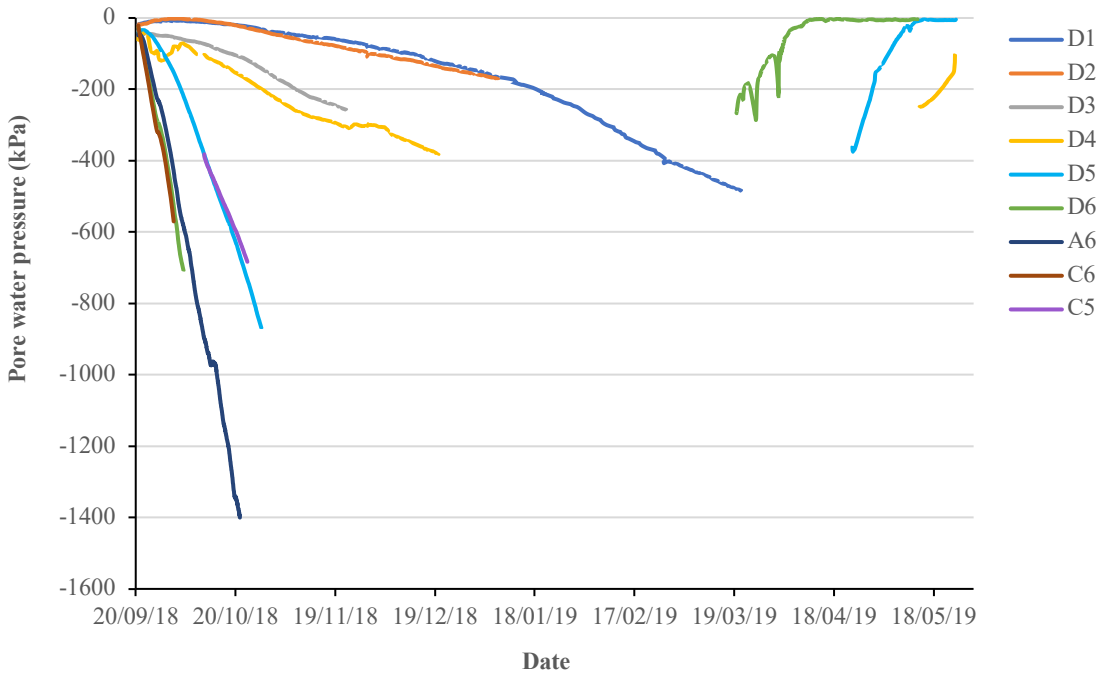

Figure 4.51 Pore water pressure profiles for different locations on the lysimeter using a high-capacity tensiometer during the drying and the wetting periods.

In the drying period, it can be observed that the tensiometers in the upper four layers immediately showed a decrease in pore water pressure after the drying started, whilst the PWPs measured in the bottom two layers stayed at a near zero value for about 20 days before showing a slow decrease. The three tensiometers in layer 6 registered the greatest decrease in pore water pressure, reaching pore water pressures as low as about -1.4 MPa after a one-month period. The tensiometers in layers 5, 4 and 3 also showed a similar tenancy of decreasing in PWPs as layer 6, but with stepwise reduced decreasing rates. Across the data by all the tensiometers, strong agreements were found between the probes at the same depth for the soil columns.

In the wetting period, in order that the widest possible range of suction could be recorded, it was planned to re-install the tensiometers in the lysimeter ports once the corresponding instrumentation layer was wetted to the suction range just below the cavitation value of

the tensiometers (expected to be around 600 to 700 kPa). Practically, three tensiometers were re-installed in layers 4, 5 and 6 on Column D to measure the pore water pressure changes in the lysimeter during the wetting period. The results of pore water pressure from three tensiometers placed in layers 4, 5 and 6 on column D are also presented in Figure 4.51. The two tensiometers in layers 4 and 6 started with PWPs at around -250 kPa and the tensiometer in layer 5 initially read at approximately -380 kPa PWP. From the PWP results for the wetting period, it clearly showed that the lysimeter sample was wetted from the top to the bottom layers, the layer 6 was the first to be wetted back to a PWP just below zero kPa and followed by the layer 5, which had also been wetted to saturation one month later.

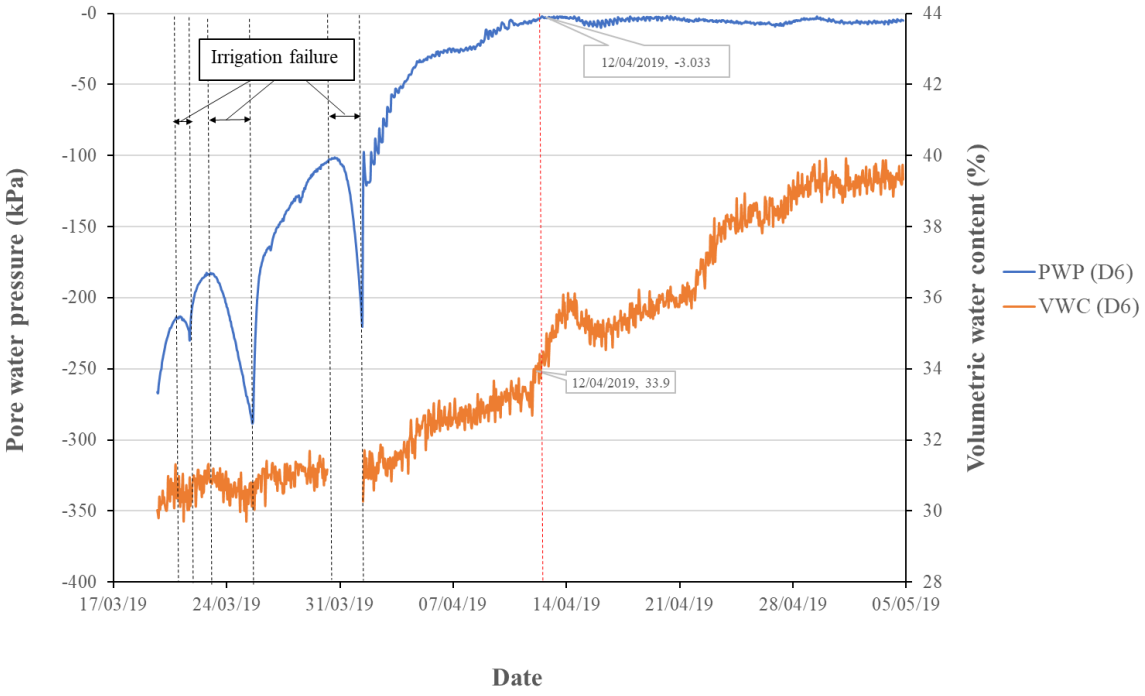

Figure 4.52 Pore water pressure and Volumetric water content data using tensiometer and TDR probe for the instrument port D6 (column D, layer 6) on the lysimeter during the wetting period.

It can also be noticed in Figure 4.51 that there were three small-scale drying-wetting activities that happened for layer 6 soil. Figure 4.52 is an enlarged picture showing the pore water pressure and volumetric water content variations of port D6 for a six-week period after installation of the tensiometer. It can be clearly seen that there were three obvious falls in pore water pressure due to the irrigation failures during the wetting process. These irrigation pauses were caused by the unexpected shut down of the irrigation system due to power issues in the laboratory. The failures in irrigation caused

small-scale drying-wetting cycles and resulted in drops in both volumetric water content and pore water pressure of soil in the near-surface layer. The result shows that a 1% reduction in volumetric water content led to a 100 kPa reduction in pore water pressure.

It can also be seen in Figure 4.52 that when the layer 6 was wetted to about 34% VWC, it was the first time for the porewater pressure measured at port D6 to reach a near-zero value, from where the pore water pressure readings started to remain consistent just below zero and the soil around the D6 port became saturated. However, the VWC measured at port D6 did not stop increasing after saturation but kept the upward trend with the persistent irrigation. This could be due to the over-wetting of soil after the saturation was reached. It means that the soil can stay swelling even when the saturation has been reached if the water is persistently added to it. This causes the increase in soil porosity and the VWC is then increasing with the increasing porosity.

4.4.4 Soil water retention curves (SWRCs) of large lysimeter test

The drying and wetting soil water retention curves for the glacial till measured in the large lysimeter are presented in Figure 4.53. All the SWRCs are established by the VWC. and suction data collected from different locations on the lysimeter using TDR probes and tensiometers. Overall, the trends for all the drying curves follow a similar shape indicating the matric suction increases with the decreasing volumetric water content. However, the curves measured at different layers and locations still show some differences. The three drying curves measured at layer 6 on column A, C and D present strong consistency and exhibit higher values of suction for a given volumetric water content than those measured at lower layers. The two drying curves measured at layer 5 show a distinct difference that the water content for a given suction measured at port D5 shows high value than those measured at C5. This indicates that the differences in SWRCs from different locations might not only be due to the depth. It could be due to the variations of the as-compacted volumetric water contents of soil from different locations. A more significant difference is shown between the wetting paths. The two wetting curves measured at port D4 and D6 present strong agreement and exhibit higher values of suction for a given volumetric water content than those obtained from port D5. In this test, hysteresis is again observed between the drying and wetting paths of SWRCs for the glacial till, showing that the VWC values following a drying path for a given suction are higher than those following a wetting path.

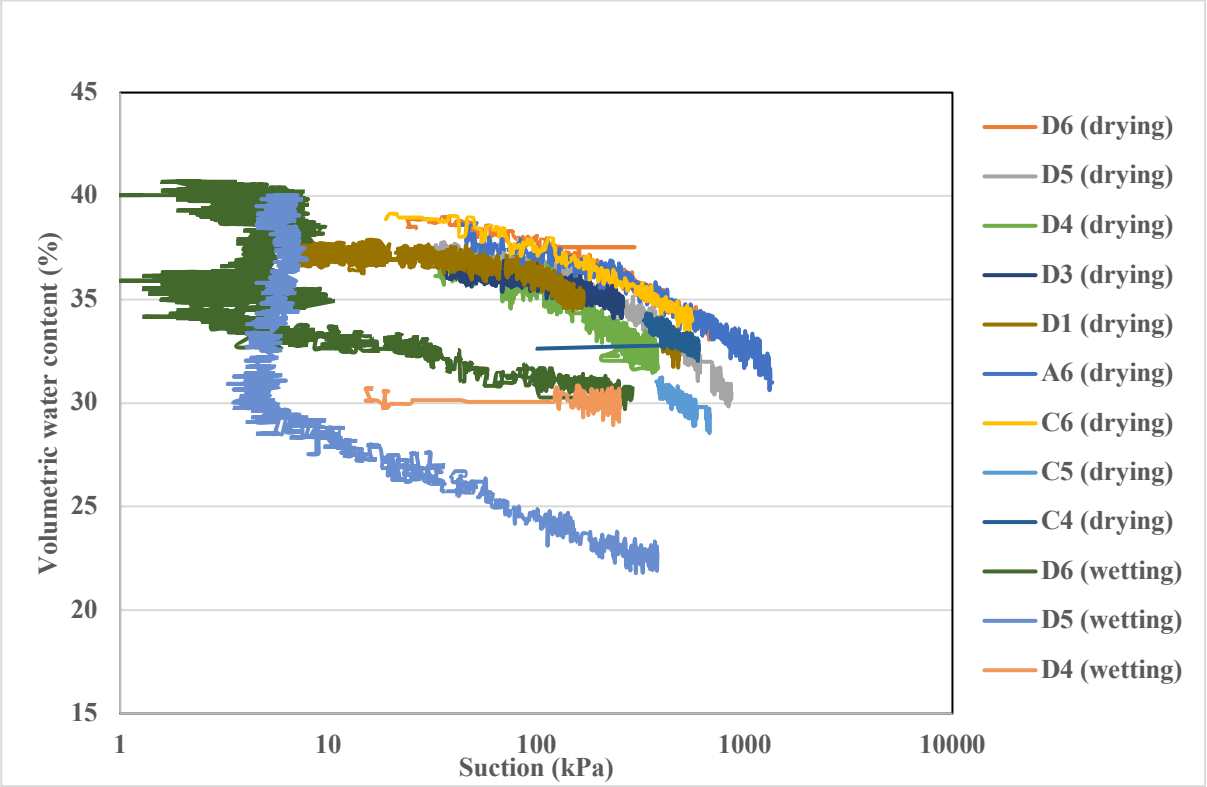

Figure 4.53 Soil water retention curves measured from different locations on the large lysimeter for the glacial till.

4.4.5 Electrical resistivity measured by TDR probes

The electrical resistivity results using TDR probes for the lysimeter during the drying and the wetting periods are presented by columns in Figure 4.54, 4.55, 4.56 and 4.57. Across all the Figures, nearly all the probes started with a resistivity value between 20 to 30 Ωm except the two probes on ports B2 and D4. The results show that the probes in layers 5 and 6 responded to the drying and wetting activities immediately once the drying was started or the irrigation was applied. Layer 6 soils registered the greatest rate of increase in resistivity during the drying period. Before the irrigation was applied, the resistivity readings from layer 6 (0.05m) on columns A, B and C increased to about 100 Ωm, whist the maximum reading from port D6 was 128 Ωm. In layer 5 (0.2m), the column D probe also measured the highest maximum resistivity at about 110 Ωm, whereas probes on other columns measured at between 70 to 90 Ωm. The data was more scattered in a high resistivity range than in a low resistivity range probably due to the limited resolution of conductivity measurement from the TDR probe. The resistivity values were converted from the conductivities measured by the TDR probe based on the reciprocal relationship between the two parameters. In the wetting period, it can be seen in the Figures that all

the near-surface (layer 6) probes responded immediately once the irrigation was applied (from the date 14/02/2019) and had a dramatic decrease in resistivity. After a three-month wetting period, the resistivities in layers 5 and 6 all reduced to about 22 - 25 Ωm, which are close to the resistivity values of the soil at the initial condition (at the beginning of drying), indicating the soils at layers 5 and 6 were wetted to near saturation. It can also be noticed that for the column A and B, the resistivities at layers 1, 2, 3 and 4 continue to rise for 1-2 months after the irrigation was applied, whilst the resistivities measured at some of these layers for columns C and D show much quicker responses to the wetting activity. This could be due to water flowing down the side of the lysimeter (between the soil and the lysimeter wall) and therefore reaching lower layers more rapidly. A gap was observed to have opened between the soil and the lysimeter wall during drying as the soil shrank.

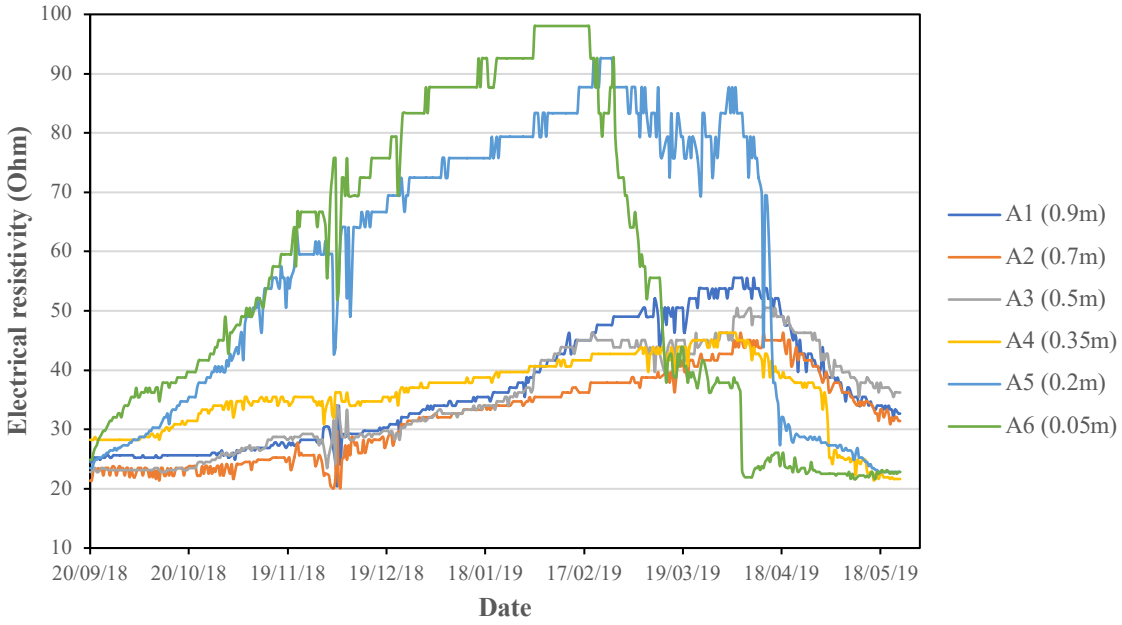

Figure 4.54 Electrical resistivity data using TDR probes for varying depths on lysimeter soil Column A

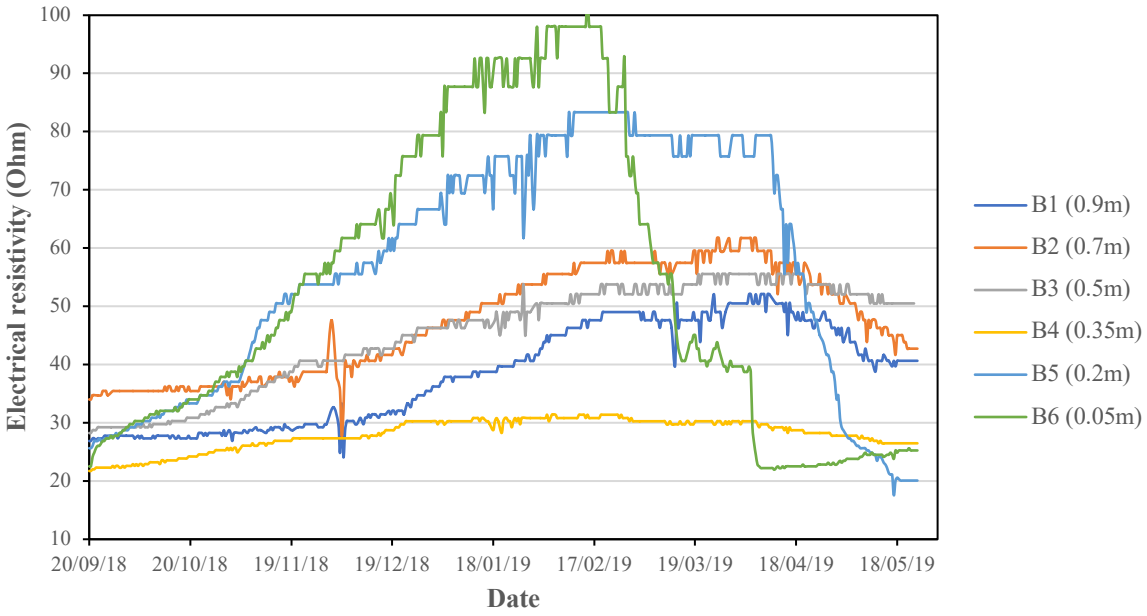

Figure 4.55 Electrical resistivity data using TDR probes for varying depths on lysimeter soil Column B

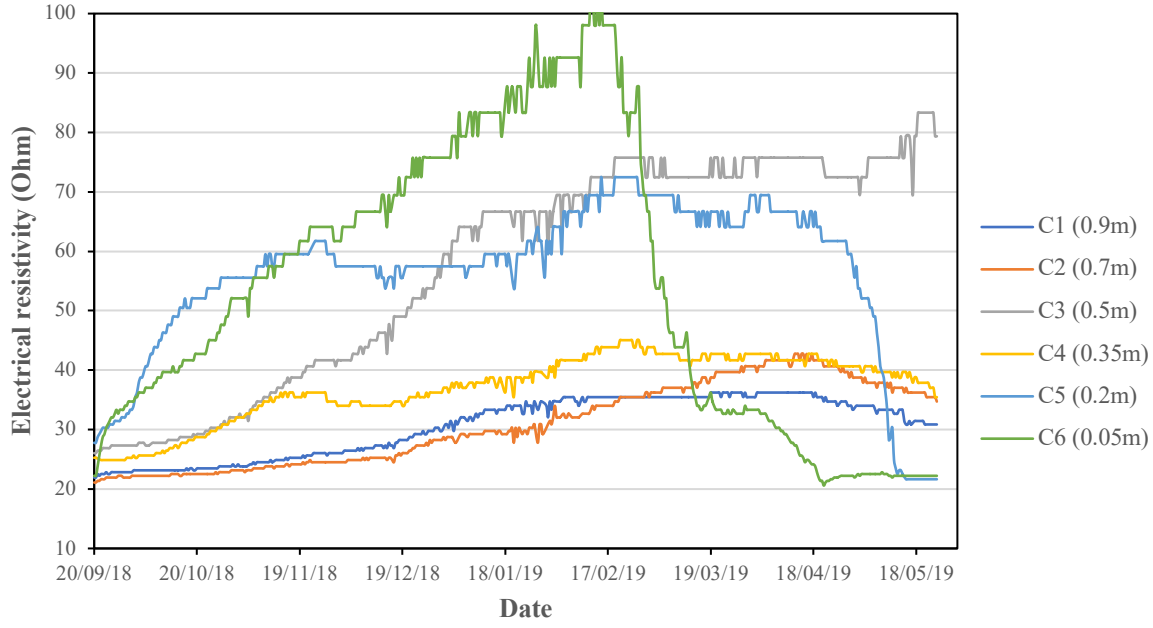

Figure 4.56 Electrical resistivity data using TDR probes for varying depths on lysimeter soil Column C

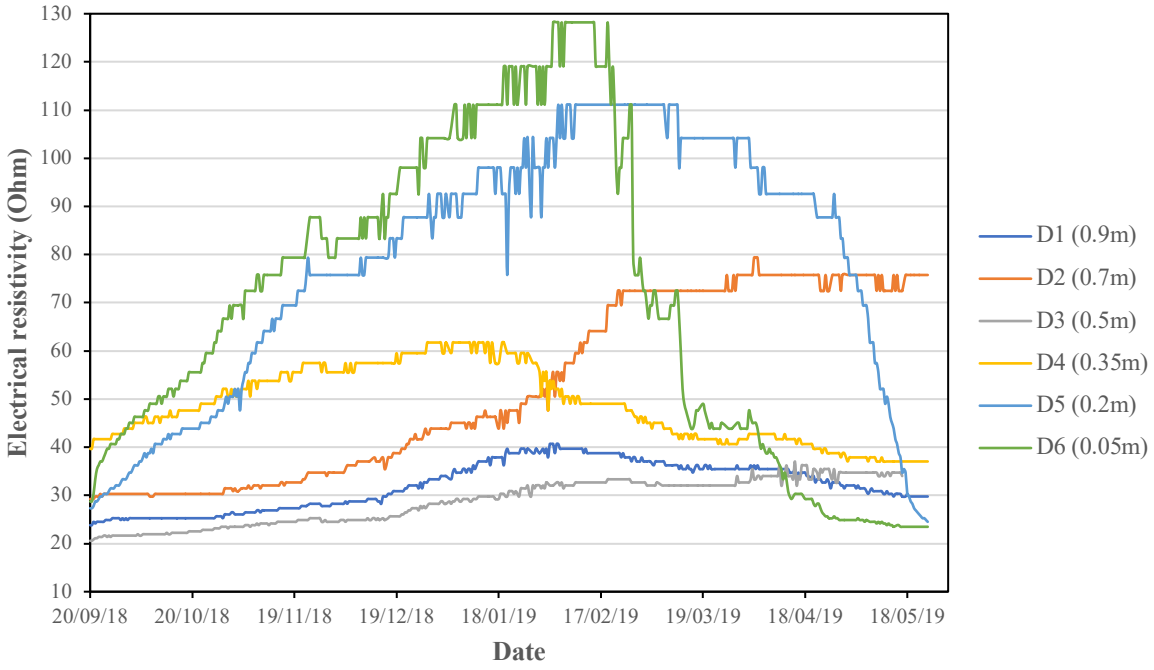

Figure 4.57 Electrical resistivity data using TDR probes for varying depths on lysimeter soil Column D

4.4.6 Comparison of soil water retention behaviour

In the previous subchapters, soil water retention curves (SWRCs) determined using different methods and on different sample sizes were presented separately for the three testing programmes. Figure 4.58 shows a comparison between the SWRCs of the primary drying-wetting cycle for the glacial till material obtained from three experiments. The drying and wetting SWRCs for large lysimeter test are presented by patterns with solid and dash lines separately to confine the variations of data obtained from different instrument ports. It can be seen that the drying curves from three experiments are in good agreements in the range where the volumetric water content is higher than about 25%, whilst the suction measured by the MPS-2 sensor in the box lysimeter experiment stay at a value of about 2500 kPa when the volumetric water content became lower. This may indicate that the working range of the MPS-2 sensor used in box experiment is up to 2500 kPa. For the wetting path, the curve determined for the small triaxial sample (shown in the FX fitting curve) shows higher VWC values when the suction is below 100 kPa and lower values when the suction is between 100 to about 300 kPa than the curve determined for the large lysimeter. The wetting curve from the large lysimeter test acts as a scanning curve of the primary wetting path as it was not completely dried out. The wetting curves

for box lysimeter and small sample shows strong agreement in the suction range between 400 to 2500 kPa whilst the wetting curve for the small sample shows a higher VWC value than that for the box lysimeter below 400 kPa suction.

It is concluded that the data are promising. The soil water retention curves from the small triaxial sample are representative of the sample from a larger scale.

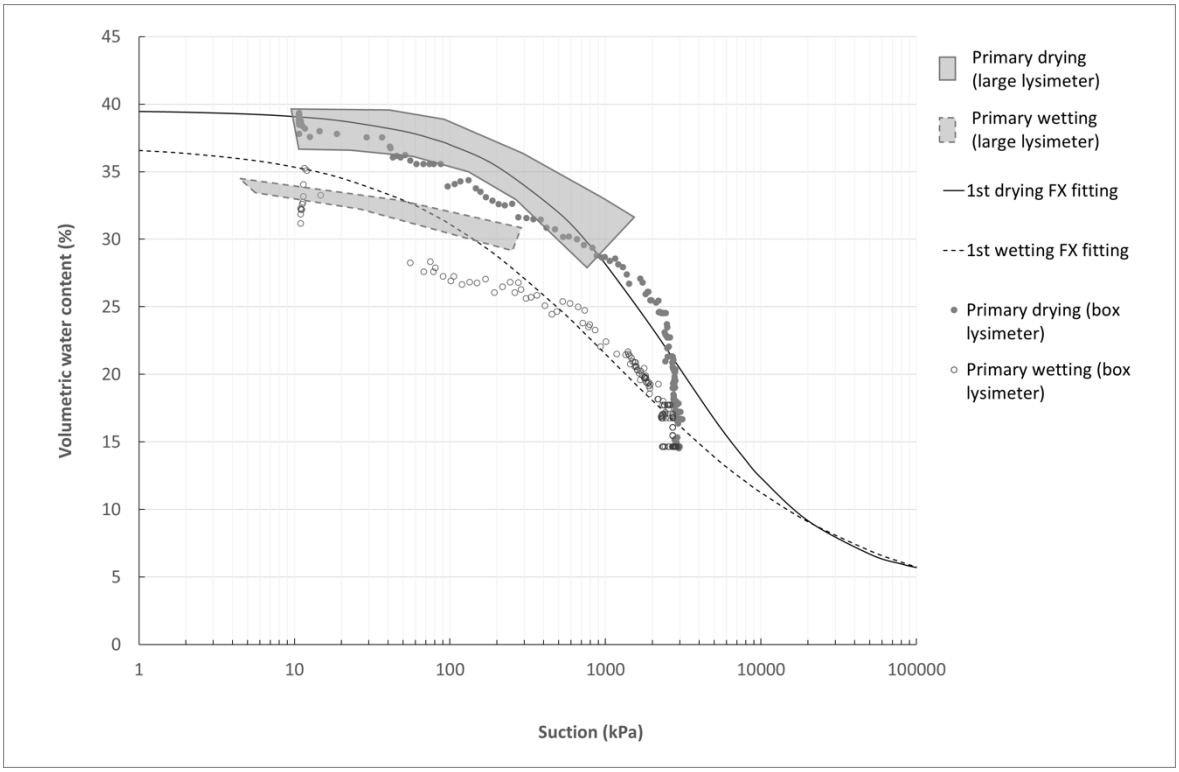

Figure 4.58 Comparison of soil water retention curves on the primary drying and wetting paths for the glacial till material determined from three testing programmes.

4.4.7 ERT-derived results

This subchapter contains the results of the electrical resistivity tomography monitoring programme of the lysimeter, over the time span of six months, starting from September 2018 when the data collection began.

4.4.7.1 The ERT model of lysimeter

The ERT data modelling was achieved using an open-source code, E4D (https://e4d.pnnl.gov/), described in Johnson et al. (2010). The code allows users to configure the ERT model based on real sample geometry.

Figure 4.59 shows a conceptual diagram of the cylindrical soil tank in the lysimeter along with the locations of the tensiometer ports for the four instrument columns. The 24 tensiometer ports were set as holes in the configuration model as they are made of insulting PVC materials. The configuration model confines the volume of the lysimeter sample as a conductive material in where the current flows are allowed to travel freely; and defines the PVC tensiometer ports as the holes, which were insulated.

A finite element mesh (FEM) for the ERT forward modelling and an inversion was then created using the mesh generation mode in E4D, as shown in Figure 4.60. It can be seen that the elements are more concentrated around the points where the electrodes are located.

The measured data sets were written into srv. files (the format of input data files in E4D) following the measurement array sequence.

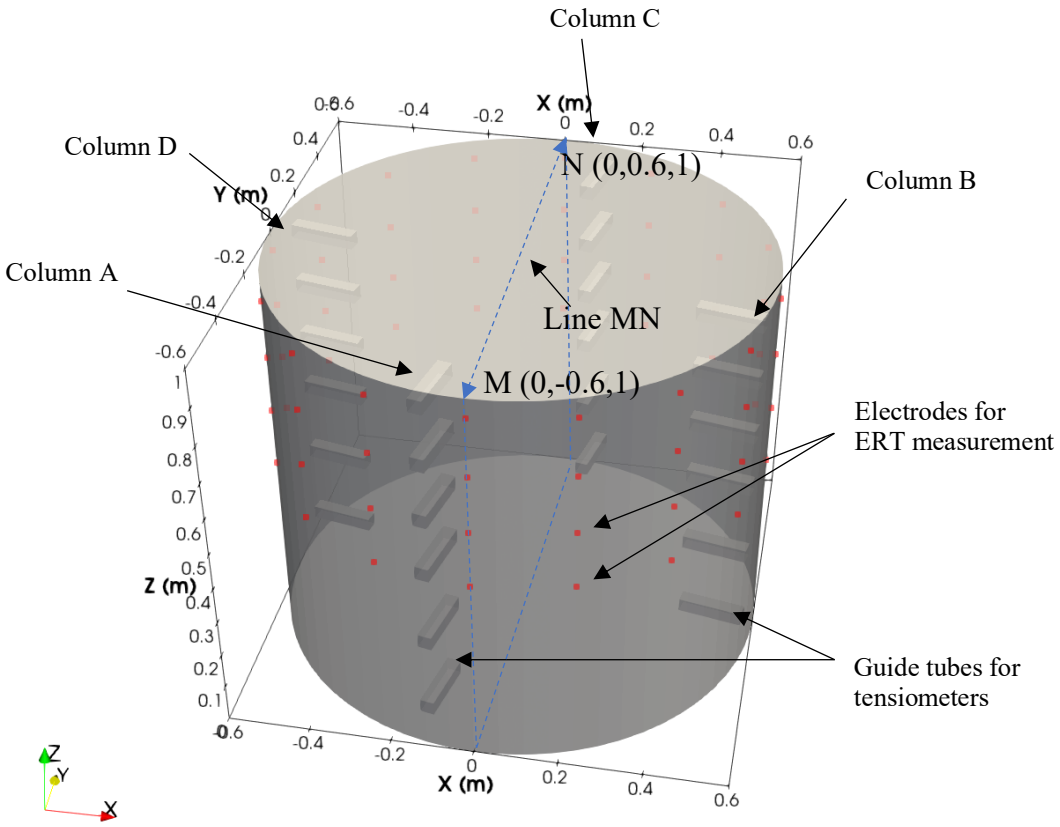

Figure 4.59 Conceptual diagram of the lysimeter sample with the locations of four soil columns and the positions of 24 plastic guide tubes for the tensiometer ports

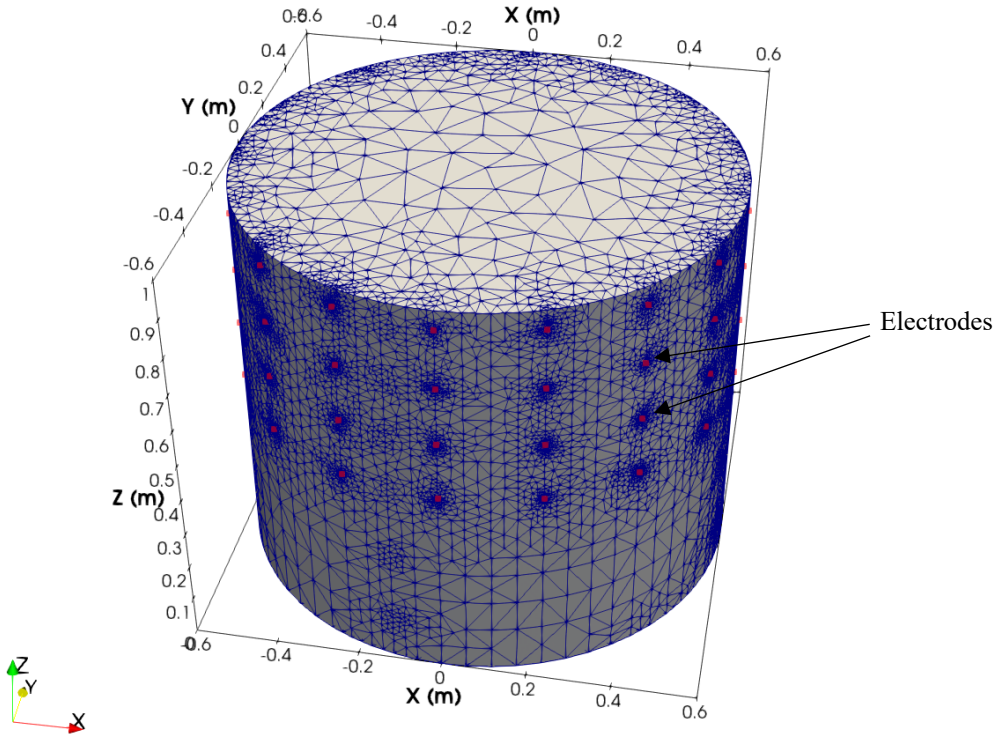

Figure 4.60 Oblique view showing the inversion mesh for the lysimeter model

4.4.7.2 2D resistivity images at monthly intervals

In order to establish the general trends in the resistivity response of the lysimeter sample during the drying and wetting periods, Figure 4.61 shows the 2D cross-sections along the plane MN (as shown to Figure 4.59) of the time-lapse 3D ERT models which present the resistivity distributions within the lysimeter sample at monthly intervals from 20th September 2018 to 20th May 2019. The images clearly show that the resistivities of the lysimeter sample started with consistent low values (less than 20 ohm.m) from the baseline model (on 20th September 2018) and increased from the top layer during the drying period until 14th February. After irrigation was applied to the top of the lysimeter sample from 14th February 2019, the resistivities gradually decreased from the top of the sample. It can be noticed that the resistivity increased more rapidly by the N side rather

than the M side from the centre top of the sample during drying, which may indicate an uneven air motion above the surface of sample. The top of the lysimeter wall is half a metre higher than the sample surface this may reduce air motion around the edge of the upper surface of the soil when compared to the centre. Consequently, stronger air motion at the centre of the upper surface may have led to the soils at the centre drying faster and becoming more resistive than the material at the edge.

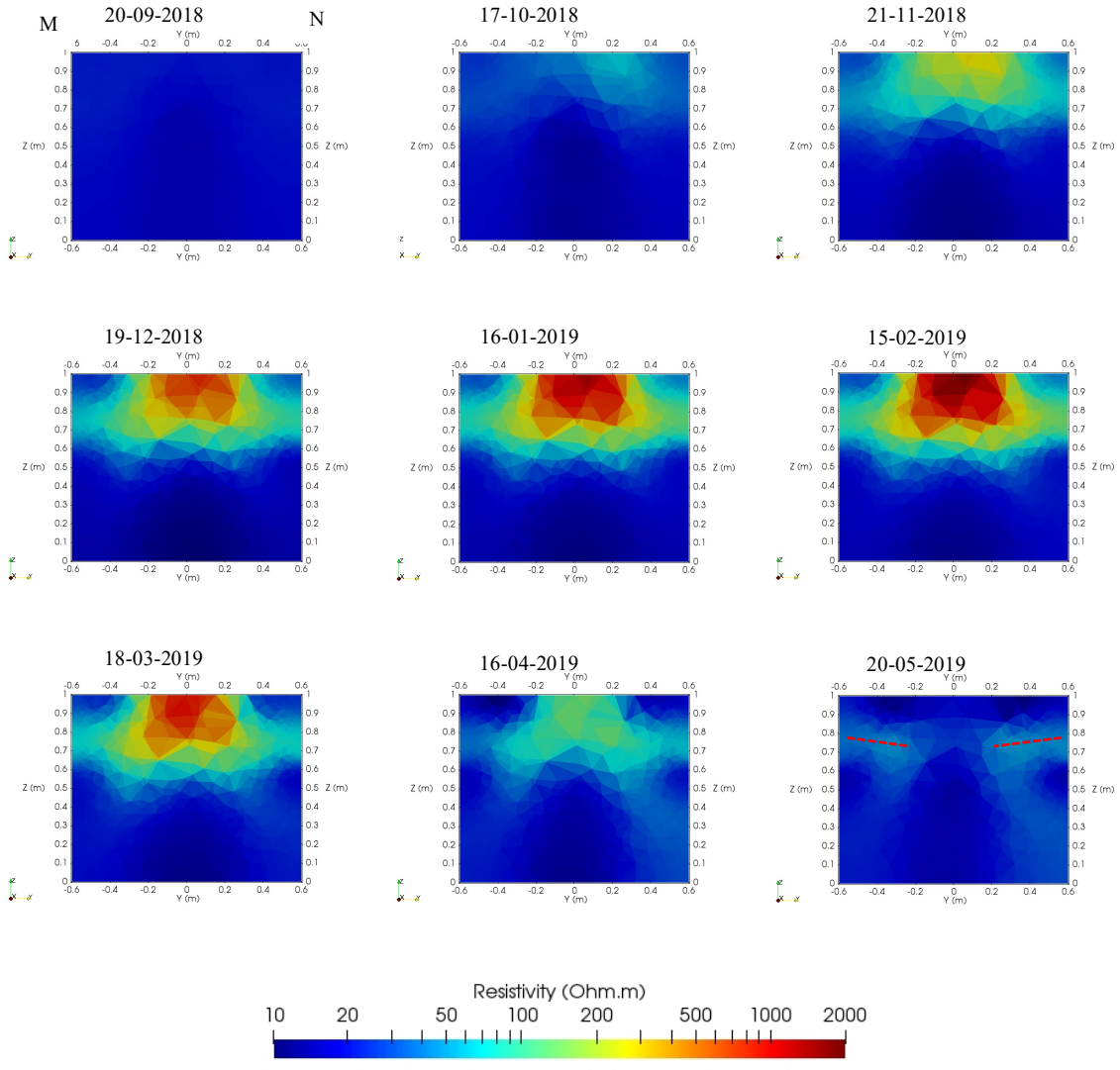

Figure 4.61 Electrical resistivity distribution at monthly intervals extracted along line MN, derived from 3D ERT data.

In addition, a horizontal zone with a high resistive response can be seen at a depth of between 0.2 and 0.3m (in which the layer 5 electrodes were installed). The presence of the high resistivity zone is thought to be as a result of the development of a cracking plane at a depth between 0.2m and 0.3m during the drying period, of which the location is

shown the imaging for the date 20/05/2019 in Figure 4.61, marked by the red dashed lines. In the wetting period (after 14/02/19), the decrease in resistivity in the lysimeter sample initialised from the edge of the upper surface to the centre of the upper surface and then gradually progressed to the lower layers. It has been mentioned in subchapter 3.4.8 that the sample was wetted by an irrigating unit that applied water radially to the sample surface such that the edge was wetted prior to the centre. It can be noticed that the high resistive zone lying at 5th layer (0.2m depth) faded gradually during wetting but still showed a relatively high resistivity response compared to the upper and lower layers until the end of the experiment.

4.4.7.3 Converted water content distributions over time

By applying the Waxman-Smiths relationship developed from small triaxial sample experiments, the 3D ERT data shown in Figure 4.61 were converted to water content using the porosity model shown in Figure 4.62, and the Waxman-Smits curve shown in Figure 4.63. In Figure 4.64, 2D time-lapse data are presented in terms of gravimetric water content for the cross-sections along plane MN.

The images clearly show that the gravimetric water content (GWC) within the lysimeter sample started from an almost saturated condition (between 20% and 25%) while the edge of the upper surface shows a little lower GWC (around 20%) than the main body of the sample (25% GWC). During the drying period, the sample generally dried from the top surface to the lower layer and the drying front moved down to 0.5m depth before irrigation was applied. The central part of the top layer dried faster than the edge due to the stronger air motion above the centre of the sample surface as explained in subchapter 4.4.7.2. It can be seen that the converted GWC of the 5th layer gradually exhibited lower value than that of the 6th layer during the drying period. This low GWC at 5th layer may not indicate a true value of GWC at the depth as it is converted from the high resistive zone in the 3D ERT data which is believed to be the result of a horizontally developed crack within the lysimeter sample during drying.

In the wetting period, data shows that the soil sample wetted from the edge of the top surface. The wetting front gradually infiltrated the central part of the top layer and then moved down toward the lower layers. The GWC for the edges of the soil sample below 0.5m showed a continuous decrease after the irrigation was applied. On 20th May 2019,

the GWC for the 5th layer shows a relatively low value between 10% and 15% that is not in accordance with the measurements from TDR probes that showed a saturated condition. Again, this low converted GWC may result from the high resistivity value caused by cracks and the low GWC zone may reveal the outline of the horizontal crack lying in the depth of the 5th layer of lysimeter sample.

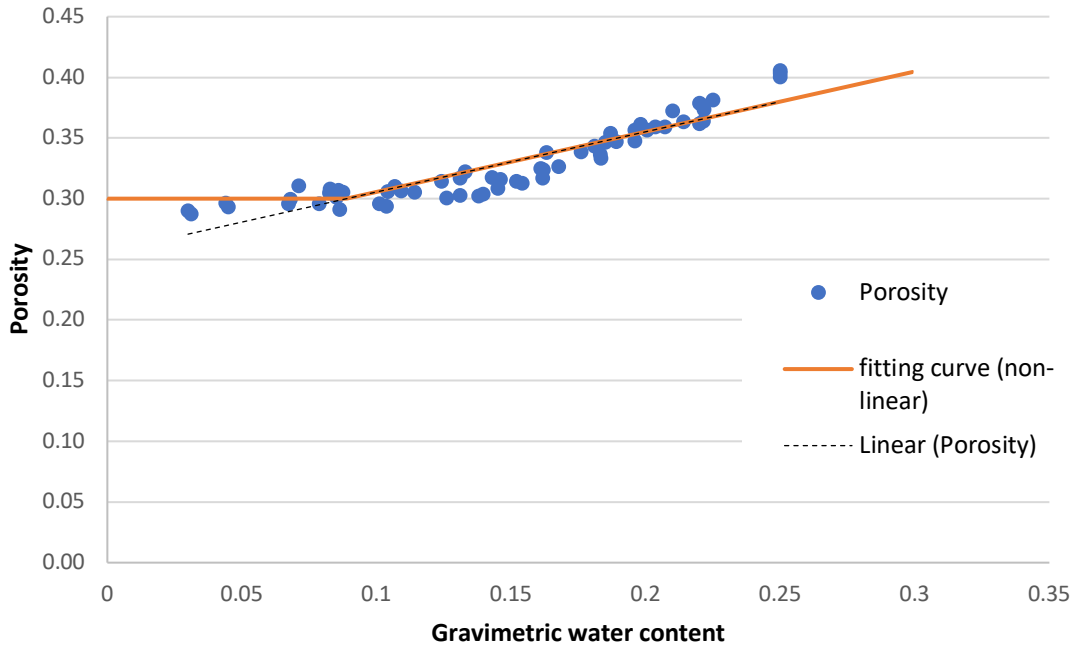

Figure 4.62 The porosity variations of glacial till material for the first drying-wetting cycle

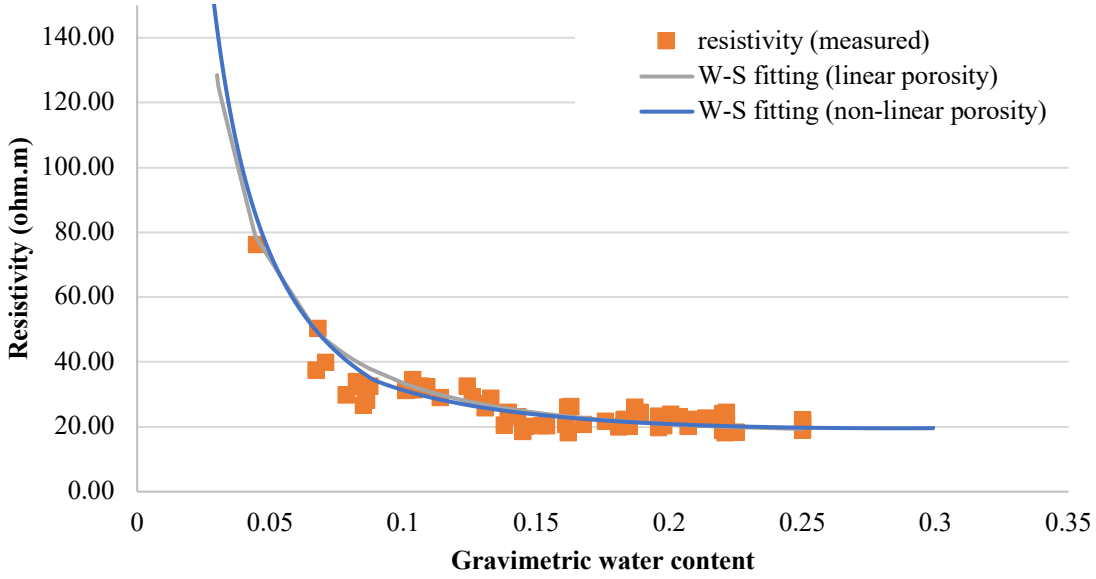

Figure 4.63 Resistivity vs. water content data of BIONICS glacial till material of the first drying-wetting cycle along with the fitting curves of Waxman-Smits model.

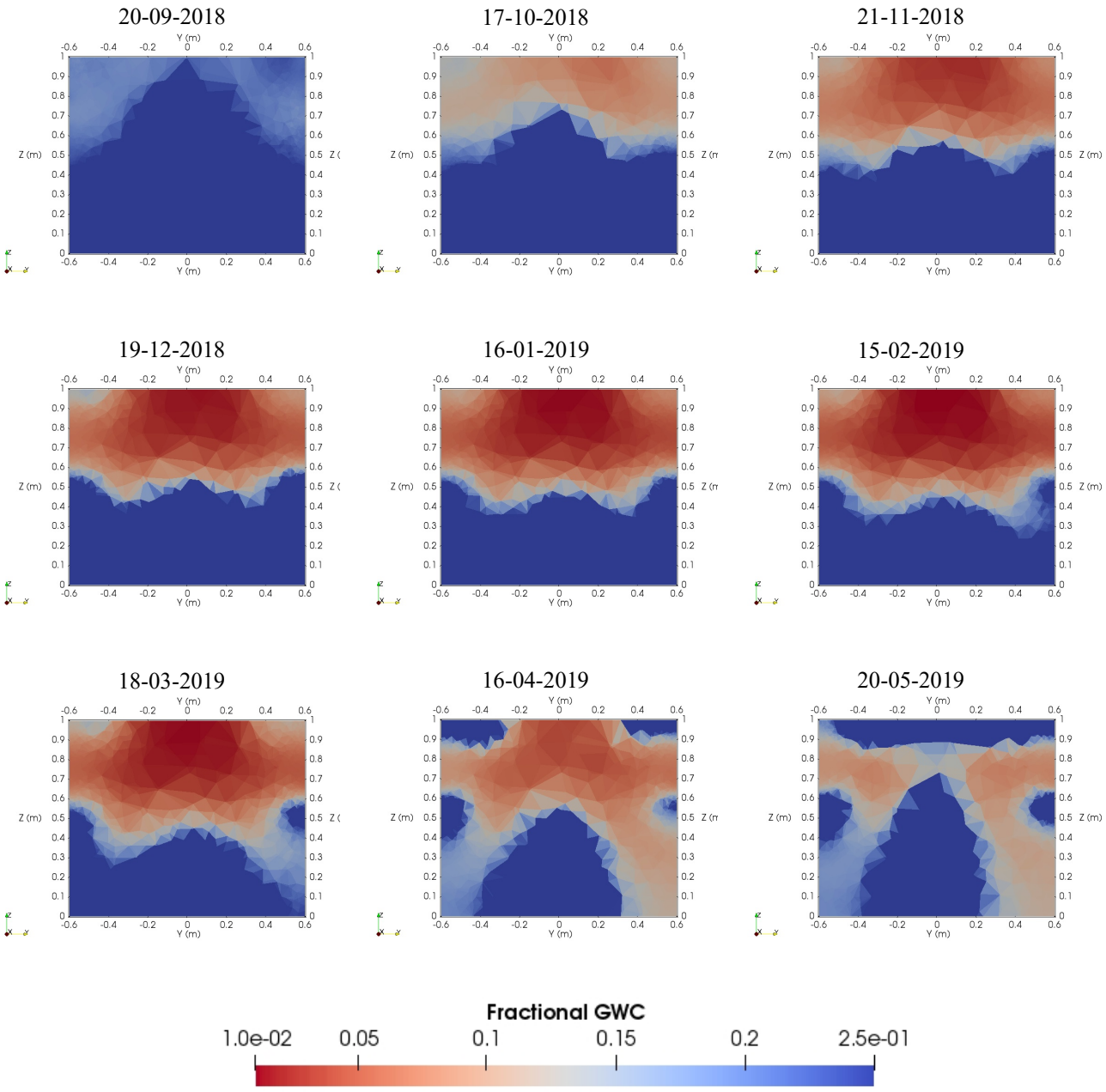

Figure 4.64 Converted gravimetric water content distributions at monthly intervals for the cross-section of lysimeter model along plane MN.

4.4.8 Comparisons of TDR and ERT derived data

4.4.8.1 Comparison of TDR and ERT derived resistivity data

Figure 4.65 shows the comparisons of measured and inferred electrical resistivity data for column A profile at different depths. For each depth of investigation, three types of resistivity data are presented: data directly measured by the TDR probe ("TDR" dataset

in the legend), data obtained by ERT ("ERT (mean)" dataset in the legend), and inferred data that derived from the VWC values measured by TDR by applying the Waxman-Smits modelling ("modelling (W-S)" dataset in the legend). The volume of an individual ERT cell confined in the mesh model (as shown in Figure 4.60) is small in the whole sample model. To compare the ERT and TDR data, the mean value of ERT resistivity of all the cells related to the location of the corresponding TDR probe was used in the comparison. An inferred resistivity dataset converted from VWC measurements of TDR probe by using the Waxman-Smits (W-S) relationship is also presented in the comparisons. Since the W-S model for the glacial till was established based on resistivity and VWC data obtained from direct methods and the use of the TDR probe on VWC determination was supported by the soil specific calibration, the W-S delivered dataset is considered as a reference resistivity data which represents a relatively true resistivity value of the lysimeter sample during the drying and wetting.

Generally, the TDR- and the ERT-derived data show similar qualitative trends in the resistivity measurements over time while the soil sample subjected to a drying and wetting cycle. Both methods indicate an increase in resistivity during drying and a decrease during wetting. However, there is a distinct difference between the two methods when quantifying the exact values of resistivity response. As can be seen for layers 1,2,3 and 6, the resistivity derived from ERT method shows a lower value than that directly measured by the TDR probe whilst for layers 4 and 5, the ERT-derived resistivity shows much higher value than that measured by TDR in a dry moisture range.

The closet agreement between ERT derived data and the W-S converted data was observed at layers 3 (0.5m) and 6 (0.05m), whilst the ERT data showed little higher resistivity values than those of W-S converted data during drying period and showed low values in the end of wetting period. At the near surface layer (0.05m), the consistent lower resistivity values observed for the ERT data (around 15 ohm.m) in comparing with the W-S converted data (around 20 ohm.m) in the wet end may be resulted from the over-wetting condition of the soils of the sample surface caused by the water pooling. Large deviations were observed between the ERT derived and W-S converted resistivity data at layers 4 (0.35m) and 5 (0.2m). This is caused by the development of the potential horizontal crack at the depth between 0.2 and 0.3m as discussed above. The crack becomes the abnormity in the ERT inversion model with very high resistivity which has

influences on all the cells in the volume close to it, causing the abnormally high values of resistivity measured by ERT at the layers 4 and 5.

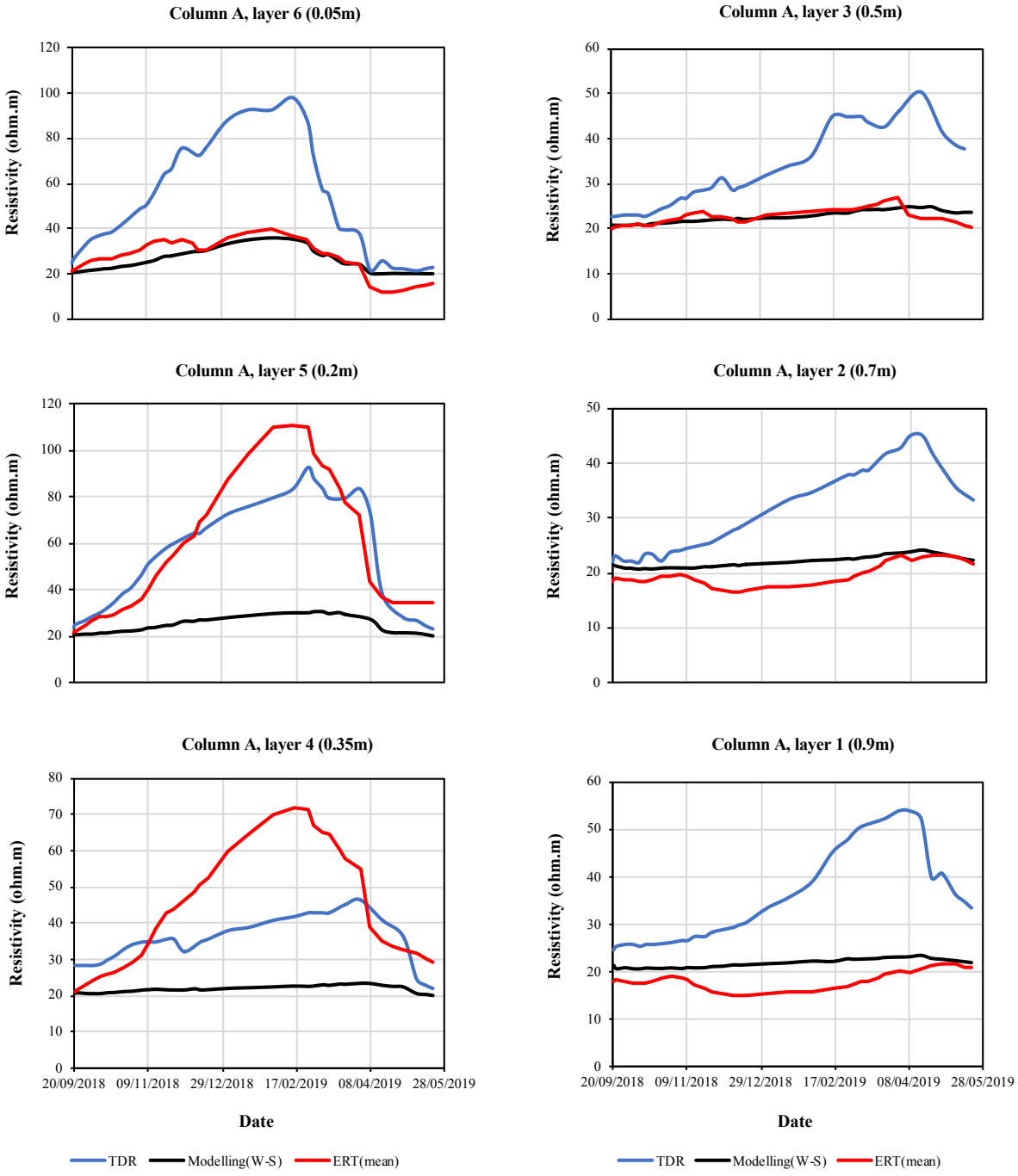

Figure 4.65 Comparison of measured and inferred electrical resistivity data for layers 1to 6 on Column A– measured resistivity data obtained from ERT imaging measurements (red curves) and the TDR probes blue curves); the inferred resistivity data (black curves) is converted from the VWC data of TDR by applying the Waxman-Smits model.

4.5 Chapter summary

A soil lysimeter test was conducted to examine a series of soil suction and moisture measurement sensors on a soil tank under cyclic drying and wetting conditions. Results suggest that for the permittivity-based point sensors, soil-specific calibration is required to ensure more accurate measurements on soil moisture. Hysteresis was found between the drying and wetting paths for the soil water retention curves and resistivity-water content relation curves when the soils were exposed to drying and wetting cycles.

A series of triaxial samples were made using three types of soils to investigate soil property relationships under multiple cycles of drying and wetting. The main findings are summarised as:

- Within the same cycle, the specimens on the drying path have higher UU shear strength and matric suction than those on the wetting path due to hysteresis.
- The behaviour of resistivity, shear strength and suction are different in different cycles. Hysteresis in the soil shear strength- moisture relationships and soil water retention behaviour are more significant in the first drying and wetting cycle and reduces as the number of cycles increases.
- Deterioration in shear strength and suction were found during multiple cycles of drying and wetting.
- The behaviour of soil electrical and geotechnical properties is influenced by cracking, volumetric change, and hysteresis.

A large scale lysimeter test was conducted to investigate the interrelationships between soil geotechnical and geophysical properties, the results suggested that:

- Both point sensor and ERT methods demonstrated similar qualitative trends in resistivity measurements during drying and wetting
- Generally, the point sensor measurement using two-point measurement showed higher reading than the ERT method which uses the four-point measurement
- Cracking was detected in the lysimeter ERT measurement and created much higher resistivity values.

5 Discussions

In this chapter, a discussion of the results of the three experimental programmes will be presented. There is a considerable correlation between the three programmes, therefore they are compared where relevant.

5.1 Laboratory testing techniques

5.1.1 Determination of soil water retention curves (SWRCs)

The soil water retention curve (SWRC) illustrates the relationship between suction and water content of the soil, which is an important component of unsaturated soil constitutive models and crucial for determining the hydraulic conductivity of unsaturated soil. The determination of SWRCs traditionally relies on filter paper method and pressure plate method, which has certain limitations. The filter paper method can deliver suction measurements over a wide range of soil water content, but it is time-consuming involving water potential equilibrium between the soil sample and the filter paper, and it relies on the use of a suitable calibration curve as an indirect method (Bicalho et al., 2011). The pressure plate method has a limited measurement range of less than 1500 kPa restricted by the air entry value of the ceramic disk, and the measurement relies on good contact between the ceramic disk and the sample surface, especially for dry samples. Another limitation of using the pressure plate method is the long time for potential equilibrium (Pan et al., 2010).

There is no available technique for measuring soil matric suction over the entire moisture range (Delage et al., 2008; Pan et al., 2010). Most studies regarding the drying and wetting SWRCs for fine-grained soils have been carried out at the low suction range with limited studies performed on the high suction range (Agus and Schanz, 2006; Al-Mahbashi et al., 2018). In previous studies, the SWRCs at low suction range (i.e. less than 1500 kPa) were usually obtained by techniques that measures matric suction, such as the axis translation technique (Fredlund and Morgenstern, 1977; Tarantino et al., 2000) and high capacity tensiometer technique (Ridley and Burland, 1993; Ridley and Burland, 1995; Tarantino and Mongiovì, 2001; Lourenço et al., 2006; Mendes, 2011; Toll et al., 2013). In the high suction range (i.e. greater than 1500 kPa), techniques that measures total suction are mainly used, such as the psychrometer technique (Campbell and Gardner, 1971; Rawlins

and Campbell, 1986; Woodburn et al., 1993; Ridley and Wray, 1996) and chilled-mirror hygrometer (Gee et al., 1992; Leong et al., 2003; Tang and Cui, 2005; Agus and Schanz, 2006). However, data of SWRC are limited for expansive soils over both the low and high suction range under repeated drying and wetting cycles. Determination of SWRCs over a wide range of suction can be performed using the combination of different techniques (Agus and Schanz, 2006; Delage et al., 2008). Since it is crucial to have the matric suction determined over a larger range to gain a more completed understanding of SWR behaviour for unsaturated soils over drying-wetting cycles, which meet one of the objectives of the thesis, SWRCs were determined for glacial till material using a combination of high capacity tensiometer and chilled-mirror technique (i.e. performed using WP4C PotentiaMeter) to cover a more complete suction range. Both the high capacity tensiometer and the WP4C PotentiaMeter provides rapid measurements on soil suction (i.e. few minutes for tensiometer and around 10 minutes for WP4C). Although the WP4C provides measurements for a wide range of suction—from 1 to 300 MPa, it has less accuracy for wet specimens with suction lower than 1 MPa (Campbell et al., 2007). To maintain the measurement range, a high capacity tensiometer apparatus was used to measure SWR data for the low suction range where the suction was lower than 1 MPa. The combination of two techniques allows the SWRCs to be determined for glacial till over a moisture range from saturation to residual water content under repeated drying and wetting.

In the box lysimeter testing programme, the dielectric water potential sensors MPS-1, MPS-2 and MPS-6 manufactured by Decagon Devices Inc. were also used to determine the matric suction of the soil sample during successive drying and wetting cycles. These sensors measure the dielectric constant to determine the volumetric water content (VWC) of the porous ceramic sensor head and provide indirect measurements of soil matric suction by converting the VWC into suction using a default calibration retention curve for the ceramic plate. Although the MPS-2 and MPS-6 sensors have a working range between -9 to -100000 kPa, they are only well calibrated between -9 and -100 kPa by the manufacture (Decagon, 2016). The promising performance of such sensors relies on the accurate calibration retention curve of the ceramic plate and good contact between the soil and the sensor heads. In this study, MPS-1,2&6 sensors and tensiometer were used to measure the matric suction of soil sample under drying and wetting cycles in a box lysimeter. As can be seen from Figure 4.4, during the drying process, the readings of MPS

sensors and tensiometer show good agreement in the range of 0 to -300 kPa, whereas only MPS-2 water potential is in good agreement with the reading of tensiometer below -300 kPa up to about -1200 kPa. The accuracy of water potential sensors to measure low suctions (i.e. < about 500kPa) has also been verified in many previous studies (Kammerer et al., 2014; Nolz and Kammerer, 2017; Walthert and Schleppi, 2018). Although the working range of MPS-2 and MPS-6 sensors indicated by the manufacture is up to -100 MPa, little information can be found in the literature to substantiate the use of water potential sensors in the high suction range (Nolz and Kammerer, 2017). All three MPS sensors show a lower limit in determining the water potential in this study: for MPS-1, it is down to approximately -500 kPa, which is in accordance with the manual (Decagon, 2009); for MPS-2 and MPS-6, there is a lower limit at approximately -3000 kPa and -1200 kPa, respectively. It can also be evident from Figure 4.58 that the water potential sensor is failure to measure high suctions above about 3000 kPa while the water content of the clay sample reduces continuously. Some previous studies have pointed out that the measurement of these sensors at high suction range are not reliable (Tripathy et al., 2016; Walthert and Schleppi, 2018). The failure of MPS sensors to measure high suctions may be attributed to multiple factors. Firstly, in Figure 5.1, it can be seen that the ceramic's water retention curve of MPS-2 and MPS-6 tends to be flat at water potential between -1000 to -10000 kPa, which means that the large change in the applied water potential causes small change in the water content within the sensor ceramic in this range, resulting in a low sensitivity zone for the water potential measurement. Additionally, the shrinkage of clay material at a dry condition may introduce air into the interface between the sensor and the soil sample, creating discontinuities in the water phase between the sensor and the sample, thus disturbing the water flow (Tripathy et al., 2016).

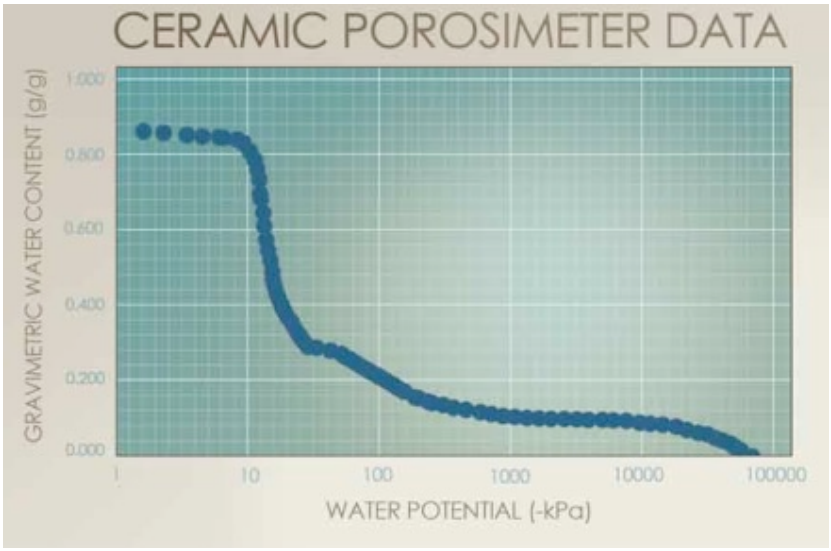

Figure 5.1 Calibration curve of MPS-2 and MPS-6 sensor ceramic by the manufacture (Decagon, 2016)

5.1.2 Point sensors for determination of soil water content

Several point sensors were used to determine the VWC of soil samples during drying and wetting in the box lysimeter and large cylindrical lysimeter testing programme. All the moisture sensors determine VWC by measuring the apparent permittivity, ε_a, of soil using different principles: i.e., time domain reflectometry (TDR probes), frequency domain reflectometry (5TE sensors) and amplitude domain reflectometry (ML2x probe). The sensor responses are related to soil dielectric permittivity, thus are converted into volumetric water contents according to the calibration relationship between soil apparent permittivity and VWC. The success of using TDR techniques as well as other dielectric sensors to determine soil water content depends on two phases, the first of which is to accurately measure the bulk permittivity of the soil. The second is to determine a reliable conversion relationship between the measured apparent permittivity and the soil water content (Robinson et al., 2003a). The empirical relationship between soil water content and apparent permittivity proposed by Topp (1980) are widely used as the factory calibration of these dielectric sensors for measuring the water content. As can be seen in Figure 4.1, the calibration results show a linear relationship between the refractive index (i.e. square root of the apparent permittivity) and the VWC, which is consistent with the literature (Malicki et al., 1996; Schaap et al., 1997; Robinson et al., 1999; Asquith, 2015). However, most of the calibration lines obtained by soil-specific calibration of these dielectric water content sensors are offset from the empirical Topp model. This has been

noted in many previous studies involving different soil types (Whalley, 1993; Schaap et al., 1997; Jones et al., 2002; Curioni, 2013; McCann et al., 2013; Asquith, 2015). As stated above, the calibration procedure for the dielectric sensors should involves two stages, first of which is the instrument calibration to ensure the accurate measurements on soil relative permittivity, and the second is the instrument independent calibration on the conversion relationship between soil permittivity and water content. The former is normally conducted based on the electrophysical theories of the techniques and applying two-point calibration to calibrate the permittivity measurement in water and air (Heimovaara, 1993; Robinson et al., 2003a; Decagon, 2010). In practice, the bulk permittivity measurement of soil medium is more complex than that of the water and air and affected by numbers of factors, such as the bulk density and the solution electrical conductivity. The soil bulk conductivity has a small effect on TDR but a more significant effect on capacitance probe. The permittivity measurement of the TDR probe is also affected by the cable length (Heimovaara, 1993), the frequency of propagation signals (Thomas et al., 2010b) and temperature (Curioni, 2013). The A soil-specific calibration is required for these point sensors to determine the VWC for a clay material given that the dry density of clay changes over time under repeated drying-wetting cycles. Additionally, good contact between the soil and the sensor is crucial for using the dielectric moisture sensors since the prongs of most sensors are sensitive to the entrapped air around them. Poor contact issues were found in both box lysimeter and large lysimeter experiments and the problematic sensors resulted in an underestimation of soil water content.

5.2 Soil property interrelationships

5.2.1 Soil water retention curves

Soil water retention curves have been determined in this study on different sample size and using different techniques as stated in section 5.1.1. In triaxial sample experiment, the total suction values were measured by WP4C, which can substitute matric suctions in a suction range of greater than about 1000 kPa, at where the osmatic suctions take minor proportion in high suction range (Fredlund and Rahardjo, 1993). In the low suction range, soil water retention data were measured using tensiometer apparatus to cover the measurements of suction range less than 1000 kPa. By combining these two sets of data

a full range SWRC data set with respect to the matric suction was determined for glacial till under multiple drying and wetting cycles. SWRCs for glacial till under cyclic drying and wetting were then made using Fredlund and Xing (1994) model as shown in Figure 4.15. Generally. Distinct hysteretic SWR behaviour has been evident herein from the SWRCs of this study. The saturated volumetric water content at the beginning of the first drying path is shown to be about 39% and dropped to around 34% when the second drying path started, and subsequently dropped to about 32.5% while the third drying path started, indicating a deterioration in water retention capacity as the number of drying-wetting cycle increases.

The results of SWRCs from the three testing programmes show clear hysteresis between the drying and the wetting paths in a drying-wetting loop. which demonstrates a higher VWC on the drying path than that of the wetting path at a given suction. The hysteresis of SWRCs has been found and discussed in many previous studies (Fredlund and Rahardjo, 1993; Leong and Rahardjo, 1997; Likos et al., 2014). Tuller and Or (2004) has concluded the mechanisms of hysteresis to several factors: the 'ink bottle' effect, different contact angles between water and soil particle, the effect of entrapped air due to incomplete saturation during the wetting process, and volumetric changes of unsaturated soils due to swelling and shrinking behaviour of soil that is subjected to drying and wetting.

The results of SWRCs in Chapter 4 shows that hysteresis of the drying-wetting loop is more significant at low suction range than that at high suction range. This may be attributed to the different water retention mechanisms of soil in the range of low and high water content. Tuller et al. (1999) has proposed that the matric suction of soil is governed by two individual mechanisms: capillary and adsorption. Capillarity is caused by surface tension of water that takes place at the water-air interfaces (menisci) within the soil pores, which is governed by the pore size distribution. The adsorption water at the surface area of the soil particles results from the interaction between water and soil particles, especially the clay minerals, due to the presence of electric double layer and the exchangeable cations (Tuller and Or, 2004). In the high water content (low suction) range, the water retention behaviour is mainly dominated by capillary mechanism, which is related to the "inkbottle" effect, soil-water contact angle, entrapped air and volumetric changes due to swelling and shrinkage. In the low water content range (high suction),

adsorption controls the soil water retention, which is governed by the mineralogy and clay activity. Since the adsorption and desorption processes are physically reversible, this makes the hysteresis at high suction range less pronounced (Lu and Khorshidi, 2015).

According to the SWRCs results presented in the Results Chapter, it has been found that the degree of hysteresis between the drying and wetting path is most pronounced in the first drying-wetting cycle and is less significant in the subsequent cycles. Similar results were reported for unsaturated soils in previous studies (Goh et al., 2014; Glendinning et al., 2018; Stirling et al., 2020; Wen et al., 2020). This may be attributed to the changes in the microstructure and the swelling-shrinkage behaviour of the soil material driven by the successive drying and wetting cycles. As stated above, the hysteresis of SWRC is dominated by the capillarity which is highly related to the pore size distribution, pore connectivity, pore shape and angularity which is governed by the soil micro-structure (Tuller et al., 1999). The main effect of drying and wetting cycles on expensive soils (e.g. clays) is the irreversible changes of soil micro-structure driven by repeated swelling and shrinkage (Al-Homoud et al., 1995; Basma et al., 1996; Estabragh et al., 2015). The continuous reconstruction and reorientation of soil fabric and particles during repeated swelling and shrinkage may result in destruction of large clay aggregates, disorientation of structural elements (Basma et al., 1996), cracking and fatigue to structures (Al-Homoud et al., 1995; Hen-Jones, 2018; Stirling et al., 2020), and the changes in pore size distributions (Kong et al., 2018; Azizi et al., 2020). These micro-structural changes also influence the swelling potential of clay, leading to an increase (e.g. as observed on London Clay and Hollin Hill Clay in this study) or a decrease (e.g. as observed Glacial till in this study) of void ratio over drying-wetting cycles depends on the aging history and the as-compacted conditions of samples (Day, 1994). Furthermore, the volumetric changes of soils during swelling-shrinking cycles were also found to be most pronounced in the first cycle and decreased with increasing cycles, which has a similar trend to the changes in hysteresis of cyclic SWRCs. This may imply the strong correlation between the SWRC hysteresis and volumetric changes. Additionally, the SWRC results showed that soil suction in both the box lysimeter test and the small triaxial sample test, representing different sample sizes, deteriorated with the drying-wetting cycle as the number of cycles increased. It may imply that this deterioration is consistent across different sample sizes and could be scaled to field conditions.

5.2.2 Resistivity-water content relationships

Figure 4.31 illustrates the relationships between electrical resistivity and degree of saturation for glacial till under three cycles of drying and wetting. In general, datasets from all the drying and wetting paths established an inverse power relationship between resistivity and degree of saturation, indicating an increase in soil resistivity as the degree of saturation decreases in a testing S_r range of 20% to 100%. The resistivity values increased slowly from full saturation to a S_r of approximately 70% from about 20 Ωm to 30~40 Ωm and grew more dramatically to a residual S_r of about 20%.

Generally, the resistivity measured on the second and third drying-wetting cycle at a given water content or S_r showed higher value than that on the first cycle. This might be due to the development of micro-cracks during drying processes, which interrupt the continuities of water fluid and block the current flows within the soil specimen, thereby resulting in higher resistivities.

Noticeably, the relationships between resistivity and degree of saturation generally changed over time as the number of drying-wetting cycles increased; the trends of this evolution in the relationship do not remain consistent between the drying and wetting paths or between the different cycles. Figure 4.31 demonstrates that the resistivities show higher values in the second drying-wetting cycle than in the first and third cycles for glacial till material, and the resistivity characteristic curves of the third drying-wetting cycle lie between the curves of the first and second cycles; this implies that soil resistivity behaviour is complex and that it is affected by multiple factors when clay material subjected to successive drying and wetting. For instance, as for the glacial till material in this study, the successive development of micro-scale cracks and fractures within the soil samples in the drying processes cycles leads to an increase in resistivity over cycling (Hen-Jones, 2018), whereas the reduction in void ratio over drying-wetting cycles results in a decrease in resistivity for a given water content over cycling (Hassan, 2014). In this case, the cracking and volumetric changes caused by drying-wetting cycles has an opposite effect on resistivity, such that the ultimate effect of drying-wetting cycles on soil resistivity behaviour is uncertain and the weight and susceptibility of each effect may need to be assessed. Therefore, when interpreting the changes in resistivity-water content relationships of clay under repeated drying and wetting cycles, the volumetric changes of

clays due to cyclic swelling and shrinking must also be considered in addition to the water content changes and cracking.

5.2.3 Strength-water content relationships

Hysteresis is shown between the drying and wetting path of the C_u-w relationship for all the drying-wetting cycles. The specimens exhibited higher shear strength values in the drying path than in the wetting path at a given water content. The hysteresis in C_u-w relationships might be related to the hysteresis between the drying and wetting of the soil water retention behaviour. The lower suctions of the wetting path might result in lower suction-induced shear strengths, causing the reductions in wetting path shear strengths. However, the hysteretic relationship between C_u and w may also be due to micro-scale cracking or volumetric changes (swelling and shrinking) in the clay material during cyclic drying and wetting.

All the drying stages exhibit a drop in shear strength at a given suction from the before to the next drying-wetting cycle. This shows a deterioration in shear strength, which demonstrates a progressive loss in the shear strength at a given water content as the number of drying and wetting cycles increases. Noticeably, the deterioration of shear strength is shown to be more significant between the first and second cycles than between the second and third cycles, which is consistent with the deterioration which has been observed in the cyclic SWRCs; an explanation for this may be that the progressive loss in suction, as observed in the cyclic SWR behaviour, reduces the suction-induced shear strength, resulting in a progressive deterioration in soil shear strength during repeated drying-wetting cycles.

The results of the relationships between shear strength and suction as presented in Subchapter 4.3.3 reflect that the micro-cracks directly cause a reduction in shear strength independent of the suction-induced shear strength with increasing numbers of drying-wetting cycles; this indicates that the development of micro-cracks has a direct influence on the performance of soil shear strength. In a conclusion, the deterioration in soil shear strength behaviour is driven by both the cyclic SWR behaviour and the development of micro-cracks under repeated processes of drying and wetting.

5.3 Soil deterioration of clay materials under drying-wetting cycling

The work presented in the results chapter provides evidence for a deterioration in fabric of compacted clay materials during successive drying and wetting cycles. This soil fabric deterioration described a progressive rearrangement of clay aggregates associated with the development of micro-scale cracks during successive drying and wetting cycles.

All the results from three laboratory experiments conducted on different sample sizes suggest the hysteretic nature of SWR behaviour, wherein the measured suctions on the drying path for given water contents were higher than those on the wetting path. The mechanism driving the hysteresis for the primary SWRC loop has been suggested and summarised in many related studies, as reviewed in Subchapter 2.2.3.2. A key observation from the laboratory results in this study is that the suctions measured on the second and third drying paths did not follow the primary drying path and showed lower values of suction for given water contents than those on the drying path of the previous cycle, indicating that the clay material progressively lost its ability to produce the same amount of suction at a given water content with increasing numbers of drying and wetting cycles. The rate of this progressive degradation in suction detected in SWRCs, driven by repeated drying-wetting cycles, is inconsistent, with the most significant change observed between the primary and second drying paths. This phenomenon was found in different scales of testing, such as the triaxial sample experiment for the small-scale and the box lysimeter experiment for the medium-scale laboratory test. Similar hysteric behaviour and deterioration has also been observed in results of undrained shear strength. This indicates that the SWR behaviour associated with a deterioration in suction contributes to a progressive loss in soil shear strength under repeated moisture cycling. Deterioration in both the suction and shear strength are most pronounced in the first drying and wetting cycle, as observed in the triaxial testing results. Similar results have been reported by Goh et al. (2014).

It is worth noting that the deterioration of soils during drying-wetting cycles cannot be considered in isolation from the microstructure changes and development of micro-scale cracks driven by the repeated swelling and shrinkage. The continuous reconstruction of soil fabric and aggregates promotes the developments of micro-cracks (Hen-Jones, 2018; Stirling et al., 2020) and makes the voids of be occupied by a greater portion of larger pores (Azizi et al., 2020). These influence the soil water retention behaviour and

contribute to the deterioration in soil suction under drying and wetting cycles. The results of the relationships between shear strength and suction presented in Subchapter 4.3.3 demonstrate a reduction in shear strength that independent of suction over increasing numbers of drying-wetting cycles. This may also be attributed to the development of micro-cracks and larger porosity during repeated drying and wetting cycles, which has a direct influence on the performance of soil shear strength (Chen et al., 2018; Hen-Jones, 2018), since it breaks the continuity of the soil fabric, producing more potential failure planes in a micro-scale within the soil. Thus, this becomes an additional mechanism of driving the deterioration in soil shear strength in addition to the SWR behaviour.

The implications of progressive soil deterioration on slope stability are considered involving two aspects. Firstly, the engineered slopes that constructed with clay materials undergo a progressive deterioration in soil suction and soil fabric driven by the actions of drying and wetting, resulting in a progressive loss of soil shear strength and, subsequently, more potential slope failures. Secondly, the deterioration of important geotechnical parameters used for assessing the long-term stability of slopes as well as other engineered infrastructures should be considered, a critical range of which can be defined from a deterioration model that developed from laboratory tests, as the soil properties change gradually over time due to progressive soil deterioration driven by the seasonal moisture cycles. By investigating the undrained shear strength and soil-water retention behaviour of unsaturated clay materials that subjected to multiple cycles of drying and wetting, an improved understanding of weather-driven deterioration of engineered soils has been presented in this study. This improved understanding can help with the development of deterioration models, such as that proposed by Glendinning et al. (2018), that can be used to predict the evolution of key geotechnical parameters used in stability analyses, providing a more critical assessment of the long-term stability of engineered earthworks, particularly for those influenced by changing climate and extreme weather.

5.4 Implementation of ERT in slope monitoring

Traditionally, the monitoring and assessment of slope stability has relied on point sensor networks, which are normally installed in drilled boreholes. The installation of these sensors disturbs the continuity of the near-surface soils. Recently, the ERT method has become popular for monitoring slope stability and multi-purpose engineering disciplines

as it is a non-invasive and fast means of obtaining spatial information on electrical resistivity in the subsurface of the earth. The latest multi-channel systems also allow numerous potential electrode pairs to be measured at the same time, speeding up the acquisition process of ERT (Samouëlian et al., 2005). Many other studies have suggested that the ERT method is suitable for observing qualitative changes in subsurface soil structures (Sass, 2007; Hirsch et al., 2008; Hsu et al., 2010; Chambers et al., 2012). However, to use the ERT method as a means of monitoring the moisture dynamics of engineered slopes, ERT-derived data must also be quantitatively interpreted to extrapolate specific geotechnical properties. In establishing this geotechnical-geophysical property transformation, the geotechnical properties in a large-scale, such as those in the field, become possible to be measured based on the ERT-derived data by applying laboratory-obtained proxy relationships, for example the proxy relationship between soil water content and resistivity and the SWRCs.

To achieve this extrapolation of geotechnical data from the ERT-derived data, the glacial till material was compacted into a large cylindrical lysimeter with a diameter of 1.2 m to simulate field conditions. To perform a quantitative investigation, volumetric water content and bulk conductivity were measured using TDR probes from different depths and locations of lysimeter sample to compare with the ERT-derived data. Electrical resistivity tomography was employed to map the distribution of soil resistivity over time as well as to map the water content distributions based on the Waxman-Smits relationship between soil resistivity and VWC, as established through the small-scale laboratory measurements on triaxial specimens with diameters of 38 mm. In Figure 4.65, a comparison between the ERT- and TDR-derived and WS-converted resistivity data was made for the quantitative analysis of the ERT-derived data. The results indicate that the ERT-measured resistivity closely agrees with the data converted from the VWC measurement of the TDR probes using W-S modelling in lysimeter sample except for the crack-influenced layers (layers 4 and 5). This also indicates close agreement between the VWC data measured by the ERT and the TDR. However, there are still several deviations observed between the ERT-derived resistivity data and the WS-converted resistivity data in the drying period for layers 1, 2, 3 and 6, which is considered to be caused by the artefact for the ERT modelling. The artefact of ERT modelling has been reported by most of the studies involving ERT methods and can result from systematic ERT configurations,

random errors in ERT data, high contact resistance issues during the drying of soil and misestimation of the error level in ERT inversion (Koestel et al., 2008).

Furthermore, the resistivity measured directly from TDR probes showed a much higher estimation of VWC than that measured by ERT. This may be due to the different methodologies of ERT and TDR in resistivity/conductivity measurements as the ERT method uses a four-electrode array whilst TDR is based on a two-point method. Previous research has shown that resistivity measured from the two-point method showed higher values than in the four-point measurement of the same type of soil (Hen-Jones, 2018). Another potential cause for the overestimation in TDR probe resistivity is because the calibration of the TDR probe for conductivity measurement is conducted using the factory calibration process (Decagon Devices, 2013), which may not be suitable for the glacial till material in this study, therefore a soil specific calibration may be required for the TDR probes to measure the resistivity.

Additionally, the development of a horizontal crack was detected in the lysimeter sample between layers 4 (0.35 m) and 5 (0.2 m) during the drying period in the ERT images, as discussed in Subchapter 4.4.8.2. The crack generated during drying produced high resistivity zones in the inverted ERT model, which influenced the resistivity response of the surrounding cells by dramatically increasing the resistivity measured by ERT. The same observations were reported in a number of other studies (Hassan, 2014; Hen-Jones, 2018; Tang et al., 2018b), indicating that the ERT method can detect the development of cracks associated with soil drying activities. Furthermore, the crack generated in the large lysimeter sample in this study affected the resistivity response of ERT for the adjacent instrument layers, making it impossible to compare ERT data with the TDR-derived data of these layers. Unfortunately, since the lysimeter walls are not transparent and are made of black PVC material, crack development was not really observed.

As discussed above, the ERT method was proven to have the ability to describe the moisture dynamics of the engineered soil both qualitatively and quantitatively, aiding with the geotechnical-geophysical proxy relationship. However, it has been proven from the laboratory tests that the proxy relationships between the geotechnical properties and resistivity changes over time due to soil fabric deterioration driven by the repeated processes of drying and wetting. This aging effect on soil fabric has also been observed

in the field tests (Glendinning et al., 2018; Hen-Jones, 2018; Stirling et al., 2020). If the ERT data are directly used to convert the geotechnical parameters in the stability assessment of an engineered slope exposed to a changing climate, the converted data may become misfits over time due to this aging effect driven by soil deterioration. Nevertheless, the results from this study also demonstrate that the change in the water content–resistivity relationship among cycles is less significant than that of the geotechnical relationships, such as SWRCs and the shear strength water content relationships. Thus, the ERT data is a suitable water content indicator for unsaturated soils that undergo repeated drying and wetting cycles. In this case, if used in association with viable deterioration models, the electrical resistivity method has the potential to monitor the deterioration of soils in-situ (Glendinning et al., 2018; Hen-Jones, 2018).

6 Conclusions and Recommendations

6.1 Conclusions

A large portion of engineered slopes and cuttings for the UK's transport networks are constructed on compacted clay soils, which are exposed to the changing climatic conditions. The deterioration of soil fabric driven by repeated moisture cycling affects the determination of soil geotechnical properties are important for the assessment of slope stability, since the properties are likely changing over time with deterioration. Given that soil electrical resistivity is popularly used as a water content indicator, the aims of this thesis were 1) to investigate how soil deterioration influences unsaturated soil property relationships during successive water content cycling, and 2) to use resistivity methods to quantify the changes in soil properties under drying and wetting cycles in association with proxy relationships. In order to investigate the soil deterioration of engineered soils affected by the changing climate, several objectives were made to investigate the interrelationships between the mechanical properties and the water content of unsaturated soils under repeated drying and wetting cycles, as the water content of soil is a key factor governed by the drying-wetting cycles. In establishing these property relationships by multi-scale laboratory tests, an improved understanding of soil deterioration driven by repeated drying and wetting cycles has been successfully obtained in this study. Simultaneously, to investigate the potential use of resistivity method for quantifying and monitoring the long-term changes of soil geotechnical properties under drying-wetting cycles, the proxy relationship between resistivity and water content in multi-scale laboratory experiments has been investigated in this study, since the water content is closely related to the geophysical properties (e.g. resistivity and permittivity), and can be used as a good proxy parameter for soil to bridge the geophysical and other geotechnical properties.

To achieve these purposes, this study investigated the interrelationships between soil geotechnical and geophysical properties by outlining the relationships between soil resistivity, water content, suction and undrained shear strength on samples of various sizes and soil types using different testing techniques through three phases of laboratory testing programmes. Samples tested were also subjected to repeated drying and wetting cycles to investigate the effects of changing climate and weather-driven soil fabric

deterioration on soil property relationships. A summary of the conclusions drawn from each subject of the results and discussions is given in the following sections.

- **Soil water retention behaviour of engineered clay materials under drying and wetting cycles has been investigated** through laboratory experiments in this study. The soil water retention curves have been determined for different types of clay material over a wide suction range under multiple cycles of drying and wetting. Particularly, for the glacial till material, of which the SWRCs have been determined for different sample sizes and using different techniques. In the box lysimeter test, soil suction and water content were determined using MPS sensors and water content point sensors, respectively; in the small-scale triaxial sample experiment, the combination of tensiometer and chilled-mirror techniques allowed the SWRCs to be determined for glacial till in an entire water content range from saturation to the residual water content under repeated drying and wetting; and in the large cylindrical lysimeter test, the SWRCs were obtained by tensiometers and TDR probes. The hysteretic soil water retention behaviour was observed in the first and the subsequent drying and wetting cycles for three different types of soils, indicating different SWR behaviour during drying and wetting that the suction value at a given water content on the drying path is higher than that on the wetting path. The SWRC data determined from different laboratory scales associated with different sample sizes shows close agreement in the first drying and wetting cycle, as shown in Figure 4.58. The slight differences between the wetting curves of different experiments were attributed to the different wetting rates and different measurement techniques applied during wetting process, or it may be explained that the drying curves in the box and in the cylindrical lysimeters present a scanning curve, and the drying curve of the small samples represents more closely to a primary drying curve due to the different drying-wetting history. The degree of hysteresis of the SWRCs were found more pronounced in the low suction range than in the high suction range, which could be explained by different mechanisms controlling the water retention behaviour in the low suction and high suction ranges. The hysteresis of SWRC has been observed to be most significant in the first cycle of drying and wetting, and the degree of hysteresis decreases over cycling, with the largest decrease occurring between the first and second cycles. This could be explained as being

related to the reconstruction of microstructure and the volumetric changes of the clay material driven by repeated swelling and shrinking during the drying-wetting cycling. These changes in soil microstructure and volumetric behaviour lead to changes in the pore size distribution and the development of cracks (Hen-Jones, 2018; Azizi et al., 2020; Stirling et al., 2020), and thus a reduction in the degree of hysteresis, with the main changes occurring during the first drying-wetting cycle. The SWRCs for clays changes progressively over time under repeated drying and wetting cycles, evolving into curves with decreasing suctions as the number of drying-wetting cycles increases. This evolution indicates a progressive loss in soil suction at a given water content over cycling due to soil fabric deterioration. The degree of deterioration in soil suction observed from SWRCs is not consistent over cycling and is most significant after the first cycle.

- **Mechanical behaviour of unsaturated clay materials under successive drying and wetting cycles has been investigated in this study through laboratory experiments.** The undrained shear strength was measured using unconsolidated undrained triaxial test for three types of engineered clay materials subjected to multiple cycles of drying and wetting. Characteristic curves of undrained shear strength against water content have been obtained to study the mechanical behaviour of unsaturated clays under drying-wetting cycles. Results have shown that shear strength-water content relationship evolves over time under drying-wetting cycles. A hysteresis was found between the drying and wetting curves, suggesting that for a given water content, the shear strength on the drying path is higher than that on the wetting path. Hysteresis of shear strength characteristic curves was found to be most pronounced in the first drying-wetting cycle and decreased with cycling. It has also been found that the relationship between soil shear strength and water content changed over drying-wetting cycling, showing a loss in soil shear strength at a given water content with increasing number of cycles, with the greatest loss occurring at between the first cycle and the second cycle. These are in consistent with the tendencies that have been found for the SWRCs, indicating that the shear strength behaviour of unsaturated soils is closely related to and controlled by the SWRC. The deterioration in suction driven by the drying-wetting cycles affects the suction-induced shear strength, resulting in progressive deterioration in soil shear strength. Additionally, it was also found in

this study that the relationship between undrained shear strength and suction varies with drying-wetting cycles, suggesting that the shear strength at a given suction reduced with increasing number of drying-wetting cycles, as shown in Figure 4.28. This is thought to be due to the volumetric changes and the development of micro-cracks in the clay during drying and wetting cycles, which becomes another mechanism driving the deterioration in soil shear strength, independent of SWR behaviour.

- In this study, an improved understanding of the soil deterioration driven by the changing climate has been established by investigating the soil water retention behaviour and shear strength behaviour of three clay materials under repeated drying and wetting cycles, as concluded in above. Soil deterioration describes a progressive reconstruction and reorientation of clay fabric and aggregates associated with the volumetric changes and development of microcracks due to the repeated processes of swelling and shrinkage driven by successive moisture cycles. This progressive deterioration in soil fabric and microstructure affects the pore size distribution and thus the soil water retention behaviour, reducing the ability of soil to maintain suction at a given water content with increasing number of drying-wetting cycles. The deterioration in soil suction further influences the soil's mechanical behaviour and leads to a reduction in soil shear strength over drying-wetting cycles. Soil fabric deterioration also directly results in decreases in shear strength independent of suction behaviour due to the development of micro-cracks and larger pores. The soil fabric deterioration results in higher values of resistivity due to cracking. The aging effect of the fabric deterioration on soil property relationships under drying-wetting cycles was found to be more pronounced during the first cycle and decreases as the number of drying-wetting cycles increases. This is likely because the reconstruction of soil microstructure is the most pronounced in the first drying-wetting cycle, decreasing in subsequent cycles and eventually reaching equilibrium after several cycles. The implication of this improved understanding of soil deterioration driven by drying and wetting cycles is to take the evolvement of geotechnical properties into account when assessing the long-term stability of engineered slopes and other infrastructures affected by the seasonally changed climate.

- Point sensors were used in this study as alternative techniques to determine the soil geotechnical and electromagnetic properties in laboratory for investigating the soil property inner-relationships. In box lysimeter experiments, MPS series sensors and tensiometer were employed to measure matric suction of soil sample under cyclic drying and wetting. The MPS-1, MPS-2 and MPS-6 sensor fit well with the tensiometer readings in the suction range of 0 to 300 kPa, only MPS-2 sensor showed a good agreement with tensiometer reading in the suction range over 300 kPa until the tensiometer was cavitated at 1200 kPa. The MPS sensors are sometimes not reliable in the high suction range due to the limitation of factory calibration in high suction range and the contact issues caused by shrinkage of clay during drying. The water content sensors were used in this study to monitor volumetric water content changes of soil sample during drying-wetting cycles. The soil-specific calibration of the water content sensors was performed in this study. The results show that the calibration lines for different sensors are different and deviate from the empirical calibration curve (i.e. the Topp model), indicating the use of empirical calibration can lead to over- or underestimation of volumetric water content. This is likely due to the influences of density and solution conductivity on the permittivity measurement. A soil-specific calibration of point sensors on the desired testing range is necessary for ensuring the accuracy of water content measurements during drying and wetting. It was also found the point sensor overestimates soil resistivity because it uses a two-point method. In addition, the performance of the point sensors relies on good contact between the sensor prongs/head and the surrounding soils. Data indicated that the sensors in poor contact with soil overestimate resistivity and underestimate VWC. This is due to the air gaps introduced between the sensor and the soil, with extreme low permittivity and high resistivity.

- The proxy relationships between soil electrical resistivity (ER) and water content were established for different types of soil from different scales of laboratory testing. The proxy relationships changed over time with the drying-wetting cycling, and the trends of this evolution in the ER-water content relationship do not remain consistent between the drying and wetting paths or the different cycles,

since the resistivity characteristics are affected by multiple factors. In the box lysimeter test, clear hysteresis was found between the drying and wetting curves of the ER-water content relationship determined by point sensors, demonstrating that the resistivity of the wetting path is higher in the low water content range, and is lower in the high water content range than that of the drying path. Whereas in the triaxial sample experiment, little hysteresis could be observed between drying and wetting path and showed a constantly lower resistivity on the wetting path than that on the drying path. These differences in hysteresis of resistivity characteristic curves are likely due to the different saturation history, different measurement techniques are used, and the microstructure changes of soil sample during drying and wetting associated with the development of micro-scale fractures. Hysteresis in resistivity-water content/Sr relationships was also found over drying and wetting cycles. Generally, the resistivity for a given water content or degree of saturation on the subsequent drying-wetting cycles has a higher value than that of the first drying-wetting cycle due to the development of micro-cracks. Additionally, the proxy relationship between soil resistivity and water content is also controlled by the volumetric changes of soils because of the swelling and shrinkage driven by repeated drying-wetting cycles, since higher dry density/lower void ratio results in a lower resistivity response for the soil of a given water content or degree of saturation.

- To investigate the use of resistivity methods in quantifying and monitoring the property changes of engineered soil subjected to drying and wetting cycles, a 64-elecrode ERT system was used in a 1.2m diameter cylindrical lysimeter to measure the spatial resistivity information of soil sample during the drying-wetting cycles. The time-lapse 3D ERT data was successfully obtained to quantify and map the continuous changes in resistivity distributions within the large lysimeter sample, which represents a large-scale laboratory test. The TDR network was also employed in this study for providing reference measurements of soil VWC and resistivity. The ERT derived resistivity data were in good agreement with the point sensor results in qualitatively describing the relative changes in the spatial resistivity distribution of soil sample with changing water content, indicating a decrease with increasing VWC and an increase with decreasing VWC. The ERT data have also been successfully used to provide

quantitative assessment of the moisture dynamics in the large-scale laboratory test with applying the proxy relationship established through the small-scale laboratory test. The ERT-derived resistivity data matched well with the inferred resistivity data that converted from the VWC results of TDR, whereas it showed large deviations from the resistivity data that directly measured by TDR. This indicate the ERT data is capable for estimating the VWC of soil in long-term monitoring. The difference between ERT and TDR data may be because ERT uses four-point method and TDR uses two-point method. According to the literature, the two-point measurement over-estimate resistivity values. Furthermore, the ERT method can detect the development of cracks, which are shown as anomalies with high resistivity in the ERT inversion models. The anomalies such that caused by cracking can mislead the interpretation of the inverted resistivity data so that it is important to accurately define any anomalies within the ERT model.

6.2 Recommendations for future work

- **Small-scale laboratory testing**

Future research could apply the methodologies of this study to other essential clay materials. Stiffness, permeability, shear strength parameters and other important geotechnical properties of soil should be added into this evaluation for a more thorough analysis of the evolution of soil property relationships under repeated moisture cycling. A scanning electron microscope (SEM) or X-ray scanning technique could be employed to directly observe the mechanism of soil fabric evolution during the successive processes of drying and wetting. Further drying and wetting cycles should also be applied to testing soils in future work to obtain a deeper understanding of soil fabric deterioration and its long-term impact on the behaviour of soil geotechnical properties. In establishing the comprehensive soil property relationships, a long-term deterioration model for soil material can be developed to be used in the monitoring and assessment of slope stability.

- **Lysimeter testing**

With the first cycle of drying and wetting finished for the large lysimeter testing, subsequent drying-wetting cycles can be continued as it was before but ideally with a

suite of reliable tensiometers installed on as many ports as possible to fully capture the SWR behaviour for the lysimeter sample. The ERT array used in the lysimeter testing should also be extended to achieve full coverage of the lysimeter sample to aid the sensitivity of the ERT array for the bottom layers.

A scaled-down version of the lysimeter with an apparent wall and denser ERT array may be interesting in future work as it would allow for the development of cracks to be observed more directly from both the top and the lateral surfaces of the soil sample, and the ERT images would be produced in a higher resolution. Such an approach would also drive the drying-wetting cycles to be more rapid, thereby providing faster quantitative assessments for the other essential source materials that create unstable slopes in the UK, such as the London Clay Formation, Lisa Group and Gault Formation.

- **ERT system in field testing**

A comprehensive laboratory testing programme was conducted in this study to investigate and validate the potential uses of electrical resistivity methods in evaluating the geotechnical behaviour of compacted clays. The results of this study clearly prove that ERT methods can be used as a strong water indicator to quantitively assess the moisture dynamics of soils under drying and wetting cycles in a large-scale laboratory test. Future work should focus on how to extend this use to a field test, in conjunction with the development of the deterioration model, to provide more efficient assessments of slope stability.

References

Agus, S. and Schanz, T., 2006. Drying, wetting, and suction characteristic curves of a bentonite-sand mixture, Unsaturated Soils 2006, pp. 1405-1414.

Aitchison, G.D., 1961. Relationships of moisture stress and effective stress functions in unsaturated soils, Pore pressure and suction in soils: conference organised by the British National Society of the International Society of Soil Mechanics and Foundation Engineering. Butterworths, pp. 47-52.

Aizebeokhai, A.P., 2010. 2D and 3D geoelectrical resistivity imaging: Theory and field design. Scientific Research and Essays, 5(23): 3592-3605.

Al-Homoud, A., Basma, A., Husein Malkawi, A. and Al Bashabsheh, M., 1995. Cyclic swelling behavior of clays. Journal of geotechnical engineering, 121(7): 562-565.

Al-Mahbashi, A.M., Elkady, T.Y. and Al-Shamrani, M.A., 2018. Hysteresis soil-water characteristic curves of highly expansive clay. European Journal of Environmental and Civil Engineering, 22(9): 1041-1059.

Antonio-Carpio, R., Perez-Flores, M., Camargo-Guzman, D. and Alanis-Alcantar, A., 2004. Use of resistivity measurements to detect urban caves in Mexico City and to assess the related hazard. Natural Hazards and Earth system science, 4(4): 541-547.

Asquith, J., 2015. Use of Large Lysimeters to Monitor Unsaturated Hydraulic Properties of Amended Soils, Durham University.

ASTM, 2001. Standard Test Method for Field Measurement of Soil Resistivity Using the Wenner Four-Electrode Method, G57-95A. ASTM International, West Conshohocken, PA.

ASTM, 2005. Standard test method for measurement of soil resistivity using the two-electrode soil box method, G187–05. American Society for Testing and Materials.

Azizi, A., Musso, G. and Jommi, C., 2020. Effects of repeated hydraulic loads on microstructure and hydraulic behaviour of a compacted clayey silt. Canadian Geotechnical Journal, 57(1): 100-114.

Baker, J. and Allmaras, R., 1990. System for automating and multiplexing soil moisture measurement by time-domain reflectometry. Soil Science Society of America Journal, 54(1): 1-6.

Bao, C.G., Gong, B.-w. and Zhan, L.-t., 1998. Properties of unsaturated soils and slope stability of expansive soils, Keynote Lecture, Proceedings of the 2nd International Conference on Unsaturated Soils (UNSAT 98). Beijing, China, pp. 71-98.

Basma, A.A., Al-Homoud, A.S., Malkawi, A.I.H. and Al-Bashabsheh, M.A., 1996. Swelling-shrinkage behavior of natural expansive clays. Applied Clay Science, 11(2-4): 211-227.

Beck, Y.-L., Lopes, S.P., Ferber, V. and Côte, P., 2011. Microstructural interpretation of water content and dry density influence on the DC-electrical resistivity of a fine-grained soil. Geotechnical Testing Journal, 34(6): 694-707.

Bichler, A., Bobrowsky, P., Best, M., Douma, M., Hunter, J., Calvert, T. and Burns, R., 2004. Three-dimensional mapping of a landslide using a multi-geophysical approach: the Quesnel Forks landslide. Landslides, 1(1): 29-40.

Bishop, A.W., 1959. The principle of effective stress. Tecknisk Ukeblnd, 106(39): 859-863.

Bishop, A.W. and Blight, G., 1963. Some aspects of effective stress in saturated and partly saturated soils. Geotechnique, 13(3): 177-197.

Blonquist, J., Jones, S.B. and Robinson, D., 2005. Standardizing characterization of electromagnetic water content sensors. Vadose Zone Journal, 4(4): 1059-1069.
Brooks, R. and Corey, T., 1964. Hydraulic properties of porous media. Hydrology Papers, Colorado State University, 24: 37.
Bryson, L.S., 2005. Evaluation of geotechnical parameters using electrical resistivity measurements, Earthquake Engineering and Soil Dynamics, pp. 1-12.
BSI, 1990a. BS 1377-2:1990. Methods of test for soils for civil engineering purposes. Classification tests. BSI, London.
BSI, 1990b. BS 1377-3: 1990. Methods of test for soils for civil engineering purposes (chemical and electro-chemical tests). BSI London, UK.
BSI, 1990c. BS 1377-4: 1990. Methods of test for soils for civil engineering purposes. Compaction-related tests. BSI London, UK.
BSI, 1990d. BS 1377-7:1990. Methods of test for soils for civil engineering purposes. Shear strength tests (total stress), London: British Standards Institution.
BSI, 1990e. BS 1377-8:1990. Methods of test for soils for civil engineering purposes. Shear strength tests (effective stress), London: British Standards Institution.
Bulut, R., Hineidi, S. and Bailey, B., 2002. Suction measurements—filter paper and chilled mirror psychrometer, Proceedings of the Texas Section American Society of Civil Engineers, Fall Meeting, Waco, pp. 2-5.
Bulut, R. and Leong, E.C., 2008. Indirect measurement of suction, Laboratory and Field Testing of Unsaturated Soils. Springer, pp. 21-32.
Cai, G.J., Liu, S.Y., Cheng, Y., Zou, H.F., Du, G.Y., Ren, B.B. and Puppala, A.J., 2013. In situ evaluation of relative density from piezocone penetration tests of clean sand from China, Geotechnical and Geophysical Site Characterization : Proceedings of the 4th International Conference on Site Characterization ISC-4. Boca Raton, pp. 207-211.
Campanella, R. and Weemees, I., 1990. Development and use of an electrical resistivity cone for groundwater contamination studies. Canadian Geotechnical Journal, 27(5): 557-567.
Campbell, G.S., 1974. A simple method for determining unsaturated conductivity from moisture retention data. Soil science, 117(6): 311-314.
Campbell, G.S. and Gardner, W.H., 1971. Psychrometric measurement of soil water potential: temperature and bulk density effects. Soil Science Society of America Journal, 35(1): 8-12.
Carbonel, D., Rodríguez, V., Gutiérrez, F., McCalpin, J.P., Linares, R., Roqué, C., Zarroca, M., Guerrero, J. and Sasowsky, I., 2014. Evaluation of trenching, ground penetrating radar (GPR) and electrical resistivity tomography (ERT) for sinkhole characterization. Earth Surface Processes and Landforms, 39(2): 214-227.
Carpentier, S., Konz, M., Fischer, R., Anagnostopoulos, G., Meusburger, K. and Schoeck, K., 2012. Geophysical imaging of shallow subsurface topography and its implication for shallow landslide susceptibility in the Urseren Valley, Switzerland. Journal of applied geophysics, 83: 46-56.
Castiglione, P. and Shouse, P., 2003. The effect of ohmic cable losses on time-domain reflectometry measurements of electrical conductivity. Soil Science Society of America Journal, 67(2): 414-424.
CCRA, 2012. Summary of the key findings from the UK Climate Change Risk Assessment. Department for Environment Food and Rural Affairs (DEFRA), London.
Chambers, J., Gunn, D., Wilkinson, P., Meldrum, P., Haslam, E., Holyoake, S., Kirkham, M., Kuras, O., Merritt, A. and Wragg, J., 2014. 4D electrical resistivity

tomography monitoring of soil moisture dynamics in an operational railway embankment. Near Surface Geophysics, 12(1): 61-72.
Chambers, J., Meldrum, P., Gunn, D., Wilkinson, P., Kuras, O., Weller, A. and Ogilvy, R., 2009. Hydrogeophysical monitoring of landslide processes using automated time-lapse electrical resistivity tomography (ALERT), Near Surface 2009-15th EAGE European Meeting of Environmental and Engineering Geophysics.
Chambers, J., Ogilvy, R., Kuras, O., Cripps, J. and Meldrum, P., 2002. 3D electrical imaging of known targets at a controlled environmental test site. Environmental Geology, 41(6): 690-704.
Chambers, J., Weller, A., Gunn, D., Kuras, O., Wilkinson, P., Meldrum, P., Ogilvy, R., Jenkins, G., Gibson, A. and Ford, S., 2008. Geophysical anatomy of the Hollin Hill Landslide, North Yorkshire, UK, Near Surface 2008-14th EAGE European Meeting of Environmental and Engineering Geophysics. European Association of Geoscientists & Engineers, pp. cp-64-00049.
Chambers, J., Wilkinson, P., Kuras, O., Ford, J., Gunn, D., Meldrum, P., Pennington, C., Weller, A., Hobbs, P. and Ogilvy, R., 2011. Three-dimensional geophysical anatomy of an active landslide in Lias Group mudrocks, Cleveland Basin, UK. Geomorphology, 125(4): 472-484.
Chambers, J., Wilkinson, P., Wardrop, D., Hameed, A., Hill, I., Jeffrey, C., Loke, M., Meldrum, P., Kuras, O. and Cave, M., 2012. Bedrock detection beneath river terrace deposits using three-dimensional electrical resistivity tomography. Geomorphology, 177: 17-25.
Chen, R., Xu, T., Lei, W., Zhao, Y. and Qiao, J., 2018. Impact of multiple drying–wetting cycles on shear behaviour of an unsaturated compacted clay. Environmental Earth Sciences, 77(19): 1-9.
Chiu, C., Cui, Y., Delage, P., De Laure, E., Haza, E., Tarantino, A. and Romero, E., 2005. Lessons learnt from suction monitoring during centrifuge modeling, Proceedings of the international symposium on advanced experimental unsaturated soils mechanics EXPERUS, Trento, Balkema, pp. 3-8.
Clapp, R.B. and Hornberger, G.M., 1978. Empirical equations for some soil hydraulic properties. Water resources research, 14(4): 601-604.
Clarke, D. and Smethurst, J., 2010. Effects of climate change on cycles of wetting and drying in engineered clay slopes in England. Quarterly Journal of Engineering Geology and Hydrogeology, 43(4): 473-486.
Cosenza, P., Marmet, E., Rejiba, F., Cui, Y.J., Tabbagh, A. and Charlery, Y., 2006. Correlations between geotechnical and electrical data: A case study at Garchy in France. Journal of Applied Geophysics, 60(3-4): 165-178.
Croney, D., 1952. The movement and distribution of water in soils. Géotechnique, 3(1): 1-16.
Croney, D. and Coleman, J., 1961. Pore pressure and suction in soil, Pore Pressure & Suction In Soils Conf, Butterworth, London, UK, pp. 31-37.
Croney, D., Coleman, J. and Black, W., 1958. Movement and distribution of water in soil in relation to highway design and performance. Highway Research Board Special Report(40).
Curioni, G., 2013. Investigating the seasonal variability of electromagnetic soil properties using field monitoring data from Time-Domain Reflectometry probes, University of Birmingham.
Dahlin, T. and Zhou, B., 2004. A numerical comparison of 2D resistivity imaging with 10 electrode arrays. Geophysical Prospecting, 52(5): 379-398.

Daily, W., Ramirez, A., Binley, A. and LeBrecque, D., 2004. Electrical resistance tomography. The Leading Edge, 23(5): 438-442.
Dalton, F., Herkelrath, W., Rawlins, D. and Rhoades, J., 1984. Time-domain reflectometry: Simultaneous measurement of soil water content and electrical conductivity with a single probe. Science, 224(4652): 989-990.
Dasberg, S. and Dalton, F., 1985. Time domain reflectometry field measurements of soil water content and electrical conductivity. Soil Science Society of America Journal, 49(2): 293-297.
Davies, M.P. and Campanella, R.G., 1995. Piezocone technology: downhole geophysics for the geoenvironmental characterization of soil, Symposium on the Application of Geophysics to Engineering and Environmental Problems 1995. Society of Exploration Geophysicists, pp. 171-180.
Day, R.W., 1994. Swell-shrink behavior of compacted clay. Journal of geotechnical engineering, 120(3): 618-623.
Dean, T., Bell, J. and Baty, A., 1987. Soil moisture measurement by an improved capacitance technique, Part I. Sensor design and performance. Journal of Hydrology, 93(1-2): 67-78.
Decagon, 2009. MPS-1 Dielectric Water Potential Sensors Operator's Manual. Decagon Devices, Inc., Pullman, WA.
Decagon, 2010. 5TE, water content, EC and temperature sensors: Operator's manual, version 6. Decagon Devices, Pullman, WA.
Decagon, 2016. MPS-2 & MPS-6 dielectric water potential sensors operator's manual. Decagon Devices, Pullman, WA.
Dehn, M., Bürger, G., Buma, J. and Gasparetto, P., 2000. Impact of climate change on slope stability using expanded downscaling. Engineering Geology, 55(3): 193-204.
Delage, P., 1987. Unnouvel appareil triaxial pour les sols non satures, 9th Eur. Conf. of Soil Mechanics, pp. 26-28.
Delage, P., Romero, E. and Tarantino, A., 2008. Recent developments in the techniques of controlling and measuring suction in unsaturated soils, Unsaturated Soils. Advances in Geo-Engineering. CRC Press, pp. 44-63.
Demoulin, A., Pissart, A. and Schroeder, C., 2003. On the origin of late Quaternary palaeolandslides in the Liège (E Belgium) area. International journal of earth sciences, 92(5): 795-805.
Di Maio, R. and Piegari, E., 2012. A study of the stability analysis of pyroclastic covers based on electrical resistivity measurements. Journal of Geophysics and Engineering, 9(2): 191-200.
Dijkstra, T. and Dixon, N., 2010. Climate change and slope stability in the UK: challenges and approaches. Quarterly Journal of Engineering Geology and Hydrogeology, 43(4): 371-385.
Dobecki, T.L. and Upchurch, S.B., 2006. Geophysical applications to detect sinkholes and ground subsidence. The Leading Edge, 25(3): 336-341.
Drahor, M.G., Göktürkler, G., Berge, M.A. and Kurtulmuş, T.Ö., 2006. Application of electrical resistivity tomography technique for investigation of landslides: a case from Turkey. Environmental Geology, 50(2): 147-155.
Drungil, C., Abt, K. and Gish, T., 1989. Soil Moisture Determination in Gravelly Soils with Time Domain Reflectometryd. Transactions of the ASAE, 32(1): 177-0180.
Edlefsen, N. and Anderson, A., 1943. Thermodynamics of soil moisture. Hilgardia, 15(2): 31-298.

Edwards, L., 1977. A modified pseudosection for resistivity and IP. Geophysics, 42(5): 1020-1036.
Escario, V. and S´ez, J., 1987. Discussion: The shear strength of partly saturated soils. Géotechnique, 37(4): 523-524.
Estabragh, A., Parsaei, B. and Javadi, A., 2015. Laboratory investigation of the effect of cyclic wetting and drying on the behaviour of an expansive soil. Soils and foundations, 55(2): 304-314.
Evett, S., Heng, L., Moutonnet, P. and Nguyen, M., 2008. Field estimation of soil water content: A practical guide to methods, instrumentation, and sensor technology. IAEA: Vienna.
Evett, S.R., Howell, T.A., Steiner, J.L. and Cresap, J.L., 1993. Evapotranspiration by soil water balance using TDR and neutron scattering. Management of Irrigation and Drainage Systems, Irrigation and Drainage Div./ASCE: 914-921.
Foster, C., Jenkins, G.O. and Gibson, A., 2007. Landslides and mass movement processes and their distribution in the York District (Sheet 63).
Fredlund, D., Morgenstern, N.R. and Widger, R., 1978. The shear strength of unsaturated soils. Canadian geotechnical journal, 15(3): 313-321.
Fredlund, D., Rahardjo, H. and Gan, J., 1987. Non-linearity of strength envelope for unsaturated soils, Proc. 6th Int. Conf. Expansive Soils, New Delhi, pp. 49-54.
Fredlund, D.G., 1973. Volume change behavior of unsaturated soils, University of Alberta.
Fredlund, D.G., 2006. Unsaturated soil mechanics in engineering practice. Journal of geotechnical and geoenvironmental engineering, 132(3): 286-321.
Fredlund, D.G. and Morgenstern, N.R., 1977. Stress state variables for unsaturated soils. Journal of Geotechnical and Geoenvironmental Engineering, 103(ASCE 12919).
Fredlund, D.G. and Rahardjo, H., 1993. Soil mechanics for unsaturated soils. John Wiley & Sons.
Fredlund, D.G. and Xing, A., 1994. Equations for the soil-water characteristic curve. Canadian geotechnical journal, 31(4): 521-532.
Fredlund, D.G., Xing, A., Fredlund, M.D. and Barbour, S., 1996. The relationship of the unsaturated soil shear strength to the soil-water characteristic curve. Canadian geotechnical journal, 33(3): 440-448.
Friedel, S., Thielen, A. and Springman, S.M., 2006. Investigation of a slope endangered by rainfall-induced landslides using 3D resistivity tomography and geotechnical testing. Journal of Applied Geophysics, 60(2): 100-114.
Friedman, S.P., 2005. Soil properties influencing apparent electrical conductivity: a review. Computers and electronics in agriculture, 46(1-3): 45-70.
Gallipoli, M., Lapenna, V., Lorenzo, P., Mucciarelli, M., Perrone, A., Piscitelli, S. and Sdao, F., 2000. Comparison of geological and geophysical prospecting techniques in the study of a landslide in southern Italy. European Journal of Environmental and Engineering Geophysics, 4: 117-128.
Gambetta, M., Armadillo, E., Carmisciano, C., Stefanelli, P., Cocchi, L. and Tontini, F.C., 2011. Determining geophysical properties of a near-surface cave through integrated microgravity vertical gradient and electrical resistivity tomography measurements. Journal of cave and karst studies, 73(1): 11-15.
Gardner, W., 1956. Calculation of Capillary Conductivity from Pressure Plate Outflow Data 1. Soil Science Society of America Journal, 20(3): 317-320.
Gariano, S.L. and Guzzetti, F., 2016. Landslides in a changing climate. Earth-Science Reviews, 162: 227-252.

Garven, E. and Vanapalli, S.K., 2006. Evaluation of empirical procedures for predicting the shear strength of unsaturated soils, Proceedings of the Fourth International Conference on Unsaturated Soils 2006, pp. 2570-2592.

Gee, G., Campbell, M., Campbell, G.S. and Campbell, J., 1992. Rapid measurement of low soil water potentials using a water activity meter. Soil Science Society of America Journal, 56(4): 1068-1070.

Giese, K. and Tiemann, R., 1975. Determination of the complex permittivity from thin-sample time domain reflectometry improved analysis of the step response waveform. Advances in Molecular Relaxation Processes, 7(1): 45-59.

Glendinning, S., Helm, P., Rouainia, M., Stirling, R., Asquith, J., Hughes, P., Toll, D., Clarke, D., Hudson, A. and Powrie, W., 2018. Infrastructure Slopes: Sustainable Management And Resilience Assessment: iSMART Final report.

Glendinning, S., Helm, P., Rouainia, M., Stirling, R., Asquith, J., Hughes, P., Toll, D., Clarke, D., Powrie, W. and Smethurst, J., 2015. informed design, management and maintenance of infrastructure slopes: development of a multi-scalar approach, IOP Conference Series: Earth and Environmental Science. IOP Publishing, pp. 012005.

Godio, A. and Bottino, G., 2001. Electrical and electromagnetic investigation for landslide characterisation. Physics and Chemistry of the Earth, Part C: Solar, Terrestrial & Planetary Science, 26(9): 705-710.

Godio, A., Strobbia, C. and De Bacco, G., 2006. Geophysical characterisation of a rockslide in an alpine region. Engineering geology, 83(1-3): 273-286.

Goh, S., Rahardjo, H. and Leong, E., 2014. Shear strength of unsaturated soils under multiple drying-wetting cycles. Journal of Geotechnical and Geoenvironmental Engineering, 140(2): 06013001.

Grantz, D., 1990. Plant response to atmospheric humidity. Plant, Cell & Environment, 13(7): 667-679.

Guan, G.S., Rahardjo, H. and Choon, L.E., 2009. Shear strength equations for unsaturated soil under drying and wetting. Journal of Geotechnical and Geoenvironmental Engineering, 136(4): 594-606.

Guan, Y. and Fredlund, D., 1997. Use of the tensile strength of water for the direct measurement of high soil suction. Canadian Geotechnical Journal, 34(4): 604-614.

Gunn, D., Chambers, J., Dashwood, B., Lacinska, A., Dijkstra, T., Uhlemann, S., Swift, R., Kirkham, M., Milodowski, A. and Wragg, J., 2018. Deterioration model and condition monitoring of aged railway embankment using non-invasive geophysics. Construction and Building Materials, 170: 668-678.

Gunn, D. and Ogilvy, R., 2010. Alert-me: new technologies for embankment warning systems. Rail Technology Magazine.

Gunn, D.A., Chambers, J.E., Uhlemann, S., Wilkinson, P.B., Meldrum, P.I., Dijkstra, T.A., Haslam, E., Kirkham, M., Wragg, J., Holyoake, S., Hughes, P.N., Hen-Jones, R. and Glendinning, S., 2015. Moisture monitoring in clay embankments using electrical resistivity tomography. Construction and Building Materials, 92: 82-94.

Gunn, D.A., Ogilvy, R., Chambers, J., Meldrum, P., Haslam, E., Holyoake, S. and Wragg, J., 2010. The first trials of the British Geological Survey's new ALERT-ME system for monitoring embankments using resistivity imaging have thrown up some fascinating results. Ground Engineering, Sept 2010: 12-14.

Gupta, S.C. and Hanks, R., 1972. Influence of water content on electrical conductivity of the soil 1. Soil Science Society of America Journal, 36(6): 855-857.

Habberjam, G.M. and Watkins, G.E., 1967. The Use of a Square Configuration in Resistivity Prospecting *. Geophysical Prospecting, 15(3): 445-467.

Haines, W.B., 1927. Studies in the physical properties of soils: IV. A further contribution to the theory of capillary phenomena in soil. The Journal of Agricultural Science, 17(2): 264-290.

Hallof, P., 1957. On the interpretation of resistivity and induced polarization measurements. PhD thes is, MIT.

Hassan, A., Ahmed, 2014. Electrical Resistivity Method for Water Content Characterisation of Unsaturated Clay Soil, Durham University.

Hauck, C., Vonder Mühll, D. and Maurer, H., 2003. Using DC resistivity tomography to detect and characterize mountain permafrost. Geophysical prospecting, 51(4): 273-284.

He, H., Dyck, M., Zhao, Y., Si, B., Jin, H., Zhang, T., Lv, J. and Wang, J., 2016. Evaluation of five composite dielectric mixing models for understanding relationships between effective permittivity and unfrozen water content. Cold Regions Science and Technology, 130: 33-42.

Heimovaara, T., 1993. Design of triple-wire time domain reflectometry probes in practice and theory. Soil Science Society of America Journal, 57(6): 1410-1417.

Heimovaara, T. and Bouten, W., 1990. A computer-controlled 36-channel time domain reflectometry system for monitoring soil water contents. Water Resources Research, 26(10): 2311-2316.

Heimovaara, T., Focke, A., Bouten, W. and Verstraten, J., 1995. Assessing temporal variations in soil water composition with time domain reflectometry. Soil Science Society of America Journal, 59(3): 689-698.

Heincke, B., Günther, T., Dalsegg, E., Rønning, J.S., Ganerød, G.V. and Elvebakk, H., 2010. Combined three-dimensional electric and seismic tomography study on the Åknes rockslide in western Norway. Journal of Applied Geophysics, 70(4): 292-306.

Hen-Jones, R., Hughes, P., Stirling, R., Glendinning, S., Chambers, J., Gunn, D. and Cui, Y., 2017. Seasonal effects on geophysical–geotechnical relationships and their implications for electrical resistivity tomography monitoring of slopes. Acta Geotechnica, 12(5): 1159-1173.

Hen-Jones, R.M., 2018. Quantitative electrical imaging of slope moisture dynamics, Newcastle University.

Hen-Jones, R.M., Hughes, P.N., Glendinning, S., Gunn, D.A., Chambers, J.C., Wilkinson, P.B. and Uhlemann, S., 2014. Determination of moisture content and soil suction in engineered fills using electrical resistivity. Unsaturated Soils: Research & Applications, Vols 1 and 2: 1695-1699.

Herkelrath, W., Hamburg, S. and Murphy, F., 1991. Automatic, real-time monitoring of soil moisture in a remote field area with time domain reflectometry. Water Resources Research, 27(5): 857-864.

Hesse, A., Jolivet, A. and Tabbagh, A., 1986. New prospects in shallow depth electrical surveying for archaeological and pedological applications. Geophysics, 51(3): 585-594.

Hibert, C., Grandjean, G., Bitri, A., Travelletti, J. and Malet, J.-P., 2012. Characterizing landslides through geophysical data fusion: Example of the La Valette landslide (France). Engineering Geology, 128: 23-29.

Hilbich, C., Fuss, C. and Hauck, C., 2011. Automated time-lapse ERT for improved process analysis and monitoring of frozen ground. Permafrost and Periglacial Processes, 22(4): 306-319.

Hirsch, M., Bentley, L.R. and Dietrich, P., 2008. A comparison of electrical resistivity, ground penetrating radar and seismic refraction results at a river terrace site. Journal of Environmental & Engineering Geophysics, 13(4): 325-333.
Hobbs, P., Hallam, J., Forster, A., Entwisle, D., Jones, L., Cripps, A., Northmore, K., Self, S. and Meakin, J., 2002. Engineering geology of British rocks and soils: mudstones of the Mercia Mudstone Group. British Geological Survey.
Hsu, H.-L., Yanites, B.J., Chen, C.-c. and Chen, Y.-G., 2010. Bedrock detection using 2D electrical resistivity imaging along the Peikang River, central Taiwan. Geomorphology, 114(3): 406-414.
Huggel, C., Clague, J.J. and Korup, O., 2012. Is climate change responsible for changing landslide activity in high mountains? Earth Surface Processes and Landforms, 37(1): 77-91.
Hughes, P., Glendinning, S., Mendes, J., Parkin, G., Toll, D., Gallipoli, D. and Miller, P., 2009. Full-scale testing to assess climate effects on embankments, Proceedings of the Institution of Civil Engineers-Engineering Sustainability. Thomas Telford Ltd, pp. 67-79.
Huisman, J. and Bouten, W., 1999. Comparison of calibration and direct measurement of cable and probe properties in time domain reflectometry. Soil Science Society of America Journal, 63(6): 1615-1617.
Huisman, J., Lambot, S. and Vereecken, H., 2006. Determining soil water content variation along the TDR probe with inverse modelling: theory, practice and challenges. Proceedings of TDR.
Huisman, J.A., Hubbard, S.S., Redman, J.D. and Annan, A.P., 2003. Measuring soil water content with ground penetrating radar: A review. Vadose zone journal, 2(4): 476-491.
IPCC, 2014. Climate change 2013-the physical science basis: working group i contribution to the fifth assessment report of the intergovernmental panel on climate change. Cambridge University Press.
Izdebska-Mucha, D. and Wójcik, E., 2013. Testing shrinkage factors: comparison of methods and correlation with index properties of soils. Bulletin of Engineering Geology and the Environment, 72(1): 15-24.
Jacobsen, O.H. and Schjonning, P., 1995. Comparison of TDR calibration functions for soil water determination, Proceedings of the Symposium: Time-Domain Reflectometry Applications in Soil Science, pp. 25-33.
Jenkins, G. and Lowe, J., 2003. Handling uncertainties in the UKCIP02 scenarios of climate change. Met Office.
Jennings, J., 1961. A revised effective stress law for use in the prediction of the behaviour of unsaturated soils, Pore pressure and suction in soils, pp. 26-30.
Jennings, J.E.B. and Burland, J.B., 1962. Limitations to the use of effective stresses in partly saturated soils. Géotechnique, 12(2): 125-144.
Jones, S.B., Wraith, J.M. and Or, D., 2002. Time domain reflectometry measurement principles and applications. Hydrological processes, 16(1): 141-153.
Kammerer, G., Nolz, R., Rodny, M. and Loiskandl, W., 2014. Performance of Hydra Probe and MPS-1 soil water sensors in topsoil tested in lab and field. Journal of Water Resource and Protection, 6(13): 1207.
Kaufmann, G., 2014. Geophysical mapping of solution and collapse sinkholes. Journal of Applied Geophysics, 111: 271-288.
Kearey, P., Brooks, M. and Hill, I., 2002. An introduction to geophysical exploration, 4. John Wiley & Sons.

Keller, G., 1966. Dipole method for deep resistivity studles. Geophysics, 31(6): 1088-1104.
Keller, G.V., 2017. Electrical properties of rocks and minerals, Handbook of Physical Properties of Rocks (1982). CRC Press, pp. 217-294.
Kemp, S. and Wagner, D., 2006. The mineralogy, geochemistry and surface area of mudrocks from the London Clay Formation of southern England. British Geological Survey Internal Report, IR/06/060. 81pp.
Khalili, N. and Khabbaz, M., 1998. A unique relationship for χ for the determination of the shear strength of unsaturated soils. Geotechnique, 48(5): 681-687.
Kiessling, D., Schmidt-Hattenberger, C., Schuett, H., Schilling, F., Krueger, K., Schoebel, B., Danckwardt, E. and Kummerow, J., 2010. Geoelectrical methods for monitoring geological CO2 storage: First results from cross-hole and surface–downhole measurements from the CO2SINK test site at Ketzin (Germany). International Journal of Greenhouse Gas Control, 4(5): 816-826.
Kilsby, C., Glendinning, S., Hughes, P.N., Parkin, G. and Bransby, M., 2009. Climate-change impacts on long-term performance of slopes, Proceedings of the Institution of Civil Engineers-Engineering Sustainability. Thomas Telford Ltd, pp. 59-66.
Klute, A., 1986. Water retention: laboratory methods. Methods of soil analysis: part 1—physical and mineralogical methods(methodsofsoilan1): 635-662.
Koestel, J., Kemna, A., Javaux, M., Binley, A. and Vereecken, H., 2008. Quantitative imaging of solute transport in an unsaturated and undisturbed soil monolith with 3‐D ERT and TDR. Water resources research, 44(12).
Kong, L., Sayem, H.M. and Tian, H., 2018. Influence of drying–wetting cycles on soil-water characteristic curve of undisturbed granite residual soils and microstructure mechanism by nuclear magnetic resonance (NMR) spin-spin relaxation time (T 2) relaxometry. Canadian Geotechnical Journal, 55(2): 208-216.
Koorevaar, P., Menelik, G. and Dirksen, C., 1983. Elements of soil physics, 13. Elsevier, Amsterdam, The Netherlands.
LaBrecque, D.J., Miletto, M., Daily, W., Ramirez, A. and Owen, E., 1996. The effects of noise on Occam's inversion of resistivity tomography data. Geophysics, 61(2): 538-548.
LaBrecque, D.J. and Yang, X., 2001. Difference inversion of ERT data: A fast inversion method for 3-D in situ monitoring. Journal of Environmental & Engineering Geophysics, 6(2): 83-89.
Lane, P. and Mackenzie, D., 2001. Field and laboratory calibration and test of TDR and capacitance techniques for indirect measurement of soil water content. Soil Research, 39(6): 1371-1386.
Lapenna, V., Lorenzo, P., Perrone, A., Piscitelli, S., Sdao, F. and Rizzo, E., 2003. High-resolution geoelectrical tomographies in the study of Giarrossa landslide (southern Italy). Bulletin of Engineering Geology and the Environment, 62(3): 259-268.
Lee, C.C., Yang, C.H., Liu, H.C., Wen, K.L., Wang, Z.B. and Chen, Y.J., 2008. A Study of the hydrogeological environment of the lishan landslide area using resistivity image profiling and borehole data. Engineering Geology, 98(3-4): 115-125.
Lee, H. and Wray, W., 1995. Techniques to evaluate soil suction-a vital unsaturated soil water variable, Proceedings of the first international conference on unsaturated soils, Volume 2, Paris, France.

Leong, E.-C., Tripathy, S. and Rahardjo, H., 2003. Total suction measurement of unsaturated soils with a device using the chilled-mirror dew-point technique. Geotechnique, 53(2): 173-182.
Leong, E.C. and Rahardjo, H., 1997. Review of soil-water characteristic curve equations. Journal of geotechnical and geoenvironmental engineering, 123(12): 1106-1117.
Likos, W.J., Lu, N. and Godt, J.W., 2014. Hysteresis and uncertainty in soil water-retention curve parameters. Journal of Geotechnical and Geoenvironmental Engineering, 140(4): 04013050.
Lin, C.-P. and Tang, S.-H., 2007. Comprehensive wave propagation model to improve TDR interpretations for geotechnical applications. Geotechnical Testing Journal, 30(2): 90-97.
Loke, M., 2001. Tutorial: 2-D and 3-D Electrical Imaging Surveys.
Loke, M.H., 2004. Tutorial: 2-D and 3-D electrical imaging surveys. Birmingham, UK.
Loke, M.H., Chambers, J.E. and Kuras, O., 2011. Instrumentation, electrical resistivity. Encyclopedia of Solid Earth Geophysics: 599-604.
Lourenço, S., Gallipoli, D., Toll, D.G. and Evans, F.D., 2006. Development of a commercial tensiometer for triaxial testing of unsaturated soils. Geotechnical Special Publication, 147(2): 1875.
Lu, N. and Khorshidi, M., 2015. Mechanisms for soil-water retention and hysteresis at high suction range. Journal of Geotechnical and Geoenvironmental Engineering, 141(8): 04015032.
Mahler, C.a.F. and Diene, A.A., 2007. Tensiometer Development for High Suction Analysis in Laboratory Lysimeters. In: T. Schanz (Editor), Experimental Unsaturated Soil Mechanics. Springer Berlin Heidelberg, Berlin, Heidelberg, pp. 103-115.
Malicki, M., Plagge, R. and Roth, C., 1996. Improving the calibration of dielectric TDR soil moisture determination taking into account the solid soil. European Journal of Soil Science, 47(3): 357-366.
Malicki, M. and Walczak, R., 1999. Evaluating soil salinity status from bulk electrical conductivity and permittivity. European journal of soil science, 50(3): 505-514.
Matyas, E.L. and Radhakrishna, H., 1968. Volume change characteristics of partially saturated soils. Géotechnique, 18(4): 432-448.
McCann, I., Fraj, M. and Dakheel, A., 2013. Evaluation of the decagon® 5te sensor as a tool for irrigation and salinity management in a sandy soil, International Conference on Agricultural Engineering: New Technologies for Sustainable Agricultural Production and Food Security 1054, pp. 153-160.
McGillivray, P.R. and Oldenburg, D.W., 1990. Methods for calculating Fréchet derivatives and sensitivities for the non-linear inverse problem: a comparative study. Geophysical Prospecting, 38(5): 499-524.
McKee, C. and Bumb, A., 1984. The importance of unsaturated flow parameters in designing a monitoring system for hazardous wastes and environmental emergencies, Proceedings of the Hazardous Materials Control Research Institute, National Conference, pp. 50-58.
McKee, C. and Bumb, A., 1987. Flow-testing coalbed methane production wells in the presence of water and gas. SPE formation Evaluation, 2(04): 599-608.
Meilani, I., Rahardjo, H., Leong, E.-C. and Fredlund, D.G., 2002. Mini suction probe for matric suction measurements. Canadian Geotechnical Journal, 39(6): 1427-1432.
Mendes, J., 2011. Assessment of the impact of climate change on an instrumented embankment: an unsaturated soil mechanics approach, Durham University.

Meric, O., Garambois, S., Jongmans, D., Wathelet, M., Chatelain, J.-L. and Vengeon, J., 2005. Application of geophysical methods for the investigation of the large gravitational mass movement of Séchilienne, France. Canadian Geotechnical Journal, 42(4): 1105-1115.

Merritt, A., 2014. 4D geophysical monitoring of hydrogeological precursors to landslide activation. University of Leeds.

Mohr, O., 1900. Welche Umstände bedingen die Elastizitätsgrenze und den Bruch eines Materials. Zeitschrift des Vereins Deutscher Ingenieure, 46(1524-1530): 1572-1577.

Mualem, Y., 1984. A modified dependent-domain theory of hysteresis. Soil Science, 137(5): 283-291.

Mualem, Y., 1986. Hydraulic conductivity of unsaturated soils: prediction and formulas. Methods of Soil Analysis: Part 1 Physical and Mineralogical Methods, 5: 799-823.

Muñoz-Carpena, R., Shukla, S. and Morgan, K., 2004. Field devices for monitoring soil water content. University of Florida Cooperative Extension Service, Institute of Food and Agricultural Sciences, EDIS., pp. 1-24.

Munoz-Castelblanco, J., Pereira, J.-M., Delage, P. and Cui, Y.-J., 2011. The influence of changes in water content on the electrical resistivity of a natural unsaturated loess. Geotechnical Testing Journal, 35(1): 11-17.

Nadler, A., Dasberg, S. and Lapid, I., 1991. Time domain reflectometry measurements of water content and electrical conductivity of layered soil columns. Soil Science Society of America Journal, 55(4): 938-943.

Nakashima, M., Inoue, M., Sawada, K. and Nicholl, C., 1998. Measurement of soil water content by amplitude domain reflectometry method and its calibration. Journal of Groundwater Hydrology, 40(4): 509-519.

Naudet, V., Lazzari, M., Perrone, A., Loperte, A., Piscitelli, S. and Lapenna, V., 2008. Integrated geophysical and geomorphological approach to investigate the snowmelt-triggered landslide of Bosco Piccolo village (Basilicata, southern Italy). Engineering Geology, 98(3-4): 156-167.

Nishimura, S., 2006. Laboratory study on anisotropy of natural London Clay, Imperial College London (University of London).

Nolz, R. and Kammerer, G., 2017. Evaluating a sensor setup with respect to near-surface soil water monitoring and determination of in-situ water retention functions. Journal of hydrology, 549: 301-312.

Öberg, A. and Sällfors, G., 1997. Determination of shear strength parameters of unsaturated silts and sands based on the water retention curve. Geotechnical Testing Journal, 20(1): 40-48.

Ogusnsuyi, O., 2010. Geophysical characterization of Peace River landslide. University of Alberta, Canada, MS Thesis.

Or, D. and Tuller, M., 1999. Liquid retention and interfacial area in variably saturated porous media: Upscaling from single - pore to sample - scale model. Water Resources Research, 35(12): 3591-3605.

Pan, H., Qing, Y. and Pei-yong, L., 2010. Direct and indirect measurement of soil suction in the laboratory. Electronic Journal of Geotechnical Engineering, 15(3): 1-14.

Pánek, T., Šilhán, K., Tábořík, P., Hradecký, J., Smolková, V., Lenart, J., Brázdil, R., Kašičková, L. and Pazdur, A., 2011. Catastrophic slope failure and its origins: Case of the May 2010 Girová Mountain long-runout rockslide (Czech Republic). Geomorphology, 130(3-4): 352-364.

Patterson, D. and Smith, M., 1981. The measurement of unfrozen water content by time domain reflectometry: Results from laboratory tests. Canadian Geotechnical Journal, 18(1): 131-144.

Peixoto, A., Pregnolato, M., Silva, A., Yamasaki, M. and Conte Junior, F., 2010. Development of an electrical resistivity measure for geotechnical and geoenvironmental characterization, Proceedings of the Second International Symposium on Cone Penetration Testing, pp. 1-09.

Peplinski, N.R., Ulaby, F.T. and Dobson, M.C., 1995. Dielectric properties of soils in the 0.3-1.3-GHz range. IEEE transactions on Geoscience and Remote sensing, 33(3): 803-807.

Perrone, A., Lapenna, V. and Piscitelli, S., 2014. Electrical resistivity tomography technique for landslide investigation: A review. Earth-Science Reviews, 135: 65-82.

Perrone, A., Vassallo, R., Lapenna, V. and Di Maio, C., 2008. Pore water pressures and slope stability: a joint geophysical and geotechnical analysis. Journal of Geophysics and Engineering, 5(3): 323-337.

Rahardjo, H. and Leong, E., 2006. Suction measurements, Proceedings of the Fourth International Conference on Unsaturated Soils 2006, pp. 81-104.

Ravindran, A. and Prabhu, M., 2012. Groundwater exploration study using Wenner-Schlumberger electrode array through W-4 2D Resistivity Imaging systems at Mahapallipuram, Chennai, Tamilanadu, India. Res. J. Recent Sci, 1(11): 36-40.

Rawlins, S.L. and Campbell, G.S., 1986. Water potential: Thermocouple psychrometry. Methods of Soil Analysis: Part 1 Physical and Mineralogical Methods, 5: 597-618.

Reynolds, J.M., 2011. An introduction to applied and environmental geophysics. John Wiley & Sons.

Richards, L., 1941. A pressure-membrane extraction apparatus for soil solution. Soil Sci, 51(5): 377-386.

Ridley, A. and Burland, J., 1993. A new instrument for the measurement of soil moisture suction. Géotechnique, 43(2): 321-324.

Ridley, A. and Burland, J., 1995. Measurement of suction in materials which swell. Applied Mechanics Reviews, 48(10): 727-732.

Ridley, A. and Wray, W., 1996. Suction measurement: a review of current theory and practices, PROCEEDINGS OF THE FIRST INTERNATIONAL CONFERENCE ON UNSATURATED SOILS/UNSAT'95/PARIS/FRANCE/6-8 SEPTEMBER 1995. VOLUME 3.

Robinson, D., Gardner, C. and Cooper, J., 1999. Measurement of relative permittivity in sandy soils using TDR, capacitance and theta probes: comparison, including the effects of bulk soil electrical conductivity. Journal of Hydrology, 223(3-4): 198-211.

Robinson, D., Jones, S.B., Wraith, J., Or, D. and Friedman, S., 2003a. A review of advances in dielectric and electrical conductivity measurement in soils using time domain reflectometry. Vadose Zone Journal, 2(4): 444-475.

Robinson, D., Schaap, M., Jones, S., Friedman, S. and Gardner, C., 2003b. Considerations for improving the accuracy of permittivity measurement using time domain reflectometry: Air-water calibration, effects of cable length. Soil Science Society of America Journal, 67(1): 62-70.

Robock, A., 2015. HYDROLOGY, FLOODS AND DROUGHTS| Soil Moisture, Encyclopedia of Atmospheric Sciences. Elsevier, pp. 232-239.

Rogers, L.E. and Wright, S.G., 1986. The effects of wetting and drying on the long-term shear strength parameters for compacted Beaumont clay.

Rosset, E., Hilbich, C., Schneider, S. and Hauck, C., 2013. Automatic filtering of ERT monitoring data in mountain permafrost. Near Surface Geophysics, 11(4): 423-433.

Roth, K., Schulin, R., Flühler, H. and Attinger, W., 1990. Calibration of time domain reflectometry for water content measurement using a composite dielectric approach. Water resources research, 26(10): 2267-2273.

Samouëlian, A., Cousin, I., Tabbagh, A., Bruand, A. and Richard, G., 2005. Electrical resistivity survey in soil science: a review. Soil and Tillage research, 83(2): 173-193.

Santos, F.A.M. and Afonso, A.R.A., 2005. Detection and 2D modelling of cavities using pole–dipole array. Environmental Geology, 48(1): 108-116.

Sass, O., 2007. Bedrock detection and talus thickness assessment in the European Alps using geophysical methods. Journal of Applied Geophysics, 62(3): 254-269.

Schaap, M., De Lange, L. and Heimovaara, T., 1997. TDR calibration of organic forest floor media. Soil Technology, 11(2): 205-217.

Schmidt-Hattenberger, C., Bergmann, P., Bösing, D., Labitzke, T., Möller, M., Schröder, S., Wagner, F. and Schütt, H., 2013. Electrical Resistivity Tomography (ERT) for Monitoring of CO2 Migration - from Tool Development to Reservoir Surveillance at the Ketzin Pilot Site. Energy Procedia, 37: 4268-4275.

Schmidt, J. and Dikau, R., 2004. Modeling historical climate variability and slope stability. Geomorphology, 60(3-4): 433-447.

Schmutz, M., Guérin, R., Andrieux, P. and Maquaire, O., 2009. Determination of the 3D structure of an earthflow by geophysical methods: the case of Super Sauze, in the French southern Alps. Journal of Applied Geophysics, 68(4): 500-507.

Schwartz, B.F., Schreiber, M.E. and Yan, T., 2008. Quantifying field-scale soil moisture using electrical resistivity imaging. Journal of Hydrology, 362(3-4): 234-246.

Seaton, W.J. and Burbey, T.J., 2002. Evaluation of two-dimensional resistivity methods in a fractured crystalline-rock terrane. Journal of Applied Geophysics, 51(1): 21-41.

Shan, C., Bastani, M., Malehmir, A., Persson, L. and Engdahl, M., 2014. Integrated 2D modeling and interpretation of geophysical and geotechnical data to delineate quick clays at a landslide site in southwest Sweden. Geophysics, 79(4): EN61-EN75.

Sharma, P.V., 1997. Environmental and engineering geophysics. Cambridge university press.

Slater, L.D., Binley, A. and Brown, D., 1997. Electrical imaging of fractures using ground-water salinity change. Groundwater, 35(3): 436-442.

Smith, M. and Patterson, D., 1984. Determining the unfrozen water content in soils by time-domain reflectometry: Research note. Atmosphere-Ocean, 22(2): 261-263.

Sposito, G., 1981. The thermodynamics of soil solutions. Oxford University Press.

Stirling, R.A., Hughes, P.N., Davie, C.T. and Glendinning, S., 2014. Cyclic relationship between saturation and tensile strength in the near-surface zone of infrastructure embankments. Unsaturated Soils: Research & Applications, Vols 1 and 2: 1501-1505.

Stirling, R.A., Toll, D.G., Glendinning, S., Helm, P.R., Yildiz, A., Hughes, P.N. and Asquith, J.D., 2020. Weather-driven deterioration processes affecting the performance of embankment slopes. Géotechnique: 1-13.

Take, W. and Bolton, M., 2003. Tensiometer saturation and the reliable measurement of soil suction. Géotechnique, 53(2): 159-172.

Tang, A.-M. and Cui, Y.-J., 2005. Controlling suction by the vapour equilibrium technique at different temperatures and its application in determining the water retention properties of MX80 clay. Canadian Geotechnical Journal, 42(1): 287-296.

Tang, A.M., Hughes, P.N., Dijkstra, T.A., Askarinejad, A., Brenčič, M., Cui, Y.J., Diez, J., Firgi, T., Gajewska, B. and Gentile, F., 2018a. Atmosphere–vegetation–soil interactions in a climate change context; impact of changing conditions on engineered transport infrastructure slopes in Europe. Quarterly Journal of Engineering Geology and Hydrogeology, 51(2): 156-168.

Tang, C.-S., Wang, D.-Y., Zhu, C., Zhou, Q.-Y., Xu, S.-K. and Shi, B., 2018b. Characterizing drying-induced clayey soil desiccation cracking process using electrical resistivity method. Applied Clay Science, 152: 101-112.

Tarantino, A. and Mongiovi, L., 2003. Calibration of tensiometer for direct measurement of matric suction. Géotechnique, 53(1).

Tarantino, A. and Mongiovì, L., 2001. Experimental procedures and cavitation mechanisms in tensiometer measurements, Unsaturated Soil Concepts and Their Application in Geotechnical Practice. Springer, pp. 189-210.

Tarantino, A. and Mongiovì, L., 2002. Design and construction of a tensiometer for direct measurement of matric suction, Proceedings of the 3nd International Conference on Unsaturated Soils, Recife, Brazil, pp. 319-324.

Tarantino, A., Mongiovì, L. and Bosco, G., 2000. An experimental investigation on the independent isotropic stress variables for unsaturated soils. Géotechnique, 50(3): 275-282.

Tekinsoy, M., Kayadelen, C., Keskin, M. and Söylemez, M., 2004. An equation for predicting shear strength envelope with respect to matric suction. Computers and Geotechnics, 31(7): 589-593.

Terzaghi, K., 1943. Theoretical soil mechanics. Chapman And Hall, Limited.; London.

Thomas, A., Chapman, D., Rogers, C. and Metje, N., 2010a. Electromagnetic properties of the ground: Part I–Fine-grained soils at the Liquid Limit. Tunnelling and Underground Space Technology, 25(6): 714-722.

Thomas, A., Chapman, D., Rogers, C. and Metje, N., 2010b. Electromagnetic properties of the ground: Part II–The properties of two selected fine-grained soils. Tunnelling and Underground Space Technology, 25(6): 723-730.

Tinga, W.R., Voss, W. and Blossey, D., 1973. Generalized approach to multiphase dielectric mixture theory. Journal of applied physics, 44(9): 3897-3902.

Toll, D., 1990. A framework for unsaturated soil behaviour. Géotechnique, 40(1): 31-44.

Toll, D. and Ong, B., 2003. Critical-state parameters for an unsaturated residual sandy clay. Géotechnique., 53(1): 93-103.

Toll, D.G., Asquith, J.D., Hughes, P.N. and Osinski, P., 2016. Soil Water Retention Behaviour of a Sandy Clay Fill Material. Procedia Engineering, 143: 308-314.

Toll, D.G., Lourenço, S.D. and Mendes, J., 2013. Advances in suction measurements using high suction tensiometers. Engineering Geology, 165: 29-37.

Topp, G. and Davis, J., 1985. Measurement of soil water content using time-domain reflectrometry (TDR): A field evaluation. Soil Science Society of America Journal, 49(1): 19-24.

Topp, G., Davis, J. and Annan, A., 1982. Electromagnetic determination of soil water content using TDR: I. Applications to wetting fronts and steep gradients. Soil Science Society of America Journal, 46(4): 672-678.

Topp, G., Yanuka, M., Zebchuk, W. and Zegelin, S., 1988. Determination of electrical conductivity using time domain reflectometry: Soil and water experiments in coaxial lines. Water Resources Research, 24(7): 945-952.

Topp, G., Zegelin, S. and White, I., 2000. Impacts of the real and imaginary components of relative permittivity on time domain reflectometry measurements in soils. Soil Science Society of America Journal, 64(4): 1244-1252.

Topp, G.C., Davis, J. and Annan, A.P., 1980. Electromagnetic determination of soil water content: Measurements in coaxial transmission lines. Water resources research, 16(3): 574-582.

Topp, G.C., Davis, J.L. and Annan, A.P., 2003. The early development of TDR for soil measurements. Vadose Zone Journal, 2(4): 492-499.

Tripathy, S., Al-Khyat, S., Cleall, P.J., Baille, W. and Schanz, T., 2016. Soil suction measurement of unsaturated soils with a sensor using fixed-matrix porous ceramic discs. Indian Geotechnical Journal, 46(3): 252-260.

Tuller, M. and Or, D., 2004. Retention of water in soil and the soil water characteristic curve. Encyclopedia of Soils in the Environment, 4: 278-289.

Tuller, M., Or, D. and Dudley, L.M., 1999. Adsorption and capillary condensation in porous media: Liquid retention and interfacial configurations in angular pores. Water resources research, 35(7): 1949-1964.

Uchaipichat, A., 2010. Experimental investigation on loading collapse curve of unsaturated soils under wetting and drying processes. Geomechanics and Engineering, 2(3): 203-211.

Uhlemann, S., Chambers, J., Wilkinson, P., Maurer, H., Merritt, A., Meldrum, P., Kuras, O., Gunn, D., Smith, A. and Dijkstra, T., 2017. Four-dimensional imaging of moisture dynamics during landslide reactivation. Journal of Geophysical Research: Earth Surface, 122(1): 398-418.

van Genuchten, M.T., 1980. A closed-form equation for predicting the hydraulic conductivity of unsaturated soils. Soil science society of America journal, 44(5): 892-898.

Vanapalli, S., Fredlund, D., Pufahl, D. and Clifton, A., 1996. Model for the prediction of shear strength with respect to soil suction. Canadian Geotechnical Journal, 33(3): 379-392.

Walthert, L. and Schleppi, P., 2018. Equations to compensate for the temperature effect on readings from dielectric Decagon MPS-2 and MPS-6 water potential sensors in soils. Journal of Plant Nutrition and Soil Science, 181(5): 749-759.

Watts, G., Battarbee, R.W., Bloomfield, J.P., Crossman, J., Daccache, A., Durance, I., Elliott, J.A., Garner, G., Hannaford, J. and Hannah, D.M., 2015. Climate change and water in the UK–past changes and future prospects. Progress in Physical Geography, 39(1): 6-28.

Waxman, M.H. and Smits, L., 1968. Electrical conductivities in oil-bearing shaly sands. Society of Petroleum Engineers Journal, 8(02): 107-122.

Wen, T., Shao, L., Guo, X. and Zhao, Y., 2020. Experimental investigations of the soil water retention curve under multiple drying–wetting cycles. Acta Geotechnica, 15(11): 3321-3326.

Whalley, W., 1993. Considerations on the use of time-domain reflectometry (TDR) for measuring soil water content. Journal of Soil Science, 44(1): 1-9.

Whiteley, J., Chambers, J., Uhlemann, S., Wilkinson, P. and Kendall, J., 2019. Geophysical Monitoring of Moisture-Induced Landslides: A Review. Reviews of Geophysics.

Widomski, M.K., Stępniewski, W. and Musz-Pomorska, A., 2018. Clays of different plasticity as materials for landfill liners in rural systems of sustainable waste management. Sustainability, 10(7): 2489.

Wilkinson, P., Chambers, J., Uhlemann, S., Meldrum, P., Smith, A., Dixon, N. and Loke, M.H., 2016. Reconstruction of landslide movements by inversion of 4 - D electrical resistivity tomography monitoring data. Geophysical Research Letters, 43(3): 1166-1174.

Williams, J., Prebble, R., Williams, W. and Hignett, C., 1983. The influence of texture, structure and clay mineralogy on the soil moisture characteristic. Soil Research, 21(1): 15-32.

Williams, P.J., 1982. The surface of the earth: an introduction to geotechnical science. Addison-Wesley Longman Ltd, New York.

Woodburn, J.A., Holden, J.C. and Peter, P., 1993. The transistor psychrometer: a new instrument for measuring soil suction, Unsaturated soils. ASCE, pp. 91-102.

Zhou, M., Wang, J., Cai, L., Fan, Y. and Zheng, Z., 2015. Laboratory investigations on factors affecting soil electrical resistivity and the measurement. IEEE Transactions on Industry Applications, 51(6): 5358-5365.